An Experimental Study of Elastic and Inelastic Electron Scattering From Molecules

by

Isabella M. Mapstone

A thesis submitted in partial fulfilment

of the requirements for the degree of

Doctor of Philosophy

University of London

1990

Abstract

The high resolution electron spectrometer designed and constructed for the present work is described. Throughout the design particular attention was paid to the window and pupil positions, beam and pencil angles and the effect of these parameters on the overall resolution of the spectrometer. Two sets of 180° hemispherical analysers, fitted with Jost type correction plates to reduce the fringing fields, were used to define the energy spread in the incident electron beam and analyse the energy of the scattered electrons. Instrumental energy resolutions of around 50 to 60meV for primary beam currents of 2 to 3nA across the interaction region were achieved.

Details of the interface built for a BBC microcomputer and the programs written to control it are given. This interface was used to collect the experimental data by generating a ramp voltage under the control of the BBC micro. For each of the 1024 steps in the ramp voltage it was possible to count pulses simultaneously from two independent electron detectors, these counts being stored in two 1024 element arrays. On completion of the required number of scans the energy loss spectrum could be displayed. The number of scans, step time, and initial and final steps in the ramp are all input parameters in the data acquisition programs.

The spectrometer and interface were used to carry out a series of measurements of the elastic differential cross sections of methane, ethene and ethane and of the excitation of vibrational levels in the electron impact energy range 3eV to 15eV for scattering angles of 30 to 140°. Equations are derived to enable the calculation of elastic and inelastic differential cross sections from these measurements and the details of the programs written to fit the energy loss spectra are given.

Methane, ethane and to a lesser extent ethene are all present in the atmospheres of Jupiter, Saturn and its satellite Titan. These molecules are also of interest due to their different symmetries, and as a testing ground for collision theory. Recent developments in computational techniques allow accurate calculations of the cross sections of large molecules to be made, consequently good experimental data is required for critical comparison.

Contents

List of Tables

List of Figures

List of Plates

Acknowledgements

To Dr W R Newell for his supervision and encouragement during the course of this work.

To Mr I Rangué for constructing the electron spectrometer and for his invaluable assistance in maintaining the vacuum system and experimental tank.

To Mr E. Oldfield for building the BBC micro interface, designing the layout of the circuit boards and for maintaining and upgrading the spectrometer power supplies.

To Mr W M Johnstone and Dr N J Mason for useful discussions and for keeping me up to date with the publications relevant to this work since my departure from college.

To my husband Paul for his support and assistance at all times and for his excellent work in the preparation of this thesis.

Chapter 1 - Review of Experimental and Theoretical Work

1.1 Introduction

The general physical principals behind electron - molecular scattering have been understood for over fifty years. The quantum mechanics has been described by Born (1926), Oppenheimer (1928) and Massey and Mohr (1932a,b) and were summarised by Massey and Burhop in the volume 'Electronic and Ionic Impact Phenomena' which was published in 1969.

It is only in the last twenty years however, that rapid advances in this field have been made. On the experimental side this is largely due to the developments in the field of electron optics and electron detection techniques, while the availability of powerful, high speed computers has enabled the calculation of the molecular cross sections calling for experimentalists to verify these new results. Developments in the fields of laser and plasma physics, astrophysical and atmospherical modelling have resulted in the need for extensive, accurate cross section data.

The molecules chosen for the present experiment, methane, ethene and ethane are of particular interest firstly because they have been identified as important constituents of the atmospheres of the planets Jupiter and Saturn and the moon Titan (Hunt 1985, Wayne 1985) and secondly due to their different symmetries. Methane, ethene and ethane belong to the symmetry groups T_d , V_h and D_{3d} respectively.

In Section 1.2 the various types of scattering experiments are outlined. In Section 1.3 the experimental data available on the low energy elastic scattering from the three molecules investigated in the present experiment is reviewed, and in Section 1.4 the available vibrational data on these molecules is described. The theoretical methods and treatment of these molecules at low energies is discussed in Sections 1.5 and 1.6.

1.2 Review of Electron Scattering Experiments

The earliest scattering experiments yielded the total electron cross section of the target atom/molecule with the most successful of these being the Ramsauer type experiments. The Ramsauer experiment was first performed in 1921 (Ramsauer 1921). In this experiment photoelectrons were accelerated to a desired energy and then deflected into a circular path by a perpendicular uniform magnetic field. These electrons passed through collimating slots before entering the region of the apparatus which contained the target gas. Scattered electrons were detected at the wall of this region, while the

unscattered electrons passed through the final slot and were detected by a Faraday cup. By measuring the two currents the total cross section was found. Modified forms of the Ramsauer method are still used, however, it is now more common for electron transmission measurements to be made in a straight through, field-free, collision chamber. More sophisticated energy analysers are employed which allow elastic and inelastically scattered electrons to be separated. The success of this technique is attributable to the combination of experimental simplicity and compactness, good energy selection ability, and good angular and energy-loss discrimination for elastic and inelastic collisions (Bederson and Kieffer 1971). The problems encountered in this method are:-

1) the forward scattering into the view cone of the detector,

2) treating electrons which undergo multiple collisions and are scattered back into the view cone of the detector,

3) defining the proper path length.

In addition there are pressure and current dependent problems (multiple scattering and space charge effects) which have to be checked and minimised. Provided these points are attended to relative total cross sections accurate to a few percent may be obtained.

In more recent times total cross sections have been measured using time-of-flight apparatus to determine the energy distribution of the electrons. Ferch et al (1985a) describe a typical TOF experiment. Electrons from a thermionic cathode are accelerated to form a beam which is chopped in a gate by sweeping it across a narrow slot, so producing bursts of electrons. The electrons in each burst are decelerated to the required energy before passing through the target gas cell. The electrons emerging from the cell are re-accelerated and detected by an electron multiplier. The flight time is measured individually for each detected electron by measuring the time between its detection and the time taken for the corresponding gate voltage to reach the timing electronics.

A time-to-pulse height convertor and multichannel pulse height analyser then generates the detected electron count rates as a function of electron energy. Flight time data are accumulated both with and without the gas present allowing the attenuation of the electron beam, and hence the total cross section,to be determined as a function of impact energy. The electron resolution is normally extremely high at low energies (Ferch et al give an energy resolution of 1meV at 0.3eV) but is limited at high impact energies (above 50eV) by time resolution capabilities. Since inelastic forward scattering cannot be energetically discriminated against in the TOF measurements caution must be used on molecular systems.

Another method used to measure the total cross section is the recoil technique. This is basically a transmission experiment in which instead of a cell containing the target gas, the electron beam is crossed with a molecular beam and the attenuation of the molecular beam rather than the electron beam is measured. Although this method has been applied extensively to atomic species to date little work has been done on molecules. This is due to the difficulty of achieving the high angular resolution and accurate quantitative detection of neutral beams.

Momentum transfer cross sections are usually measured by means of the swarm technique. The two main methods employed are the 'drift velocity' method and the 'microwave method'. In the drift method the momentum transfer cross section is determined as a function of electron energy from measurements of the average velocity of electronic drift through a gas in a dc electric field. These measurements are made in a drift tube. Inside the drift region of the tube there exists a gas of number density N and an uniform electric field E, the parameter E/N determines the drift velocity and average energy of the electrons in the gas for a given gas temperature. The drift velocity is measured as a function of E/N. Cross section information may be extracted from this data as at a given E/N the steady state drift velocity is achieved by a balance between the accelerations in the field direction between collisions with the gas molecules and the velocity changes that occur during these collisions. The momentum transfer cross sections are parameters in the Boltzmann transport equations, therefore by inserting estimated collision cross sections in the Boltzmann transport equation for the swarm the electron energy distribution function may be evaluated. Then by averaging over this distribution function the electron transport coefficients for the swarm may be calculated. Comparison of the calculated coefficients with the previously measured values suggest adjustments to the input cross sections, these are then altered until the calculated and experimental values agree. At low energies where only a few collision channels are open this procedure can yield reliable and accurate cross sections. At higher energies where many channels are open ambiguities develop in fitting the observed transport to the theoretical expressions and therefore in determining the cross section.

The microwave method employs a magnetron to break down the gas contained in a resonant cavity and provide a plasma whose conductivity can be measured. The change in the cavity impedance due to the presence of free electrons is measured by using a continuous-wave tuneable magnetron and a standing wave detector. For further details see Bederson and Kieffer 1971.

Differential cross sections have been measured since the 1930s and in these experiments an electron beam intersects a gas beam or cell, and the scattered current is detected over a range of scattering angles, typically 10 to 150°. It is only in the last ten to twenty years, however, due to advances in electron optics and in the design of electron energy selectors that accurate measurements have been possible. The earliest significant works on electron optics date from the 1960s, for example 'Electron Optics' by Grivet published in 1965, followed by a publication of the same name by Kemplerer and Barnet in

1971. It is only as recently as 1976, however, that extensive lens data (Harting and Read 1976) has been available facilitating the design of high energy and high angular resolution spectrometers. A second important contributing factor is the vast improvements in electron detection, due to the use of sensitive electron multipliers, microchannel plates, and the advances made in digital electronics. Improvements in vacuum technology, pressure measurement and target gas purity have also helped the modern experimenter. The following four chapters describe the techniques used in the present experiment.

1.3 Review of Low Energy Electron Scattering Measurements

Table 1.1 lists the work published for the three molecules methane, ethene and ethane for elastic scattering of low energy electrons.

The earliest results were obtained using Ramsauer type techniques, yielding the total cross sections of methane and ethane. Brode (1925) investigated the variation of the absorption coefficient of methane with incident electrons in the energy range 2 to 360eV. The absorption coefficient is directly proportional to the total cross section at a particular electron energy. His results show a rapid rise to a maximum value at 7.5eV which falls off slowly as the incident energy increases to 360eV. He observed that the cross sections for helium and argon were similar in shape although different in absolute magnitude.

Similar measurements were carried out by Brüche (1927) over the energy range 1 to 38eV and are in reasonable agreement with those of Brode. Although the peak value is greater by approximately 20% and centred at just under 7eV, the shape of the curves are similar. Brüche also carried out these measurements on ethene and ethane (1929,1930) and found the same variation of the total cross section with electron energy for energies greater than 3eV. The peak magnitude at each energy however, increased with the size of the molecule, the peak heights for ethene and ethane being approximately 25% and 40% greater than that of methane. The ethene peak was situated at the higher energy of 9eV and this gas also displayed a smaller, narrow peak at 2.2eV, see Figures 1.1 and 1.2.

Ramsauer and Kollath (1930) extended the energy range to below 1eV, working with methane, and showed that the absorption coefficient has a minimum at 0.4eV. This 'Ramsauer' minimum is also apparent in argon and the heavier inert gases, and is explained by the wave nature of the electron.

More recently total cross sections and electron transmission functions have been obtained by measuring the attenuation of electron beams in a straight line collision chamber, without a confining magnetic field. Boness et al (1967) measured the electron transmission functions of methane, ethene and ethane searching for low lying negative ion states. For methane a broad peak with small undulations was

Author	Target Gas	†Type of Measurement	Type of Experiment	Energy Range	Angular Range
Brode (1925)	CH_4	T	RAMSAUER	2-360eV	
Brüche (1927,1929,1930)	CH_4,C_2H_4,C_2H_6	T	RAMSAUER	1-38eV	
Ramsauer and Kollath (1930)	CH_4	T	RAMSAUER	0.2-36eV	
Boness et al (1967)	CH_4,C_2H_4,C_2H_6	T	e- TRANSMISSION	0-3eV	
Sanche and Schulz (1973)	CH_4,C_2H_4	T	e- TRANSMISSION	0-20eV	
Botz and Glick (1975)	CH_4	T	e- TRANSMISSION	5-15eV	
Barbarito et al (1979)	CH_4	T	e- TRANSMISSION	0.1-16eV	
Mathur (1980)	CH_4	T	e- TRANSMISSION	1-20eV	
Ferch et al (1985b)	CH_4	T,M	TOF	0.085-12eV	
Jones (1985)	CH_4	T	TOF	1.3-50eV	
Floeder et al (1985)	CH_4,C_2H_4,C_2H_6	T	e- TRANSMISSION	5-400eV	
Sueoka and Mori (1985)	CH_4,C_2H_4,C_2H_6	T	TOF	1-400eV	
Cottrell and Walker (1965,1967)	CH_4,C_2H_6	M	SWARM	0-1eV	
Pollock (1968)	CH_4	M	SWARM	0-1eV	
Duncan and Walker (1972)	CH_4,C_2H_6	M	SWARM	0.01-1eV	
McCorkle et al (1978)	C_2H_6	M	SWARM	0-0.5eV	
Bullard and Massey (1931)	CH_4	D	GAS CELL	4-30eV	20-120°
Arnot (1931)	CH_4	D	GAS CELL	30-410,820eV	10-120°,10-50°
Mohr and Nicoll (1932)	CH_4	D	GAS CELL	30-84eV	20-160°
Hughs and McMillan (1933)	CH_4	D	GAS CELL	10-625,800eV	10-150°,10-50°
	C_2H_4			10-225eV	10-150°
Fink et al (1975)	C_2H_4,C_2H_6	D	CROSSED BEAM	100-1000eV	3-130°
Newell et al (1979)	CH_4	D	CROSSED BEAM	10eV	20-130°
Rohr (1980)	CH_4	D	CROSSED BEAM	1,2,5eV	20-120°
		D(E)		0.1-10eV	20,80°
Tanaka et al (1982)	CH_4	D,I,M	CROSSED BEAM	3-20eV	30-140°
Sohn et al (1983)	CH_4	D	CROSSED BEAM	0.6,1eV	30-105°
		D(E)		0.1-1.3eV	35°,55°,90°,110°
Vuskovic and Trajmar (1983)	CH_4	D	CROSSED BEAM	20,30,200eV	8-130°
Curry et al (1985)	CH_4,C_2H_6	D	CROSSED BEAM	7.5-20eV	30-140°
Sohn et al (1986)	CH_4	D,I	CROSSED BEAM	0.2-5eV	15-138°
Tanaka et al (1988)	C_2H_6	D,I,M	CROSSED BEAM	2-100eV	15-130°
Present work	CH_4,C_2H_4,C_2H_6	D	CROSSED BEAM	3-15eV	30-140°

† T = Total cross section
M = Momentum transfer cross section
D = Differential cross section
D(E) = Differential cross section as a function of collision energy
I = Integral cross section

Table 1.1 Summary of the total, momentum transfer and elastic differential cross section measurements on methane, ethene and ethane

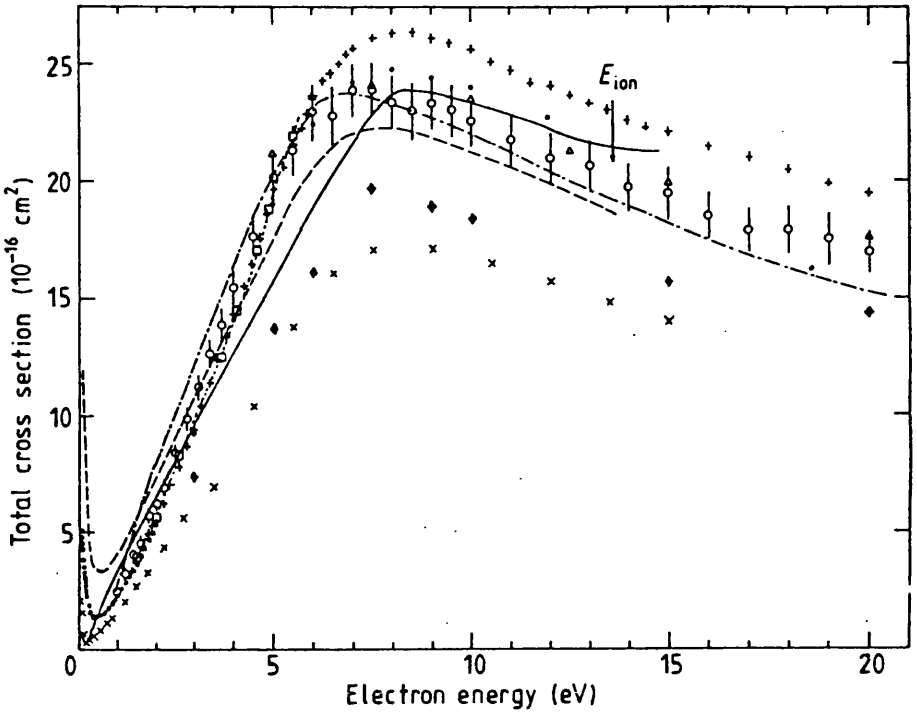

Figure 1.1 Total cross sections for electrons colliding with methane at low energies. Experimental results: o Sueoka and Mori 1985; • Ferch et al 1985; Δ Floeder et al 1985; + Jones 1985; × Barbarito et al 1979; - - - Brüche 1927; ♦ integrated cross section of Tanaka et al 1983. Theoretical results; — AT from Jain and Thompson 1982; --- Gianturco and Thompson 1976. The arrow shows the threshold of ionisation.

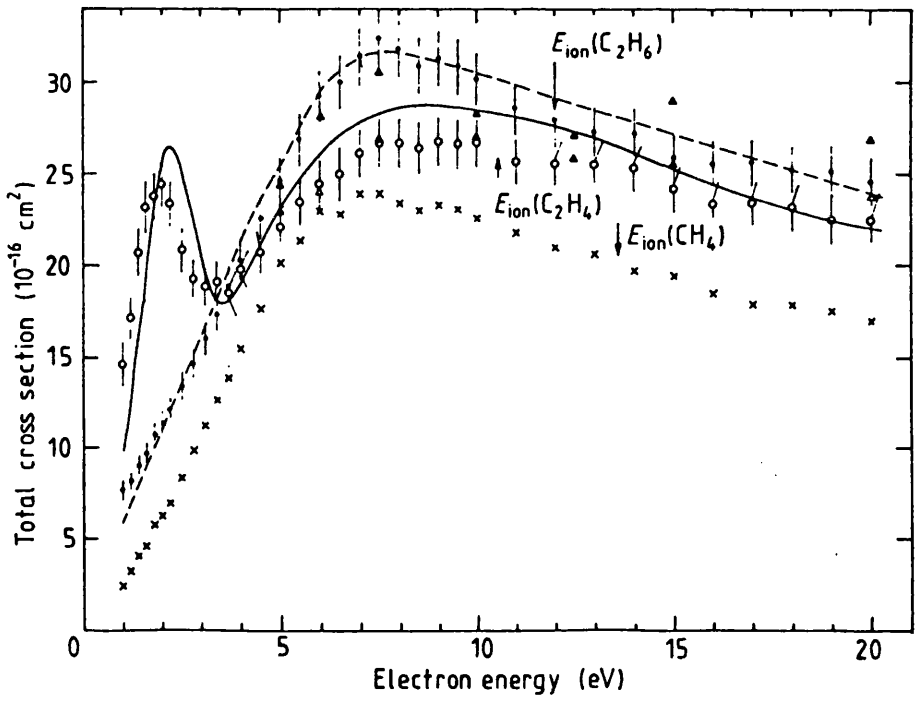

Figure 1.2 Total cross sections for electrons colliding with ethene and ethane at low energies. Experimental results: o (C_2H_4), • (C_2H_6) Sueoka and Mori 1985; Δ (C_2H_4), ▲ (C_2H_6) Floeder et al 1985; — (C_2H_4) Brüche 1929; --- (C2H6) Brüche 1930. The e^- - CH_4 data of Sueoka and Mori, × are shown for reference. The thresholds of ionisation are indicated by arrows.

obtained between 2 and 3eV, indicating the presence of a vibrational progression. Ethene showed two bands peaking at 0.2 and approximately 1.3eV. No structures were observed in ethane.

In 1973 Sanche and Schulz searched for compound states in several molecules by measuring the derivative of the current transmitted through the target gas, from this they were able to deduce the total cross sections. They found no structures in the total cross section of methane over the energy range 0 to 20eV. A broad and structureless dip, centred at 1.76eV, was observed in the plot of the transmitted current vs the electron energy for ethene, corresponding to a maximum in the total cross section. This they attributed to the formation of a temporary negative ion. They also reported a vibrational progression of resonances starting at 6.6eV and extending to 7.4eV. They did not observe any structure in the region of 0.2eV.

Botz and Glick (1975) measured the electron transmission function of methane over the energy range 5 to 15eV, using a 270° electrostatic energy selector and achieving an energy resolution of 40meV. They reported structures at 6.53, 7.37 and 8.15eV.

Barbarito et al (1979) have published total cross sections for methane obtained by measuring the attenuation of 0.1 to 16 eV electrons, their results are shown in Figure 1.1. An electron monochromator was used producing a well defined beam of approximately 80meV full width half height. The Ramsauer minimum was found to be considerably sharper and deeper (by a factor of 5), than that observed by Ramsauer and Kollath, and situated at a lower energy of 0.215eV. In general the total cross section was lower over the energy range investigated than found in previous experiments. These differences were explained by the improved energy resolution of the Barbarito experiment and the better control over the pressure value in the scattering chamber due to the use of a capacitance manometer. Barbarito et al also claimed to have observed a vibrational progression in the region of the Ramsauer minimum.

The electron transmission function of methane over the energy range 1-20eV was measured by Mathur in 1980. He reported two broad minima, corresponding to a maximum in the total cross section, at 7.8 and 12eV in addition to a broad 18.5eV resonance. The 12eV resonance appeared to be strongly angular dependant. He attributed the broad minimum at 7.8eV to the predissociation broadening characteristic of saturated hydrocarbons and pointed out that the derivative technique employed by Sanche and Schulz (1973) would not be expected to detect such a shallow minimum. No fine structure was observed between 6 and 9eV and he therefore suggested that the three sharp features observed by Botz and Glick (1975) should be viewed with suspicion. The broad structure in methane at 2.4eV observed by Boness et al (1967) was attributed to a nitrogen impurity.

Ferch et al (1985b) measured the total cross section of methane using a time-of-flight spectrometer over the energy range 0.085 to 12eV, their results are shown in Figure 1.1. They paid particular attention to the Ramsauer minimum for which they determined a minimum cross section of $1.36\times10^{-16}\,cm^2$ at an energy of 0.40eV.

On comparing their data with that of the early experiments they found excellent agreement with Ramsauer and Kollath (1930) over the energy region of the Ramsauer minimum and with Brüche (1930) covering the energy region of the maximum. A distinct disagreement, however, exists between their results and those of Barbarito et al (1979) with the data of Ferch et al being systematically higher over the whole energy range. Also the minimum in the cross section data of Barbarito et al is substantially deeper and located at a lower energy. Barbarito et al had interpreted the deviation of their results from the early measurements as a consequence of better target pressure manometry and higher electron energy resolution. Ferch et al agree that a pressure measurement off by about 25% is conceivable for an experiment performed 50 years ago. They also allow that insufficient energy resolution could indeed increase the minimum and because of its asymmetrical shape shift it towards higher energies. However, their results were obtained with a pressure measurement accuracy on the 0.1% level, employing a Baratron capacitance manometer. They also go on to compare their energy resolution with that of Barbarito et al and claim that for energies below 1.6eV their resolution is significantly better than that of Barbarito et al, rising from 4meV at 0.085eV to 1.38eV at 12eV. Finally like Barbarito et al, they also compared their argon data (Ferch et al 1985a) to that of Ramsauer and Kollath (1929), again unlike Barbarito et al the agreement with the early data is good. They conclude by attributing the discrepancies in the data to the following errors in the Barbarito experiment:-

1) Insufficient discrimination of forward scattering in the gas cell of 25mm length (1/10 of that in their experiment). This is most serious at the Ramsauer minimum where isotropic S-wave scattering vanishes.

2) Pressure enhancement in the gauge located very close to the target-gas inlet.

Both of these errors could have led to a measured cross section which is generally too low.

The data of Jones (1985) supports the above argument and is shown in Figure 1.1. He measured the absolute total cross section for methane using a time-of-flight electron transmission spectrometer for incident energies 1.3 to 50eV and obtained a broad maximum at 8.1eV. The shape of his cross section agrees well with that of Barbarito et al, but his measurements are on average 35% greater. The pressure measurements were made with a MKS capacitance manometer giving an accuracy of better than ±1.20%.

Also in 1985, Floeder et al measured the total cross section for electron scattering from methane, ethene and ethane between 5 and 400eV. Their results between 5 and 20eV are plotted in Figures 1.1 and 1.2. The transmission apparatus used has been described in detail by Deuring et al (1983). Excellent agreement was found with Ferch et al. The pressure was measured directly with a capacitance manometer, consequently the systematic error resulting from the determination of the effective target length and pressure was estimated to be ±3%. Discrimination against inelastically forward scattered particles with an energy loss of greater than 2eV was achieved by applying a retarding potential to the filter lens. As expected the total cross section for ethane was found to be consistently higher than that for methane (over the range 5-300eV it was higher by 30-50%), like methane the ethane cross section peaks at 7.5eV. Similarly the cross section of ethene is greater than that of methane, over the same energy range by about 20-40%. A single peak, situated at 10eV was observed.

Most recently the total cross sections for 1-400eV electrons colliding with methane, ethene and ethane were measured by Sueoka and Mori (1985) using a retarding potential time-of-flight method. Their cross sections between 1 and 20eV are also shown in Figures 1.1 and 1.2. and were obtained by a normalisation method rather than by absolute measurements. For all gases good agreement was found with Floeder et al, however the agreement with Brüche, particularly in the position of the low energy shape resonance in ethene, was not so good. The position of the low energy ethene peak was found to be at 2.0eV rather than at the 2.2eV value reported by Brüche.

The momentum transfer cross sections of methane and ethane have been measured by Cottrell and Walker (1965,1967) Pollock (1968, methane only), Duncan and Walker (1972) and McCorkle et al (1978, ethane only) using swarm techniques in the electron energy region of 1eV. The measurements reveal Townsend minima in the region of 0.25eV for methane and 0.12eV for ethane of magnitude 1.0 and $1.2\times10^{-16}\,cm^2$ respectively. The application of these techniques are limited however by the assumptions involved in the analysis of the results (Duncan and Walker 1972).

Ferch et al (1985b) calculated the momentum transfer cross section, $\sigma_m(E)$, up to $E=0.5$eV and obtained a Townsend minimum of $0.45\times10^{-16}\,cm^2$ at 0.29eV which is both lower in magnitude and higher in energy than that obtained in the early swarm data evaluations. They employed the 'modified effective-range theory' (MERT) which aids comparison of results obtained in beam and swarm experiments and the determination of the scattering length by providing extrapolation formula for total and momentum transfer cross sections down to zero energy. MERT was originally developed for the spherically symmetrical systems of the noble gas atoms (O'Malley 1963) and later extended to homonuclear molecules (Chang 1981). How MERT could be extended to other molecules has not been studied theoretically, however the highly symmetric configuration of the tetrahedral methane molecule suggests that this theory might be applicable as a first approximation.

The earliest measurements of methane's differential cross sections were made by Bullard and Massey (1931). Electrons of 4 to 30 eV were scattered from a target gas cell and detected over the angular range 20 to 120°. The results at 6 and 4eV are shown plotted in Figures 6.3 and 6.5 with the results of the present experiment. Again similarities with argon were observed at energies below 20eV, this is shown in Figure 1.3 in which the Argon data of Srivastava et al (1981) has been plotted with the methane data of Tanaka et al (1982) over the energy range 3 to 15eV. From their results Bullard and Massey deduced that the outer electrons determine the scattering at low energies as argon and methane have similar electron configurations in their outer shells, ie all electrons are paired. At higher energies, the incident electron will penetrate the inner shells and hence produce a divergence in the cross sections of methane and argon.

In the same year Arnot (1931) conducted similar experiments for incident electron energies of 30, 84, 205, 410 and 820eV. The scattered electrons were collected over the range 10 to 120°at 3°and 84eV, the range then reducing to 10 to 50°at 820eV. At the lowest energy, 30eV, a deep minimum is observed at 100°, it is still visible at 84eV, but with its magnitude significantly reduced. The results obtained by Mohr and Nicoll (1932), in the energy range 30 to 84eV and for scattering angles between 20 and 160°are similar, however, at 84eV the minimum has shifted from 100° to 90°.

Hughs and McMillen (1933) performed experiments with methane over the angular range 10 to 150° for energies 10 to 625eV and also at 800eV over the reduced range of 10 to 50°. Their results at 15eV are plotted in Figure 6.1. These results are in fair agreement with those of Bullard and Massey at 10eV and Arnot at 30 and 400eV, however at 50eV the cross section is significantly lower at the larger scattering angles than that obtained in the earlier measurements of Mohr and Nicoll. They also published results for ethene over the angular range of 10 to 150° for a reduced selection of energies in the range of 10 to 225eV. At 100eV and below a minimum is clearly observable, at 100eV it is only just observable and centred at 100° but it increases in magnitude and moves to 90° at the lower energies. The methane spectra at 10 and 25eV display a shoulder at 50°, this is not present in the ethene results, the cross section instead falls smoothly to the minimum at 90°.

More recently, relative elastic differential scattering results for ethene and ethane have been reported by Fink et al (1975) using a crossed beam geometry and a retarding potential analyser. The incident electron energies were in the range of 100 to 1000eV over the angular range of 3 to 130°. In these measurements ethane displays a shallow minimum centred at 80° at 100eV, this shifts to 110° at 200eV and is not visible at the higher energies. Ethene also displays a minimum at 90° at 100eV and this too is not present at the higher energies.

Newell et al (1979) used a coaxial cone spectrometer (see Brewer et al 1980), providing an energy resolution of 90meV FWHM, to measure the elastic differential cross section of methane at 10eV

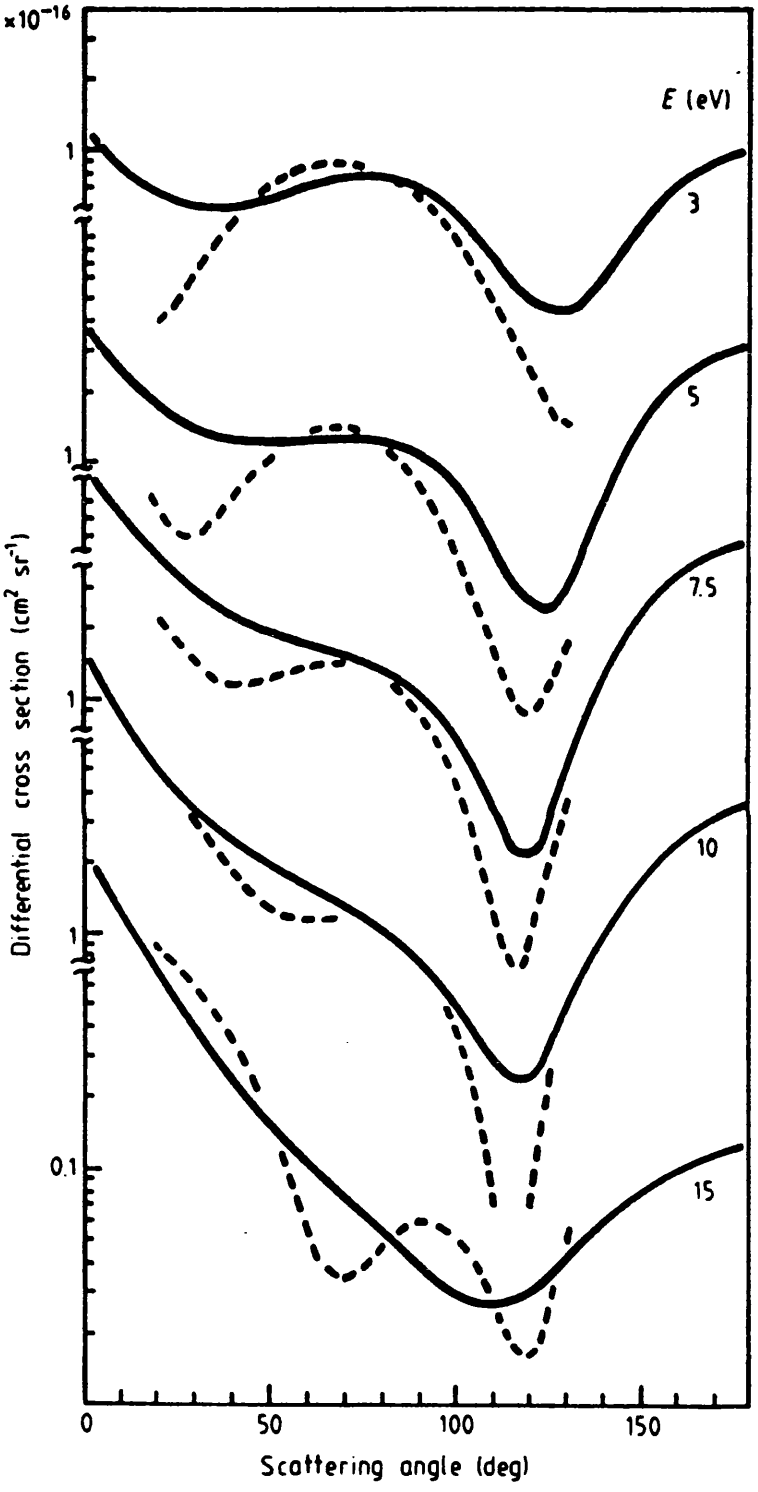

Figure 1.3 Comparison of the differential cross section of methane (solid curves, Tanaka et al 1982) with argon (broken curves, Srivastava et al 1981).

incident energy, over the angular range 20 to 130°. This spectrum displays the previously observed deep minimum at around 110° and a shallow shoulder at approximately 50°.

Rohr (1980), measured the differential cross section of methane over the incident energy range of 0.1 to 10eV at the scattering angles 20° and 80°. He employed two 127° cylindrical electrostatic selectors, with an overall energy resolution of 25meV. These cross sections display pronounced Ramsauer minima, and in addition at 80° a broad resonance structure at about 5eV. The position of the Ramsauer minimum was found to vary with angle with the minimum located at 1.5eV at 20° while at 80° it was sharper and had shifted to 0.3eV. Using the full angular range of the apparatus, of 20 to 120°, Rohr also reported results at 1, 2 and 5eV.

Tanaka et al (1982) have published results for methane over the energy range of 3 to 20eV, they also used a double 127° cylindrical electrostatic spectrometer. The scattering angle range was 30 to 140°, and an energy resolution of 50meV was achieved. These results were placed on an absolute scale using the relative flow technique (Srivastava et al 1975, Trajmar and Register 1984) and were used to normalise the measurements of the present experiment, see Section 6.2. Their data is shown in Figures 6.1 - 6.4 and 6.6 where it is compared to the results of the present experiment. By extrapolating their data between 0 to 30° and 140 to 180° they were able to calculate the integral and momentum transfer cross sections from the differential results. They compared their calculations to the measurements of Brode (1925), Brüche (1927), Ramsauer and Kollath (1930) and Barbarito et al (1979). Best agreement was found with Barbarito et al, the earlier data being considerably greater in magnitude at all energies. It should be noted, however, that the later measurement of total cross sections (eg that of Ferch et al 1985b) agree better with the early results of Ramsauer and Kollath and it is possible that the integral cross sections of Tanaka et al are in fact underestimated due to inelastic contributions to the total cross sections and/or systematic errors made in extrapolating their differential cross sections beyond the angular range of their measurements.

Sohn et al (1983), using a double 127° cylindrical electrostatic spectrometer, have reported results on methane. Their measurements were made at 0.6 and 1eV over the angular range of 30 to 120°. They also measured the energy dependence of the elastic differential cross section at scattering angles 35, 55, 90 and 110° and confirmed that the Ramsauer minimum shifts towards lower energy with increasing angle as previously reported by Rohr.

Vuskovic and Trajmar (1983) measured the elastic differential cross section of methane at incident energies of 20, 30 and 200eV. over the angular range 8 to 130°.They used a double hemispherical electrostatic spectrometer, with a FWHM energy resolution of 100meV.

Curry et al (1985), using the same apparatus as the present experiment, but different electron optics, measured the differential cross sections of both methane and ethane over the energy range 7.5 to 20eV, and over the angular range 30 to 140°. The energy resolution of this spectrometer was 80meV. The results at 15 and 7.5eV are shown in Figures 6.1 and 6.2 for methane and 6.13 and 6.14 for ethane.

Sohn et al (1986), using an improved spectrometer with an energy resolution of 20meV, have measured the elastic scattering from methane for collision energies of 0.2 to 5eV and angular range 15 to 138°. Absolute cross sections were obtained using the relative flow technique. Their data at 3, 3.5 and 5eV is compared to the present results in Figures 6.4,6.5. and 6.6. With the help of a phase shift analysis integrated cross sections were calculated. Total cross sections were estimated as the sum of these integral elastic cross sections and the vibrational cross sections (the latter being calculated using the Born approximation), reasonable agreement was found with the measurements of Ferch et al. It was noted that the integral elastic cross section differed from their calculated total cross section by 30% at 0.6eV, and they concluded that the contributions from the inelastic scattering are significant in this energy region and may even shift the minimum of the total cross section with respect to the integral cross section.

The most recent results to be reported are those of Tanaka et al (1988). Using hemispherical selectors, of energy resolution 30-40meV the elastic differential cross section of ethane over the energy range 2 to 100eV and angular range 15 to 130° has been measured. The measurements at the lower energies, 15 to 3eV, are shown in Figures 6.13-18. As for methane these results were put on an absolute scale using the relative flow technique, and have been used to normalise the present data. Integral and momentum transfer cross sections were obtained from the parametrised fits. Excellent agreement was found with the old total cross section measurements of Brüche (1930) and more recent data of Floeder et al (1985) and Sueoka and Mori (1985). An estimate of the momentum transfer cross section near 2eV obtained using the electron swarm parameters of Duncan and Walker gave a value approximately twice as large as the value obtained using the differential cross sections.

1.4 Review of Low Energy Electron Vibrational Excitation Measurements

Table 1.2 lists the work published on the low energy, vibrational excitation of the three gases methane, ethane and ethene.

In the early experiments, due to the poor monochromaticity of the electrons beams it was impossible to resolve the vibrational excitation processes. An energy resolution of better than 100meV is required for this. The importance of vibrational excitation at low incident energies has been demonstrated, however, by electron swarm experiments, when comparing the results of swarm experiments with theory, it has been found necessary to include inelastic cross section estimates with the elastic cross

Author	Target Gas	Vibrational Mode	†Type of Measurement	Type of Experiment	Energy Range	Angular Range
Barbarito et al (1979)	CH_4	ν_2	T	RAMSAUER	0.4eV	
Rohr (1980)	CH_4	$\nu_{2,4}, \nu_{1,3}$	D	CROSSED BEAM	0-4eV	20-120°
			D(E)		0-4eV	60°
Tanaka et al (1983)	CH_4	$\nu_{2,4}, \nu_{1,3}$	D	CROSSED BEAM	3-20eV	30-140°
Sohn et al (1983)	CH_4	$\nu_{2,4}, \nu_{1,3}$	D	CROSSED BEAM	0.3-1eV	30-105°
			D(E)		0.1-1.8eV	35°,75°,90°,105°
Curry et al (1985)	CH_4	$\nu_{2,4}, \nu_{1,3}$	D	CROSSED BEAM	7.5-20eV	30-140°
	C_2H_6	ν_b, ν_s				
Present work	CH_4	$\nu_{2,4}, \nu_{1,3}$	D	CROSSED BEAM	3-15eV	30-140°
	C_2H_4	ν_i, ν_j				
	C_2H_6	ν_b, ν_s				

† see key to Table 1.1

Table 1.2 Summary of the vibrational excitation measurements on methane, ethene, ethane.

sections to achieve reasonable agreement. Working with methane, Duncan and Walker (1972) demonstrated that to match experimental and calculated transport properties, it was necessary to include vibrational excitation cross sections for one or both of the infrared active modes ν_4 and ν_3 with a peak cross section of nearly $10^{-15}\ cm^2$. With ethane (1975), they included the infrared active mode ν_9, its cross section peaking at 0.18eV with a magnitude of approximately $2\times10^{-16}\ cm^2$.

Inelastic features were obtained in some of the more recent of the experiments already described in Section 1.3. Barbarito et al (1979), while measuring the total cross section of methane, detected a number of small regularly spaced peaks in the region of the Ramsauer Townsend minimum, these peaks were attributed to the electron induced excitation of the ν_2 normal mode of methane.

Rohr (1980), has investigated vibrational excitation of methane, from threshold to 4eV for the scattering angles 20 to 120°. The 40meV energy resolution of his apparatus, was insufficient to resolve the ν_1 and ν_3 modes or the ν_2 and ν_4 modes, however, it did reveal the dominance of the infra-red active modes ν_3 and ν_4 at small angles and low collisions energies, while the ν_1 and ν_2 Raman active modes appear to be stronger at the larger angles. From this Rohr concluded that in the low energy region excitation occurs essentially by the direct dipole process, via the dipole moment dependence on the internuclear separation. Rohr also measured the differential cross section for the $\nu_{1,3}$ and $\nu_{2,4}$ compo-

sites as a function of energy at the fixed scattering angle 60° and observed a sharp onset at the threshold (at approximately 0.3 and 0.15eV respectively) followed by a narrow threshold peak, for both cases. The influence of the threshold extends to approximately 1eV, after which the variation of the cross section with impact energy is small.

Tanaka et al (1983), using the same apparatus as Tanaka et al (1982), see Section 1.3, have measured the differential cross section excitation of the $\nu_{1,3}$ and $\nu_{2,4}$ composites for methane in the energy range 3 to 20eV for scattering angles 30 to 140°. These results are compared with the present data in Figures 7.8 and 7.9.

Sohn et al (1983) measured the vibrational differential cross sections of methane as a function of collision energy, over the range 0.1 to 1.8eV at scattering angles 35, 75, 90 and 105°. Although these measurements exhibit the same general features of those of Rohr, the half widths of the threshold peaks are 3 to 10 times larger, being approximately 300meV, and the ratio of the peak intensities to the cross section at 1eV are 5 to 10 times greater. Sohn et al also measured the differential cross section for the two composite peaks over the same angular range at energies 0.3, 0.6 and 1eV. The first two of these energies correspond to the maxima in the cross section due to the excitation of the $\nu_{2,4}$ and $\nu_{1,3}$ composites respectively. At 1eV, the angular distribution was observed to be isotropic. At the other two energies, a maximum at 70° and minima at 40° and 90° was observed.

The most recent measurements are those of Curry et al (1985) who determined the differential cross sections of the vibrational excitation of methane and ethane over the energy range 7.5 to 20eV. The results at 7.5 and 15eV are compared to the present data in Figures 7.8 and 7.9 for methane and 7.32 and 7.33 for ethane.

1.5 Review of the Theoretical Methods used in the Treatment of Low Energy Electron Molecular Scattering

The two major theoretical methods used for describing electron-molecular scattering are the BODY-frame fixed nuclei (FN) model with the adiabatic nuclei (AN) approximation and the LAB-frame close coupling (CC) calculations.

The FN model was first put forward by Sir Harrie Massey and his co-workers in the 1930s. He assumed that the molecular axes remain fixed during the collision process and then averaged the cross section over random orientations of these axes, with the internuclear distance fixed. Several early calculations used the Born approximation (Born 1926) within this model; a coordinate system attached to the nuclei, called the BODY-frame was employed and the resulting cross sections were then averaged

over all orientations of the nuclear axes in the space fixed laboratory frame, the so called LAB-frame. These early calculations were all concerned with the simplest molecules, hydrogen and nitrogen (Massey 1930, Massey and Mohr 1932a, Bullard and Massey 1931), and produced results which were in good agreement with the experimental data for elastic differential cross sections at high incident energies, ie 100eV.

At lower energies, however, the agreement with experiment was not so good. Massey and Mohr (1931, 1932b, 1934) identified three main fundamental physical effects, not included in the Born approximation, but which were necessary to explain the scattering process at the lower energies, ie 'distortion', 'exchange' and 'polarisation'. The first of these effects is due to the distortion of the incoming electron wave, from the asymptotic plane wave form assumed in the Born approximation, by the electrostatic field of the target molecule. The exchange effect refers to the fact that the incident and target electrons are indistinguishable during the collision process and so require the total wave function to be anti-symmetric with respect to the interchange of the co-ordinates of the incident electron with those of the target. The third physical effect is a 'backcoupling' effect. The incident electron distorts the electron charge distribution of the target molecule and the effect of the subsequent polarisation of the molecule must therefore be taken into account. However although these effects were identified in the 1930s, they could not be included fully in the calculations until more recent years due to the powerful computers required.

Massey (1930) realised that cross sections for rotational and vibrational excitation can be obtained from a generalisation of the FN model, by allowing for nuclear motion. This is known as the adiabatic nuclei (AN) approximation. This model proceeds in two stages. The scattering problem is initially solved in the BODY-frame and the scattering amplitude calculated at fixed nuclear orientations and separations by solving the Schrödinger equation. In the second stage the transformation to the LAB-frame is made and the nuclear rotation and vibration wave functions are introduced. Altshuler (1957) found that this approximation holds if the period of the target motion, rotational and vibrational, is much greater than the time for the electron to cross the region of the interaction, ie the collision time and also if the number of excited states of the target that contribute significantly to the wavefunction is limited. The AN approximation therefore is not suitable for collisions close to threshold, at the energy of a resonance or for polar molecules at small scattering angles.

An alternative approach was considered by Massey (1932). In his work on electron-polar molecule scattering, he introduced the rotation of the molecule explicitly into the treatment viewed from a laboratory fixed coordinate system (LAB-frame). By expanding the complete scattering function in terms of the quantum mechanical eigenstates of the rotor, he obtained a coupled system of partial differential equations for the coefficient functions of the expansion (also called channel functions) which depend on the coordinates of the scattered electron. By observing that there is no first order

distortion for the incident electron wave in the case of a dipole field, he concluded that the rotational excitation of weakly polar molecules can be treated at all energies in the Born approximation. This approach was elaborated upon by Gerjuoy and Stein (1955a,b) and Arthurs and Dalgarno (1960) and is known as the rotational close-coupling (CC) approach in which individual equations, representing rotational channels are connected by various coupling terms. In practice only a finite number of equations are retained and this is then called the rotational CC-approximation. In the weak coupling limit, the CC equations decouple and the distorted wave approximation (DWA) is obtained. This representation has since been refined to include the effects of exchange, polarisation, vibrational and electronic excitation.

It has been observed when analysing the results of the LAB frame CC calculations and the AN approximation for e - H_2 scattering, that if the static exchange potential is included in both treatments they give practically identical results. Fano (1970) analysed the two methods and concluded that when the electron is far away from the molecule the LAB frame is advantageous, whereas when the electron is inside or very close to the molecule the BODY frame method should be used. He proposed that the two wave functions obtained should be connected at a convenient intermediate electron-molecule distance. In some cases the connecting point may lie at infinity, in which no LAB-frame CC equations need be solved.

To date the majority of calculations on electron scattering by diatomic molecules have utilised the AN approximation and major efforts have been made in the last ten years to solve specific problems as accurately as possible. Much work has gone into developing equivalent local potentials that describe the exchange effects accurately. The inclusion of polarisation is even more difficult, the majority of calculations at both low and intermediate energies have used semi-empirical polarisation potentials with adjustable parameters. Generally the vibrational degrees of freedom of the molecule have been ignored. Choi and Poe (1977a,b), however, reported an extensive analysis of the CC equations in the rotating frame where vibrational coupling was included but rotation treated adiabatically. Vibrational coupling is needed to explain resonances, where the AN approximation does not hold.

1.6 Review of the Theoretical Treatment of Electron Methane Scattering

The theoretical treatment of electron methane scattering is summarised in Table 1.3.

The first calculations of the cross sections of methane which successfully reproduced the overall experimental features of the total cross section curve for electron scattering off methane, were performed by Gianturco and Thompson (1976). over the energy range 0 to 13.6eV. The calculations were performed within the 'fixed nuclei' approximation and required the solution of

Author	Method Used	†Type of Calculation	Energy Range	Angular Range
Gianturco and Thompson (1976)	FN + parameterized polarisation potential	T	0-13.6eV	
(1980)		T,M	0-1.4eV	
		D	9.5eV	40-140°
Jain and Thompson (1982)	FN + parameter free polarisation & local exchange potentials	T	0-15eV	
		D	3,5eV	0-180°
Abusalbi et al (1983)	LAB frame CC + energy dependent local exchange potential + 2 forms of the polarisation potential	I,M	10eV	
		D	10eV	0-180°
Lima et al (1985)	FN + static exchange potential	I	3-20eV	
		D	3-20eV	0-180°

† see key to Table 1.1

Table 1.3 Summary of the theoretical treatment of electron methane scattering.

$$[\nabla^2 + k^2 + V_0(\mathbf{r}) + V_p(r)]\, F^{p\mu}(\mathbf{r}) = \sum_i \lambda_i \varphi_i^{p\mu}(\mathbf{r}) \tag{1.1}$$

for the scattered electron wave function $F^{p\mu}$, where ∇^2 is the Laplacian operator, k is the wavenumber of the incident electron, $V_0(\mathbf{r})$ is the static potential of the molecule, $V_p(r)$ is the polarisation potential, λ_i are Lagrange multipliers and $\varphi^{p\mu}(\mathbf{r})$ are the bound orbitals of the target.

$F^{p\mu}(\mathbf{r})$ transforms, under rotations, according to the μ^{th} component of the p irreducible representation (IR) of the molecular point group, T_d for methane, and can be expanded in terms of symmetry functions $X_{Lh}^{p\mu}(\hat{\mathbf{r}})$ of this point group. The point group notation is used to describe the symmetry elements that a molecule possesses (Cotton 1971). The group T_d describes tetrahedral molecules which exhibit 3 two-fold rotation axes, 4 three-fold rotation axes and 6 mirror planes. Therefore

$$F^{p\mu}(\mathbf{r}) = \sum_{Lh} f_{Lh}^{p\mu}(r)\, r^{-1} X_{Lh}^{p\mu}(\hat{\mathbf{r}}), \tag{1.2}$$

where $X_{Lh}^{p\mu}(\hat{\mathbf{r}})$ are linear combinations of the spherical harmonics $Y_L^M(\hat{\mathbf{r}})$ and have been discussed and tabulated by Altmann and coworkers (Altmann and Cracknell 1965).

$V_0(\mathbf{r})$, the full static potential from the ground state (closed shell) configuration of methane ($1a_1^2$, $2a_1^2$, $1t_{2x}^2$, $1t_{2y}^2$, $1t_{2z}^2$) transforms according to the A_1 IR and can be expanded as

$$V_0(\mathbf{r}) = \sum_{Lh} v_{Lh}(r)\, X_{Lh}^{A_1}(\hat{\mathbf{r}}) \tag{1.3}$$

where the $v_{Lh}(r)$ parameters are calculated using single centre SCF near Hartree - Fock functions.

A polarisation potential $V_p(r)$ of the form

$$V_p(r) = \frac{\alpha}{r^4}\left[1 - \exp\left(-\frac{r}{r_0}\right)\right]^6 \tag{1.4}$$

was used where α is the static molecular polarisability (17.5 a.u. for methane) and r_0 is the 'cut off' parameter which governs the short range behaviour of $V_p(r)$. A value of $0.84a_0$ was chosen by Gianturco and Thompson for r_0 by fitting the calculated cross sections to experimental data (Brode 1925, Brüche 1930 and Ramsauer and Kollath 1930). Exchange effects in the scattering were included in an approximate manner by employing the Lagrange multipliers (λ_i) which allowed solutions of $F^{PK}(\mathbf{r})$ to be obtained which were orthogonal to the occupied bound orbitals, $\varphi_i^{PK}(\mathbf{r})$ of the same symmetry.

Gianturco and Thompson reduced Equation 1.1 to a set of coupled radial equations for the $f_{Lh}^{PK}(r)$ and retained five terms in the expansions of Equations 1.2 and 1.3. Methane has five possible scattering states, A_1, A_2, T_1, T_2 and E, these being the characters of the IR's of the symmetry elements of the molecular point group T_d. For a detailed discussion of the application of group theory to molecular structure see Cotton (1971). The total cross sections reported contain contributions from three of these states A_1, T_2 and E. The A_1 wave function contains elements with L = 0,3,4,6 and 7 but the results indicate a dominance of the s-wave. The partial waves for the T_2 wave function are L = 1, 2, 3, 4 and 5 and it exhibits a shape resonance, at approximately 7eV with strong L = 2 behaviour. At energies below 3eV the L = 1 partial wave is dominant. The E contribution is also mainly L = 2 but there is no resonance behaviour. The total cross section is shown in Figure 1.1.

This work was extended (Gianturco and Thompson 1980) following essentially the same approach, but now including momentum transfer and differential cross sections as well as the total cross sections for other values of the polarisation 'cut off'. These results contain contributions from the states A_1, T_1, T_2 and E; A_2 was not included as its leading term in the wavefunction single-centre expansion has L=6.

The total and momentum transfer cross sections were calculated in the region of the Ramsauer Townsend minimum for two values of r_0, 0.84 and 0.88, it was found that the results for $r_0 = 0.88a_0$ gave the best agreement between experiment and theory. The differential cross section was calculated for an incident electron energy of 9.5eV and $r_0 = 0.84, 0.88$ and $0.92a_0$. The results for $r_0 = 0.88a_0$ again show the best agreement with theory and are shown in Figure 1.4.

Jain and Thompson (1982) attempted to improve the agreement by introducing two important modifications to Equation 1.1. These were a parameter-free polarisation potential, $V_p'(\mathbf{r})$, given by

$$\lim_{r \to \infty} V_p'(\mathbf{r}) = -\frac{1}{2r^4}(\alpha_{11}\sin^2\theta\cos^2\varphi + \alpha_{22}\sin^2\theta\sin^2\varphi + \alpha_{33}\cos^2\theta), \tag{1.5}$$

where φ and θ are the polar and azimuthal angles respectively of the electric field induced by the incident electron and α_{ii} are the diagonal elements of the polarisability tensor. For methane, taking the z-axis along the main symmetry axis of the molecule $\alpha_{11} = \alpha_{22} = \alpha_{33}$. To obtain a potential for all r, it was assumed that the perturbation of the molecule due to the incident electron is zero if $r < r_i$, r_i being the molecular electron coordinate (Temkin 1957). This parameter free polarisation potential V_p' is substantially weaker than the empirical potential V_p used by Gianturco and Thompson (1976, 1980), V_{pmax}' is approximately $0.13V_{pmax}$.

The second modification was the introduction of a local exchange potential, $V_e(\mathbf{r})$, calculated in the Hara free-electron-gas model (HFEGE) to provide a stronger representation of exchange.

The details of the calculation are exactly as for Gianturco and Thompson (1980). Total cross sections were calculated (see Figure 1.1) and compared to the measurements of Barbarito et al (1979). The Ramsauer minimum was found to agree both in magnitude and position, however,in the region of the maximum, at approximately 7eV, the calculated cross section is larger than that reported by Barbarito et al. The differential cross sections, calculated at incident electron energies of 3 and 5eV are in good agreement with the results of Tanaka et al. They concluded that the modification of the polarisation potential and the inclusion of the local exchange potential give a more accurate representation of low energy electron-methane than that achieved in the earlier work of Gianturco and Thompson (1976, 1980). The Ramsauer minimum as determined by Barbarito et al provided an essential part in the comparison of Jain and Thompson's theory with experiment, however, as the more recent measurements (for example those of Ferch et al 1985) do not agree with the data of Barbarito et al, the parameter free polarisation of Jain and Thompson should perhaps be re-evaluated.

Abusalbi et al (1983) have performed LAB-frame CC calculations and reported rotationally summed cross sections at 10eV electron impact energy. The high degree of symmetry of the methane molecule

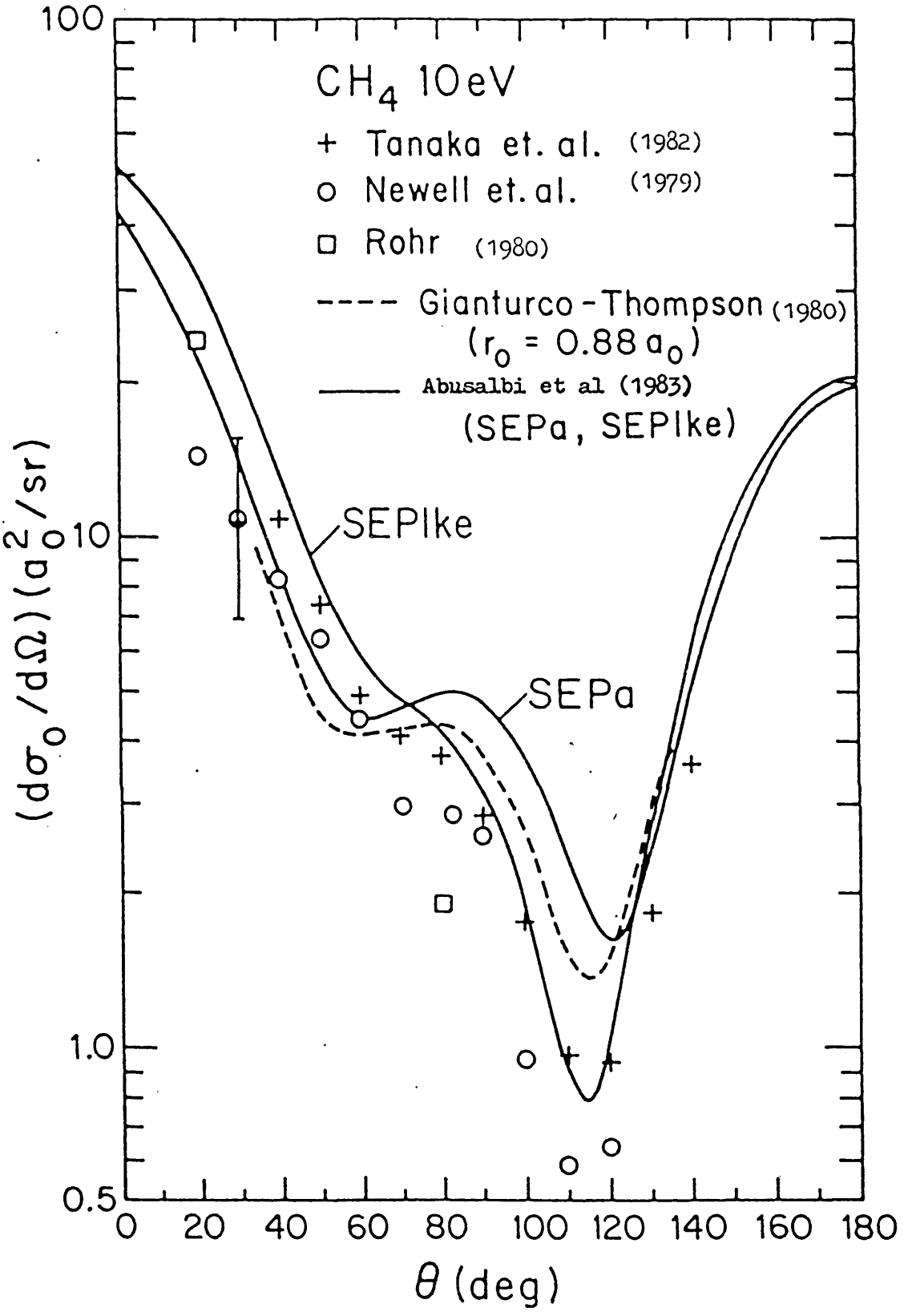

Figure 1.4 Differential cross section results for e^- - CH_4 elastic scattering at 10eV (9.5eV in the case of Gianturco and Thompson). The labels SEPa and SEPIke on the calculations of Abusalbi et al are explained in Section 1.6.

simplified the calculation in that the number of coupled states which had to be considered was significantly reduced. The interaction potential used included the static potential of the molecule, $V_s(\mathbf{r})$, an energy-dependent local exchange potential, $V_e(\mathbf{r}, E)$ and two forms of the polarisation potential.

The energy-dependent local exchange potential was calculated from the semi-classical exchange approximation (Riley and Truhlar 1975). The form of this potential was

$$V_e(\mathbf{r}, E) = \frac{[E - V_s(\mathbf{r})] - \sqrt{[E - V_s(\mathbf{r})]^2 + 4\pi\rho(\mathbf{r})}}{2}, \tag{1.6}$$

where E is the incident electron energy.

The first form of the polarisation potential was an adiabatic potential, $V_{pa}(\mathbf{r})$ (Riley and Truhlar 1975), the second a polarisation potential based on the local kinetic energy semi-classical polarisation model (Valone et al 1982) given by

$$V_{plke}(\mathbf{r},E) = \frac{V_{pa}(\mathbf{r})}{1 + [E - V_{se}(\mathbf{r},E)] \left(\frac{\alpha}{N_{val}}\right)^{1/2}}, \tag{1.7}$$

where $V_{se}(\mathbf{r},E)$ is the static + exchange potential, N_{val} is the number of electrons in the outer shell of the molecule and α is the static molecular polarisability. The adiabatic model overestimates the polarisation effect, even at low impact energies, because the scattered electron is speeded up by the field of the target and the target polarisation does not have enough time to respond fully to the scattered charge. The introduction of V_{plke} was an attempt to account for this effect, and was therefore expected to produce better results than those obtained using V_{pa} alone. The results for both polarisation potentials are shown in Figure 1.4.

The integral and momentum transfer cross sections were calculated at 10eV and compared with the integral and momentum cross sections of Tanaka et al (1982) and the total cross section measurement of Barbarito et al (1979) at the same energy. The calculated cross sections were found to be approximately 30% higher than these earlier measurements, which agrees well with the later measurements of Ferch et al (1985b), Jones (1985) etc. The differential cross section results at 10eV are also in good agreement with the experimental results at the same energy (Newell et al 1979, Tanaka et al 1982). In all cases the results using the non-adiabatic terms in the polarisation potential gave the best agreement.

Lima et al (1985) included the exchange terms in the exact solution of the methane scattering problem, rather than using a local exchange potential. To achieve this a multichannel extension of the Schwinger variational principle (SMC) was used, in which the trial scattering functions are expanded in an L^2 basis. Details of this method are given by Takasuka and McKoy (1981,1984). This allowed them to calculate an analytical approximation to the body-frame fixed-nuclei scattering amplitude for molecules of arbitrary geometry. The fixed nuclei scattering amplitude was then expanded in a partial wave series and the transformation to the laboratory frame made. They calculated the differential and integral cross sections for elastic collisions in methane for 3-20eV electrons. The calculations in the body frame included contributions from the $^2A_1$, $^2T_2$ and ^2E symmetries. All values of $L \leq 5$ were included in the partial wave expansion of the scattering amplitude.

Their results at 3, 5, 7.5 and 15eV are shown in Figure 1.5 together with the experimental data of Tanaka et al 1982. The calculated differential cross section in this range of energies are characterised by forward peaking, a minimum around 120° and a backwards peak. The minimum is rather sharp at low energies and becomes broader with increasing energy. The experimental data of Tanaka et al displays a secondary minimum, occurring near 45° at 3eV. As the incident energy increases to 7.5eV this minimum moves towards 60° and becomes a much less pronounced shoulderlike structure. The calculated static-exchange cross sections reproduce both the forward and backward peaks as well as the primary minimum near 120°. At low energies the calculated forward peak is much more pronounced than experiment and the secondary minimum is also missing, suggesting that this feature is most probably due to polarisation effects. This is supported by the data of Gianturco et al (1980), who found that when they increased their cut-off parameter from 0.84 to 0.92, making the inner region of the potential look more like the static-plus-exchange potential, the shoulder at low energy became less pronounced.

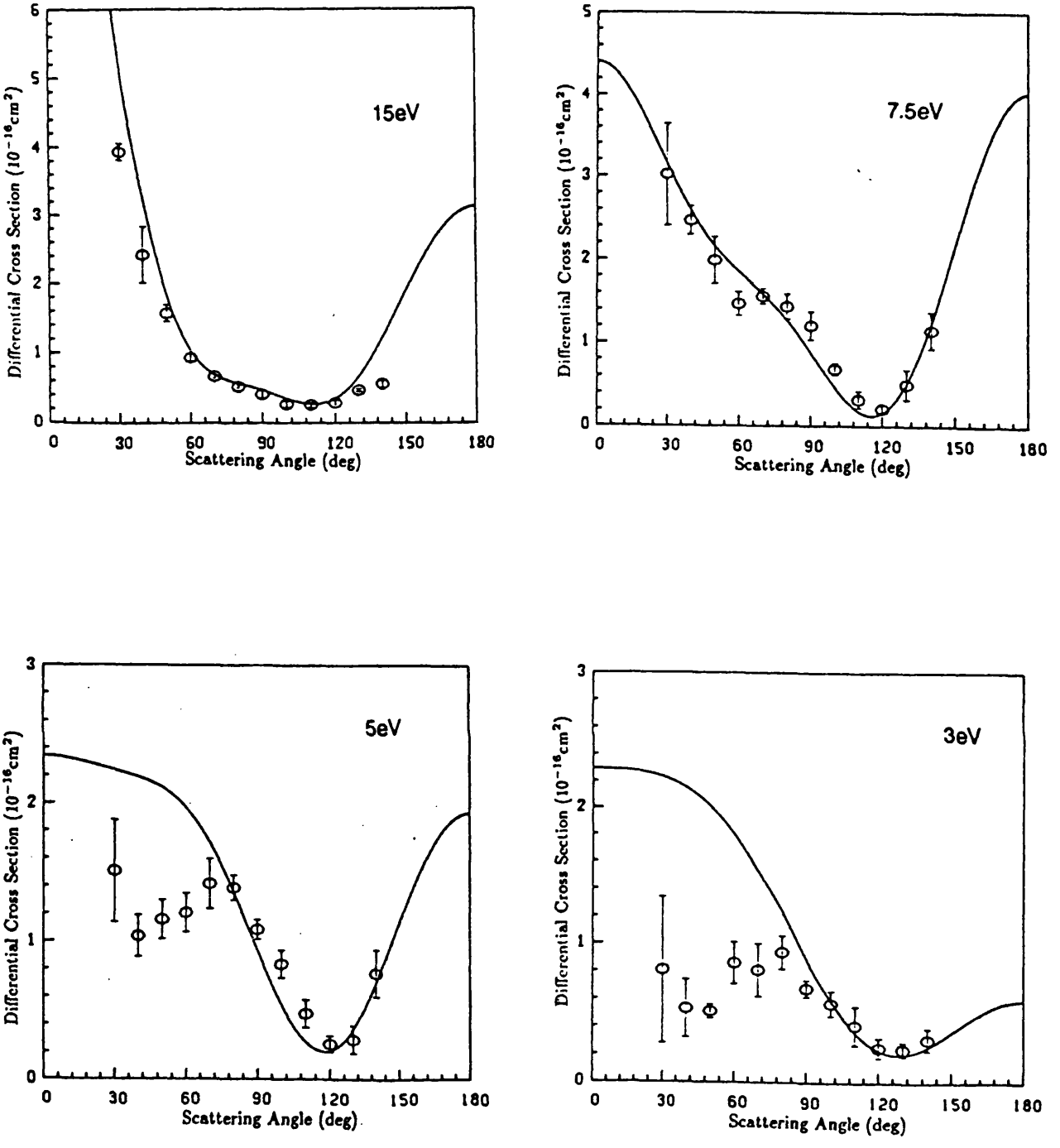

Figure 1.5 Differential cross sections for e^- - CH_4 at 15, 7.5, 5 and 3eV: —— theoretical results of Lima et al 1985; o experimental results of Tanaka et al 1982.

Chapter 2 - The Experimental Apparatus

2.1 Introduction

In the following two sections of this chapter the experimental chamber and vacuum system are described. The electron optics were shielded from the Earth's magnetic field and details of this are given in Section 2.4. The apparatus used to support the electron spectrometer and allow for the rotation of the analyser is described in Sections 2.5 and 2.6. The last section covers the gas beam source and the method used to admit gases into the chamber.

2.2 The Experimental Chamber

The experimental chamber was constructed entirely from stainless steel (type EN58B). It was manufactured in three parts, a 35mm thick base plate of 835mm diameter, a cylinder of 155mm height by 760mm diameter carrying 30mm thick flanges top and bottom, and finally a domed cover which carried a 30mm thick flange that could be bolted onto the upper flange of the cylinder (see Figure 2.1).

The base plate was mounted off the floor on four 'T' section aluminium legs. Ports were cut into the base plate, allowing the vacuum system to be suspended below the experimental chamber. The lower flange of the cylinder was bolted onto the base plate, and a vacuum seal made by compressing a 0.030 inch diameter gold wire gasket seal.

The cylinder has six side ports, 190mm in diameter. The flange of the dome was bolted onto the upper flange of the cylinder. This seal and all side port seals were made using 0.060 inch diameter indium wire.

2.3 The Vacuum System

Two pump stacks were used to evacuate the chamber. These were attached to the ports in the base plate, see Figure 2.1. Both stacks were built round oil (Convelex 10) diffusion pumps, Edwards E04 and E06. The stack with the E04 diffusion pump was attached to the base plate via a 90° elbow on a small buffer tank. This buffer tank acted as an adaptor since there was no suitably sized port in the base plate to enable the E04 stack to be attached directly.

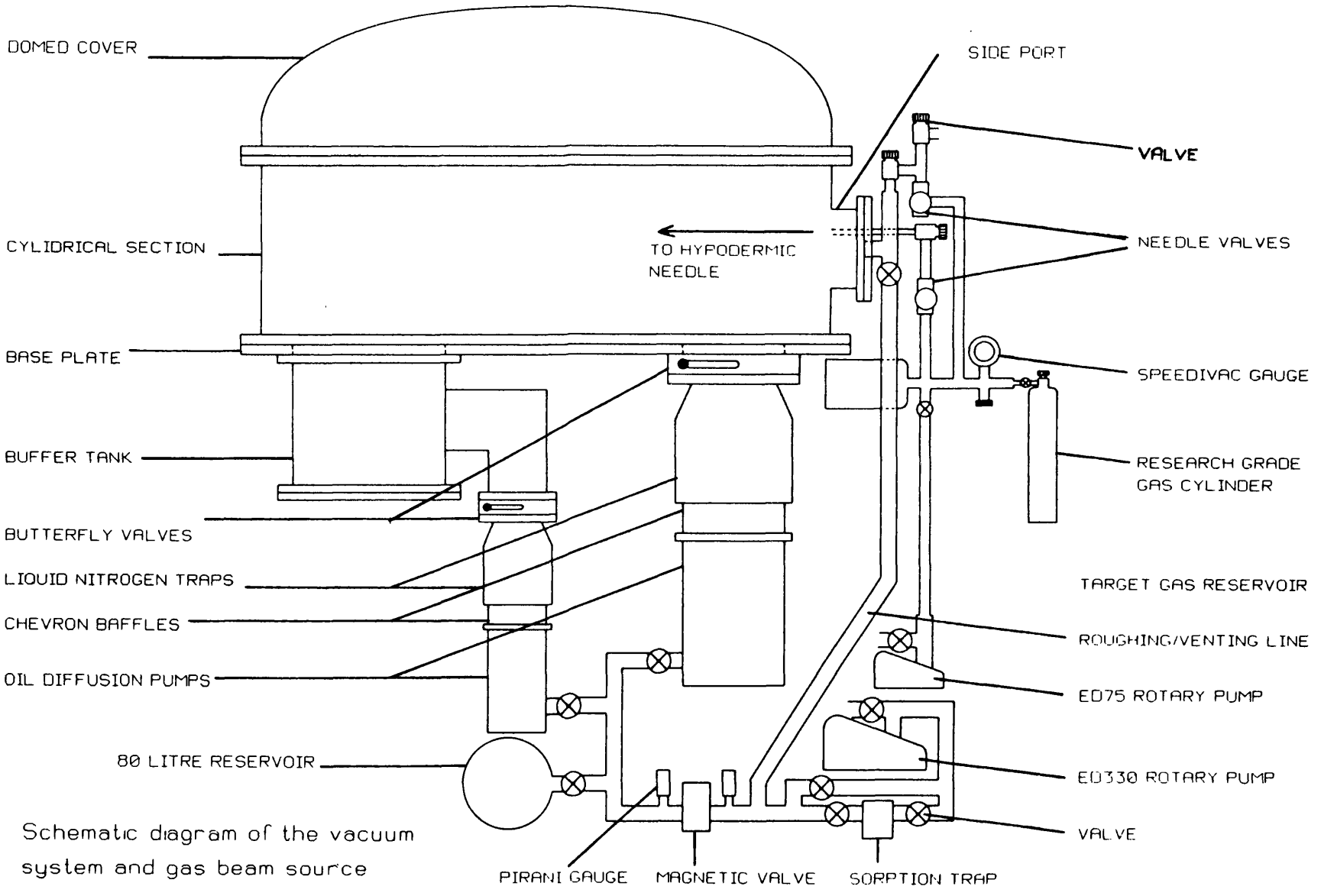

Figure 2.1 Schematic diagram of the vacuum system and gas beam source

The stacks could be isolated from the chamber by quarter swing butterfly valves, allowing the chamber to be let up to atmospheric pressure, via the valve in the roughing line, while the pumps were still active.

Liquid nitrogen traps and Peltier cooled chevron baffles were employed between the butterfly valves and the diffusion pumps. These ensured the condensation of any oil vapour leaving the diffusion pumps, and prevented contamination of the vacuum chamber. As the chamber was kept under vacuum for weeks at a time, the traps were filled automatically using a liquid nitrogen level controller (Oxford Instruments). Two probes were placed in each trap, at the required high and low liquid nitrogen levels.

Both diffusion pumps were backed by an Edwards ED330 rotary pump operating via a magnetic valve and a sorption trap. The rotary pump provided a backing pressure of around 0.01 torr, with the target gas present in the tank. The pressure in the backing line was measured by two Pirani gauges, one on either side of the magnetic valve. The sorption trap contained activated alumina which prevented rotary pump oil contaminating the high vacuum region.

A large reservoir volume of 80 litres was incorporated in the backing line so that the diffusion pumps could operate for a limited period of time with the magnetic valve closed. This volume increased the time taken for the pressure in the backing line (as monitored by the Pirani gauge on the high vacuum side of the magnetic valve), to reach the critical backing pressure of around 0.1 torr, when not being pumped by the rotary pump.

The vacuum chamber was roughed out by the roughing/venting pipeline connecting it to the rotary pump. This could be done with the diffusion pumps active by closing the magnetic valve, the exhaust from the diffusion pumps being contained in the 80 litre reservoir. Once the pressure in the tank had fallen to around 0.01 torr, as measured by the Pirani gauge (on the low vacuum side of the magnetic valve) the roughing line would be closed off, and both the magnetic valve to the diffusion pumps and butterfly valves to the chamber, opened. When roughing out the chamber the sorption trap was initially by-passed, to prevent it becoming contaminated with water vapour. As soon as the pressure in the chamber had fallen to around 0.1 torr, this trap was used again.

To vent the vacuum chamber, the butterfly valves were closed. An argon cylinder was then connected to the valve at the top of the roughing/venting line and the chamber brought up slowly to atmospheric pressure with the inert gas. The valve to the rotary pump was left closed.

The pressure in the vacuum chamber was measured using an ionisation gauge (Edwards, type IG3) mounted in one of the side flanges of the chamber. The vacuum chamber was normally pumped down to a pressure of 1×10^{-8} torr. To maintain this vacuum all surfaces in the chamber were initially cleaned

by washing with acetone (see Section 3.6) and the chamber was regularly baked overnight by four 150W, 24V halogen projector bulbs.

The experiment was protected by a series of electrical trips. If the mains or water supply failed, the whole experiment switched off. This would also happen if the backing line pressure exceeded 0.1 torr. In both cases the magnetic valve would close, protecting the diffusion pumps from contamination from any rotary pump oil which might be sucked back into the high vacuum region. If the pressure in the vacuum chamber exceeded one and a half times the full scale deflection of the ionisation gauge, the spectrometer supplies, ionisation gauge and high voltage supplies were switched off.

2.4 The Magnetic Shielding

It was necessary to minimise the deflection of the electron beam by stray electric and magnetic fields. To reduce the stray electric fields all electrical connections to the spectrometer were screened with braided cable, and the chamber earthed. To protect the spectrometer from the earths magnetic field and any nearby magnetic bodies, a double mumetal shield was used (Telcon Metals Ltd), both shields of thickness 1.6mm. To activate the mumetal, it was heated to 1000°C. Only non magnetic materials were used within the shield. To remove any residual magnetism all stainless steel nuts, bolts and studding were heated using an oxy-acetylene flame until red hot, then allowed to cool within a mumetal shield. This procedure was adopted after discovering that one of the stainless steel nuts in the monochromator had become sufficiently magnetic to prevent tuning of the beam in the pre-interaction region lens stack.

The outer shield took the form of a can with a removable lid. This fitted closely inside the cylindrical part of the chamber, resting on the baseplate (see Figure 2.2). Holes were made at the pump and side ports, their diameters were kept to a minimum to reduce the loss in shielding, in their vicinity. The inner shields consisted of two boxes that fitted around the two halves of the spectrometer (the monochromator and the analyser) and can be seen in Plate 2.1. Both shields were heat treated by baking to 1000°C. Within the shields the magnetic field was reduced to around 2 milligauss, while within the interaction region cylinder (Section 2.6), protected by only the outer shield, the field was reduced to around 5 milligauss.

2.5 The Spectrometer Support Table

As the base of the outer mumetal shield could not be used to support the spectrometer, a large circular aluminium plate (of diameter 620mm) was manufactured for this purpose, of flatness ± 0.02mm over its diameter. The plate was bolted to the base plate by eight aluminium pillars, see Figure 2.2.

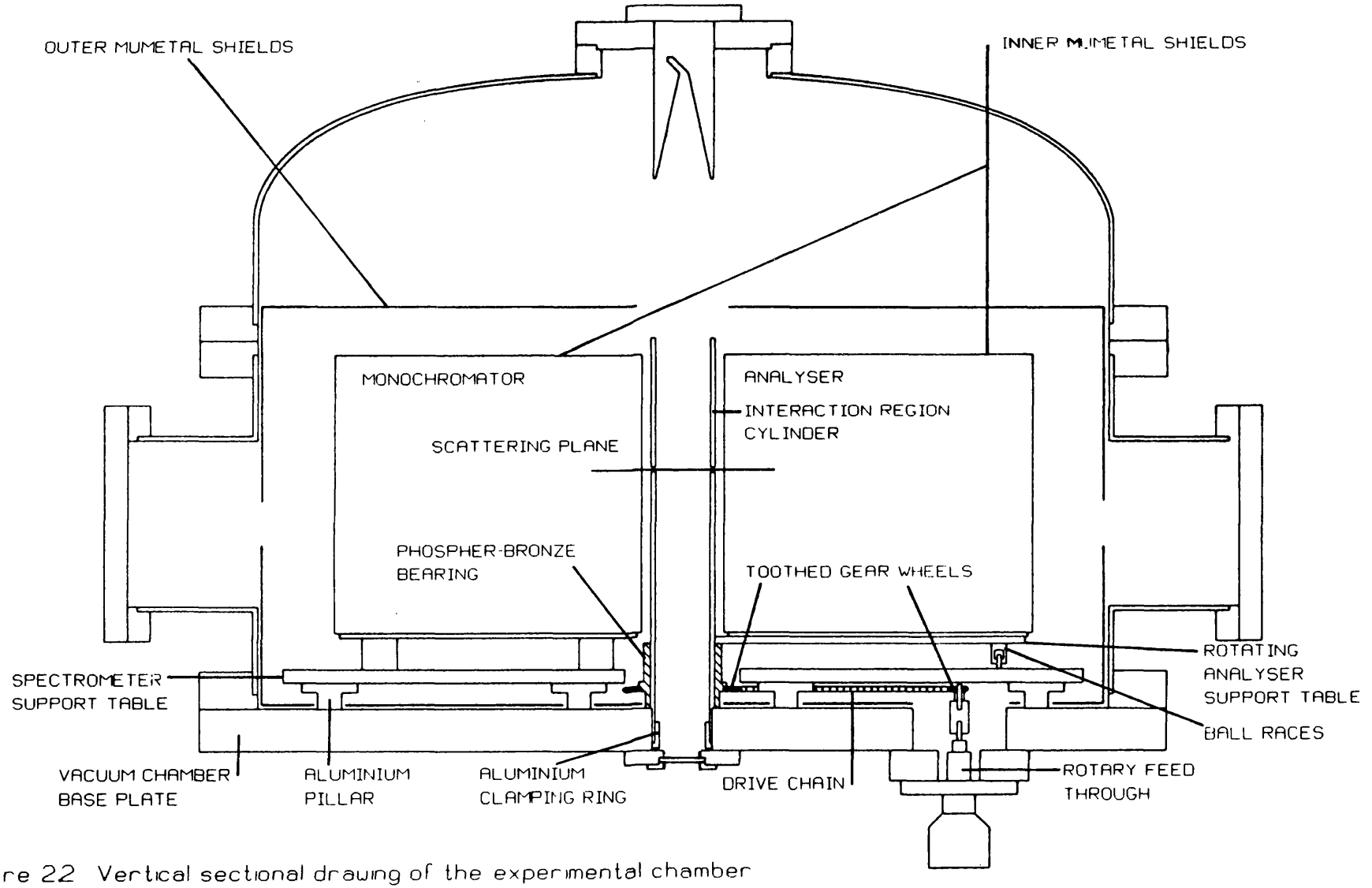

Figure 22 Vertical sectional drawing of the experimental chamber

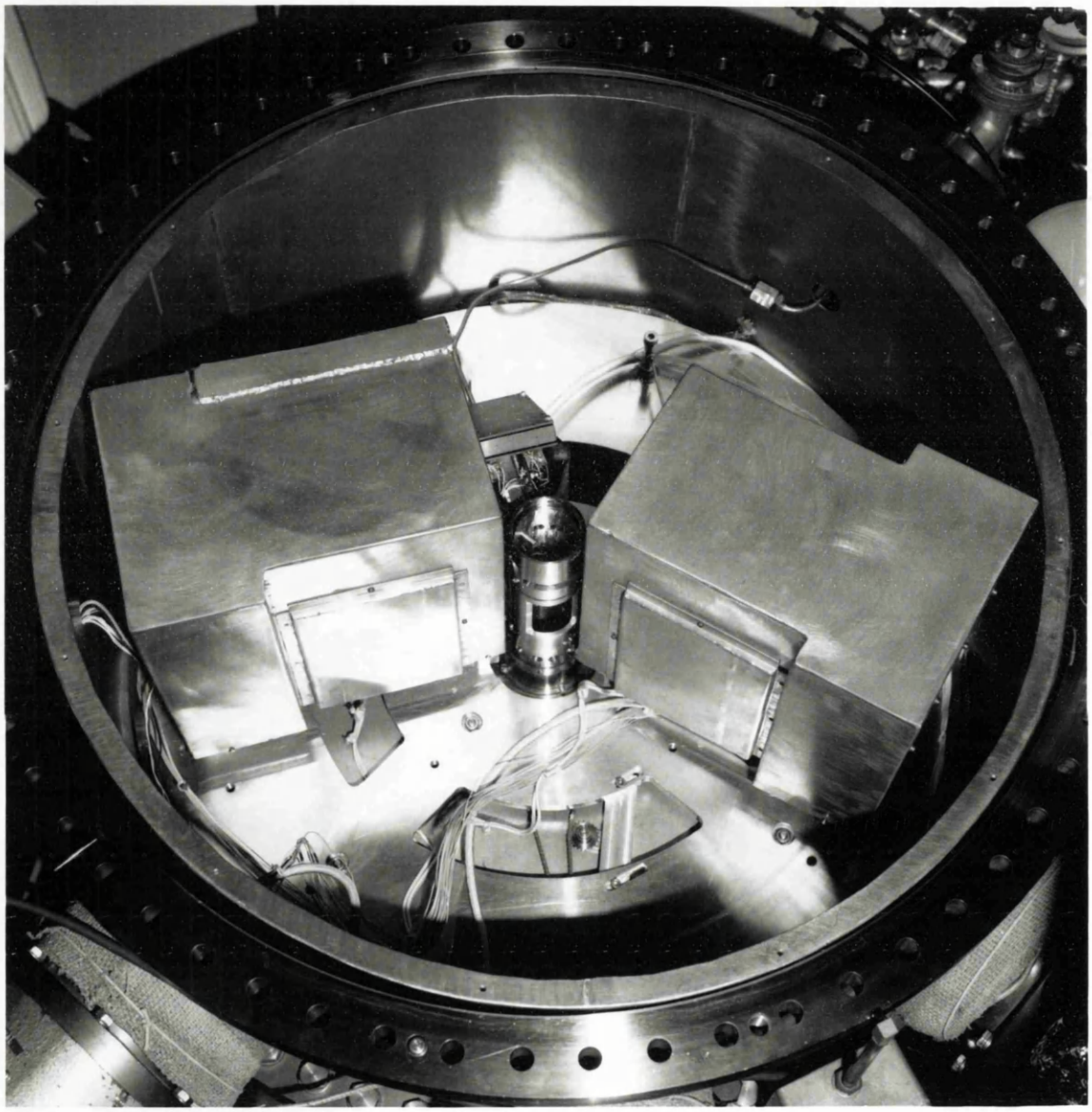

Plate 2.1. Top view of the electron spectrometer showing the monochromator (left) and analyser (right, at a scattering angle of 40°) enclosed within their mumetal boxes, the outer mumetal shield lines the experimental tank. The interaction region cylinder can be seen between the monochromator and analyser and the hypodermic needle is visible within this cylinder.

Where possible parts of the support table were cut away to facilitate pumping. A 95mm diameter hole in the centre allowed the interaction region cylinder to be mounted directly onto the chamber base plate.

2.6 The Interaction Region Cylinder and Spectrometer Rotation Mechanism

The interaction region was defined by a 330mm long stainless steel cylinder with an outside diameter of 55.8mm and a wall thickness of 4.3mm and can be seen in Plate 2.1. One end of the cylinder fitted into the central port of the chamber baseplate, and was held firmly in position by an aluminium clamping ring. Beside defining the collision region (see Section 3.5), it also provided the location for the phosphor-bronze bearing of the analyser rotating table and the hypodermic needle gas source.

The rotating support table which supported the analyser was bolted to the phosphor-bronze bearing. This was located by and rotated about the interaction region cylinder. As well as being supported by the bearing, the rotating platform incorporated a pair of ball races which were radial with respect to the interaction region cylinder axis and 268mm from it. These maintained the height of the platform and provided regular, smooth motion of the analyser over the spectrometer support table.

To enable the rotation of the analyser, a gear wheel was bolted to the base of the phosphor-bronze bearing, this was connected via a drive chain to a second gear wheel mounted on the axis of a Vacuum Generator rotary feedthrough. A third gear wheel was mounted beneath the spectrometer support table, in the plane of the drive chain, its position could be adjusted to set the required tension in the chain. The gearing ratio of the system was 8:1 and all components were made from stainless steel.

The drive mechanism produced accurate and reproducible external rotation of the analyser over the angular range -5 to 140°. A spring, attached to a aluminium support which was bolted to the spectrometer support plate (at -5°), allowed the analyser to be set to zero angle externally. The spring was electrically isolated from its support, and wired up to a feedthrough pin (also electrically isolated) in one of the side flanges of the chamber. It was positioned so that when the analyser was at zero angle, its mumetal shield would just make contact with it. This could be observed externally by measuring the resistance between the feedthrough pin and earth.

2.7 The Gas Beam Source

The gas beam was produced by a hypodermic needle, 10mm long and with an internal diameter of 0.3mm. The needle was made from demagnetised, stainless steel and soldered onto a flanged stainless steel tube. This tube located into a 6mm hole in the interaction region cylinder (see Figure 3.4),

positioning the needle in the scattering plane. A 1/4 inch copper tube connected the hypodermic needle to the external target gas supply line (see Figure 2.1).

Before letting the target gas into the experimental chamber, the supply line was evacuated using an Edwards ED75 rotary pump. The pressure in this line was measured with a 0-760 torr Speedivac gauge. Once evacuated, the pump was shut off, and the target gas cylinder opened. The supply line and gas reservoir were filled with gas up to atmospheric pressure. This was then pumped away, flushing out any impurities in the supply line. This procedure was repeated a few times before finally filling with the target gas. The needle valve to the experimental chamber was then opened slowly, allowing the gas to flow to the hypodermic needle. The needle valve was adjusted until the required gas background level had been obtained as measured by the ionisation gauge.

About 2/3 of the wall area of the interaction region was cut away, to maximise the pumping speed at the hypodermic needle source. This was to prevent the build up of gas in the cylinder, which would degrade the crossed beam geometry of the collision region by producing an enhanced 'cell' contribution to the scattering leading to the violation of the single collision condition (see Section 5.3).

The target gas could also be let directly into the chamber, from the supply line, via a 1 inch diameter pipe welded into a side flange. This gas flow was controlled by a second needle valve and provided a means of measuring the number of electrons scattered from the background gas, without the gas beam being present. The purpose of this measurement is described in Section 5.3.

All experiments were performed using research grade gas, of better than 99.9% purity. It was found that a single fill of the gas reservoir was sufficient to provide a stable gas beam for periods in excess of eight hours.

Chapter 3 - The Electron Spectrometer

3.1 Introduction

The spectrometer was designed to enable the measurement of elastic differential and vibrational excitation cross sections for various polyatomic molecules. The measurements were required over the incident electron energy range of 3 to 20eV and for scattering angles of 30° to 140°. To observe the vibrational excitation it was necessary to detect the electrons scattered from the molecular beam with energy losses in the range 0 to 0.5eV and to reduce the data collection time currents of a few nA were required in the collision region. A good angular resolution ($< 2°$) and energy resolution (of around 50 to 60meV) were considered desirable.

3.2 Design Principles

Several papers have been published which outline the design methods required to build a high resolution electron spectrometer, for example Simpson 1964, Read et al 1974, Brunt et al 1977. Principles described in these papers have been used in the present design. The definitions of the electron optical terms and the equations used in the design are given in Appendix A.

From Figure 3.1 it can be seen that a set of three lenses was used in each of the gun, pre and post-interaction region lens stacks, this allowed the window and the pupil to be focused separately. In each stack the first lens was an accelerating/decelerating lens, operating at a fixed voltage ratio, which focused the window onto the first principal plane of the following einzel lens. The einzel lens imaged the window onto its second principal plane, leaving its energy unchanged. The third lens, a zoom lens, then took the window and focused it at a fixed image distance over a range of energies. The voltage on the central element of the einzel lens was adjusted so that it focused the pupil onto the first focal plane of the zoom lens, its image then being sent to infinity by the zoom lens, resulting in a zero exit beam angle.The beam angle was set to zero on entering both the monochromator and analyser to aid the energy resolution (see Equation 3.7) and also at the interaction region to help obtain a good angular resolution (Brunt et al 1977).

Two real apertures were used in each lens stack of the spectrometer to redefine the size and position of both the window and the pupil (if necessary) and to aid the tuning of the spectrometer. The aperture sizes were such that they were always just greater than the calculated diameter of the electron beam at that point. They were positioned in the relatively high energy lenses to reduce space charge effects and at least one lens diameter away from the end of the lens in order to reduce the effect of spherical

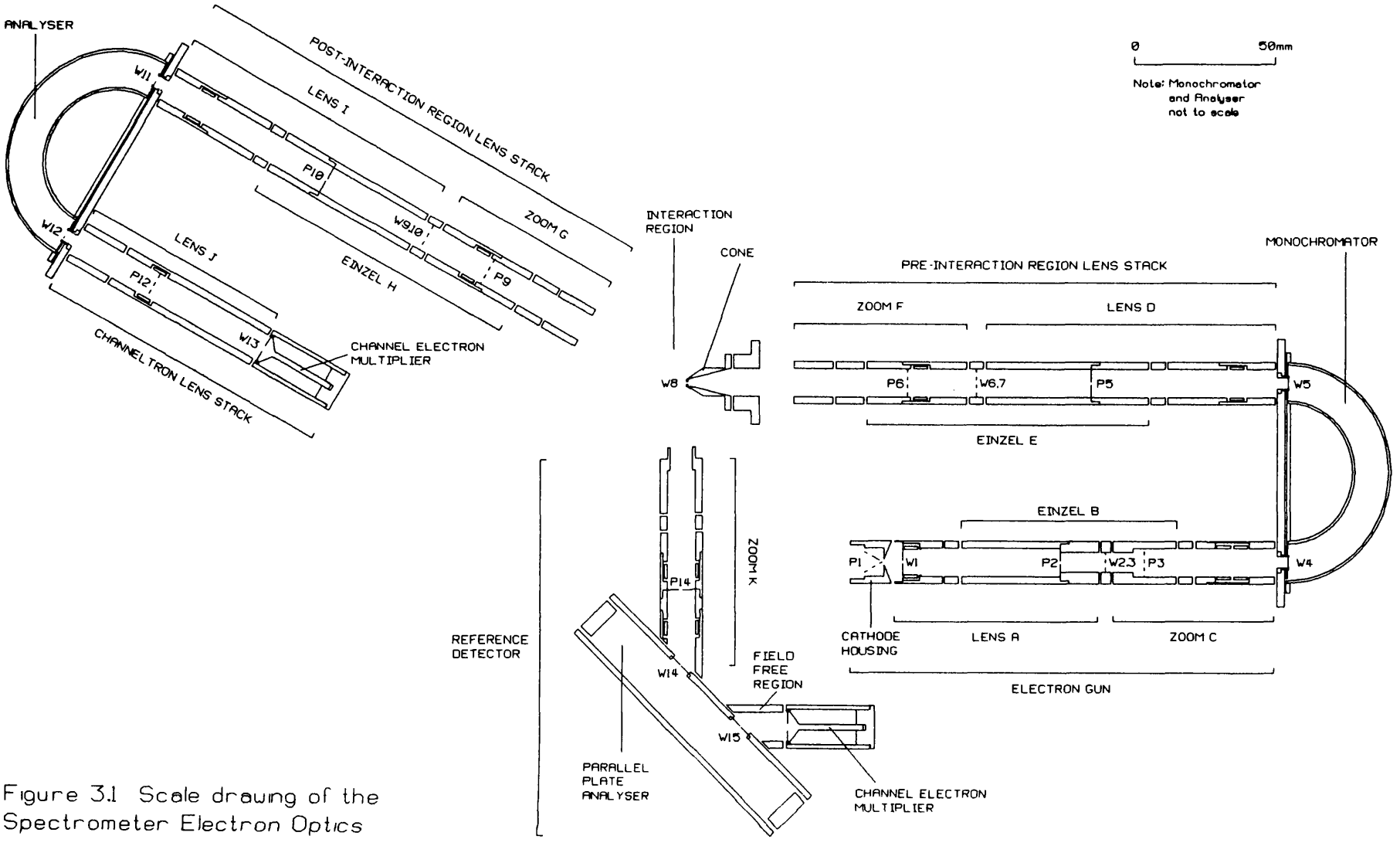

Figure 3.1 Scale drawing of the Spectrometer Electron Optics

aberration; for the same reason filling factors were kept to less than 50% (Brunt and Read 1975). A set of deflector plates was positioned between the apertures to correct for any minor misalignments and stray magnetic fields that might have effected the electron beam path.

Physical constraints were placed on the design, as the optical benches, interaction region cylinder and hemispherical analysers used with the previous spectrometer were retained. This meant that the overall length of the pre and post-interaction region and parallel plate lens stacks were set and that the lengths of the gun and channeltron lens stacks were limited. The design of the mumetal cans also put an additional constraint on the positioning of deflector sets, it being necessary for their studding to protrude into the wider part of the cans to prevent electrical shorting to earth.

Harting and Read (1976) have published data tables, listing the focal and mid-focal lengths, $f1,f2,F1,F2$, as a function of voltage ratio. These tables are available for a variety of aperture and cylindrical lenses. Cylindrical lenses were used in preference to aperture lenses, in the present experiment, as they were simpler to manufacture and also easier to fasten to the optical bench, being physically longer.The aperture lens data given by Harting and Read (1976) requires the diameter of the cylinder containing the aperture to be 5 x the size of the aperture. To utilise the existing optical bench it was necessary to limit the internal diameter of the cylinders to 10mm, this would have resulted in a lens aperture size of 2mm and hence very high filling factors. The small aperture size would also have made these lenses more sensitive to any surface contamination. Three element cylinder lenses were chosen in preference to two element lenses as they have the advantage that the lens can be fine tuned by altering the voltage on the centre element without upsetting the voltage ratios of the following or preceding lens.

For each three element cylindrical lens the lens parameters ($f1,f2,F1,F2$ and spherical coefficient terms) are listed in the data tables as a function of voltage ratio $V2/V1$ for a given $V3/V1$, V1, V2 and V3 being the voltages applied to the three elements of the cylindrical lens, numbered in the direction of travel of the electron beam. Once $V3/V1$ has been decided upon for a lens then the necessary $V2/V1$ voltage ratio can be found from this data to give the desired object and image distances (P,Q distances). The corresponding lens parameters $f1, f2$ etc are used to calculate the magnifications of the pupil and window. The image sizes may then be corrected for spherical aberration, using the coefficients listed in the tables. This correction can usually be considered as an upper estimate particularly for the case when the pupil is positioned at the first focal plane of a lens. The magnification of the pencil angle is found using the Helmholtz Lagrange Equation, and the entrance and exit beam angle are calculated by considering the path of the 'rays' defining the size of the pupil and window.

In practice, once the voltage ratio $V3/V1$ and P,Q distances had been decided upon, an estimate of $V2/V1$ was made, using the published P,Q curves, then with the aid of a computer program a more

accurate value was found. This program calculates quadratic expressions for $f1$,$f2$,$F1$ and $F2$ using the lens parameters associated with the three values of $V2/V1$ closest to the estimated value. Then using Newton's method the program solves

$$(P - F1)(Q - F2) = f1\,f2 \tag{3.1}$$

to find the best value of $V2/V1$, and its associated $f1$,$f2$,$F1$ and $F2$, for the required P,Q distances; $V2/V1$ is calculated to an accuracy of better than 0.005. To run the program the required P and Q distances are entered (in units of D, the internal diameter of the lens) together with the best estimate of $V2/V1$. Lenses were always chosen so that the middle element would be at a higher potential than the outside elements, thereby reducing the spherical aberrations (Adams and Read 1972b). The same program was used to calculate the voltage ratio $V2/V1$ for the einzel lenses, again to reduce spherical aberrations, only solutions which gave $V2/V1 > 1$ were considered (Adams and Read 1975a).

Several lens combinations were considered for each stack, the combination finally selected giving the lowest filling factors, best angular resolution and also fulfilling the physical constraints placed on the design. The method used to combine the three lenses in the gun stack was slightly different to that used to combine the lenses used in the pre and post-interaction region stacks.

The first step in combining the lenses in the gun, was to find the $V2/V1$ ratios (using the program described above) needed to focus the window for the desired P,Q distances and $V3/V1$ ratios selected for lens A and zoom lens C. The following steps, which are illustrated in Figure 3.2, were then carried out.

i) Initially it was assumed that the principal planes of the einzel lens both lay on its reference plane. This assumption may be made as the principal planes of an einzel lens always lie very close together about its reference plane for all values of $V2/V1$. The object distance of the pupil $P^{(B)}_{p\,initial}$, for the einzel lens B is therefore given by

$$P^{(B)}_{p\,initial} = Q^{(A)}_{w} - Q^{(A)}_{p}\,, \tag{3.2}$$

where $Q^{(A)}_{w}$ is the image distance of the window for lens A and $Q^{(A)}_{p}$ is the image distance of the pupil for lens A.

The image distance of the pupil is given by

$$Q^{(B)}_{p\,initial} = P^{(C)}_{w} - F2^{(C)}\,, \tag{3.3}$$

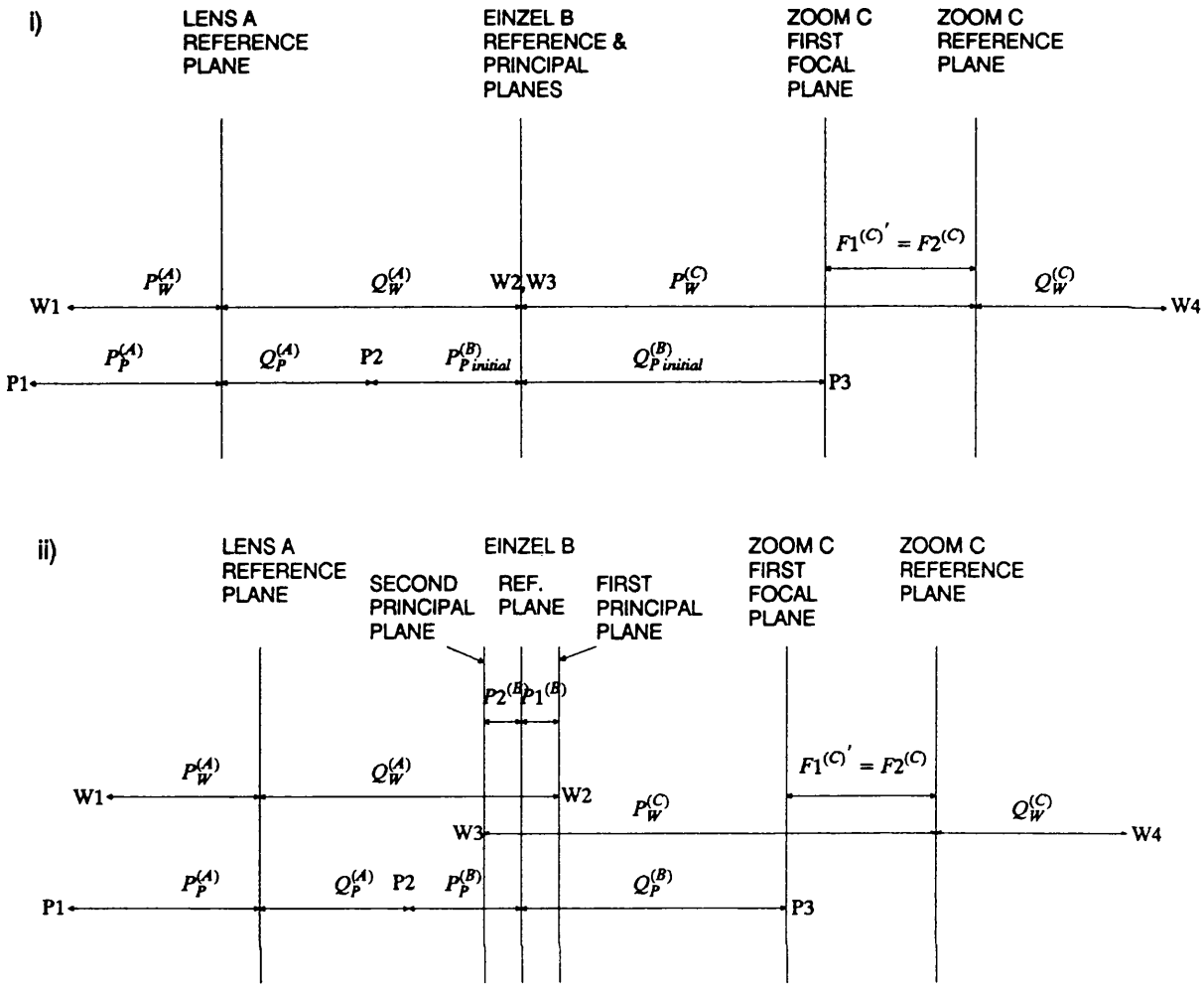

Figure 3.2 Illustration of first and last steps in the procedure followed to fit the gun stack

where $P_w^{(C)}$ is the object distance of the window for zoom lens C and $F2^{(C)}$ is the distance between the first focal plane and the reference plane of the decelerating zoom lens C.

ii) The einzel voltage ratio, $V2/V1$, required to focus the pupil was found and its associated lens parameters were used to calculate the true positions of the principal planes. To avoid changing the image distance of the window for lens A and the object distance of the window for zoom lens C, the total length of the gun was reduced by the amount $P1^{(B)} + P2^{(B)}$. It was then necessary to recalculate the pupil object and image distances for the einzel lens, using

$$P_p^{(B)} = Q_w^{(A)} - Q_p^{(A)} - P1^{(B)}, \tag{3.4}$$

$$Q_p^{(B)} = P_w^{(C)} - F2^{(C)} - P2^{(B)}, \tag{3.5}$$

where $P1^{(B)}$ is the distance between the first principal plane and reference plane of the einzel lens B and $P2^{(B)}$ is the distance between its second principal plane and the reference plane.

As the pupil object and image distances of the einzel lens B had been reduced, it was necessary to recalculate $V2/V1$ to focus the pupil correctly. The principal planes associated with the recalculated value of $V2/V1$ had shifted slightly, therefore step ii was repeated until the distances $P1^{(B)}$ and $P2^{(B)}$ were 'fixed'. This was taken to be when a further correction shifted their positions by less then 0.001D. Although this method had the advantage in that it was only necessary to adjust the voltage ratio for the einzel lens, it was only possible to use it when the total length of the lens stack could be adjusted.

As the lengths of the pre and post-interaction region lens stacks were fixed by the optical benches the method illustrated in Figure 3.3 was used to fit these lenses. Once the first estimate of the positions of the einzel's principal planes had been made, the image distance of lens D/G and object distance of lens F/I were both increased from their initial values to take this into account. It was then necessary

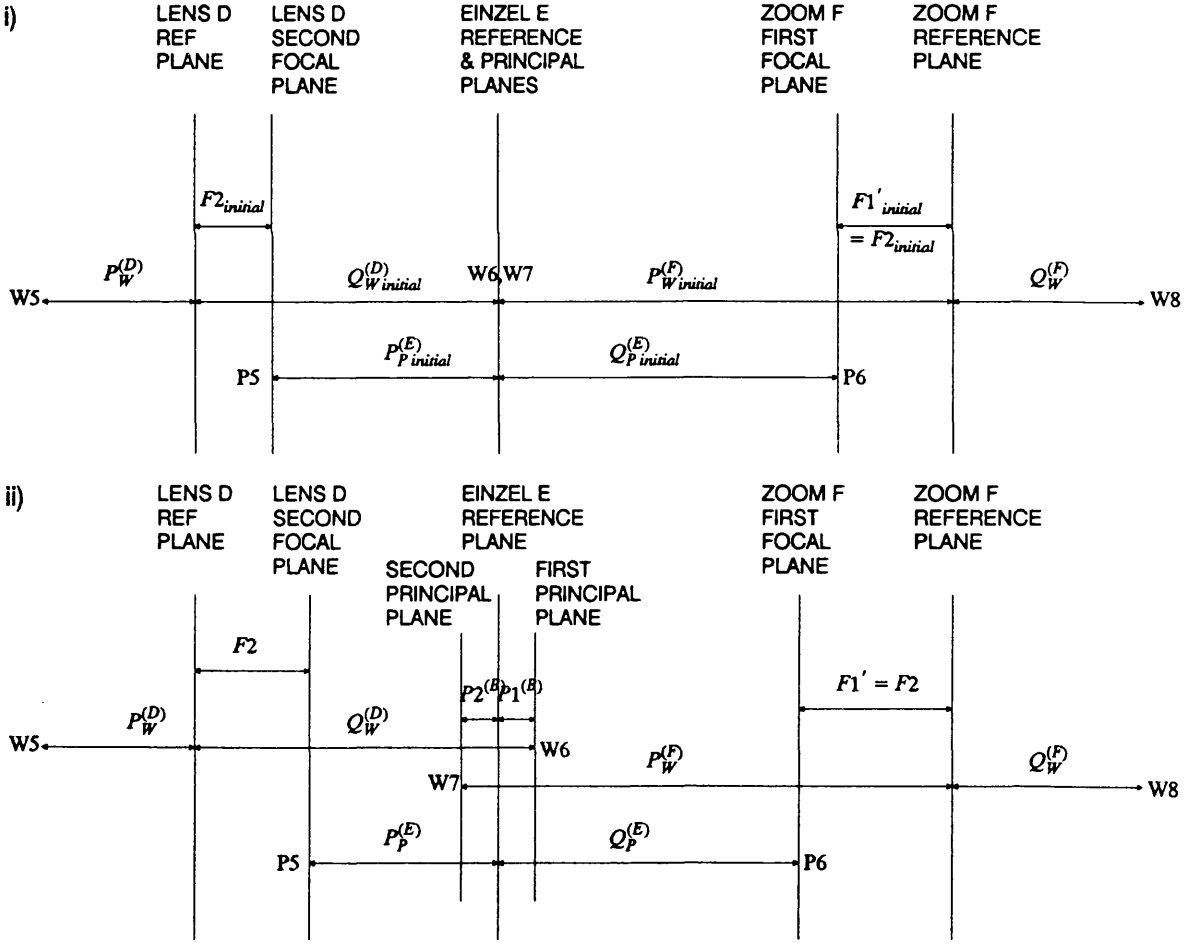

Figure 3.3 Illustration of first and last steps in the procedure followed to fit the pre-interaction region lens stack

to recalculate $V2/V1$ for both lenses D/G and F/I, resulting in a slight shift in the position of their focal planes. The voltage ratio $V2/V1$ of the einzel was then recalculated to refocus the pupil correctly, which in turn resulted in a slight shift in the positions of its principal planes. This fitting procedure was repeated until the positions of the focal planes of lenses D/G and I/K and the principal planes of the einzel lens were 'fixed'.

3.3 The Electron Spectrometer Design

The electron spectrometer designed for the present work is shown in Figure 3.1 and Plate 3.1. The design summary is given in Table 3.1 and the full lens data, voltage ratios etc are tabulated in Appendix B for each operational mode of the spectrometer. The following sections describe each part of the spectrometer in more detail.

3.3.1 The Electron Gun

The gun was originally designed to be used in conjunction with the pre and post-interaction region lens stacks previously used by Curry (1984). This spectrometer was designed to produce a minimum energy of 7.5eV in the interaction region with the monochromator operating at 7eV, therefore to produce a beam energy of 3eV in the interaction region it would have been necessary to monochromate the electrons at just under 3eV, consequently the gun was re-designed to operate over an energy range of 2.5 to 7.5eV.

A Pierce extraction system was used, based on a design by Chutjian (1974). The Pierce system's main advantage over that of the Soa, another commonly used extraction system, is in the way the electrons are sorted according to their angle of emission. The central point of the electron image is made up of electrons emitted normally to the cathode, while those emitted at increasing angles to the axis form concentric circles of increasing radius. By use of a stripper aperture (in this case the aperture at the entrance plane of the monochromator), only those electrons with transverse emission velocities below some maximum value will be transmitted (Harting and Burrows 1970).

A heated hairpin tungsten filament was used as the electron source. The pupil P1 is positioned at the filament tip with a diameter of twice the effective radius of the hairpin cathode (which is about 0.025mm (Chutjian 1979)). The window W1 is defined by the aperture in the anode. The electrons are drawn away from the filament by a anode voltage of 75V, with a small negative voltage, typically -0.6V, being applied to the cathode housing to aid this. The initial pencil angle, A_p, is calculated from (Kuyatt and Simpson 1967)

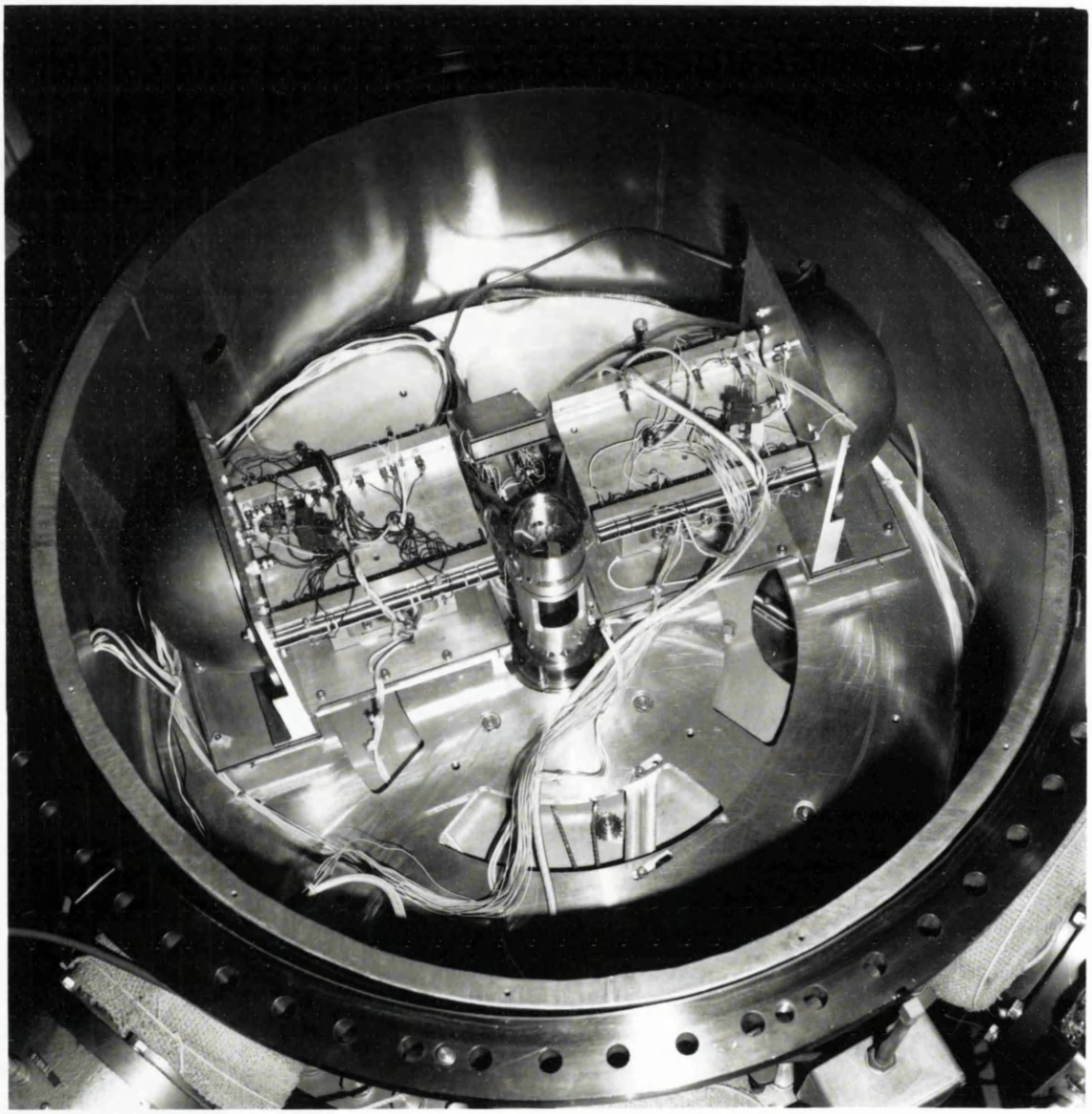

Plate 3.1. Top view of the electron spectrometer showing the monochromator (left) and analyser (right, at zero angle position) their optical benches and mounting blocks. The reference detector is mounted on the interaction region cylinder at a scattering angle of -90°

Operational energy range:	3 - 15eV
Primary beam current:	2 -3nA
Beam diameter in interaction region:	0.75 - 1.06mm
Energy resolution:	50 - 60meV
Angular resolution:	1.2 - 2.1°
Extraction system:	Pierce
Cathode:	Tungsten hairpin

LENS	ACTION
A	5:1 Decelerating Lens
B	Einzel Lens
C	2:1 Decelerating Zoom Lens
D	1:3 Accelerating Lens
E	Einzel Lens
F	8:1 - 1.5:1 Decelerating Zoom Lens
G	Accelerating Zoom Lens, inverse of F
H	Einzel Lens, inverse of E
I	Decelerating Lens, inverse of D
J	1:8 Accelerating Lens
K	2:1 - 1:2.7 Decelerating/Accelerating Zoom Lens

Lenses A-I and K are three cylinder lenses, K is a two cylinder lens. See Appendix C for voltage ratios and full lens data.

Lens filling factors: < 50%

APERTURE	SIZE
W1	0.3mm
W4	0.5mm
W5,W11,W12	0.5 x 5mm slot
W13	2.3mm
W14,W15	0.5 x 5mm slot
P2,P5,P10,P14	0.7mm

Hemispherical analyser:	Mean radius 63.5mm, analysing energy 7.5eV, real apertures, Jost type correction plates
Parallel plate analyser:	Analysing energy 7.5eV, real apertures
Ramp voltage:	All lenses after the first element of zoom lens G may be ramped
Electron detection:	Channel electron multiplier

Material of lenses:	Titanium
Material of Hemispheres and apertures:	Molybdenum
Material of parallel plate analyser:	Copper
Material of Jost type plates:	Aluminium
Surface coating of apertures and analysers:	Graphite (DAG 580)

Table 3.1 Design summary of the electron spectrometer

$$A_p = \left(\frac{V_k}{V_k + V_a}\right)^{\frac{1}{2}}, \tag{3.6}$$

where $V_k(\text{eV}) = \frac{T(K)}{11600}$ and T is the filament temperature in degrees Kelvin, and V_a is the anode voltage. The beam angle is set by the dimensions of P1, W1 and d, d being the distance between P1 and W1 (0.663mm).

As the ratio of the voltages on the anode to the final element of lens C can be seen to lie between 10 to 30, depending on the energy mode of the gun, two lenses were used to decelerate the electrons before entering the monochromator. The first of these decelerating lenses, lens A, images the real window W1 to W2, and the pupil P1 onto P2. As there is some uncertainty about the exact position of the pupil P1, P2 is defined using a real aperture of the same size as the calculated image of P1. For maximum separation of P2 and W2, $V3/V1$ for lens A had to be kept low, a large P2-W2 separation being required to enable an einzel lens to image P3 onto the first focal plane of zoom lens C. In fact it was found necessary to use an einzel lens with a smaller internal diameter than the surrounding lenses, for the P2-W2 separation (measured in units of internal diameter) to be large enough for the einzel lens to operate.

The virtual image of the window W2 is situated at the first principal plane of the einzel lens and so is imaged by this lens onto its second principal plane with its energy unchanged. The function of the decelerating zoom lens C was to focus W3 onto W4 over the required energy range 2.5 to 7.5 eV. The voltage on the central element of the einzel was set so that the pupil image of this lens, P3, always lay on the first focal plane of zoom C. This ensures that the pupil P3 is sent to infinity by this lens, resulting in a zero beam angle on entering the monochromator. As the position of the first focal plane of the zoom lens C changes with $V3/V1$, its (spatial) range, over the required energy range, was calculated before choosing a suitable einzel lens.

The final choice of lenses A and C was restricted by the permitted magnifications, both angular and spatial. Firstly, to keep the filling factor in lens C below 50% it was found necessary to keep both the pencil and beam angle low on entry. Secondly, to improve the resolution of the monochromator (see next section) it was necessary to keep the overall angular magnification of the pencil angle as low as possible, while keeping the overall magnification of the window within reasonable limits, these being related by the Helmholtz Lagrange equation. An acceptable compromise was reached.

As the position of the principal planes of the einzel lens vary with its $V2/V1$ ratio, when calculating the total physical length of the gun an average distance between their extreme positions was taken, thus 'fixing' the window object and image distance of this lens for all energy modes of operation. As the

difference in the positions of the principal planes over the required range is so small, around 0.1D, the error in the subsequent voltages of the central elements of the decelerating lenses was negligible, being of the order of 0.2V.

3.3.2 The Monochromator

A hemispherical monochromator, providing first order focusing, in two dimensions, was used to disperse the electron beam. The properties of this type of monochromator are well known (Purcell 1938) and described in detail by Kuyatt and Simpson (1967). The inner and outer hemispheres had radii of two and three inches respectively, the relatively large difference in radius minimising the effects of patch fields.

The electron beam image produced by the gun was imaged on the entrance plane of the monochromator. A real aperture, W4, in this plane allowed the central part of the image to enter the hemispheres, where the electron beam was dispersed into an image in the horizontal plane at the exit plane. The length of this image depended on the original energy spread and angular divergence in the electron beam. Only a small part of it could pass through the slot, W5, in the exit plane and this spatial restriction corresponded to a selection in energy.

The energy resolution ΔE for this type of monochromator is given by (Sevier 1972)

$$\frac{\Delta E}{E} = \frac{W}{2R_0} + A^2, \tag{3.7}$$

where E is the mean electron energy in the monochromator, R_0 is the mean radius of the hemispheres, W is the diameter of the entrance aperture and A is the half angle of the electron beam at the entrance, in this case being equal to half the pencil angle, the beam angle being set to zero.

Real apertures were used in the monochromator to ensure correct tuning of the hemispheres and following lenses. However, electron scattering from the apertures can occur and space charge effects are more pronounced, with the result that the design current is generally reduced.

A vertical slot was used in the exit plane as the long electron path in the hemispheres being around 399mm made it very susceptible to deflection by any small residual magnetic fields. With an circular exit aperture any vertical deflection of the beam within the monochromator results in loss of useful current and this problem is overcome with the use of the slot.

Although the gun had been designed to produce electron beams at the monochromator of 2.5 to 7.5 eV (the 2.5eV mode being necessary to give final beam energies of 3eV in the interaction region with the previous spectrometer) only the highest energy mode of operation was used with the redesigned spectrometer. It seemed advisable to operate the gun at the highest energy mode in order to reduce the space charge effects and scattering from the apertures W4 and W5; also any magnetic deflection of the beam in the hemispheres is reduced at the higher analysing energy. The necessity of running the instrument at the lower energy was removed when the previous spectrometer's pre and post-interaction region lens stacks were replaced by the present improved design (see Section 3.3.3).

To improve the energy resolution of the monochromator and analyser Jost (1979) type correction plates were fitted. These electrodes are designed to reduce the adverse effect of fringing fields on the beam trajectory. They consisted of two concentric rings which fitted between the two hemispheres, lying in the focusing plane. The voltage on the outer ring could be varied between the mean and outer hemisphere's potential and on the inner ring, between the mean and inner hemisphere's potential. In general best results were obtained with the rings at the same, or just below, the voltage of their corresponding hemisphere. These rings are shown in Figure 3.5.

3.3.3 The Pre/Post-Interaction Region Lenses

The pre-interaction region lens stack consists of three lenses, the first, lens D, an accelerating lens, followed by the einzel lens E and finally a decelerating zoom lens F. The purpose of this stack is to transport the focused electron image from the exit plane of the monochromator to the centre of the interaction region, a distance of 219mm, with an image size of approximately 1mm and a divergence angle of less than 2°.

Lens D images the window W5 onto the first principal plane of the einzel lens E. This einzel lens then images the window onto its second principal plane from where it is imaged by the zoom lens F to the centre of the interaction region, over the energy range 2.81 to 15 eV. The pupil, which is at infinity, is imaged by lens D onto the aperture P5 lying at its second focal plane. The size of this aperture is such that none of the electron beam should be lost. The pupil is then imaged by the einzel lens E onto the first focal plane of the zoom lens F, this lens consequently focuses the pupil at infinity, resulting in zero beam angle at the interaction region.

As with the gun, the average positions of the principal planes of the einzel lens, over the operational energy modes, were found and used to fix the window image distance of lens D and window object distance of lens F, for all final beam energies.

The post-interaction region is the mirror image of the pre-interaction region lens stack, focusing the window at the entrance aperture W11 of the analyser while at the same time sending the pupil to infinity resulting in a zero beam angle on entering the analyser.

When collecting energy loss data, a ramping voltage was applied to the post-interaction region lens stack, analyser and channeltron lens stack. The effect of this on the operation of the spectrometer is discussed in Section 3.10.

3.3.4 The Analyser

This was identical to the monochromator in design. The transmitted current was higher, however, as the space charge effects were considerably reduced in this region of the spectrometer, the beam currents being of the order of a few nAs as opposed to the 10^{-7}A measured at the monochromator.

3.3.5 The Channeltron Lens Stack

This consisted of a two element lens, lens J, which focused the electrons from W12 onto the mouth of the channel electron multiplier (Mullard, type B419BL). The aperture W13 at the mouth of the channeltron was considerably larger than the image size, its only purpose being to reduce the likelihood of any stray electrons being detected. The electrons emanating from W13 were collected over a solid angle of 6.5×10^{-4}Sr. The deflector set ensured that the beam could be re-centred if necessary.

3.4 The Reference Detector

As the purpose of this detector was to monitor any variation in the magnitude of the scattered electron beam, due to instabilities in the incident electron beam or gas beam, it was considered that the magnitude and stability of the detected electron beam was more important than its energy or angular resolution.

3.4.1 The Pre-Parallel Plate Lens Stack

A three element zoom lens, zoom K, was used to focus the window from the centre of the interaction region onto the aperture W14 in the entrance plane of the parallel plate analyser. This lens was chosen so that over the complete energy range of operation of the spectrometer, the beam and pencil angles were kept as low as possible on entering the parallel plates. The pupil is brought back from infinity by this lens to be focused at its second focal plane P14.

3.4.2 The Parallel Plate Analyser

Electrons which entered the parallel plate detector through the aperture W14 were dispersed in the field maintained between the plates to form a image at the exit aperture W15. In a similar fashion to the spectrometer's hemispherical analysers, the restricted diameter of this aperture selected the energy of those electrons transmitted to the remaining optics.

There are two major differences between hemispherical and parallel plate analysers, firstly the input beam is deflected through 90° before imaging by the parallel plate analyser, as opposed to 180° in the hemispherical analyser; hence the relative orientation of the two analysers in the spectrometer. Secondly the parallel plate analyser is only a one dimensional imaging device. The latter point gives rise to an additional term in the expression for the full half width maximum energy resolution of the parallel plate analyser ΔE, which is given by (Sevier 1972)

$$\frac{\Delta E}{E} = \frac{W}{l_0} + 2a^2 + b^2, \tag{3.8}$$

where l_0 is the entrance exit aperture separation, b is the beam half angle normal to the dispersion plane and the other symbols have the same meaning as in Equation 3.7

The energy selected electrons that were transmitted by the exit aperture W15 passed through a field free region of length 9.5mm before detection by the channel electron multiplier. Unlike the rest of the spectrometer which could be tuned with the primary electron beam and an electrometer, the optics of the parallel plate analyser had to be optimised using the relatively weak 90° elastically scattered signal of the target gas. However, with the deflectors turned down to their lens potential and the central element of lens K set to its calculated value a signal from the channel electron multiplier could always be observed on scanning the voltage on the outer plate. This could then be maximised by fine tuning lens K and using the deflectors. Count rates between 1000 to 10,000 counts/s were obtained.

3.5 The Interaction Region and Cone

The interaction region was defined by the interaction region cylinder, see Section 2.6, and Figures 2.2. and 3.4. An entrance hole for the incident electron beam, exit hole for the reference detector, and exit slot for the analyser were cut into the side of the cylinder. The holes and slot were all centred on the scattering plane and of diameter/height 10mm.

A cone was mounted on a cone support which was machined to give a good slide fit into the entrance hole, and bolted onto a milled flat in the interaction region cylinder wall. Three accurately positioned

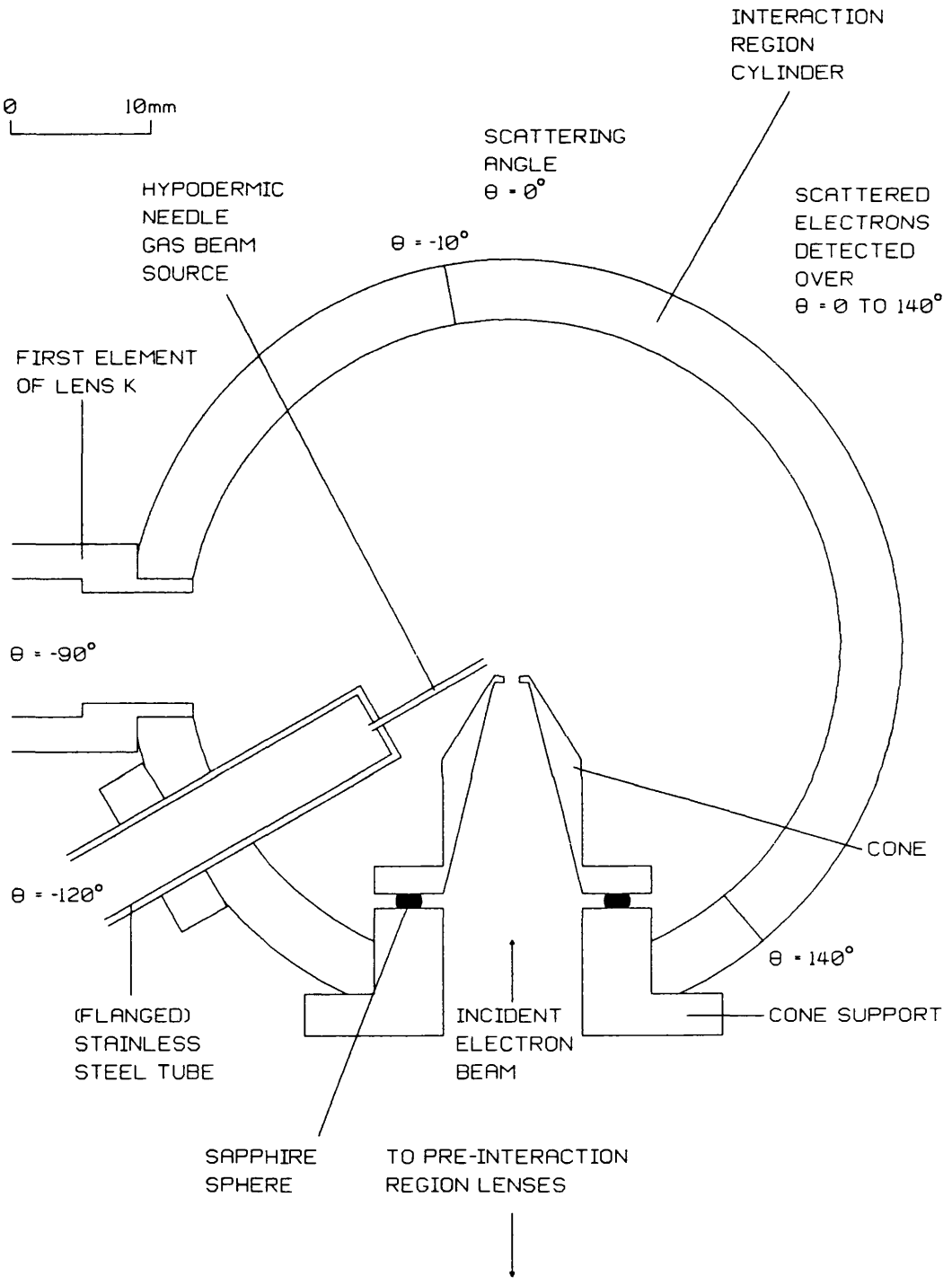

Figure 3.4 Horizontal sectional scale drawing of the interaction region cylinder

2mm diameter sapphire balls were used to insulate the cone and align its apex with the centre of the entrance hole (see Figure 3.4).

The cone terminated in a 1.2mm diameter aperture. Due to its electrical isolation from the interaction region cylinder, the cone was extremely useful in maximising the current at the centre of the interaction region, as the beam could be deflected onto its aperture and maximised there. It was then possible to deflect the beam through the aperture using the final set of deflectors in the lens zoom F.

3.6 Construction, Preparation and Alignment

The lenses were all machined from titanium, with a dimensional tolerance of ± 0.005mm. The apertures were of thickness 0.05mm and made of molybdenum. The hemispherical analysers were manufactured from spun molybdenum, the Jost plates from aluminium and the parallel plates from copper.

Besides the lenses, analysers and interaction region cylinder already mentioned, the spectrometer consists of a base plate, which supported the two mounting blocks for the optical benches and the two supporting plates for the two hemispherical analysers. These latter parts were all machined from aluminium with a dimensional tolerance of ± 0.02mm being used throughout (see Figures 3.5 and 3.6).

The optical benches and their mounts were in contact with the baseplate, all being at the same potential as the vacuum tank earth. As the plate supporting the hemispheres needed to be at a potential above this, it was insulated from the baseplate using 3mm diameter sapphire spheres. These were located between six pairs of accurately positioned holes (2.6mm in diameter) drilled in the two plates, thereby separating them by 1.5mm and providing their alignment. The hemispheres and Jost correction rings were located on the plates in the same way.

The method used to mount the lenses is shown in Figure 3.6b. Each element was attached to the optical bench by studding that passed through a horizontal slot in the optical bench and an insulating ceramic bush. By tightening a nut on this studding the lens element was pulled against two ground-glass rods, providing its alignment on, and isolating it electrically from, the optical bench. The wires carrying the lens potential were attached to the studding.

On replacing the old cone with the redesigned one, it was necessary to remove the optical bench holding the pre-interaction region lenses. Once the new cone had been installed the optical bench had to be realigned. This was achieved using three dummy lenses which were initially loosely attached to the optical bench. Two of the lenses were fastened to the ends of the optical bench closest to the hemisphere support plate, these lenses were machined to slide fit into aperture holders in the plate.

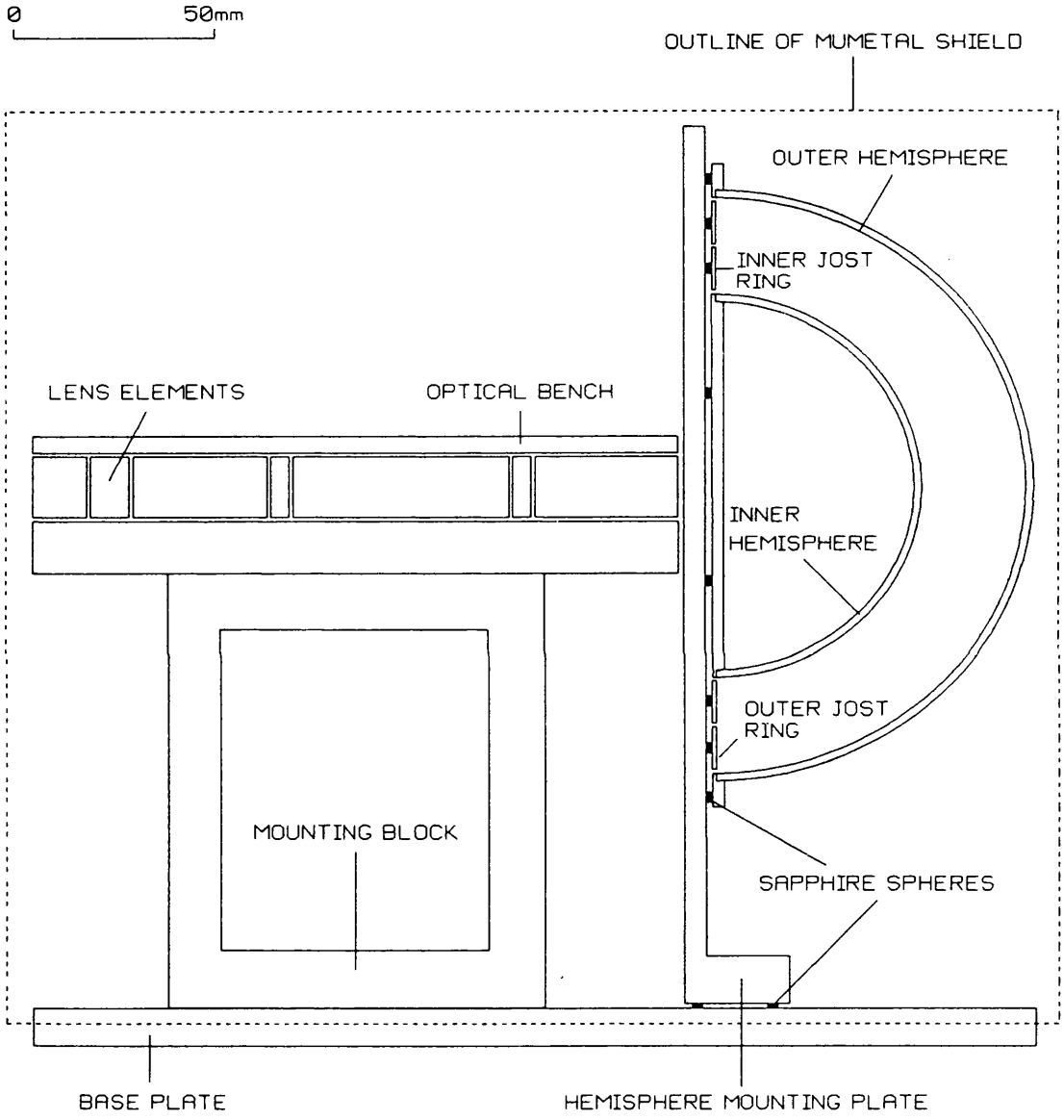

Figure 3.5 Scaled side view of the pre/post interaction region lens stack, analyser and supports

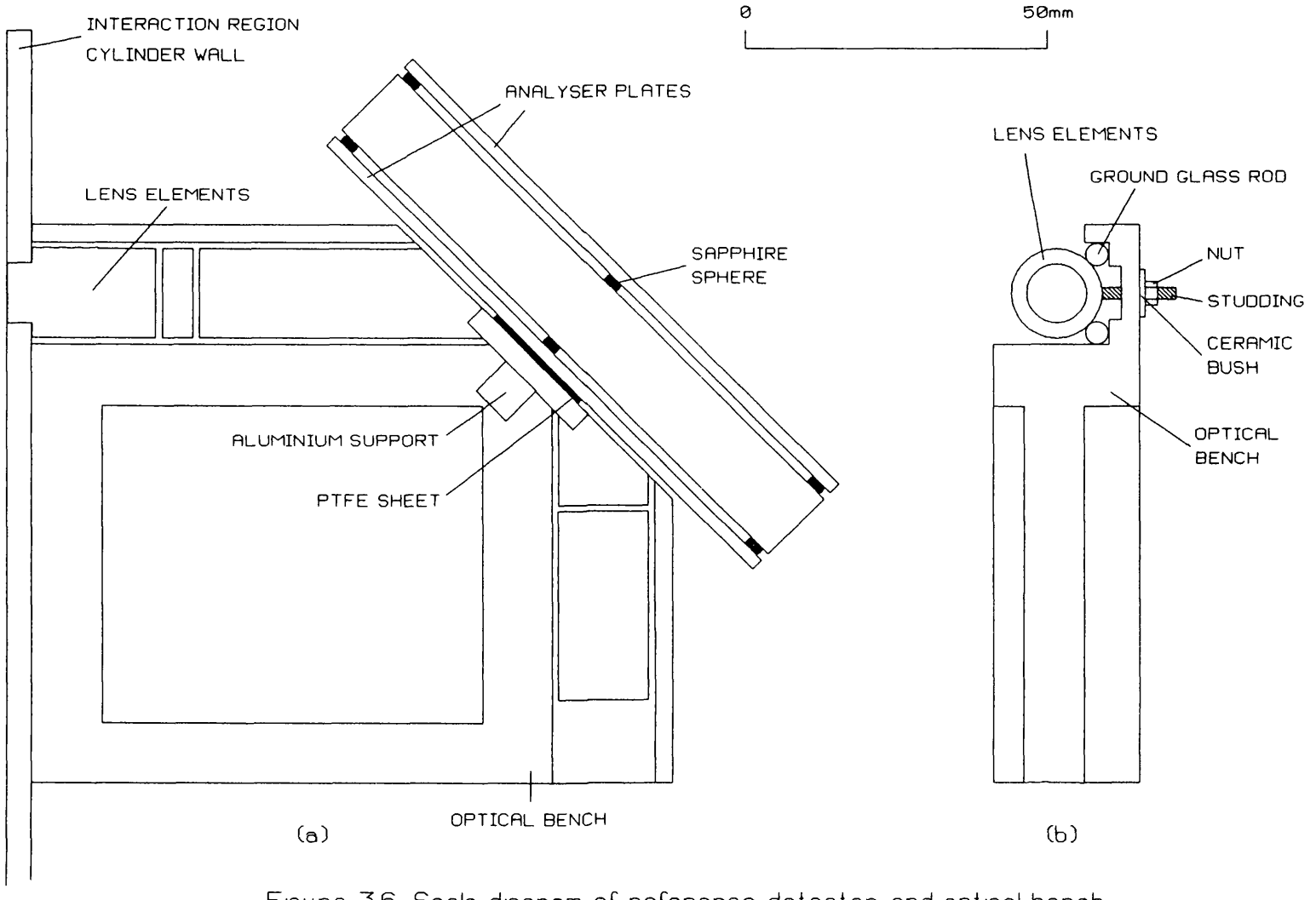

Figure 3.6 Scale diagram of reference detector and optical bench

One end of the third, cone shaped lens was machined to slide fit into the cone. When the optical bench was aligned correctly it was possible to slide all three lenses along the optical bench into their corresponding openings, simultaneously. When all three lenses were in position the optical bench was bolted to the base plate and the dummy lenses removed.

The alignment of the post-interaction region optical bench was achieved by using the same two dummy lenses at the analyser entrance and exit as were used at the monochromator. A fourth lens carried a silver steel rod which acted as a pointer. This lens was attached to the optical bench so that the pointer passed through the slot in the interaction region cylinder to the centre of the interaction region. The cone shaped, dummy lens, attached to the other optical bench, was also equipped with a pointer which could pass through the aperture in the cone. The rods were set in position so that their tips were located at the centre of the interaction region. At the same time the two dummy lenses at the analyser were inserted into the aperture holders in the plate. To check that the analyser was aligned at all angles it was rotated through to 140° and the relative position of the tips of the two pointers observed. In this way it was confirmed that the analyser observed the centre of the interaction volume independent of angle.

The first 3.0mm of the first element of lens K, in the reference detector stack, was machined to give a slide fit into its exit hole in the interaction region cylinder. This element was aligned when the wider 15mm diameter part of the lens was pushed hard against the cylinder wall, which was milled flat at the reference detector. The optical bench was aligned with this element and bolted to the flat surface on the interaction region cylinder. The parallel plate analyser was aligned using two dummy lens equipped with pointers. The analyser was moved along its aluminium support until the pointers were centred on the apertures in the entrance and exit planes.

Before assembling the new spectrometer the following cleaning procedure was observed. The lenses, apertures, hemispheres and rings were first washed with a detergent and rinsed off with distilled water. The hemispheres, rings and apertures were then cleaned with acetone by hand, while the lenses, nuts and bolts etc were placed in an acetone bath and cleaned ultrasonically. After drying with a heat gun, the process was repeated using methylated spirits instead of acetone. The sapphire spheres received the same treatment but before being cleaned in acetone were placed in concentrated nitric acid for a few seconds, to remove any surface impurities, then rinsed in distilled water. This cleaning procedure insured that any grease was removed from the lens surface and so reduced the build up of static charges which would interfere with the focussing of the optics. It was also considered important to keep all surfaces within the experimental tank clean and grease free in order to maintain the high vacuum, this being necessary for high beam stability. For this reason rubber gloves were always worn when assembling the spectrometer or working in the tank.

Once dry the apertures, internal surfaces of the hemispheres, correction rings and aperture holders in the plate were painted with a grahite solution (DAG 580) in order to reduce electron reflection and provide a uniform surface potential. Previous to using DAG 580 these surfaces were coated with a fine layer of carbon soot, using an oxy-acetylene flame. Although this method possibly produces a better surface than the grahite (McGowan 1967), it was abandoned due to the number of electrical shorts occurring when small particles of soot fell between lenses. Parker and Warren (1962) who describe a method of measuring the variation of contact potential over a 1 inch diameter plate, with an accuracy of $\pm$1meV, found that graphite had a contact potential variation, after first bakeout, of less than 10meV. Occasionally shorts did still occur, due to dust or graphite, these were detected using a megohm meter and generally removed by blowing air between the affected elements.

Once assembled and the power supplies connected up, a final check for shorts was carried out, the power supplies then switched on and the potential at each lens measured, to ensure they were all connected up correctly. The tank would then be pumped down, and baked using the four (150W, 24V) halogen projector lamps, one on each of the two optical benches, with the other two on the corresponding bases.

3.7 Power Supplies

A diagram of the overall electrical arrangement of the spectrometer power supplies is given in Figure 3.7. In this diagram A(1), A(2) and A(3) refer to the elements of lens A, numbered in the direction of travel of the electron beam.

The power supplies for the individual lenses had to fulfil the following requirements.

(a) They had to be insensitive to the small leakage currents between lens elements, since any change in their output voltage would de-tune the instrument.

(b) Their a.c. ripple had to be minimised to prevent modulation of the electron beam, which would degrade the resolution.

(c) They had to be smoothly variable to allow precise tuning of the electron beam.

Circuits were designed and built in house which had low output impedance and included ten-turn 100k potentiometers to comply with (a) and (c) respectively. These circuits did not contribute significantly to the a.c. ripple, which was limited to that present in the supply lines, and was always less than 2mV peak to peak in accordance with (b). Particular care was taken in the earthing arrangements to eliminate any loops which would increase pickup.

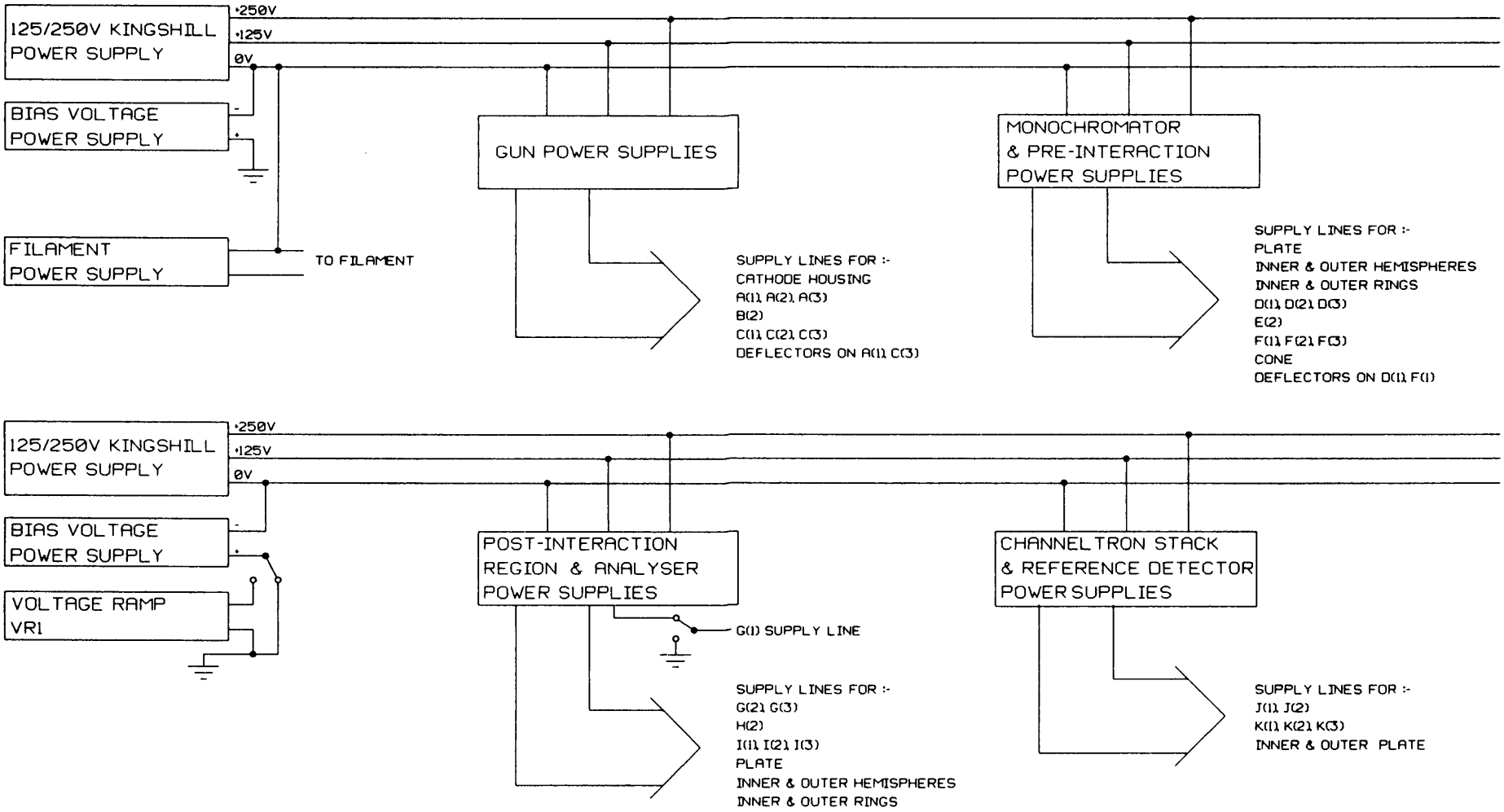

Figure 3.7 Diagram of the overall electrical arrangement of the spectrometer power supplies

The lens power supplies were connected to the vacuum tank via low current, multicore shielded cable. All the supplies were taken into the tank via feedthrough pins welded into the side port flanges, the pins being set in insulating ceramic holders. Internal connections to the lenses were made using PTFE covered, silver coated copper wire. The channeltron housing (in the channeltron lens stack) was connected electrically to the preceding element J(2) of lens J. Similarly the field free region and channeltron housing in the reference detector were connected to the last element of lens K.

Two 125/150V Kingshill Power Supplies were used to provide the high voltage lines needed to drive the lens power supplies. The bias voltage power supplies (Coutant, model LQ50/50) were used to set the energy of the electron beam in the interaction region and were connected between the 0V line and ground. All lens voltages were measured with respect to the 0V line. The filament was connected to the negative terminal of the pre-interaction bias supply, the energy of the incident electron beam was therefore varied by adjusting this bias voltage.

A voltage ramp, VR1, could be applied to the second element of lens G and all the following post-interaction region lenses and reference detector. When this ramp voltage was applied, the first element of lens G was earthed. Details of the voltage ramp generation are given in Chapter 4 and the defocusing effect of the ramp is discussed in Section 3.10.

The filament power supply and power supply for the projector bulbs (both Coutant, model LB100.2) were connected to feedthrough pins at the tank using 13A mains cable. Inside the tank thick fibre glass covered copper wire was used. The two wires to each bulb were twisted to minimise the magnetic field produced when the bulbs were on.

The same thick, well insulated, copper wire was used to connect the channeltrons to their corresponding feedthrough pins.

3.8 The Angular Resolution of the Spectrometer

The angular resolution of the spectrometer is a measure of the range in angle, about any one given angle, over which electrons may be detected at the analyser. It is determined by the angular extent of the incident beam and the acceptance angle of the analyser.

This was always measured before letting the target gas into the tank, by moving the analyser from the zero angle position and observing the fall in the current as measured at the back of the outer hemisphere of the analyser, using an electrometer. The angle through which it was necessary to move the analyser in order to reduce the current to half its maximum value, was used to calculate the 'full

width half maximum' angular resolution values, the electron beam's profile being symmetric about its maximum value.

Primary Electron Beam Energy (eV)	FWHM angular resolution
2.81	2.1° ± .3°
3.75	1.8° ± .4°
4.50	1.7° ± .3°
5.63	1.7° ± .3°
7.50	1.5° ± .3°
15.00	1.2° ± .3°

Table 3.2 Measured values of the FWHM angular resolution of the spectrometer for electron impact energy in the range 2.81 to 15eV

3.9 Contact Potential Measurement

Due to contact potentials and space charge effects, the energy of the electron as it enters the interaction region, is not equal to the energy at which it was emitted from the cathode; the difference in energies can be up to 1V (Heddle 1968). Various methods of measuring this contact potential are described by Kuyatt (1968). The method chosen in the present case, while not the most accurate, was by far the simplest with the present electron optics.

The contact potential was measured on completing a set of differential cross section measurements. It was carried out with the target gas still present in the tank. The electron beam was deflected onto the cone, which was used as a Faraday cup; the voltage on the cone was then reduced until the current was observed to fall sharply to zero. In the absence of contact potential this would have happened for a cone voltage of 0V, as measured with respect to the centre point of the filament. Due to the presence of contact potential, however, it was found necessary to apply a small negative voltage to the cone, for the current to fall to zero. This negative voltage, indicated the presence of positive contact potential of the same magnitude.

It was observed that for a given target gas the contact potential was fairly constant from day to day. Small variations occurred, however, for the different target gases used. For all gases the contact potential was always less than 0.8V.

Target Gas	Contact Potential
Helium	0.4 ± .2
Methane	0.4 ± .3
Ethene	0.5 ± .2
Ethane	0.4 ± .2

Table 3.3 Contact potentials for the target gases.

3.10 Energy Loss Mode and Transmission Characteristics of the Spectrometer

To detect the inelastically scattered electrons it was necessary to apply a voltage ramp to the power supplies in the analyser section of the spectrometer (details of the voltage ramp are given in Chapter 4).This ramp voltage was applied between the laboratory ground and the post-interaction region bias power supply (See Figure 3.7). With the ramp voltage at 0V and the analyser tuned, the primary beam was transmitted, all inelastically scattered electrons being defocused by the electron optics. With a positive (negative) ramp voltage ΔV applied, all the electrons with a energy loss (gain) of $e\Delta V$ were transmitted, the elastically scattered electrons and electrons scattered with a different energy loss being defocused by the electron optics. By collecting electrons at each step of the ramp it was possible to build up an energy loss spectrum.

The ramp was not, however, applied to the first element of zoom lens G in the post-interaction region stack, this was to avoid introducing an electric field near the collision region. To ensure that this element remained at the same potential as the interaction region, it was connected directly to the laboratory ground when the voltage ramp was applied. However, since the other two elements of this lens were ramped this resulted in a slight detuning of this lens, leading to a fall off in the transmitted current with increasing energy loss.

Various methods of measuring this effect were considered which entailed measuring the reduction in the primary electron current transmitted to the analyser (using it as a Faraday cup) at zero angle, as a function of the ramp voltage ΔV. However, to ensure that the primary beam correctly represented an energy loss beam, it was necessary to reduce the pre-interaction region bias and the voltage on the cone by the same ΔV each time. This resulted in a change in the profile of the incident electron beam, which in itself could have caused a fall off in the transmission of the electron optics. As no method of measurement could be devised which in itself did not change some property of the electron beam, the effect was calculated.

To calculate the reduction in transmission at a particular energy, the adjusted voltage ratios $V3/(V1-\Delta V)$ and $V2/(V1-\Delta V)$ were worked out for values of ΔV between -0.3 to +0.5V in steps of 0.1V and the lens parameters ($f1$,$f2$,$F1$,$F2$) associated with each pair of adjusted ratios found by interpolating the data of Harting and Read (1976). The resulting window image position, its size and the exit pencil angle for zoom lens G were then found, using the associated lens parameters, for each value of ΔV. The focusing of this image by the following einzel lens H and lens I was then calculated. For each value of ΔV, the new size and position of the window W12, and the exit pencil angle of lens I were found and used to project the image W12 onto the aperture in the entrance plane of the analyser. The percentage of the image which would pass through the aperture was then found for each of the values of ΔV given above. When the diameter of the projected image is larger than the diameter of the aperture, less current will enter the analyser, therefore these percentages give a measure of the variation in transmission with ΔV, and their reciprocals may be substituted for the transmission correction term $T_d(E) / T_d(E-\Delta E)$ in Equation 5.17.

It was found that a transmission correction was only necessary at the two lowest energies of 2.81 and 3.75eV, as at the higher operational energies of the spectrometer the transmission curves fell off by less than 1% over the full range of the ramp. The transmission curves for 2.81 and 3.75eV are shown in Figures 3.8 and 3.9 respectively.

3.11 Performance of the Spectrometer

The spectrometer performed well over the full operational energy range, producing 2 to 3nA in the interaction region, with an energy resolution of 50 to 60meV. It produced a stable electron beam (± .05nA) over the time (of up to 45 minutes) required to collect an elastic differential cross section.

To maximise the current entering the monochromator it was found necessary to increase the aperture P2 from 0.3 to 0.7mm and to increase the voltage applied to the central elements of lenses A and C by about 5 and 10% above their calculated values. This was probably a result of space charge, always a problem in gun design.

The current entering the monochromator was around 1×10^{-7}A with its transmission therefore being around 3%. The measured resolution of the monochromator was 35 to 42meV ($1/\sqrt{2}$ × the overall resolution). As the calculated resolution for this monochromator with an analysing energy of 7.5eV and pencil angle 2.11 is 40mV, it would appear that the beam angle was successfully set to zero on entry by the preceding zoom lens C.

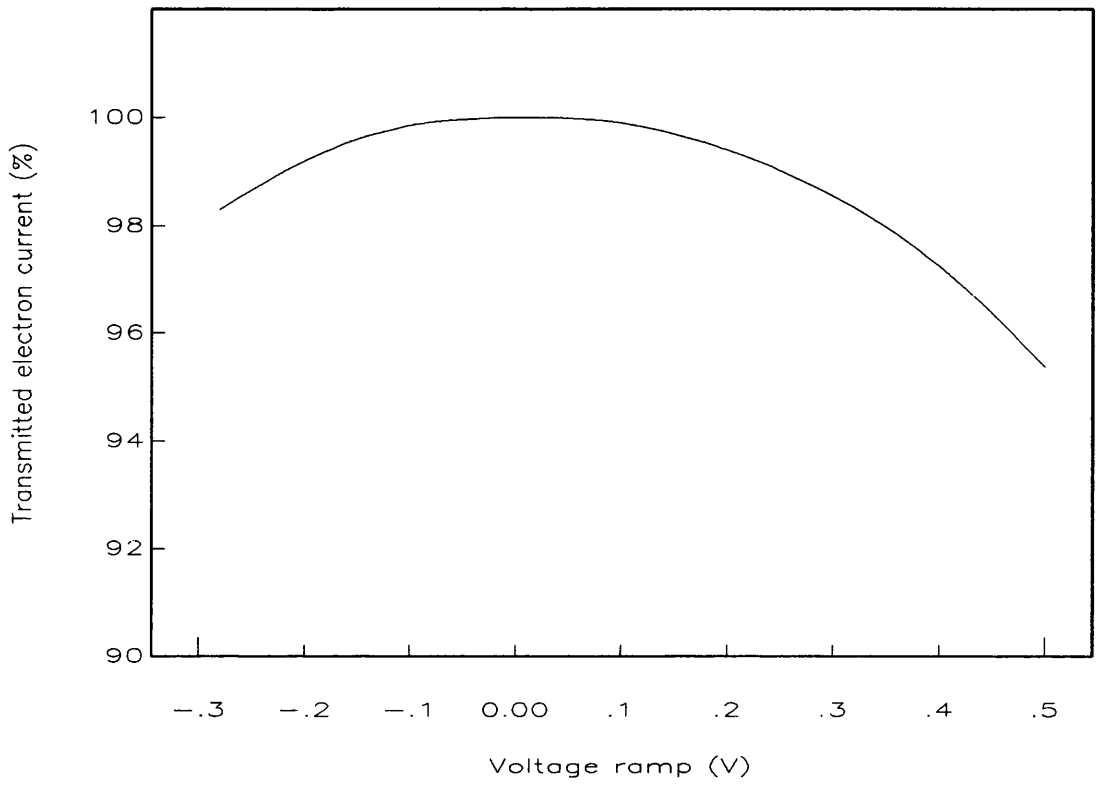

Figure 3.8 Spectrometer transmission characteristics at 2.81eV

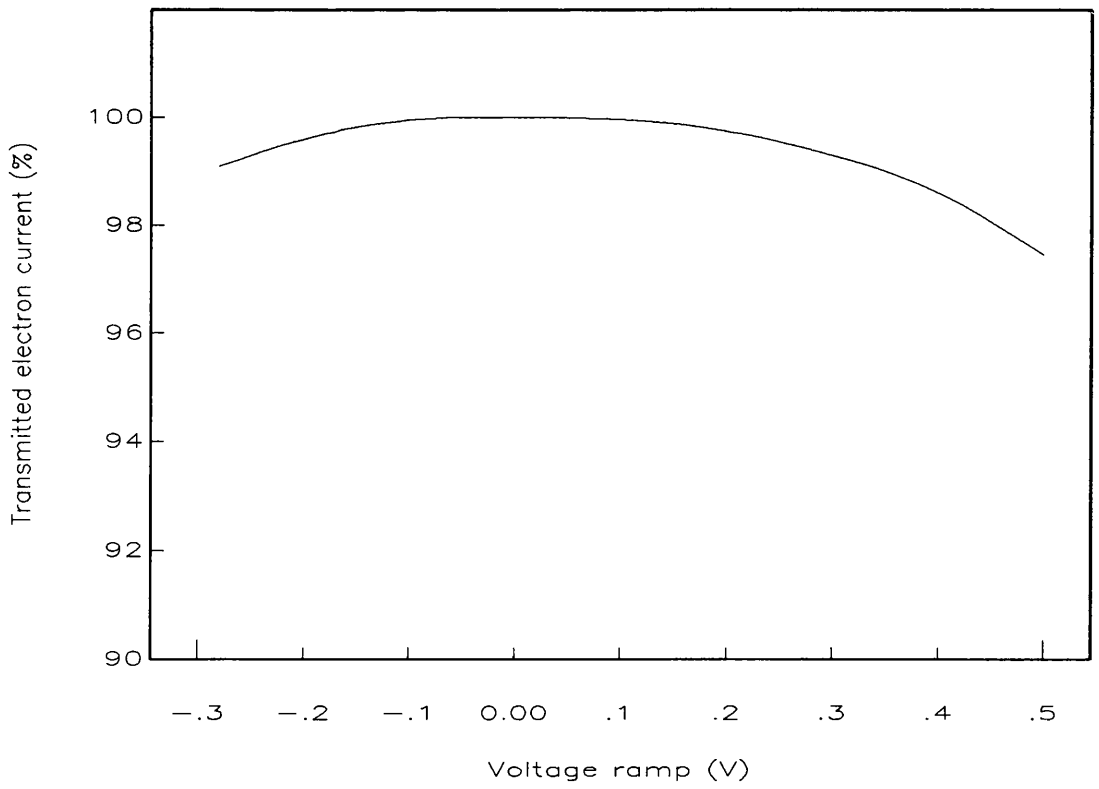

Figure 3.9 Spectrometer transmission characteristics at 3.75eV

At the lower operational energies, it was found that to maximise the current entering the analyser, it was necessary to increase the voltage on the central elements of the zoom lenses F and G by up to 10% of their calculated values, the increase needed becoming greater as the interaction region energy was decreased. This was possibly due to the contact potential at the interaction region with its defocusing effect becoming more significant at the lower energies.

The reference detector used for the elastic differential cross section measurements, worked particularly well, maintaining high count rates over the data collection period. Its energy resolution was measured to be 150meV.

Chapter 4 - Data Collection

4.1 Introduction

This chapter describes how the scattered electrons were detected and the data acquisition methods used. A BBC micro computer was used to control the data collection process and was connected up to the experiment via a purpose built interface. A general description of the interface is given in Section 4.3, its operational details in Section 4.5 and hardware specifications in Section 4.6. The software written to drive the interface is described in Section 4.4.

4.2 Signal Detection

Scattered electrons leaving the hemispherical analyser (see Figure 3.1) were detected by the electron channel multiplier (Mullard, type B419BL), operating in a pulse counting mode; the height of the output pulses being independent of the incident electron energy. The channeltron was operated at 3kV, (using a Fluke High Voltage Power Supply, model 410B) with a typical gain of 1×10^8. High count rates severely reduce this gain due to the build up of space charge in the channeltron (Petley 1971), but the signal count rates achieved in this experiment were not reduced by this effect since the output pulse height was always above the limiting threshold of the amplifying devices.

The pulses from the channeltron were fed into a charge sensitive pre-amplifier with a gain of 10 (Petley 1971), which produced positive, unipolar pulses of approximately 60mV. By feeding test pulses into the preamplifier (using a square wave generator), it was observed that it was the preamplifier which put an upper limit on the maximum measurable count rate as the output signal of the pre-amplifier was observed to fall off very sharply for count rates above $40{,}000s^{-1}$. For scattering angles of 20° or greater, however, this limit was not reached; the maximum count rates obtained from the channeltron being around $35{,}000s^{-1}$.

The pulses from the preamplifier were in turn amplified by a spectroscopic amplifier (Ortec, model 451) which had a variable voltage gain, and were subsequently fed into a discriminator (Nuclear Enterprises, model 4623). With the amplifier gain set to 20 and the lower level of the discriminator set to cut out pulses of height less than 0.2V, the background count rate due to electrical noise was virtually eliminated, being of the order of $0.01s^{-1}$. To achieve this very low count rate great care was taken with the earthing arrangements within the preamplifier, and all connections between the channeltron and BBC micro computer were carefully shielded. The pulses at the output of the

discriminator were approximately Gaussian in shape with an average base width of 300ns and height of +5V.

An identical signal detection system was used for the electrons scattered into the reference detector situated at a fixed angle of -90° (see Figure 3.1).

When initially tuning the spectrometer at a given scattering angle, the discriminator outputs were fed into a ratemeter (Ortec, model 441). When ready to collect data, the data and reference detector discriminator outputs were connected to Inputs 1 and 2 of the interface respectively, as shown in Figure 4.1. The pulses were counted by counters in the interface under the control of the BBC micro computer which was connected to the interface via the 1MHz bus.

4.3 The Interface

Under the control of the BBC Micro, the interface is capable of outputting a bipolar voltage ramp of 1024 steps. The voltage ramp, VR1, which is shown in Figure 4.1 may be applied to the second element of lens G (see Figure 3.7) and all the following lenses. The ramp output can also be varied manually over the range of 0 to ± 2.3V. In the present experiment the ramp output was always set to ±0.5V, allowing electrons with an energy gain/loss of up to ±0.5eV to be detected, with a energy step resolution of 0.97meV.

For the duration of each of the 1024 steps of the ramp, the +5V pulses from the discriminators can be counted. For each of the discriminators, the sum of the counts, for each step, is stored in the corresponding element of a 1024 element array inside the BBC micro computer (the two integer arrays, for the data and reference detector, being called C1% and C2% respectively). By changing the software a range of pulse collection techniques can be used. For example the pulses may be collected for a given number of complete scans of the voltage ramp, for a minimum number of counts to accumulate in any one particular element of either array, for the sum of all counts in an array to have reached a minimum number, or for a given collection time.

The circuit was designed so that the ICs required to generate a voltage ramp and act as a single counter are contained on a 'daughter' board which plugs into the 'mother' board. The mother board holds the circuitry common to all the daughter boards. In the present experiment two daughter boards were used but only one of the daughter boards was fully utilised providing the voltage ramp VR1 and counting the pulses arriving at Input 1. The other board was used to count the pulses arriving at Input 2. The mother board can support up to eight of these boards, however, allowing for eight voltage ramps and eight pulse counting inputs (see Sections 4.5 and 4.6).

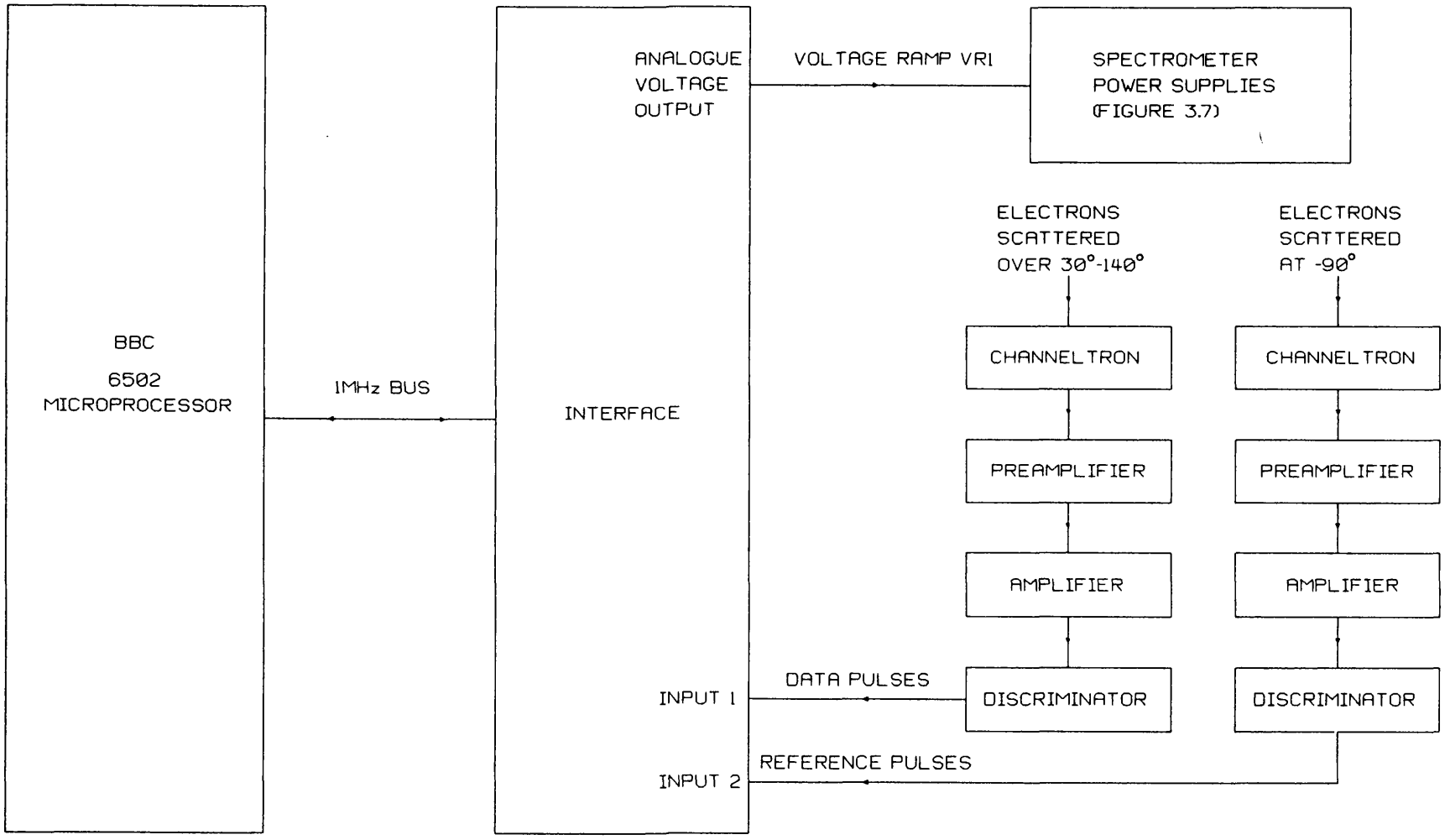

Figure 4.1 Block diagram of data acquisition system

4.4 Software

Separate programs were used to collect the elastic and inelastic cross section data. Both programs are menu driven and written in a modular form. BBC BASIC is well suited to this as it allows for the use of procedures. Procedures resemble subroutines but are called by name from the main program and may have parameters passed to them. The variables within a procedure are localised where possible making it easy for the same procedure to be used in other programs.

Another advantage of BBC BASIC is that it allows 6502 assembly language programs to be included within a BASIC program. To deal with interrupts from the interface (Section 4.5) and to reduce the dead time when collecting data, it was necessary to write parts of the data collection procedure in assembly language.

Error trapping routines are included in both programs, to ensure as far as possible that programs would not crash, and data be lost, due to user errors. These routines try to predict the most likely errors and provide error messages within the programs as necessary.

4.4.1 Inelastic Measurements

On running E-LOSS the program to collect the inelastic measurements, the procedure PROCinit is called (see listing in Appendix C). This procedure initialises the interface. The following menu is then displayed:-

```
1. COLLECT DATA
2. DISPLAY DATA
3. PLOT DATA
4. SAVE DATA ON DISC
5. LOAD DATA FROM DISC
6. END PROGRAM
```

If an error occurs, or the user presses the escape key at any time, this menu is redisplayed. While at this menu the user can submit operating system commands (such as format disk) by pressing the '*' key.

On selecting the first option, the user is prompted to enter the required step time, (in the range 0 to 65536μs), the number of scans (ie the number of times the ramp is to be repeated) and the initial and final step numbers. In this experiment it was only necessary to detect elastically scattered and energy loss electrons, therefore to minimise the data collection time the initial and final step numbers were usually set to 200 and 1023, resulting in an output voltage ramp in the range -0.3 to +0.5V. An energy

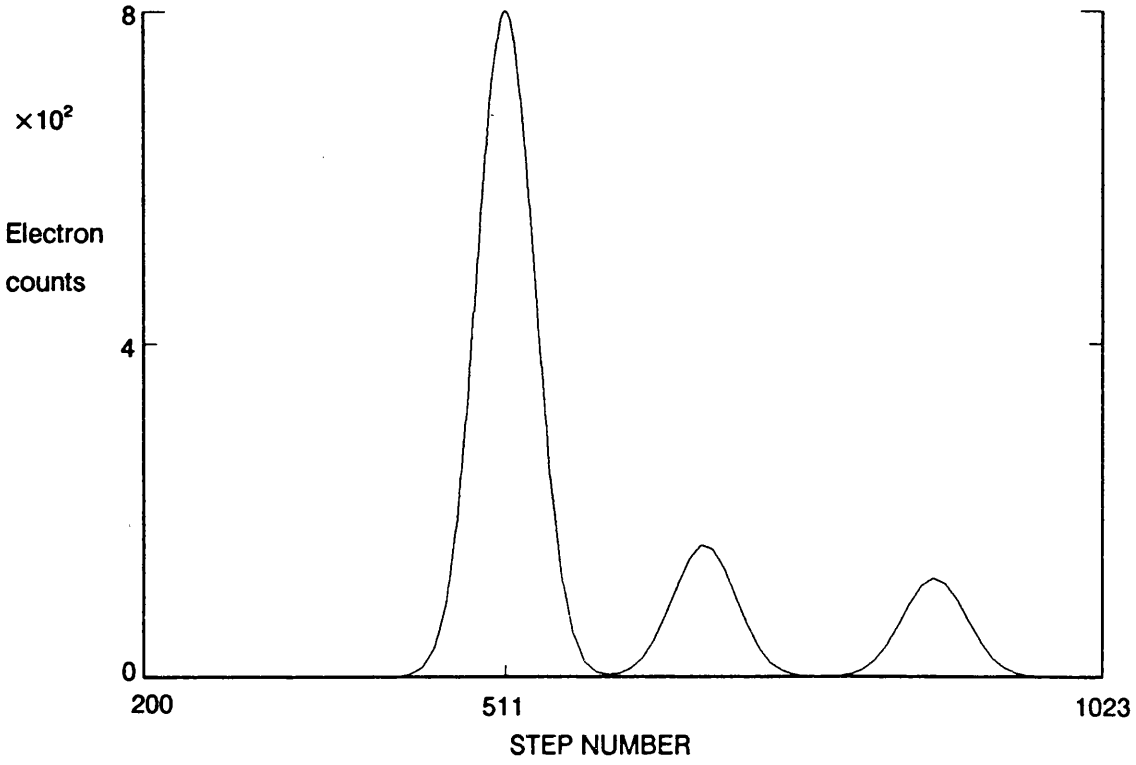

Figure 4.2 A typical energy loss spectrum obtained with the step range 200-1023 steps

loss spectrum obtained with this voltage range is illustrated in Figure 4.2, the elastic peak is centred at step 511 and the peaks due to the inelastically scattered electrons are positioned at higher step numbers. By using this reduced step range the time taken for one voltage ramp, using the maximum step width, was reduced from 70.4s to 56.7s. While scanning the 'WORKING' message is displayed together with the current scan number.

When the required number of scans have been completed the program redisplays the main menu. The data may now be viewed in a tabular format by selecting option 2, or plotted, as shown in Figure 4.2, by selecting option 3. The plot procedure displays the spectrum, by plotting the contents of C1% along the y-axis vs the step number along the x-axis. The y-axis is initially scaled so that the highest point of the spectrum is plotted in the upper half of the screen while the graduations along this axis increase by a factor of 1,2 or 5. On hitting the space bar, the y-axis is expanded by a factor of 5 allowing the inelastic peaks to be seen more clearly. It is also possible to have a partial plot of the x-axis, allowing the spectrum to be expanded horizontally. The graphs produced could be sent to the printer, if connected, or saved on disc to be printed at a later date.

If the energy loss peaks are not sufficiently well defined (ie the area under the smallest peak contains less than the 10,000 counts required for a 1% error), option 1 may be reselected and additional data collected. At this point the user is asked whether the data is to be added to the current values in C1% or if a new spectrum is to be generated, in which case the array is zeroed.

When the energy loss spectrum is sufficiently well defined the data may be saved by selecting option 4. The energy loss spectra (contents of the arrays C1% vs step number) are saved on disc as an ASCII file. If at a later date the user wishes to view the spectrum, the data may be loaded back into the array C1% by selecting option 5.

4.4.2 Elastic Measurements

To allow for the calculation of the differential cross section at a given scattering angle, it was necessary to take the ratio of the height of the elastic peak detected at the required scattering angle to the height of the elastic peak detected by the reference detector, situated at a fixed angle of -90° (see Section 5.3 for details of this calculation). Hence to determine the differential cross section, the count rates at the centre step of both elastic peaks are measured simultaneously.

To achieve this it is necessary:-

1. To determine the centre step of both elastic peaks.

2. If this step is not the same for both peaks, to alter the analysing potential on the reference detector to bring the two peaks into line.

3. To collect data for the minimum number of scans required for a least 10,000 counts to have accumulated at the centre step of both elastic peaks.

The program DIFF was used to operate the interface in such a way that the above could be achieved, the program listing is given in Appendix D.

On running DIFF, PROCinit is called, this procedure initialises the interface allowing data to be collected from both detectors simultaneously. The following menu is then displayed:-

```
1. SET STEP RANGE
2. PLOT DATA
3. COLLECT DATA
4. COLLECT NOISE
5. DISPLAY DATA
6. CALCULATE COUNT RATES
7. END PROGRAM
```

If an error occurs, or the user presses the escape key at any time, this menu is redisplayed. While at this menu the user can submit operating system commands (such as format disk) by pressing the '*' key.

The first option 'SET STEP RANGE' is used to determine the centre step numbers for both elastic peaks. When tuning the spectrometer, lens voltages were set to the nearest 0.01V, however the energy loss spectrum has an energy step resolution of 0.97meV, therefore the elastic peaks were often shifted from the centre 0V ramp step (511) by up to 10meV.

On selecting this option the user is prompted to enter the number of scans, the estimated centre step of the spectrum (typically 511), and the required step range (typically ± 50). Data is then collected from both detectors over the requested step range about the estimated centre step for the required number of scans.The step duration is automatically set to its maximum value of 65535μs.

These elastic peaks may then be plotted by selecting option 2. The user may plot the single peak obtained from either the data or reference detector or both peaks together. Figure 4.3 illustrates the spectra obtained using a step range of 461 to 561 steps. In this example the elastic peaks measured by the data and reference detectors are separated by approximately 15meV. The centre step of each peak is determined visually with the aid of a vertical pointer which can be moved along the x-axis, reading the step number. If the peaks are separated, the potential on the outer plate of the reference analyser may be adjusted to bring them into line (the change in potential required being determined by the displacement of the two centre voltage steps, normally a few mV). Options 1 and 2 would then be repeated to check the two elastic peaks were indeed aligned.

Once both peaks have the same centre step option 6, 'CALCULATE COUNT RATES', is selected. This calculates and displays the count rates together with their errors for the central steps of both peaks.

Option 3, 'COLLECT DATA', is then selected. The user is prompted to enter the minimum number of counts required in either of the peaks (a typical input being 10,000). Using this input value, and the previously calculated count rates, the minimum number of further scans required to achieve this minimum number of counts in both elastic peaks is calculated and displayed. Next the user is prompted to enter the centre step (as previously determined from option 1) and the required step range (usually set to 0). If the selected step range is outside the range used in option 1, the user is warned that the data already collected will be deleted and the variable storing the number of completed scans zeroed, otherwise the new counts are added to the values already stored in the arrays C1% and C2%. Finally the required voltage step(s) is sent out and the pulses arriving from both discriminators counted. When the required number of scans are complete, option 6 is reselected from the main menu and the count

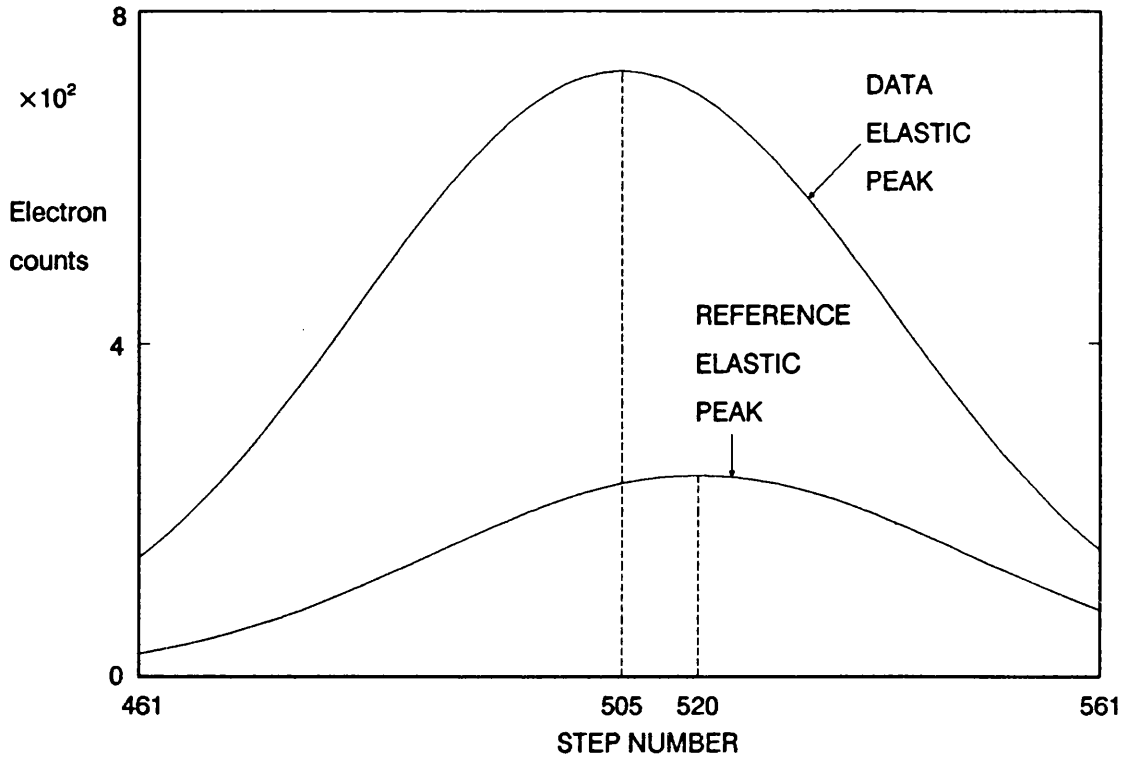

Figure 4.3 Typical spectra obtained with a step range of 461-561. The elastic peaks of the data and reference detectors are centred at steps 505 and 520 respectively

rates of the centre steps recalculated. If the electron beam intensities have fallen off during the data collection, more scans may be necessary to attain the required accuracy, option 3 is therefore repeated until this has been achieved.

On moving the analyser to another scattering angle, the whole procedure was repeated, however, the peak position normally remained constant over the time required to complete a set of angular measurements, so it was unnecessary to adjust the reference detector potential.

By selecting option 4, 'COLLECT NOISE', the d.c. background level may be found. The user is prompted to enter the required number of scans, the -0.5V step (step 0) is then sent out and data collected for the requested number of scans. The background level was measured before and after a differential cross section had been collected, and was found to be fairly constant on any one day and of the order $.01s^{-1}$.

As in the E-LOSS program, option 6, displays the counts recorded in the arrays C1% and C2% vs step number.

4.5 Operational Details of the Interface

The following section describes how the programs E-LOSS and DIFF control the interface.

On running E-LOSS an initialisation procedure (PROCinit) is automatically called. This procedure sets up the registers of the 6522 Versatile Interface Adaptor (1), which is in the interface box. The 6522 VIA contains 16 internal registers which may be directly addressed. The operational mode of this IC is set by loading the relevant registers (see 6522 VIA data sheet for details of these 8 bit registers). The 6522 VIA also contains two, 16 bit, timers T1 and T2. T2 of the 6522 VIA (1) is set up to act as a counter by this procedure and T1 to act as a timer.

Once the user has selected the 'COLLECT DATA' option from the main menu, and entered valid parameters for the stepwidth, number of scans required and initial and final step numbers, the procedure PROCcollect is called. This procedure sends out the first step of the ramp and sets the interface to collect pulses for the required step time. The pulses are collected in the counter T2 in the 6552 VIA (1) and at the end of the step time this counter is read. The next voltage step is then sent out and the process repeated until data has been collected for each step of the ramp. The ramp is repeated for the requested number of times.

To achieve the above, PROCcollect has three main parts:-

1. To enable and handle interrupts from the interface.

2. To send out a voltage step.

3. To start the counter T2 in the 6552 VIA (1), and to read this counter at the end of the step.

These points, and the operation of the interface, are described in more detail below. In the following text, numbers preceded by the '&' sign are hexadecimal.

When the computer is switched on the operating system continually services interrupts from the screen, keyboard etc (even when a program is running). Each time the 6502 microprocessor is interrupted (about 100 times a second) the operating system jumps to a reserved memory address (&206) where it finds the address of the interrupt service routine. To enable interrupts from the interface to be serviced it is necessary to intercept this service routine by changing the address found at &206 for the address of code used to handle interrupts generated by the interface. The final part of this code must send the operating system to the address originally contained at &206, allowing interrupts from the keyboard etc to be serviced using the standard interrupt routine, otherwise the

computer will crash. Once interrupts have been enabled in this way, when an interrupt is received by the 6502, the interrupt handling code checks to see if it is coming from the 6522 VIA(1) in the interface before going on to check the keyboard etc. If the interrupt has come from the interface, a flag will be set in the 6522 VIA (1) flag register. On finding this, the interface interrupt handling routine resets the flag and sets a memory location (&70) to 1. The significance of this is explained later.

After sending out the first step of the ramp voltage (see Section 4.6.8 for detail of this), the memory location, &70, is set to zero and the timer, T1, in the 6522 VIA(1) loaded with the required step time. Having loaded the timer, the BBC program then waits for the memory location &70 to be set to 1, by the machine code interrupt handling routine.

As soon as the lower byte of the step time is loaded into T1, the VIA starts decrementing it at the clock rate. At the same time it causes the voltage level output on one of the pins of the VIA, (PB7), to fall from +5V to 0V, this is used to enable a gate (774LS423) so letting the pulses from the data discriminator reach T2 and be counted.

When T1 has decremented to zero, it sets the time out interrupt flag in the interrupt register, and interrupts the 6502 microprocessor of the BBC Micro by pulling the interrupt request line to 0V (see Section 4.6.1). This interrupt is serviced as explained above. The voltage on PB7 reverts to its original level on the time out interrupt flag being set, stopping the pulses from the data discriminator getting through to the counter

As soon as the memory location &70 is set to 1, by the interrupt handling routine, the BBC program (which has been waiting for this event) continues, the counter T2 is read and its contents stored in the element of C1% which corresponds to that step number.

The program then sends out the next step of the ramp and the whole process is repeated. On completing the last ramp step, the program either returns to the menu if the requested number of scans has been completed, or else starts another ramp. In each subsequent ramp the new counts at each step are added to those already stored in the array C1%. Before returning to the main menu interrupts from the interface are disabled.

The program DIFF works in essentially the same way, however the initialisation procedure also writes to the control registers in the 6522 VIA (2), setting its T2 timer to act as a counter.The voltage output on pin PB7 of the 6522 VIA(1), occurring when its timer T1 is decrementing, is used to gate both the data and reference discriminators, the T2 counters of both VIAs are read on timeout.

Most of the data collection procedure was written in assembly language to minimise the dead time of the interface and so reduce the necessary data collection time. A scan of 1024 steps, with the maximum step duration of 65536μs took 70.4s, 3.29s of this therefore being dead time, the dead time, being the time needed to send out each step of the ramp and read the counters.

4.6 The Hardware

Figure 4.4 is a block diagram of the main components of the interface, showing their connections to the BBC micro. The circuit diagram of the mother board and first daughter board is given in Figure 4.5.

The mother board contains the circuitry common to both boards, the cleanup circuit, address decoder, buffer and gate. The daughter boards are identical, both containing a 6522 VIA and the circuit required to produce the analogue output voltage. In the present experiment, the second daughter board was only used to count pulses from Input 2, so the components required to generate a second voltage ramp are not shown in Figure 4.4. The following section describes each component of Figure 4.4 in more detail.

4.6.1 The BBC Micro and 1MHz Bus

The interface is connected to the 1MHz bus of the BBC Micro. This bus contains the eight data lines D0 to D7, the eight low address lines, A0 to A7 and two lines, NPGFC and NPGFD, signalling whether JIM or FRED are being addressed. JIM and FRED are names of two pages of memory, &FC and &FD respectively. Each page contains 256 memory locations and each location within the page is accessed by the low address byte. Both JIM and FRED contain some memory locations which have been set aside for user purposes, for FRED these addresses lie between &80 and &FF, and were used to access the registers in the 6522 VIAs in the interface.

The 1MHz bus also contains some logic lines. Of these the 1MHz line (1MHzE), reset (NRST), read/write (R/NW) and interrupt request (NIRQ) are used.The 1MHz line is connected to the φ_2 pins of both 6522 VIAs, and 'clocks' the two VIAs. The reset line is usually at +5V, on pressing the <BREAK> key on the BBC micro keyboard, this line is pulled down to 0V, resetting the registers in both 6522 VIAs. The read/write line is set to +5V by the BBC when the 6502 processor is executing a read operation and to 0V when executing a write operation. This line is connected to the R/NW pins of both 6522 VIAs; when a register in the VIA is addressed and this line is at low, data is transferred from the data bus and loaded into the register, correspondingly when a register is addressed and this line is high, the contents of the register are transferred to the data bus. The interrupt request line is

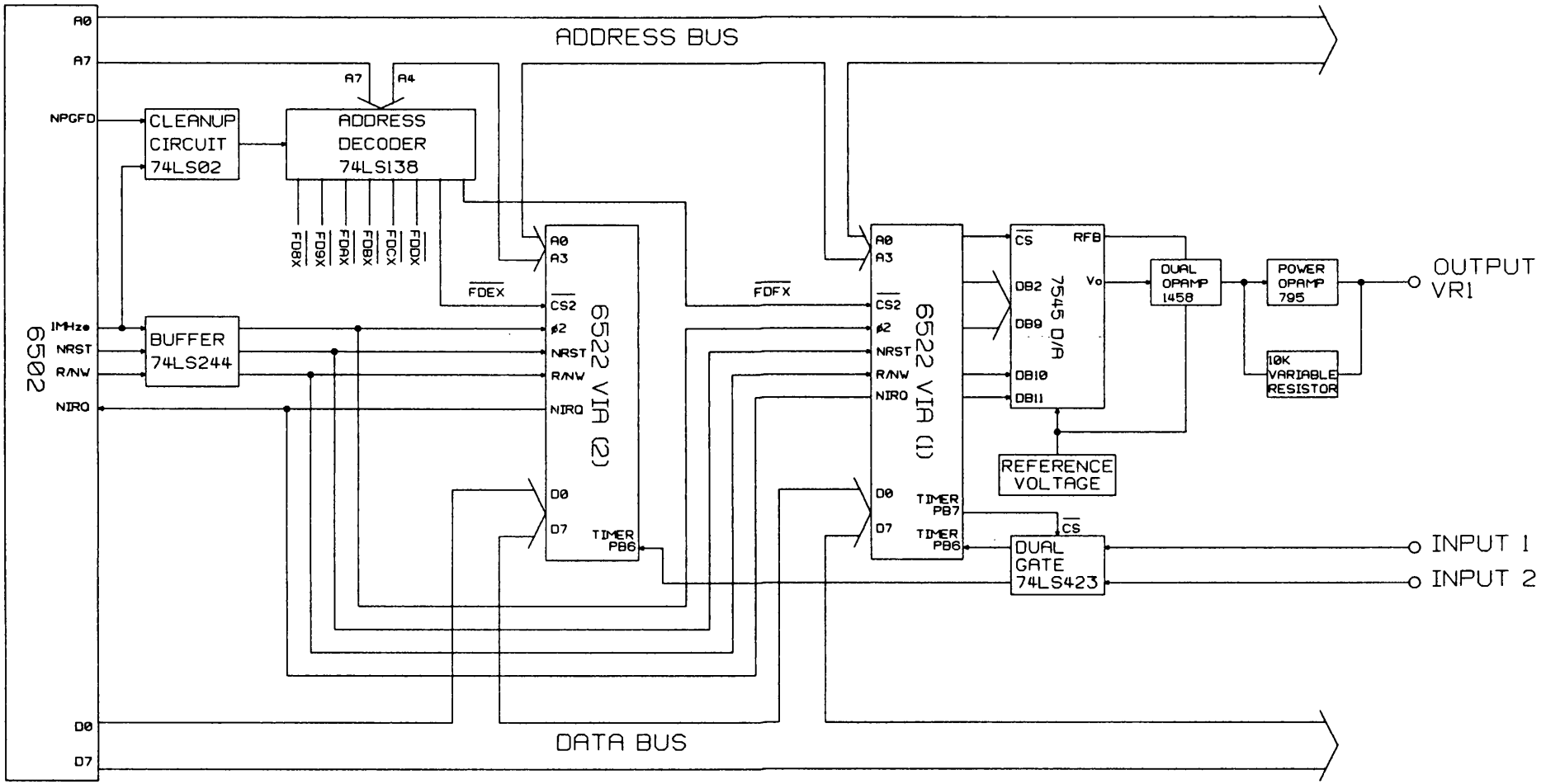

Figure 4.4 Block diagram of interface

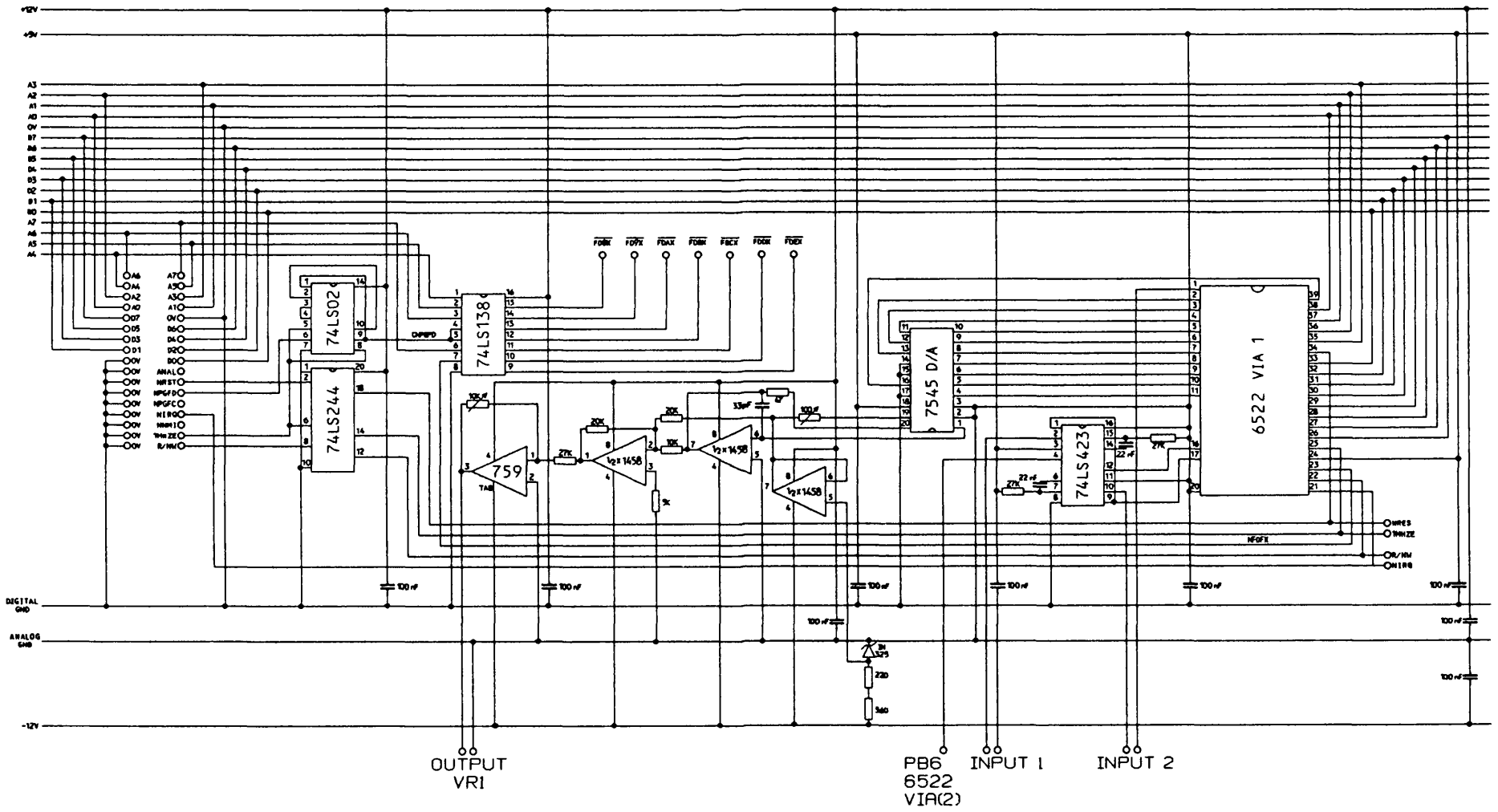

Figure 4.5 Circuit diagram of interface showing mother board and first daughter board

usually at +5V, and is connected to the NIRQ pins of both VIAs. When this line is pulled down to 0V, the 6502 is interrupted and jumps to an interrupt routine, the address of which is stored at the memory location &206. Section 4.6.5 gives more details of the operation of the 6522 VIA.

4.6.2 Clean Up Circuit (74LS02)

This IC is necessary because the 6502 microprocessor in the BBC Micro runs at 2MHz while all the 1MHz bus peripherals are clocked by a 1MHz square wave. Therefore after generating a valid 1MHz address a 'slow down' circuit stretches the clock high period, however the stretched wave suffers from spurious glitches which can result in the incorrect addressing of the 1MHz bus devices. The Clean Up Circuit overcomes this problem, for further details see the BBC Advanced Users Guide.

4.6.3 Buffer (74LS244)

No more than one low power Schottky TTL load should be presented to any of the logic lines of the BBC Micro, therefore all logic lines were buffered for each peripheral.

4.6.4 Address Decoder (74LS138)

This IC partially decodes the memory in FRED which is reserved for user applications, ie &FD80 to &FDFF. Address lines A4 to A7 are decoded so that each of the eight outputs, &FD8X, &FD9X to &FDFX, can be used to enable 16 addresses, X taking the values 0 to &F. When an address in the range &FDF0 to &FDFF is selected (when one of the 6522 VIA (1) registers is written to), the &FDEX line goes low. This line is connected to the chip select pin ($\overline{CS2}$) of the VIA (1), when this pin is low, data may be read from/written to the data bus (the operation being determined by the status of the R/NW line).

4.6.5 6522 Versatile Interface Adaptor (1)

The 6522 VIA (1) has 16 internal registers, including an interrupt flag register, interrupt enable register and two function control registers (PCR and ACR), its operational mode depends on how these registers are set. In the present experiment it is used to control the output from the digital to analogue convertor (7454 D/A), to control the gating of the incoming signal pulses and to count the pulses arriving from the pulse Input 1.

Port A and pins 0 and 1 of Port B are used to control the digital output to the D/A. To produce a ramp voltage of 1024 steps the numbers 000 to &3FF are written sequentially to these ports. This digital

data is latched into the D/A by a control pulse from pin CA2. CA2 is connected to the chip select pin ($\overline{CS}$) of the D/A and is preset to go low, by one of the 6522 VIA (1) control registers (PCR), for one cycle following a write operation to Port A.

Timer 1 is loaded with the required step time. It is preset, by one of the 6522 VIA (1) control registers (ACR), to start decrementing this number on loading the low byte, at the clock rate, and on reaching 0 to set the corresponding interrupt flag in the flag register. As soon as this timer starts to decrement, PB7 is set to zero, and is therefore used to enable the 74LS243 IC and so gate the incoming discriminator pulses.

Timer 2 is used as a counter. It is loaded with the number &FFFF at the start of each step and is set to decrement for each negative going pulse arriving at pin PB6. In this way the gated pulses from the data detector are counted for the duration of the step time. When Timer 1 has decremented to zero and set its interrupt flag, Timer 2 is read. The input pulses at Timer 2 require a minimum pulse width of $2\mu s$ and to be separated by $2\mu s$. In practice the input pulses were stretched to approximately $3\mu s$, limiting the maximum count rate that could be handled by the interface to 2.5×10^5, well above the maximum count rate which can be passed by the preamplifier.

4.6.6 6522 Versatile Interface Adaptor (2)

This is used to count the gated, negative going pulses from the reference detector, on pin PB6.

4.6.7 The Gate (774LS423)

This device gates pulses from both discriminators under the control of the output from pin PB7 of 6522 VIA (1). These signal pulses were inverted and stretched to approximately $3\mu s$ by this IC.

4.6.8 The Digital to Analogue Convertor (7545)

Although this is a 12 bit D/A only the 10 most significant bits were used as only 1024 steps were required in the output voltage ramp, the pins corresponding to the lowest two bits were therefore tied to 0V. The pins corresponding to the bits 2 to 11 were connected to Port A and pins 0 and 1 of Port B of the 6522 VIA (1). Data is latched into the D/A under the control of a negative pulse from pin CA2 of 6522 VIA (1). Table 4.1 shows the voltage levels at each of the 12 pins of the D/A and the corresponding output voltage for the ramp steps 0,510,511,512 and 1023 (1 corresponds to +5V and 0 to 0V).

	D/A PIN LEVEL												1458 OUTPUT	VR1 OUTPUT
step	11	10	9	8	7	6	5	4	3	2	1	0		
1023	1	1	1	1	1	1	1	1	1	1	1	1	-6.2 × 2044/2048	+0.499
512	1	0	0	0	0	0	0	0	0	1	0	0	−6.2 × 4/2048	+0.001
511	1	0	0	0	0	0	0	0	0	0	0	0	0V	0.000
510	0	1	1	1	1	1	1	1	1	1	1	1	+6.2 × 4/2048	-0.001
0	0	0	0	0	0	0	0	0	0	0	0	0	+6.2 × 2048/2048	-0.500

Table 4.1 Analogue Output voltages for steps 0-1023

4.6.9 The Reference Voltage and Dual Opamp 1458

The reference voltage is generated by the diode IN325 and half of a 1458 dual opamp, it produces a steady -6.2V. The other 1458 dual opamp amplifies the bipolar voltage output of the D/A up to the value of the reference voltage (see Table 4.1).

4.6.10 The Power Op-Amp (759) and 10K Variable Resistor

The power op-amp inverts the output from the dual opamp and reduces the maximum output range by a factor of 10/27 ie to a maximum output of ±2.3V. The ramp range may be further reduced, down to 0V, by means of the 10K variable resistor. In the present experiment, the range was set manually to ±0.5V, giving a step resolution of just under 1mV.

4.6.11 The Supply Lines

As no power should be drawn from the BBC micro computer, external ±12V and +5V power supplies were necessary to power the components in the interface.These were designed and built in house.

4.6.12 Earthing

The power supplies to each IC are decoupled from ground, as is the -6.2V reference voltage and the power rails themselves. This is to reduce the ripple voltage on the analogue output voltage. To reduce the ripple even further, to below 2mV, it was necessary to connect the disc drive box, monitor case, interface box, power supply box and all the cable shields, directly to the laboratory earth. The most

critical earth connection was found to be between the GRD of the video output of the BBC Micro and the laboratory earth.

Chapter 5 - Cross Section Calculation and Collision Region Geometry

5.1 Introduction

In the first section of this chapter the advantages of the collision region geometry used in the present experiment are described. The scattering equation used to calculate the elastic differential cross sections is then derived, followed by a description of the experimental procedure. Section 5.5 shows how a volumetric correction was found and applied to the elastic data. In Section 5.6, the equation used to calculate the inelastic differential cross sections is developed, and finally, in Section 5.7, the condition for single collision scattering is determined for each of the target gases.

5.2 The Collision Region Geometry

When conducting scattering experiments, two collision region geometries are commonly used, the 'cell' configuration and the 'crossed beam'. When a gas cell is used, the gas is confined in a collision chamber whose pressure and temperature can be measured accurately. Various collisions chambers which have been used are described in detail by Kuyatt (1968). In the crossed beam configuration, a target gas beam may be produced by flowing the gas through either a fine hole, capillary tube or an array of capillaries. Beam forming systems commonly used include hypodermic needles (eg Andrick and Bitsch 1975) and capillary arrays (eg Srivastava et al. 1975). The resultant gas beam is set up to intersect a monochromatic electron beam usually at 90°. For both cell and crossed beam configurations the energy and angular distributions of the electrons, scattered by the target molecules, may be determined as functions of the energy of the incident electron beam.

When a perfectly monochromatic electron beam is incident on a gas, there will be a spread in the interaction energy due to the thermal motion of the gas molecules, this spread in energy is called the Doppler Broadening and this broadening has been calculated by Chantry (1971). The full width at half maximum of his calculated energy distribution is given by

$$W_{\frac{1}{2}} = \sqrt{11.1\,\gamma\,k\,T\,E_0}\,, \tag{5.1}$$

where $\gamma = \dfrac{m}{m+M}$,

m = mass of projectile electron,

M = mass of target molecule,

k = Boltzmann's constant,

T = temperature of target gas (K),

E_0 = energy of incident electron (eV).

This expression may be simplified to

$$W_{\frac{1}{2}} = 12.3\left(\frac{E_0}{A}\right)^{\frac{1}{2}} \text{ meV} \tag{5.2}$$

assuming a gas beam temperature of 290K. A is the mass of the target molecule in atomic mass units.

For high resolution work the crossed beam technique is preferable to using a scattering chamber, as the Doppler Broadening can be significantly reduced (Read 1975). The reduction factor in the broadening, when using a gas beam, is of the order of $\frac{1}{2}\Delta_B$, where Δ_B is the full angular range (in radians) at half maximum intensity of the beam. Only in the case of a small aperture, when the gas has a cosine intensity distribution, which results in a Δ_B of 120°, is the Doppler broadening not reduced by using the crossed beam configuration. By using a hypodermic needle, the density distribution is much smaller and therefore Δ_B is considerably reduced. If the dimensions of the hypodermic needle and the gas pressure behind the needle are known Δ_B may be deduced using the data published by Lucas (1972). In the present experiment a needle of 0.3mm internal diameter and length 10mm was used and the gas pressure behind the needle was typically 5Torr; Δ_B for methane was therefore 50°, increasing to approximately 60° for ethene and ethane.

The maximum Doppler broadening would occur when using the target gas with the lowest molecular mass, ie methane, and when scattering at the highest electron energy, 15eV. From Equation 5.2, and after applying the reduction factor for the crossed beam configuration, the expected Doppler broadening for these conditions is of the order of 5meV.

By using the crossed beam geometry high target gas intensities can be obtained, of the order of 1000:1 with respect to the background gas intensity. Such ratios are advantageous as they give high scattering intensities while devices such as the electron channel multiplier, which are adversely affected by high pressures, can operate. The open geometry also allows stray electrons to escape.

5.3 The Scattering Equation

The detected electron current, of incident electron energy EeV, which has been elastically scattered at an angle θ from a single gas molecule is given by (Kuyatt 1968)

$$I_s(E,\theta) = I_0(E)\, n\, l \frac{d\sigma(E,\theta)}{d\Omega} T(E)\, d\Omega \ , \tag{5.3}$$

where $I_0(E)$ = incident electron current,

n = number of molecules per unit volume,

l = path length of electron beam through gas,

$\frac{d\sigma}{d\Omega}$ = elastic differential cross section,

$T(E)$ = transmission efficiency of the analyser ie) ratio of electrons entering the analyser optics to those detected by the channeltron,

$d\Omega$ = detector solid angle.

The product $l\, d\Omega$ is usually known as the effective path length of the electron beam through the gas.

For a fixed energy, the count rate recorded at the data detector, at scattering angle θ, is given by

$$D(\theta) = \frac{I_s(\theta)}{e} + \frac{I_0}{e} W(\theta) + Z_d \, , \tag{5.4}$$

where $\frac{I_0}{e} W(\theta)$ = count rate due to I_0 scattering off the cone aperture etc.
This is dependent on I_0 but independent of the pressure in the gas beam,

Z_d = count rate recorded which is independent of I_0, ie electrical noise,

e = electronic charge.

From Equations 5.3 and 5.4 the differential cross section at an energy E may be expressed as

$$\frac{d\sigma(\theta)}{d\Omega} = \frac{[D(\theta) - Z_d]\, e - I_0\, W(\theta)}{I_0\, n\, l\, d\Omega\, T} \,. \tag{5.5}$$

If all the quantities on the right hand side of Equation 5.5 could be measured absolutely, then $d\sigma(\theta)/d\Omega$ could be obtained. However, at low energies $ld\Omega$ cannot be measured with any great certainty, due to the electron lens aberrations and surface contact potentials introducing large uncertainties in the absolute electron density and flux distribution. Consequently it was decided that relative differential cross sections would be measured and these measurements put on an absolute scale by some other means as recommended by Register et al (1980).

One of the major sources of error in scattering experiments is the long term stability of the particle beams involved. Although the electron beam may be easily monitored during the collision experiment, the variation in the number density of a neutral molecular gas beam is less easily measured. In order to eliminate this dependence, a second, reference detector was used. This detector collected electrons scattered at a fixed angle, -90°

The following treatment shows how the data collected simultaneously at the two detectors was used to calculate the differential cross section, independently of the gas number density and $\frac{I_0}{e} W(\theta)$, the extraneous electrons scattered from the aperture in the cone etc.

Although a gas beam is used as a target, scattering also occurs from the background gas cell ie) the gas molecules which have diffused out of the beam. With the gas beam present in the apparatus the background pressure in the experimental tank increased from 1×10^{-8} to around 2×10^{-5}Torr. This background gas which is the same species as the target gas, will produce contributions to the scattered electron signals at both the data and reference detectors. Hence under normal operating conditions the observed electron scattering occurs not solely from the gas beam produced by the hypodermic needle but from a combination of the gas beam plus a 'gas cell' produced by the background target gas in the experimental chamber. By adopting the procedure (Andrick and Bitsch 1975, Newell et al 1981) of measuring the differential cross section for a 'cell plus beam' configuration with a primary electron beam I_0, and then repeating the measurements for the 'cell only' configuration with a primary electron beam I_0' and the cell pressure adjusted to the value of the measured background pressure produced by the presence of the gas beam in the first experiment, the effect of the cell background may be evaluated.

Equations 5.3 and 5.4 can now be rewritten as

$$D_{bc}(\theta) = \frac{I_0}{e}\left[n_b\, g_b(\theta) + n_c\, g_c(\theta)\right] \frac{d\sigma(\theta)}{d\Omega}\, T_d + \frac{I_0}{e}\, W(\theta) + Z_d \,, \tag{5.6}$$

where the bc subscript denotes that electrons scattered from both the gas beam and the cell contribution are being detected, $g_b(\theta)$ and $g_c(\theta)$ are the geometrical factors for the gas beam and cell respectively, replacing the quantities $(l\, d\Omega)_b$ and $(l\, d\Omega)_c$ and,

n_b = number density of gas beam,

n_c = number density of gas cell,

T_d = transmission of data analyser optics,

Z_d = dc noise measured by the data detector.

Similarly the count rate recorded at the reference detector is given by

$$R_{bc}(-90°) = \frac{I_0}{e}\left[n_b g_b(-90°) + n_c g_c(-90°)\right]\frac{d\sigma(-90°)}{d\Omega} T_r + \frac{I_0}{e} W(-90°) + Z_r . \tag{5.7}$$

By 'switching off' the gas beam but keeping the background gas pressure constant, the scattering due to the cell contribution may be measured (see Section 2.7 for details of this).

The data count rate for the gas cell measurements is given by

$$D_c(\theta) = \frac{I_0'}{e} n_c g_c(\theta)\frac{d\sigma(\theta)}{d\Omega} T_d' + \frac{I_0'}{e} W'(\theta) + Z_d' . \tag{5.8}$$

And the count rate at the reference detector by

$$R_c(-90°) = \frac{I_0'}{e} n_c g_c(-90°)\frac{d\sigma(-90°)}{d\Omega} T_r' + \frac{I_0'}{e} W'(-90°) + Z_r' . \tag{5.9}$$

Provided $W'(\theta) = W(\theta)$, then by combining Equations 5.6, 5.7, 5.8 and 5.9, it can be shown that

$$\frac{\frac{d\sigma}{d\Omega}(\theta)\left[T_d n_b g_b(\theta) + (T_d - T_d')\, n_c g_c(\theta)\right]}{\frac{d\sigma}{d\Omega}(-90°)\left[T_r n_b g_b(\theta) + (T_r - T_r')\, n_c g_c(\theta)\right]}$$

$$= \frac{D_{bc}(\theta) \quad - \frac{I_0}{I_0'} D_c(\theta) \quad - \left(Z_d - Z_d' \frac{I_0}{I_0'}\right)}{R_{bc}(-90°) - \frac{I_0}{I_0'} R_c(-90°) - \left(Z_r - Z_r' \frac{I_0}{I_0'}\right)}. \tag{5.10}$$

Finally, provided $T_d = T_d'$ and $T_r = T_r'$, this reduces to

$$\frac{\frac{d\sigma}{d\Omega}(\theta)}{\frac{d\sigma}{d\Omega}(-90°)} = \left\{ \frac{D_{bc}(\theta) \quad - \frac{I_0}{I_0'} D_c(\theta) \quad - \left(Z_d - Z_d' \frac{I_0}{I_0'}\right)}{R_{bc}(-90°) - \frac{I_0}{I_0'} R_c(-90°) - \left(Z_r - Z_r' \frac{I_0}{I_0'}\right)} \right\} \frac{T_r}{T_d} \frac{g_b(-90°)}{g_b(\theta)}. \tag{5.11}$$

As already stated, the major advantage of using Equation 5.11 rather than 5.5 to find the differential cross section, is that there is no longer any dependency on the gas number density. In the present experiment, therefore the number density of the gas beam was not measured.

Equation 5.11 is also independent of $\frac{I_0}{e} W(\theta)$, the electrons scattered from the aperture in the cone etc.

5.4 Procedure For Collecting The Elastic Differential Cross Sections.

The following procedure was carried out when collecting differential cross sections.

1. The electron beam was tuned for the required incident energy. This being set by the bias voltage applied between ground and the earth of the lens power supplies (see Figure 3.7).

2. The angular resolution of the electron beam was measured, and the analyser then returned to the zero angle position (see Section 3.8).

3. The gas beam was let into the tank for the required background pressure (see Sections 2.7 and 5.7).

4. The incident electron beam, I_0, was measured, by deflecting it onto the cone in the interaction region.

5. The bias voltages were measured.

6. The electrons arriving at both the data and reference detectors were counted simultaneously (see Section 4.4.2), as a function of angle. At each angle the collection time was sufficient for at least 10,000 counts to have been collected from both detectors, so giving a statistical accuracy of better than 1%. For each angle the count rates, D_{bc} and R_{bc}, were calculated and recorded.

7. The incident electron beam current, I_0, was remeasured.

8. The gas beam was switched off, and gas let into the experimental chamber via an opening in a side flange (Section 2.7) to give the same background gas pressure.

9. The incident electron beam current, I_0', was measured.

10. The count rates D_c and R_c were measured as a function of scattering angle θ as described in 6 above.

11. The incident electron beam current, I_0', was remeasured.

12. The bias voltages were remeasured.

The whole procedure was repeated four or five times, allowing the term on the left hand side of Equation 5.12 to be found:

$$\frac{d\sigma(\theta)}{d\Omega} g_b(\theta)\, K = \frac{D_{bc}(\theta) \quad - \frac{I_0}{I_0'} D_c(\theta) \quad - \left(Z_d - \frac{I_0}{I_0'} Z_d' \right)}{R_{bc}(-90°) - \frac{I_0}{I_0'} R_c(-90°) - \left(Z_r - \frac{I_0}{I_0'} Z_r' \right)}, \tag{5.12}$$

where

$$K = \frac{T_d}{T_r} \frac{1}{g_b(-90°) \frac{d\sigma}{d\Omega}(-90°)} \tag{5.13}$$

and is constant for a given molecular target

The cell contribution was found to contribute not more than 5% to the total scattered current.

As already mentioned in Section 4.4.2, the electrical background was usually extremely low allowing the terms in Z in Equation 5.12 to be neglected. However, the noise count rate was measured regularly over the period in which data was being collected and if it was found to approach 1% of the data or reference count rates its value was substituted into Equation 5.12.

Initially when using the reference detector, the term $\frac{I_0}{e} W$ was found to contribute significantly to the count rate, being up to 50% of R_{bc}. Although this would not effect the measurement of the elastic differential cross section, it made the initial tuning of the reference detector difficult. To overcome this a copper shield was made for this detector, the shield fitting around its optical bench. This prevented the electrons which were scattered off the interaction region cylinder from reaching the reference channeltron.

When using Equation 5.12, the assumptions that $T_r = T_r'$, $T_d = T_d'$ and $\frac{T_r}{T_d}$ are constant have to be made. For this to be true it is necessary that the spectrometer voltages are constant for the beam plus cell and cell alone measurements. For this reason on completing a set of angular measurements for the beam plus cell configuration at a given energy, the corresponding cell measurements were made straight away. The output of the bias supplies were checked at the beginning and end of each run. Only the data for which the bias voltages had remained unchanged (within ± 2mV) were recorded.

The volumetric term $g_b(\theta)$ in Equation 5.12 varies with angle and must be evaluated to allow the differential cross section to be found, the method used to evaluate this term is described in the next section.

5.5 The Volumetric Correction

As $g_b(\theta)$ is dependant on the scattering angle for most geometries, a geometrical correction factor must be found to enable the differential cross section to be determined. Only in the ideal case when the FWHM of the gas beam is well inside the acceptance angle of the detector will this correction be unnecessary, as in the experiment described by Shyn et al (1972). Previously a $\sin\theta$ correction has been applied to this apparatus (Curry 1984), however as shown by Brinkman and Trajmar (1980), this can lead to serious error. To find this term therefore, the experiment was repeated with helium. The elastic differential cross section for helium was measured as described in Section 5.4, for the same

energies and over the same angular range as was used for the three molecules being investigated. These measurements were substituted into the right hand side of Equation 5.12 yielding the term

$$\left[\frac{d\sigma(\theta)}{d\Omega}\right]^{(He)} g_b(\theta)^{(He)} K^{(He)} .$$

Williams (1979) has published the phase shifts of helium, calculated from his absolute measurements, with a stated accuracy of better than 5%. These phase shifts were interpolated for the energies used in the present experiment and the corresponding absolute cross sections calculated using the formula given by Nesbit (1979). On substituting the values measured in the present experiment into the right hand side of Equation 5.12, and the value of the absolute cross section into the LHS, the term $g_b(\theta)^{(He)} K^{(He)}$ may be found for helium.

Then provided

$$g_b(\theta)^{(molecule)} \propto g_b(\theta)^{(He)}$$

the relative cross sections for the any molecular target may be determined.

In the present experiment the pre and post-interaction region lenses were tuned identically to produce and receive a focussed electron beam which had a diameter of the order of 1mm at the centre of the collision region. Therefore the overlap of the incident electron beam with the acceptance cone of the detector was always within the gas beam for all the target gases (the tip of the hypodermic needle being 2.2mm from the centre of the collision region and Δ_B increasing from 40° for helium to 60° for ethane). The above proportionality is therefore valid.

5.6 The Measurement Of The Inelastic Differential Cross Sections

As already described in Section 4.4.1, energy loss spectra were collected over the energy range 0 - 0.5eV. For a fixed scattering angle θ, the scattered electrons with an energy loss ΔE are given by

$$I_s(E - \Delta E) = I_0 n l d\Omega \frac{d\sigma(E - \Delta E)}{d\Omega} T(E - \Delta E) . \qquad (5.14)$$

The count rate recorded at the data detector for the elastically scattered electrons is given by

$$D_{bc}(E) = \frac{I_0}{e}(n_b g_b + n_c g_c)\frac{d\sigma(E)}{d\Omega}T(E) + \frac{I_0}{e}W + Z_d \tag{5.15}$$

and for the electrons scattered with energy loss ΔE,

$$D_{bc}(E - \Delta E) = \frac{I_0}{e}(n_b g_b + n_c g_c)\frac{d\sigma(E - \Delta E)}{d\Omega}T(E - \Delta E) + \frac{I_0}{e}W + Z_d . \tag{5.16}$$

From Equations 5.15 and 5.16 the ratio of the cross section for the inelastically scattered electrons to the cross section for elastically scattered electrons is given by

$$\frac{\frac{d\sigma}{d\Omega}(E - \Delta E)}{\frac{d\sigma}{d\Omega}(E)} = \left\{\frac{D_{bc}(E - \Delta E) - \frac{I_0}{e}W - Z_d}{D_{bc}(E) \quad - \frac{I_0}{e}W - Z_d}\right\}\frac{T_d(E)}{T_d(E - \Delta E)}. \tag{5.17}$$

The quantities within the brackets may all be determined from the energy loss spectra, the dc electrical noise, Z_d, appearing as a horizontal continuum, $\frac{I_0}{e}W$ (when present) as a sloping continuum, falling smoothly from the centre of the spectrum and D_{bc} by the magnitude of the peaks. The transmission correction term was calculated as described in Section 3.10.

Once the energy loss spectrum has been corrected for the terms T_d, $\frac{I_0}{e}W$ and the transmission correction, the areas under the elastic peak $A(E)$ and inelastic peak $A(E - \Delta E)$ may be found (see Section 7.2). The inelastic cross section is then given by

$$\frac{d\sigma(E - \Delta E)}{d\Omega} = \frac{A(E - \Delta E)}{A(E)}\frac{d\sigma(E)}{d\Omega}. \tag{5.18}$$

Absolute inelastic cross section may be obtained if absolute elastic cross sections are substituted into the above equation.

5.7 Determination Of The Background Pressure For Single Collisions

Equation 5.3 is only valid for single collision conditions, ie an incident electron experiences only one molecular collision before being detected. It was necessary therefore to find the maximum gas flow at which single collisions still occurred. To do this the scattered electron count rate, at a fixed scattering angle (40°) and incident electron energy of 2.81eV, was measured as a function of the background gas

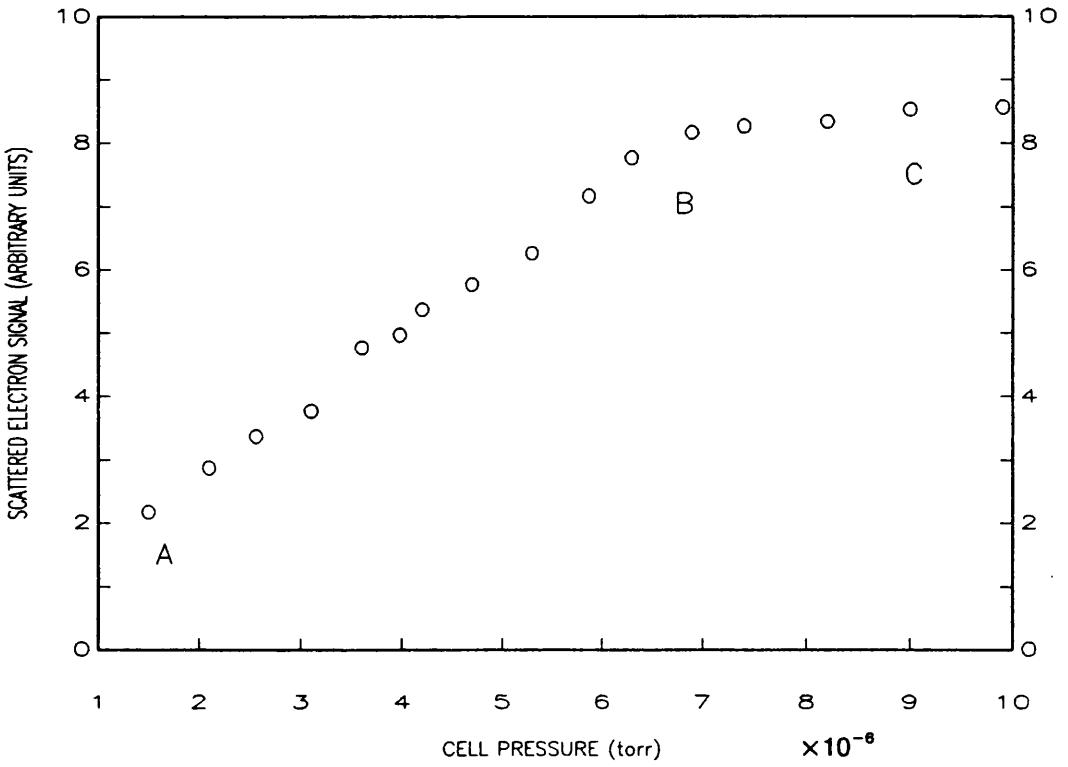

Figure 5.1 Elastically scattered electron signal vs cell pressure for helium

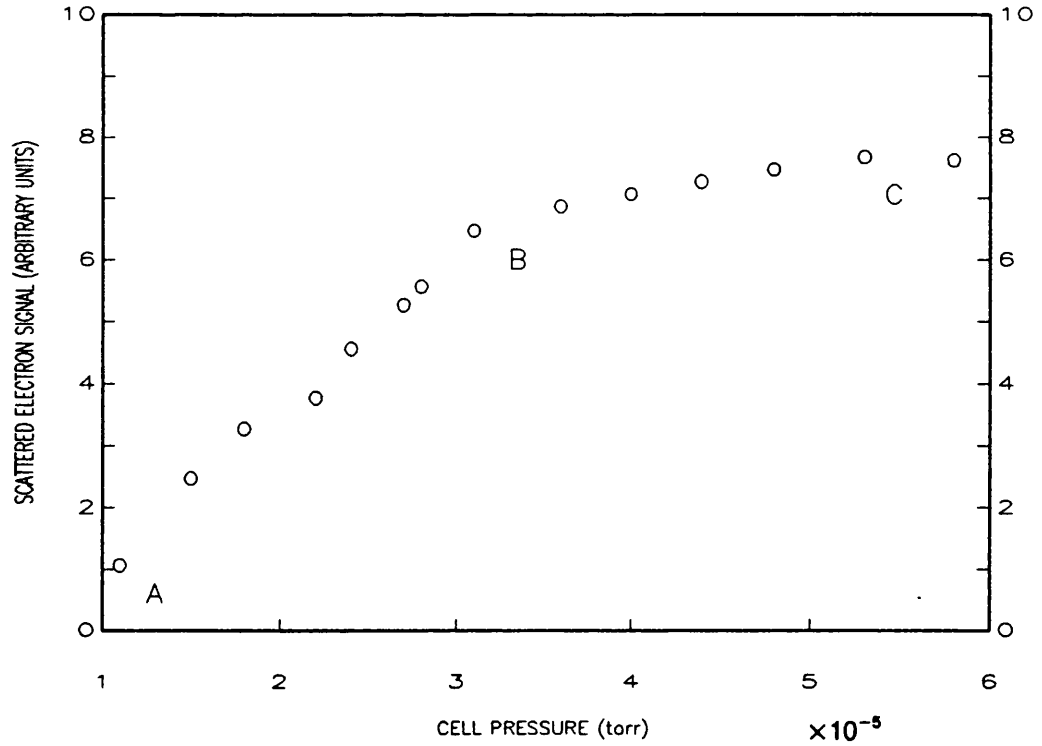

Figure 5.2 Elastically scattered electron signal vs cell pressure for methane

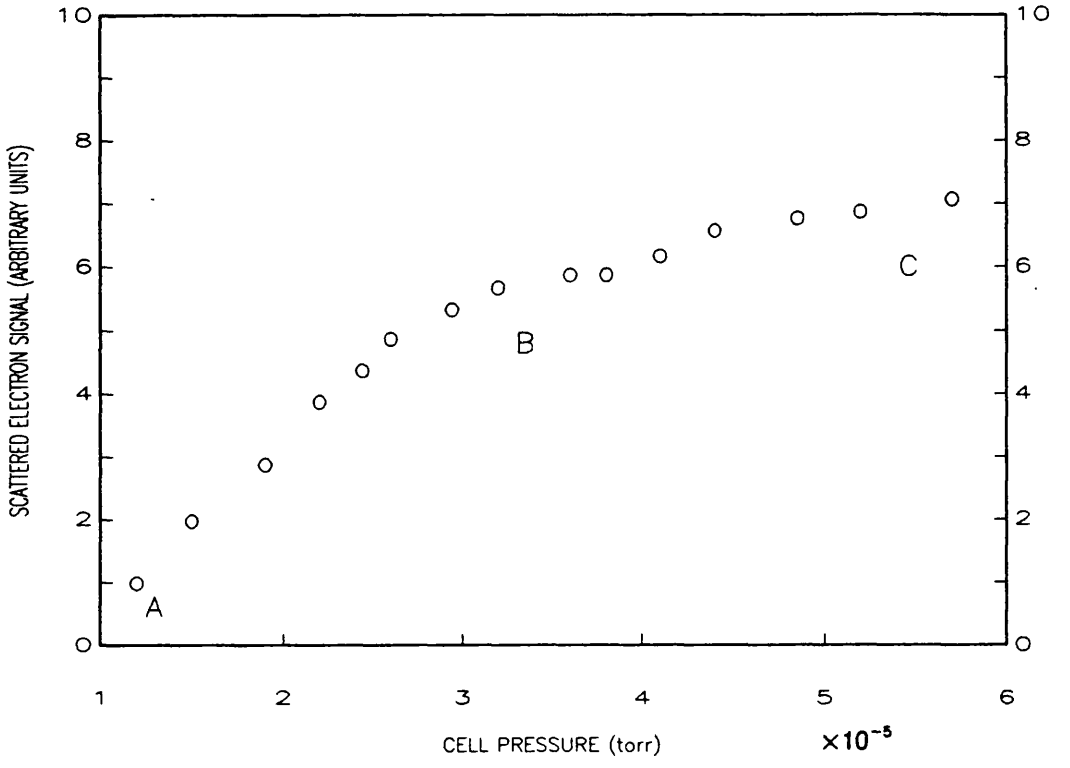

Figure 5.3 Elastically scattered electron signal vs cell pressure for ethene

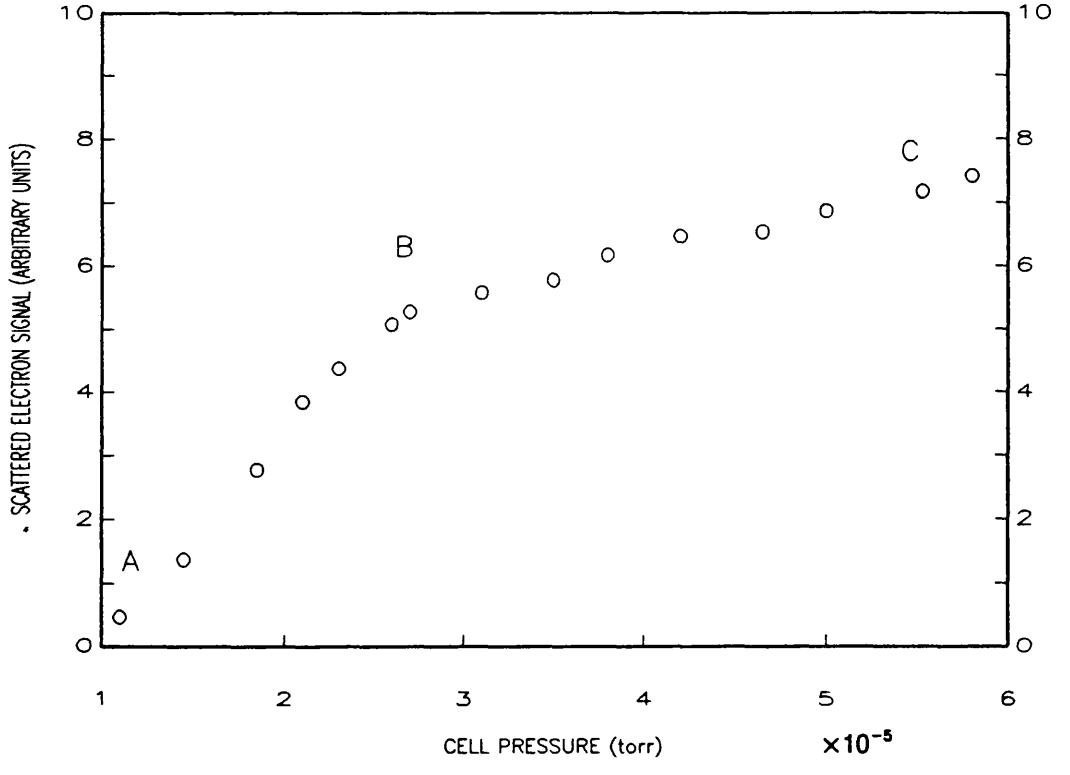

Figure 5.4 Elastically scattered electron signal vs cell pressure for ethane

pressure, as the flow of gas to the hypodermic needle was increased in stages. After each increase in the gas flow I_0 was measured so that the count rates could be corrected for any variation in the incident electron beam intensity. These measurements were carried out for each of the target gases used, methane, ethene, ethane and helium and are shown in Figures 5.1 to 5.4.

The initial linear region, between A and B corresponds to single collision conditions. This is followed by a non linear region B to C, indicating the onset of multiple scattering. The maximum permissible background pressure for each of the target gases was found from these graphs and is shown in Table 5.1.

Gas	Maximum Background pressure /Torr
helium	5×10^{-6}
methane	2×10^{-5}
ethene	2×10^{-5}
ethane	2×10^{-5}

Table 5.1 Pressure below which single electron - molecule collisions occur.

Chapter 6 - Elastic Scattering of Electrons From Methane, Ethene and Ethane

6.1 Introduction

The elastic differential scattering cross section results for methane,ethene and ethane are presented in this chapter. Knowledge of the elastic electron scattering properties of various gases is of central importance in the study of a wide variety of plasma phenomena because the effective momentum transfer cross section of electrons in gases is usually dominated by the elastic scattering process for electron energies below the threshold for electronic excitation. It is the variation of the momentum transfer cross section with incident energy that produces the corresponding variations in the expressions for the electron conductivity, diffusion coefficients and other transport properties of electrons in gases. Consequently, the magnitude and energy dependence of the elastic scattering differential cross sections for the gaseous media strongly influence the passage of electrons through the gas.

The hydrocarbons studied in the present experiment are all constituents of the planetary atmospheres of Jupiter and Saturn and its moon Titan. It is only in the last ten years that significant advances have been made in the study of these planetary atmospheres from the earlier Pioneer spacecraft and more recently the Voyager missions. The two space probes Voyager 1 and 2 made flybys of Jupiter in 1979 and Saturn in 1981 and 1982 and increased the understanding of these planets significantly. Although only making up a few percent of the overall atmosphere, the hydrocarbon presence is significant, and in the case of Jupiter the presence of ethene has been used in one of the many theories concerning the existence of the Great Red Spot (Hunt 1980). Good cross section data is required for realistic modeling of these atmospheres.

6.2 Analysis of Results

The data for the calculation of the elastic differential cross sections was collected, over the angular range $30° \leq \theta \leq 140°$ for each incident electron energy, as described in Section 5.4 and substituted into the right hand side of Equation 5.12 to give $M(\theta)$ where

$$M(\theta) = \frac{d\sigma(\theta)}{d\Omega} g_b(\theta) K \ . \tag{6.1}$$

This procedure was repeated four or five times, then for a particular molecular target and energy the mean value of M(θ) was found, together with its statistical error $\Delta M(\theta)$, for each value of θ.

From Equation 6.1 the relative differential cross section for any molecule is given by

$$\frac{d\sigma(\theta)}{d\Omega} \propto \frac{M(\theta)}{g_b(\theta)}, \tag{6.2}$$

therefore to determine the relative cross section the angular dependent term $g_b(\theta)$ must be found. In the present experiment (see Section 5.5)

$$g_b(\theta)^{(molecule)} \propto g_b(\theta)^{(He)}, \tag{6.3}$$

where

$$g_b(\theta)^{(He)} \propto \frac{M(\theta)^{(He)}}{\frac{d\sigma}{d\Omega}(\theta)^{(He)}}. \tag{6.4}$$

The measurements described in Section 5.4 were therefore repeated with helium and $M(\theta)^{(He)}$ found. The differential cross section of helium, $d\sigma(\theta)/d\Omega^{(He)}$, has been measured many times (eg Andrick and Bitsch 1975, Steph et al 1979, Newell et al 1981), in the present experiment it was calculated from the phase shifts published by Williams (1979). The relative differential cross section for any target gas may then be calculated from

$$\frac{d\sigma(\theta)^{(rel)}}{d\Omega} \propto M(\theta) \frac{\frac{d\sigma(\theta)^{(He)}}{d\Omega}}{M(\theta)^{(He)}}, \tag{6.5}$$

and the associated error is given by

$$\left(\frac{\Delta d\sigma(\theta)/d\Omega^{(rel)}}{d\sigma(\theta)/d\Omega^{(rel)}}\right)^2 = \left(\frac{\Delta M(\theta)}{M(\theta)}\right)^2 + \left(\frac{\Delta d\sigma(\theta)/d\Omega^{(He)}}{d\sigma(\theta)/d\Omega^{(He)}}\right)^2 + \left(\frac{\Delta M(\theta)^{(He)}}{M(\theta)^{(He)}}\right)^2. \tag{6.6}$$

Wherever possible the data was normalised to put it on an absolute scale. In the case of methane the data was normalised to the fitted measurements of Tanaka et al (1982) at scattering angle 80°. This angle was chosen as it is equidistant from the minima which occur at 40 and 120°. The data of Tanaka et al was plotted and interpolated to find the absolute differential cross sections for the energies used in the present experiment. The experimental data for ethane was normalised to that of Tanaka et al (1988) in the same way. However for this gas the normalisation angle was chosen to be 50° as at this angle the smoothest curve of $d\sigma/d\Omega$ vs energy was obtained with the data of Tanaka et al allowing for

the most accurate normalisation. It was only possible to normalise the data of ethene at the two highest energies of 15 and 7.5eV, the only communicated data being that of McKoy (1987). The angle of normalisation was taken to be 50°.

The absolute differential cross section for methane is therefore found from

$$\frac{d\sigma(\theta)^{(abs)}}{d\Omega} = M(\theta)\, V(\theta)\, N(\theta)\,, \tag{6.7}$$

where

$$V(\theta) = \frac{\dfrac{d\sigma(\theta)^{(He)}}{d\Omega}}{M(\theta)^{(He)}}\,,$$

$$N(\theta) = \frac{\dfrac{d\sigma(80°)^{(Tanaka)}}{d\Omega}}{\dfrac{d\sigma(80°)^{(rel)}}{d\Omega}}\,.$$

The associated error is given by

$$\left(\frac{\Delta d\sigma(\theta)/d\Omega^{(abs)}}{d\sigma(\theta)/d\Omega^{(abs)}}\right)^2 = \left(\frac{\Delta M(\theta)}{M(\theta)}\right)^2 + \left(\frac{\Delta V(\theta)}{V(\theta)}\right)^2 + \left(\frac{\Delta N(\theta)}{N(\theta)}\right)^2 \tag{6.8}$$

which is equivalent to

$$\left(\frac{\Delta d\sigma(\theta)/d\Omega^{(abs)}}{d\sigma(\theta)/d\Omega^{(abs)}}\right)^2 = \left(\frac{\Delta M(\theta)}{M(\theta)}\right)^2 + \left(\frac{\Delta d\sigma(\theta)/d\Omega^{(He)}}{d\sigma(\theta)/d\Omega^{(He)}}\right)^2 + \left(\frac{\Delta M(\theta)^{(He)}}{M(\theta)^{(He)}}\right)^2 + \left(\frac{\Delta d\sigma(80°)/d\Omega^{(Tanaka)}}{d\sigma(80°)/d\Omega^{(Tanaka)}}\right)^2$$

$$+ \left(\frac{\Delta M(80°)}{M(80°)}\right)^2 + \left(\frac{\Delta d\sigma(80°)/d\Omega^{(He)}}{d\sigma(80°)/d\Omega^{(He)}}\right)^2 + \left(\frac{\Delta M(80°)^{(He)}}{M(80°)^{(He)}}\right)^2. \tag{6.9}$$

The absolute differential cross sections for ethene and ethane are found in the same way, their normalisation terms being given by

$$N(\theta)=\frac{\frac{d\sigma(50°)^{(McKoy)}}{d\Omega}}{\frac{d\sigma(50°)^{(rel)}}{d\Omega}} \tag{6.10}$$

and

$$N(\theta)=\frac{\frac{d\sigma(50°)^{(Tanaka)}}{d\Omega}}{\frac{d\sigma(50°)^{(rel)}}{d\Omega}} \tag{6.11}$$

respectively.

The values of the elastic differential cross sections and the associated errors were calculated using the above expressions and are listed in Tables 6.1, 6.2 and 6.3. The data has been plotted in Figures 6.1 to 6.18 together with other published data at the same (or similar) incident electron beam energies. The incident electron energies given for the present measurements have been corrected for the contact potentials listed in Table 3.3 and are given in the legend of each graph. The energies given in the graph titles are those of the nearest comparison data. These values are used throughout, even when no comparison data exists, to aid comparison between the different molecules.

6.3 Discussion of the Elastic Results for Methane and Comparison with Other Work

Methane is the simplest of all organic molecules and has therefore attracted extensive experimental and theoretical studies since the early 1930s. These investigations which were reviewed in Chapter 1 have shown the existence of a Ramsauer minimum (at 0.4eV) followed by a broad maximum possibly due to a shape resonance (centred near 8eV) in the total cross section.

Methane has become of particular interest to atmospheric physics since it was found to contribute significantly to the greenhouse effect. Absolute differential cross sections are needed as a test of the latest developments in theory and to verify other experimental methods and results.

Resonances are quasi discrete states of the molecule plus electron that may be formed during a scattering process; they are embedded in and interact with a continuum of scattering states and their existence is inferred from structure in the appropriate scattering cross section function, occurring at energies around the energy of the resonance state. When a electron approaches a molecule with large collision angular momentum there is a repulsive centrifugal force $L^2/2\mu r^2$, where L is the angular

momentum and μ is the electron-molecule reduced mass; when this repulsive potential is taken in conjunction with the static attractive electron-molecule interaction, a barrier can be formed. This potential barrier is such a shape to allow the existence of a resonance state whose energy is above the limit of the parent molecular state. This resonance state decays into available channels, the ground state and perhaps vibrationally excited states of the molecule so that structure is observed in the elastic and perhaps other scattering cross section functions.

From the shape of the differential cross sections it is possible to deduce that a resonance state has been excited. This is because usually only one partial wave is expected to participate in a resonance scattering which gives rise to a characteristic shape in the differential cross section curve. If no resonant scattering has occurred, at very low energies the differential cross section is nearly isotropic (because the centrifugal barrier excludes all but the s-wave scattering). As the incident electron energy increases, the differential cross section generally becomes more forward peaked as more partial waves contribute to the scattering process and also the electron transfers less and less momentum to the molecule.

Figures 6.1 to 6.6 show the elastic differential cross section of methane as a function of scattering angle and incident energy. Also included are the previous experimental results of Bullard and Massey (1931), Hughs and McMillan (1933), Tanaka et al (1982), Curry et al (1985) and Sohn et al (1986) together with the theoretical results of Jain and Thompson (private communication 1989). The results of Hughs and McMillan (1933) and Bullard and Massey (1931) were published in relative units and have therefore been normalised to Tanaka et al (1982) at 80° to aid comparison with the present data.

	Incident energy (eV)					
Angle (deg)	15.4eV	7.9eV	6.0eV	4.9eV	4.2eV	3.2eV
30	3.57 ± 0.50	3.48 ± 0.55	1.81 ± 0.60	1.45 ± 0.37	0.78 ± 0.08	0.40 ± 0.07
40	2.21 ± 0.41	2.20 ± 0.35	1.35 ± 0.31	1.14 ± 0.15	0.85 ± 0.12	0.46 ± 0.09
50	1.75 ± 0.22	1.80 ± 0.28	1.42 ± 0.30	1.16 ± 0.16	1.11 ± 0.15	0.54 ± 0.09
60	1.08 ± 0.12	1.43 ± 0.22	1.30 ± 0.24	1.25 ± 0.16	1.19 ± 0.17	0.94 ± 0.16
70	0.65 ± 0.09	1.39 ± 0.20	1.42 ± 0.26	1.36 ± 0.19	1.19 ± 0.16	0.81 ± 0.15
80	0.50 ± 0.06	1.32 ± 0.21	1.38 ± 0.25	1.30 ± 0.18	1.14 ± 0.16	0.85 ± 0.16
90	0.40 ± 0.06	0.98 ± 0.14	1.18 ± 0.20	1.02 ± 0.15	1.01 ± 0.15	0.83 ± 0.14
100	0.29 ± 0.04	0.62 ± 0.09	0.81 ± 0.12	0.86 ± 0.10	0.86 ± 0.13	0.62 ± 0.10
110	0.27 ± 0.04	0.27 ± 0.08	0.41 ± 0.10	0.46 ± 0.07	0.73 ± 0.11	0.34 ± 0.08
120	0.32 ± 0.04	0.17 ± 0.03	0.22 ± 0.06	0.26 ± 0.06	0.42 ± 0.09	0.22 ± 0.06
130	0.43 ± 0.06	0.46 ± 0.15	0.45 ± 0.08	0.40 ± 0.09	0.25 ± 0.06	0.20 ± 0.08
140	0.57 ± 0.10	0.94 ± 0.20	0.80 ± 0.15	0.73 ± 0.11	0.53 ± 0.15	0.27 ± 0.09

Table 6.1 Differential elastic cross sections for CH_4 ($10^{-16}cm^2\ sr^{-1}$)

Figure 6.1 Methane 15eV

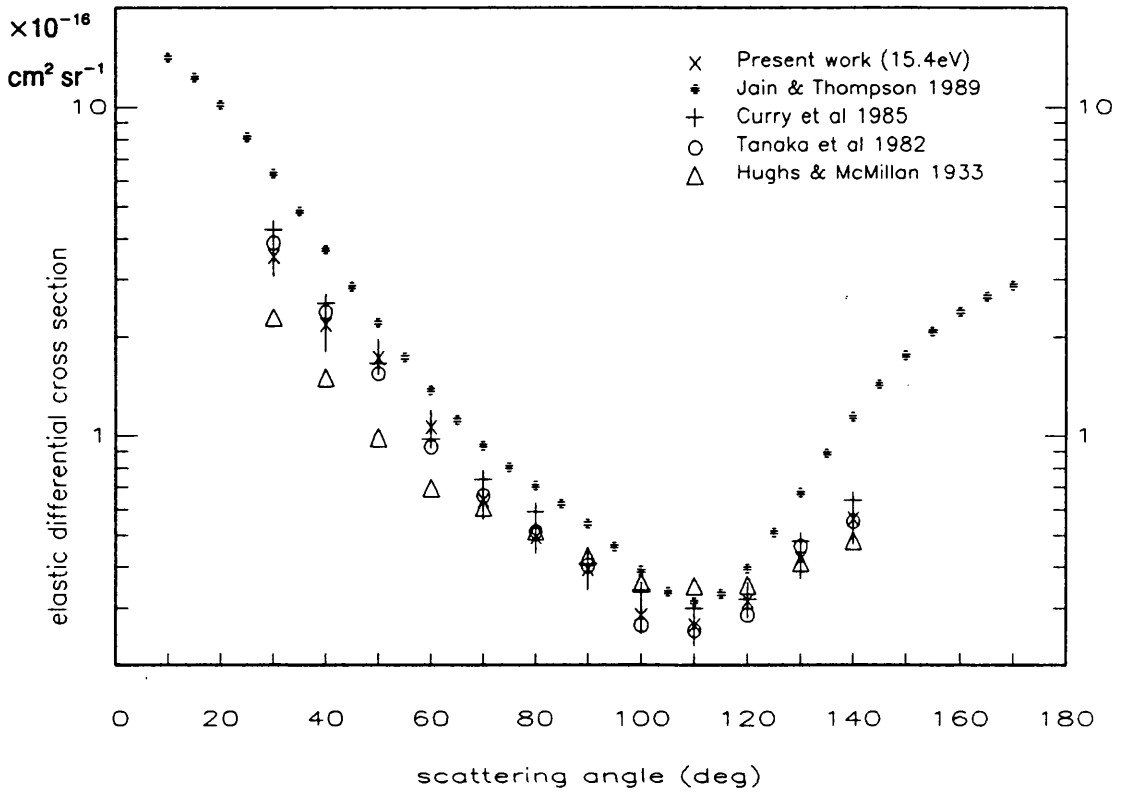

Figure 6.2 Methane 7.5eV

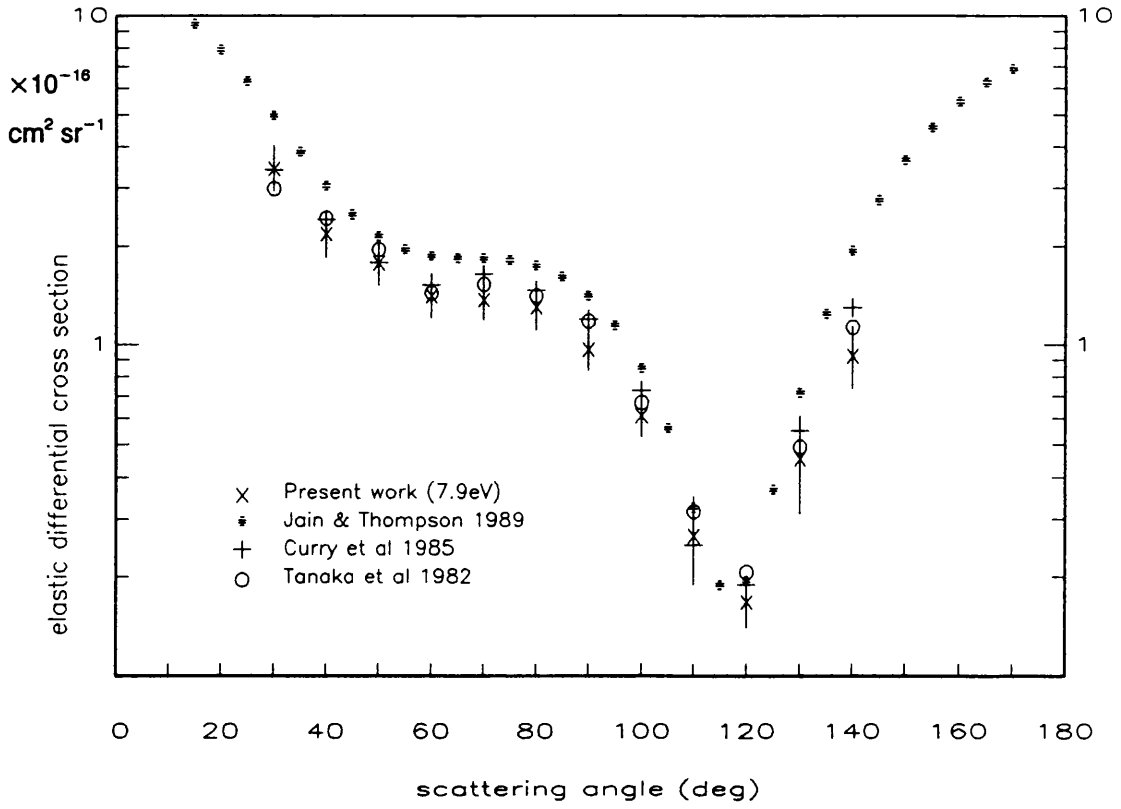

Figure 6.3 Methane 6eV

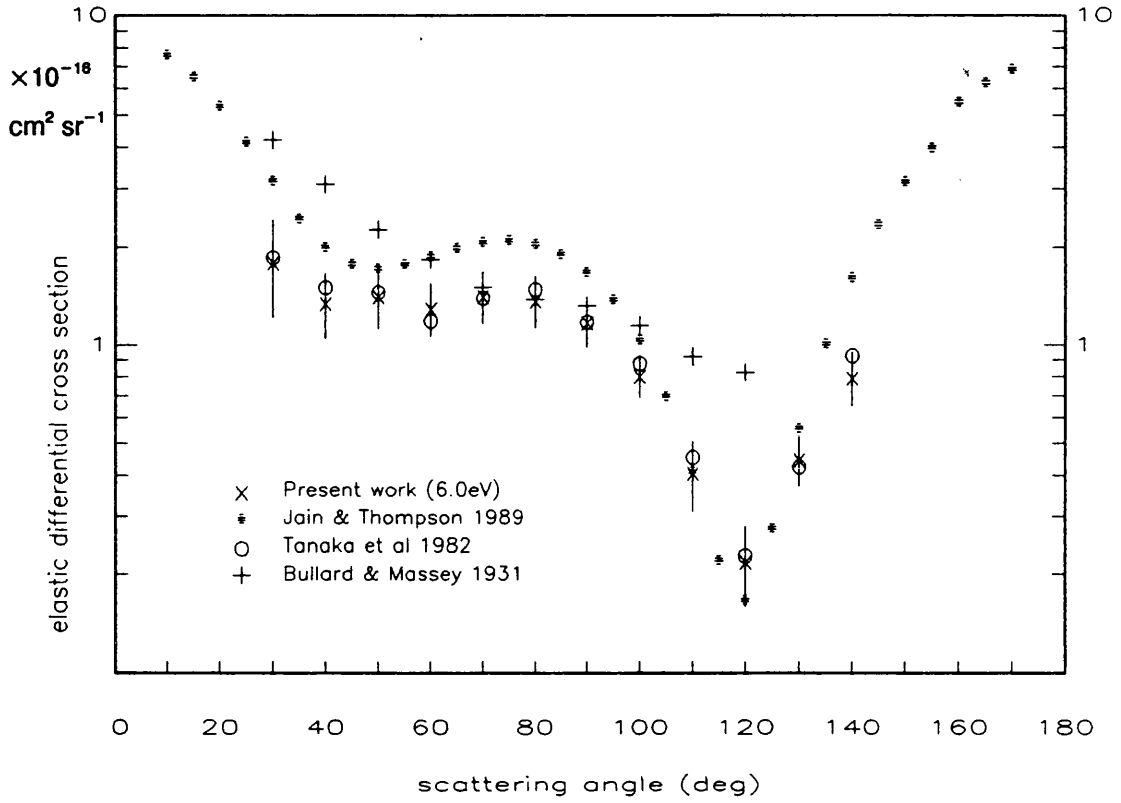

Figure 6.4 Methane 5eV

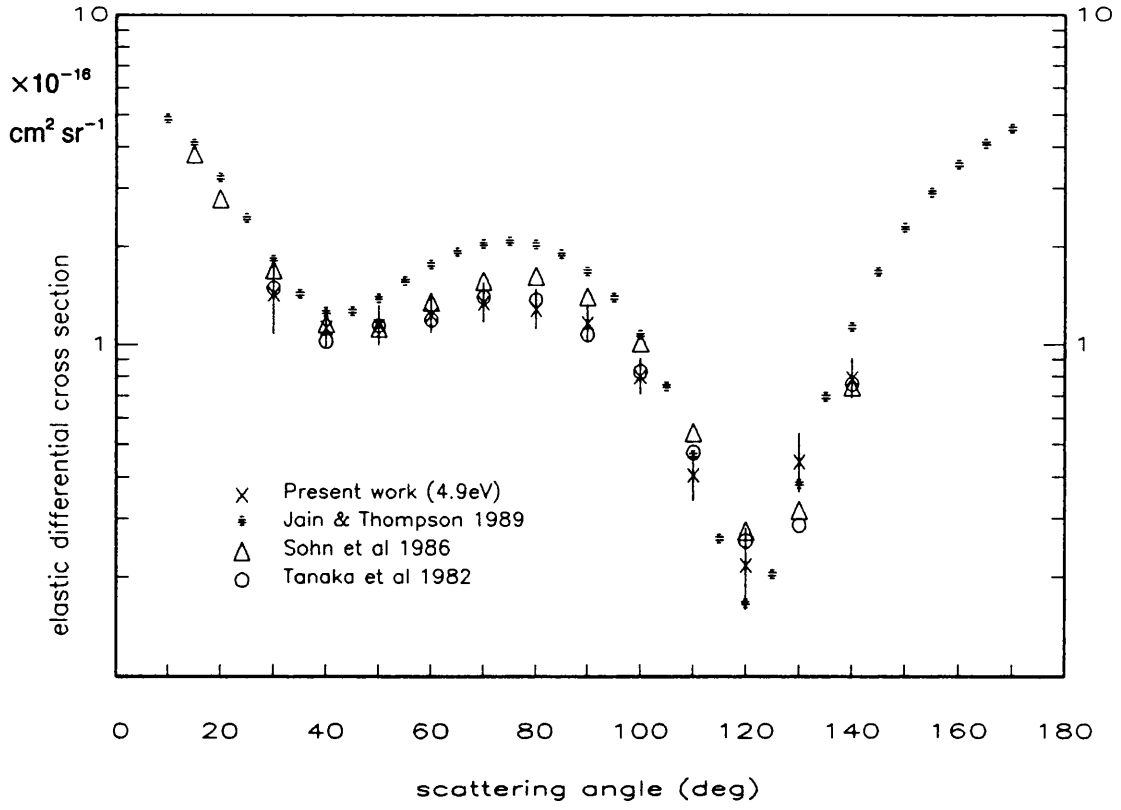

Figure 6.5 Methane 4eV

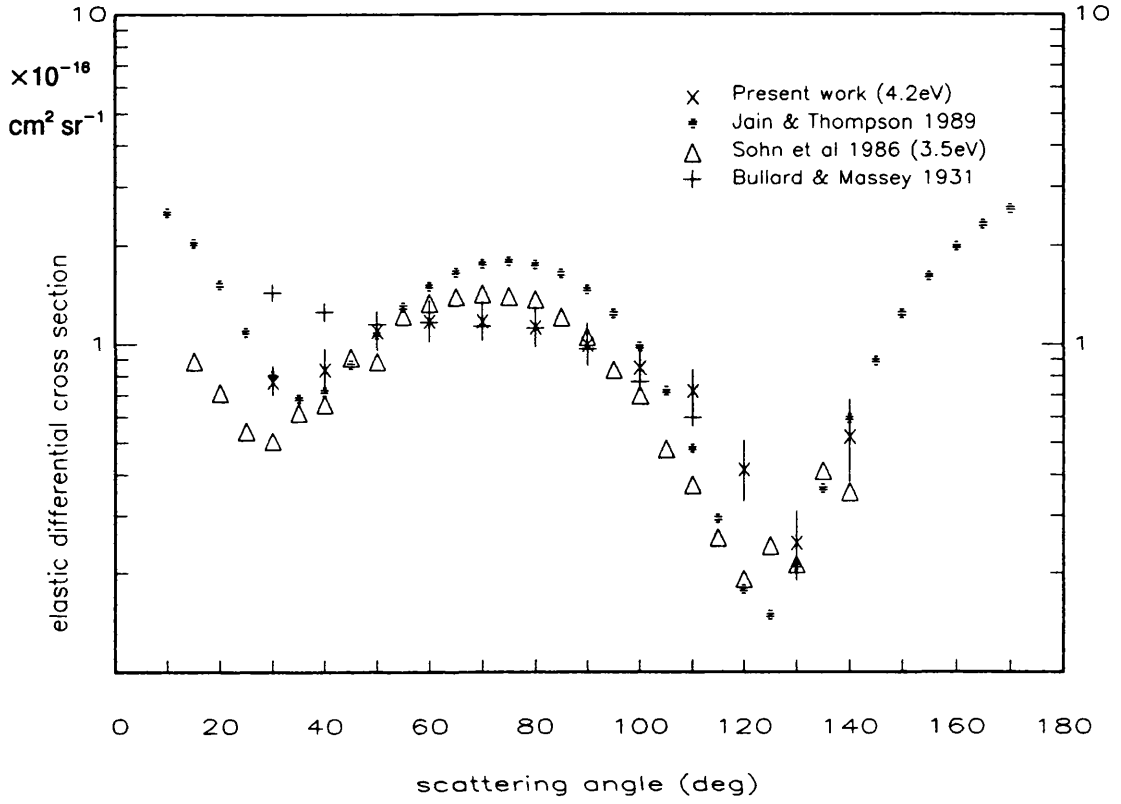

Figure 6.6 Methane 3eV

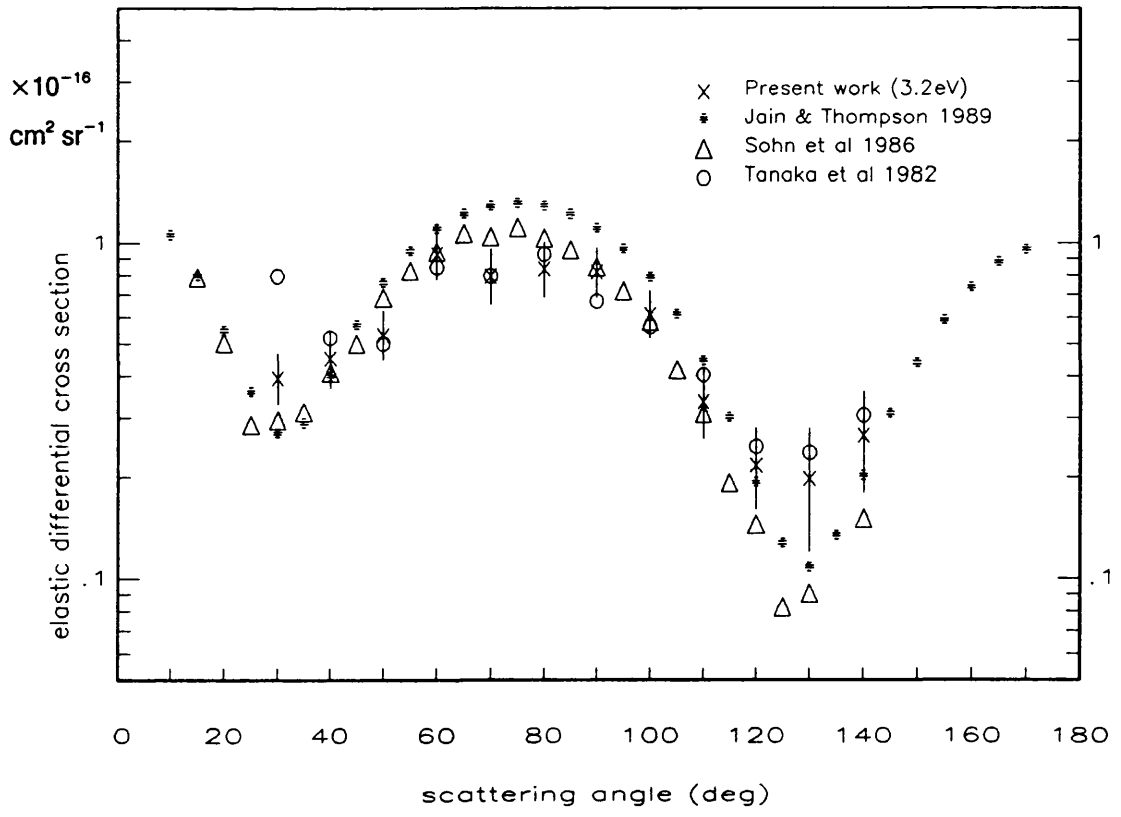

At 15eV the present results are in good agreement with both the measurements of Tanaka et al and Curry et al, the major feature in the cross section being a broad minimum at 110°. The earlier results of Hughs and McMillan also display this minimum, although theirs is slightly broader than the present result. The largest discrepancy, however, occurs between 30 and 60°. Here the magnitude of their differential cross section is considerably lower, by approximately a factor of 2. The theoretical results of Jain and Thompson display the same shape as the present data but is generally greater in magnitude, this is particularly noticeable at the higher angles.

At 7.5eV, a shallow minimum at 60° is apparent in the present data and also in that of Tanaka et al and Curry et al. The theoretical data displays a shoulder between 50 and 80°. The sharper minimum at the higher angle has shifted slightly to 120° in all the data sets.

In Figure 6.3, the present results are compared to those of Tanaka et al and Bullard and Massey. Both the present data and that of Tanaka et al and Jain and Thompson show a deep minimum at 120°. At the lower angles there is a shallow minimum between 40 and 60° in both the present data, that of Tanaka et al and in that of Jain and Thompson. This minimum is not apparent in the data of Bullard and Massey.

At 5eV the present data is compared with that of Tanaka et al, Sohn et al and Jain and Thompson. The agreement is good, all data showing a broad minimum centred between 40 and 50°, and a much deeper minimum at 120°.

In Figure 6.5 the present data at 4.2eV has been plotted with that of Sohn et al at 3.5eV, and that of Bullard and Massey and Jain and Thompson at 4eV. The data of Bullard and Massey has no strong characteristics at this energy, falling off slowly from 30° to a plateau between 50 and 80°, then again falling slightly to 110°, their highest angle at this energy whereas the other sets of data display minima between 30 and 40° and 120 and 130°. The data of Sohn et al is significantly lower than the calculated values of Jain and Thompson between the angles 15 and 30°, however this may be a consequence of the difference in collision energies, as the cross section between these angles is significantly lower at 3eV (see Figure 6.6).

In Figure 6.6 the 3eV data of Tanaka et al, Sohn et al and Jain and Thompson has been plotted with the 3.2eV data of the present experiment. All sets of data display a well defined maximum between 60 and 80°. The data of Sohn et al, Jain and Thompson and possibly the present data also display minima at 30 and 130°. The low angle minimum of Tanaka et al is positioned at 40° and is at variance with the present work and current theory.

To summarize, the present cross sections show a deep minimum which moves from 110° at 15.4eV to 130° at 3.2eV,becoming less pronounced as the incident electron energy is decreased. As the electron energy is reduced a second minimum becomes visible, appearing initially as a plateau centred at 60° at 7.9eV then moving to 40° at the lower energies while at the same time becoming deeper and less broad.

The shape of the curves at the lower energies indicate a fairly large contribution from d-wave scattering, this being characterised by two minima near 60 and 120° with a maximum at 90°. As the impact energy increases the influence of the d-wave scattering decreases, the minimum at 60° changing to a plateau at 7.5eV and disappearing at 15eV. Methane belongs to the symmetry group T_d and has the ground state configuration $1a_1^2 2a_1^2 1t_x^2 1t_y^2 1t_z^2$, yielding an $^1A_1$ ground state. In their total cross section calculations (discussed in Section1.6) Gianturco and Thompson (1976) have attributed the broad resonance structure at about 7eV to a T_2 wavefunction contribution with a strong $L = 2$ partial wave portion. Based on group theory Read (1968) has given general expressions for the angular distribution for resonant scattering of electrons by the cubic T_d molecules. According to that work, the dominant partial waves for this experiment are expected to be p and d waves, the latter characterising the present angular distribution in the low energy range.

Generally good agreement is found with the measurements of Tanaka et al, Curry et al and Sohn et al. When compared with the earlier data of Hughs and McMillan and Bullard and Massey the agreement is not so good. The discrepancies between the curves of Bullard and Massey, Hughs and McMillan and the present data can be accounted for by the lower angular and energy resolution of the earlier experiments. The higher angular resolution possible with modern spectrometers allows narrower structures to be observed. The superior energy resolution ensures that there is no contribution to the elastically scattered signal from electrons which have undergone energy loss/gain. Further evidence for this may be seen by the improved agreement between these early results and the recent measurements of Tanaka et al (1982) at the higher energy of 20eV; at this energy there are no narrow minima, and the vibrational cross sections are small and of less importance.

As first observed by Bullard and Massey (1931), there is some similarity between the elastic differential cross section of methane and that of argon (see Figure 1.3). Both molecules display two minima at low impact energies, ie below 10eV. The first minimum of argon is consistently at a lower angle and deeper than that of methane, the second minimum, however, like that of methane, is situated between 110 and 130°. These results suggest that methane and argon present similar effective scattering potentials to low energy electrons. There is no resemblance between the cross sections for electron energies greater than 10eV.

The calculations of Jain and Thompson are in reasonable agreement with the present data at all energies covered ie 3 to 15eV. As discussed in Section 1.6 they employed a localised Hara exchange potential and developed a parameter free polarisation potential. The theoretical results of Jain and Thompson are in far better agreement with the experimental data than those of Lima et al (shown in Figure 1.5) over the energy range 3 to 7.5eV, displaying the low angle minima apparent in the measured differential cross sections over this energy range. Lima et al did not include a polarisation potential in their calculations, which do not display the low angle minima, it would appear therefore that this potential makes a significant contribution to the scattering at low angles at 7.5eV and below.

6.4 Discussion of the Results of Ethene and Ethane and Comparison with Other Work

Similarly to methane, ethene and ethane both exhibit a broad peak, centred around 8eV in their total cross sections (Sueoka and Mori 1985), ethene also displays a peak at approximately 2eV. Absolute differential cross sections are required for both gases to demonstrate the influence of resonances on their total cross sections. Very little published data exists for either of these molecules, particularly ethene.

Figures 6.7 to 6.12 show the elastic differential scattering of ethene, over the energy range 3.3 to 15.5eV. The present data is compared to the theoretical data of McKoy (private communication 1987) at 15 and 7.5eV and has been normalised to this data to put it on an absolute scale. The cross sections at

	Incident energy (eV)					
Angle (deg)	15.5eV	8.0eV	6.1eV	5.0eV	4.3eV	3.3eV
30	5.96 ± 0.62	6.01 ± 0.59	6.20 ± 0.69	6.62 ± 0.68	6.95 ± 0.8	7.22 ± 0.72
40	3.24 ± 0.29	3.42 ± 0.35	2.82 ± 0.36	2.41 ± 0.29	2.91 ± 0.35	4.01 ± 0.34
50	1.59 ± 0.15	2.82 ± 0.27	3.23 ± 0.35	3.43 ± 0.35	3.56 ± 0.32	3.72 ± 0.35
60	1.07 ± 0.1	2.32 ± 0.25	2.47 ± 0.21	2.77 ± 0.26	3.02 ± 0.27	2.85 ± 0.25
70	0.75 ± 0.06	1.20 ± 0.11	1.69 ± 0.15	1.64 ± 0.14	1.62 ± 0.16	1.43 ± 0.12
80	0.60 ± 0.05	0.87 ± 0.1	0.88 ± 0.08	1.01 ± 0.08	1.03 ± 0.09	0.96 ± 0.1
90	0.61 ± 0.05	0.85 ± 0.09	0.88 ± 0.07	0.96 ± 0.08	0.98 ± 0.09	1.02 ± 0.09
100	0.66 ± 0.07	1.14 ± 0.11	1.16 ± 0.1	1.19 ± 0.09	1.45 ± 0.15	1.38 ± 0.13
110	0.77 ± 0.09	1.24 ± 0.16	1.55 ± 0.14	1.62 ± 0.16	1.70 ± 0.13	1.64 ± 0.17
120	0.80 ± 0.08	1.39 ± 0.15	1.77 ± 0.15	1.86 ± 0.19	2.16 ± 0.21	2.63 ± 0.29
130	0.97 ± 0.12	1.43 ± 0.19	2.28 ± 0.28	2.31 ± 0.26	2.34 ± 0.26	3.25 ± 0.36
140	1.03 ± 0.15	1.42 ± 0.26	2.32 ± 0.32	2.46 ± 0.34	2.51 ± 0.32	3.33 ± 0.41

Table 6.2 Differential elastic cross sections for C_2H_4 ($10^{-16}cm^2\,sr^{-1}$ at 15 & 7.5eV)

Figure 6.7 Ethene 15eV

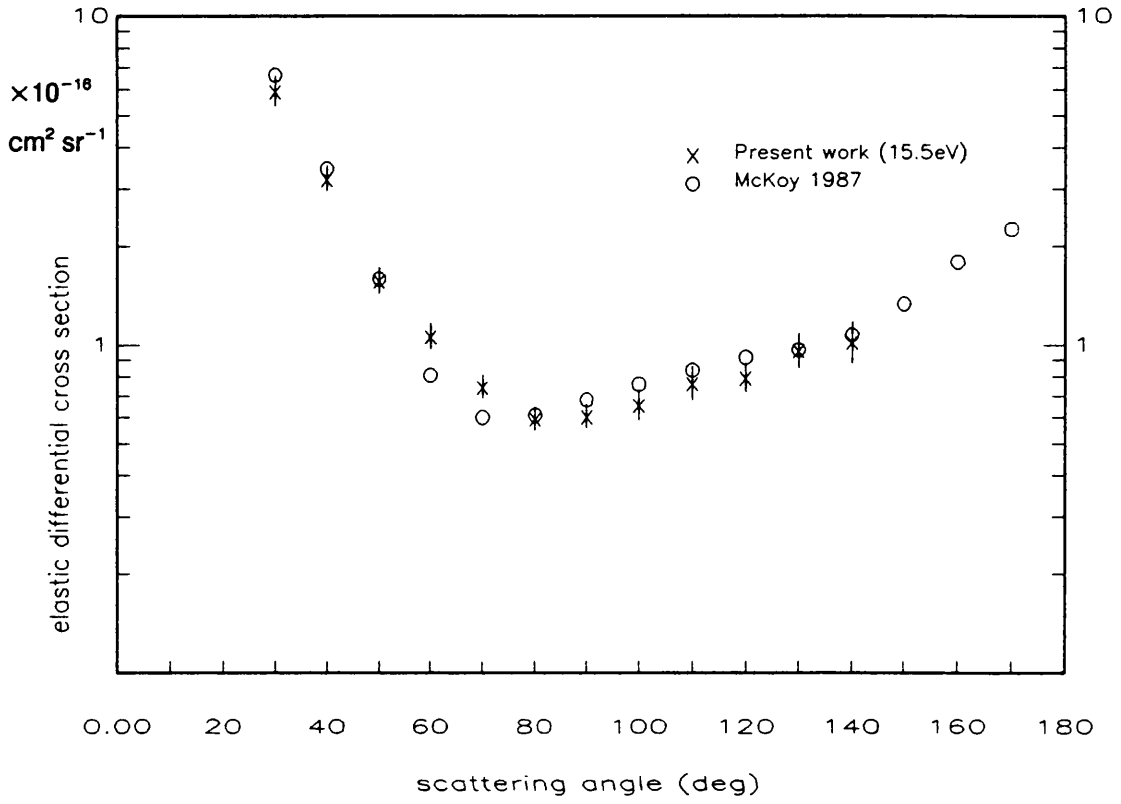

Figure 6.8 Ethene 7.5eV

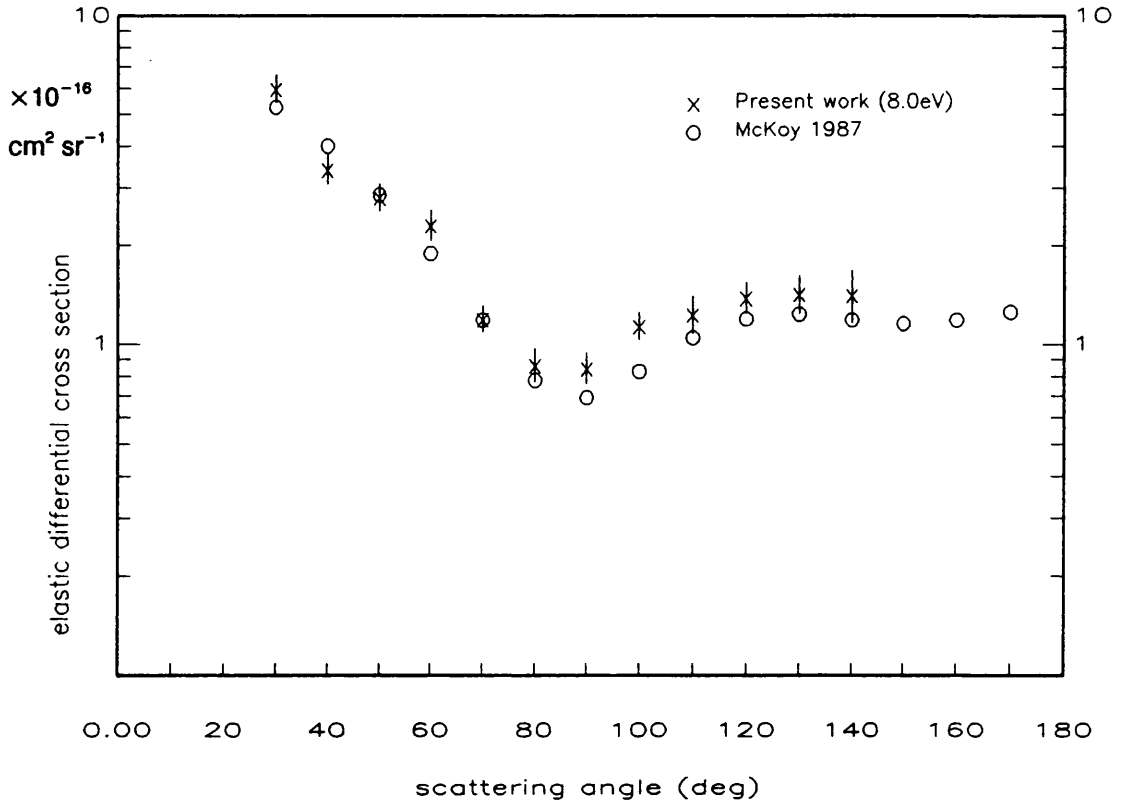

Figure 6.9 Ethene 6eV

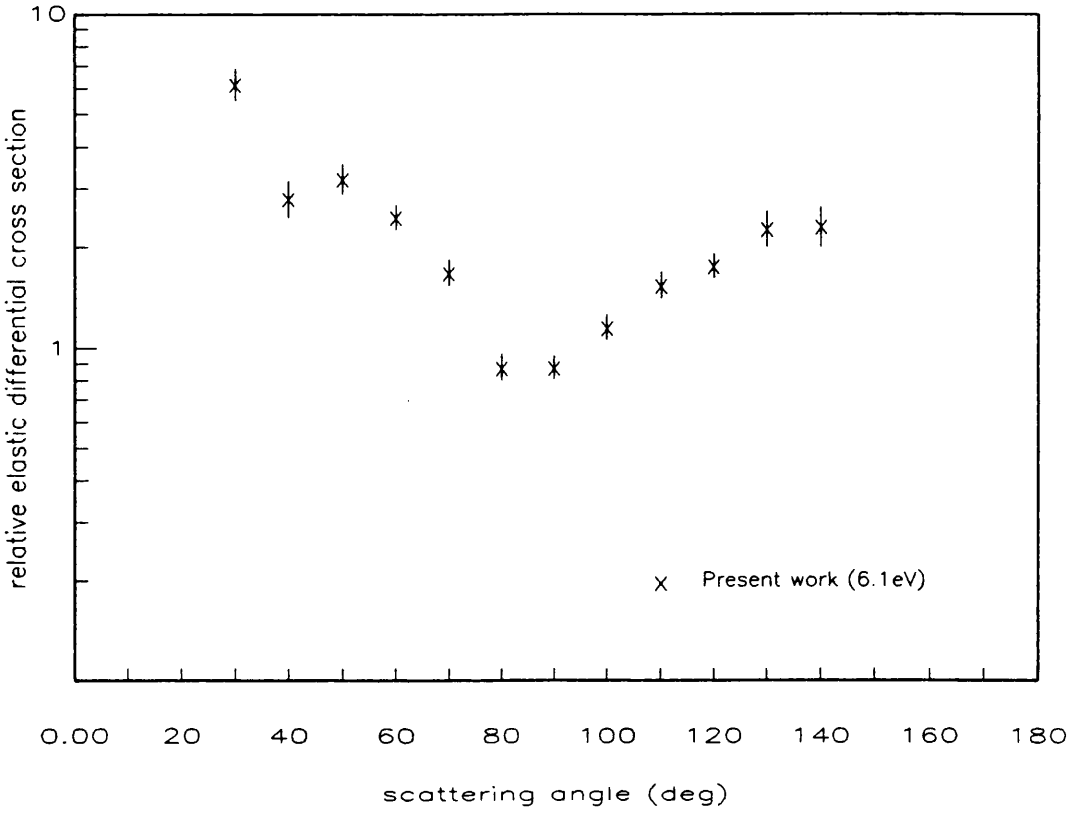

Figure 6.2 Ethene 5eV

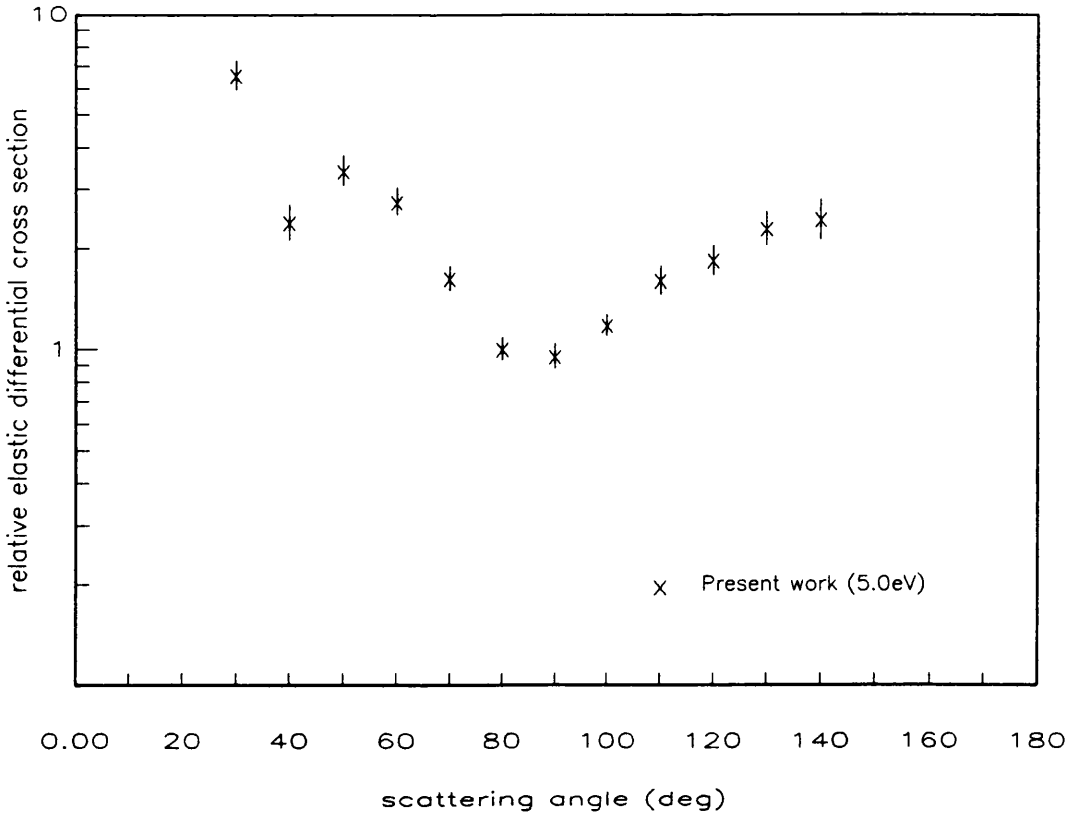

Figure 6.11 Ethene 4eV

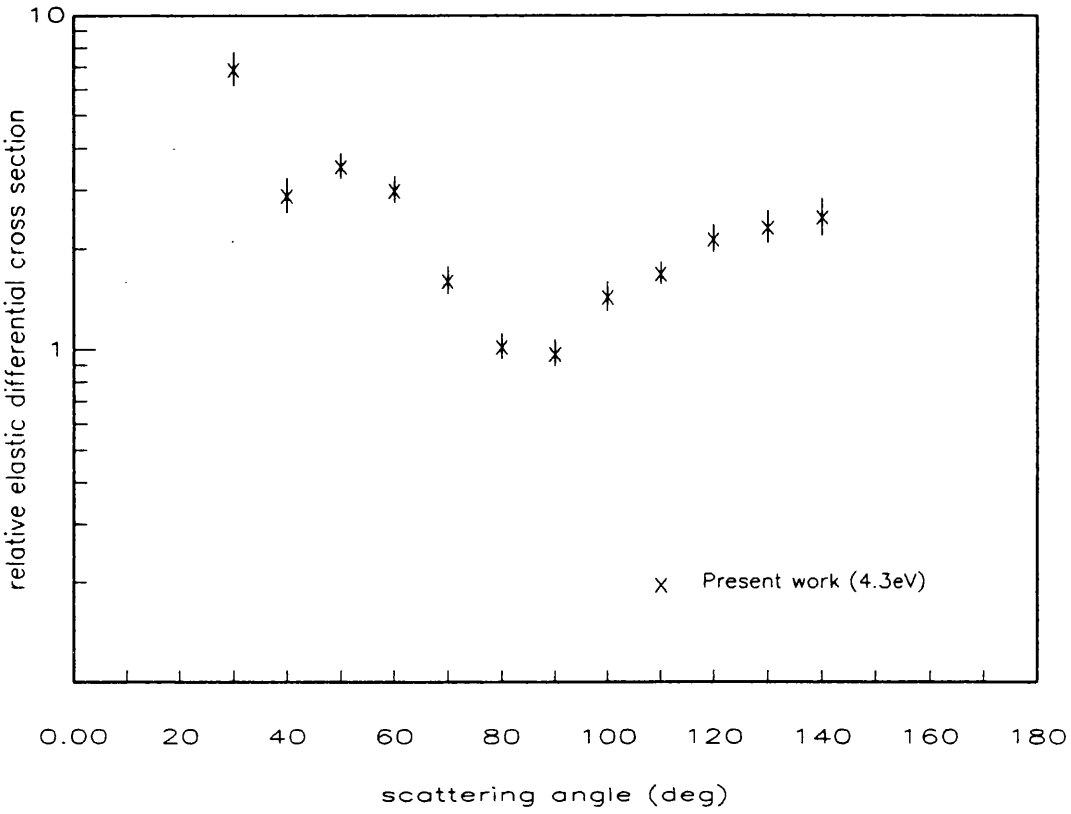

Figure 6.12 Ethene 3eV

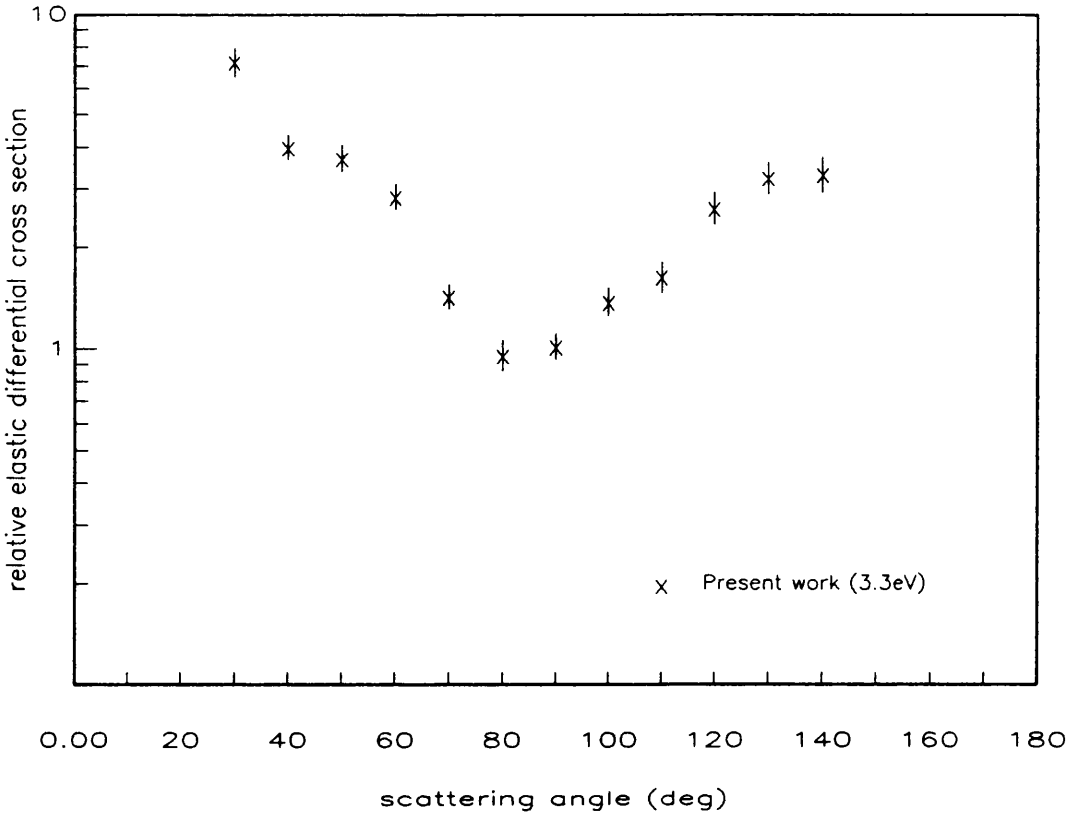

the lower energies are relative as there are no published differential cross sections for this molecule in the energy range 3 to 6eV.

At 15 and 7.5eV, the curves are similar. The present data has a broad minimum centred at 80°, while a similar minimum is observed in the calculated data, but centred between 70 and 80°. At 7.5eV the agreement with McKoy improves, both curves having slightly sharper minimum centred at 90°. McKoy used the same method as Lima et al (1985) to calculate the differential cross section, employing a static exchange potential but no polarisation potential. It would appear that at 15 and 7.5eV that the polarisation potential has very little effect on the shape of the cross section.

In the present experiment the minimum at 90° remains virtually unchanged as the incident electron energy is decreased to 3.3eV. A second much smaller dip, centred at 40°, can be observed at 6.1eV and below and the cross section starts to display characteristics associated with an f-wave resonance, ie a minimum at about 45° followed by a local maximum around 65° and a deeper minimum at 90°.

Figures 6.13 to 6.18 show the present data for ethane compared with that of Curry et al (1985) and Tanaka et al (1988), there is no theoretical data available for comparison. As for methane there are two minima in the curves, the one at the lower angle becoming more pronounced as the incident energy falls, while the minimum at the higher scattering angle becomes broader and less deep, although always lower than the first minimum.

	Incident energy (eV)					
Angle (deg)	15.4eV	7.9eV	6.0eV	4.9eV	4.2eV	3.2eV
30	3.71 ± 0.93	5.21 ± 1.30	3.65 ± 0.81	3.02 ± 0.59	3.16 ± 0.77	1.61 ± 0.31
40	2.24 ± 0.46	3.24 ± 0.61	2.42 ± 0.52	2.04 ± 0.41	1.55 ± 0.36	1.27 ± 0.24
50	1.57 ± 0.31	2.37 ± 0.47	2.12 ± 0.40	1.88 ± 0.37	1.60 ± 0.31	1.14 ± 0.22
60	1.16 ± 0.22	2.22 ± 0.42	2.27 ± 0.43	2.08 ± 0.40	2.35 ± 0.45	1.22 ± 0.23
70	0.77 ± 0.15	1.80 ± 0.34	1.88 ± 0.35	1.82 ± 0.36	2.23 ± 0.42	1.29 ± 0.25
80	0.72 ± 0.13	1.07 ± 0.20	1.10 ± 0.21	1.18 ± 0.22	2.12 ± 0.39	1.26 ± 0.24
90	0.55 ± 0.11	0.87 ± 0.15	0.83 ± 0.15	0.82 ± 0.16	1.97 ± 0.37	1.17 ± 0.22
100	0.56 ± 0.11	1.07 ± 0.20	0.78 ± 0.15	0.62 ± 0.12	1.50 ± 0.28	0.87 ± 0.17
110	0.57 ± 0.10	1.58 ± 0.30	1.22 ± 0.23	0.74 ± 0.14	1.18 ± 0.24	0.71 ± 0.14
120	0.60 ± 0.11	1.73 ± 0.36	1.72 ± 0.32	0.97 ± 0.22	0.98 ± 0.26	0.54 ± 0.10
130	0.74 ± 0.19	2.15 ± 0.45	2.07 ± 0.39	1.28 ± 0.32	1.02 ± 0.28	0.52 ± 0.10
140	0.89 ± 0.23	2.19 ± 0.49	2.21 ± 0.47	1.69 ± 0.45	1.11 ± 0.27	0.51 ± 0.10

Table 6.3 Differential elastic cross sections for C_2H_6 ($10^{-16}cm^2\ sr^{-1}$)

Figure 6.13 Ethane 15eV

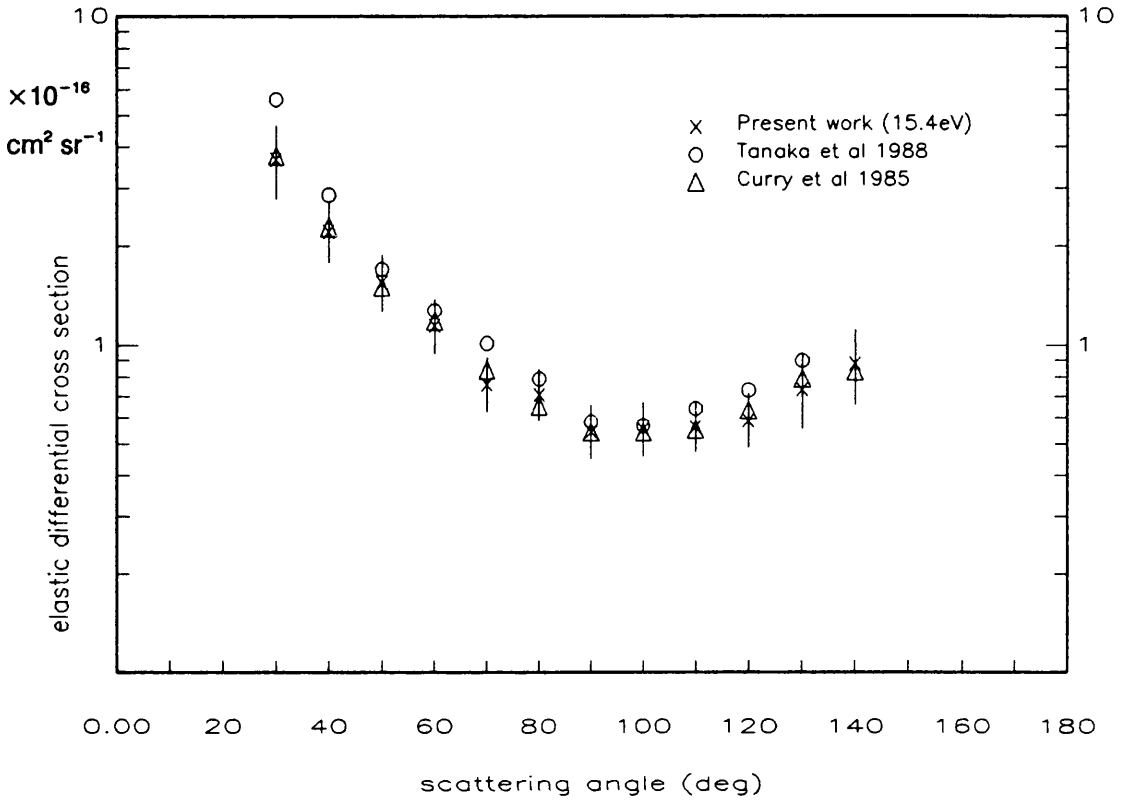

Figure 6.14 Ethane 7.5eV

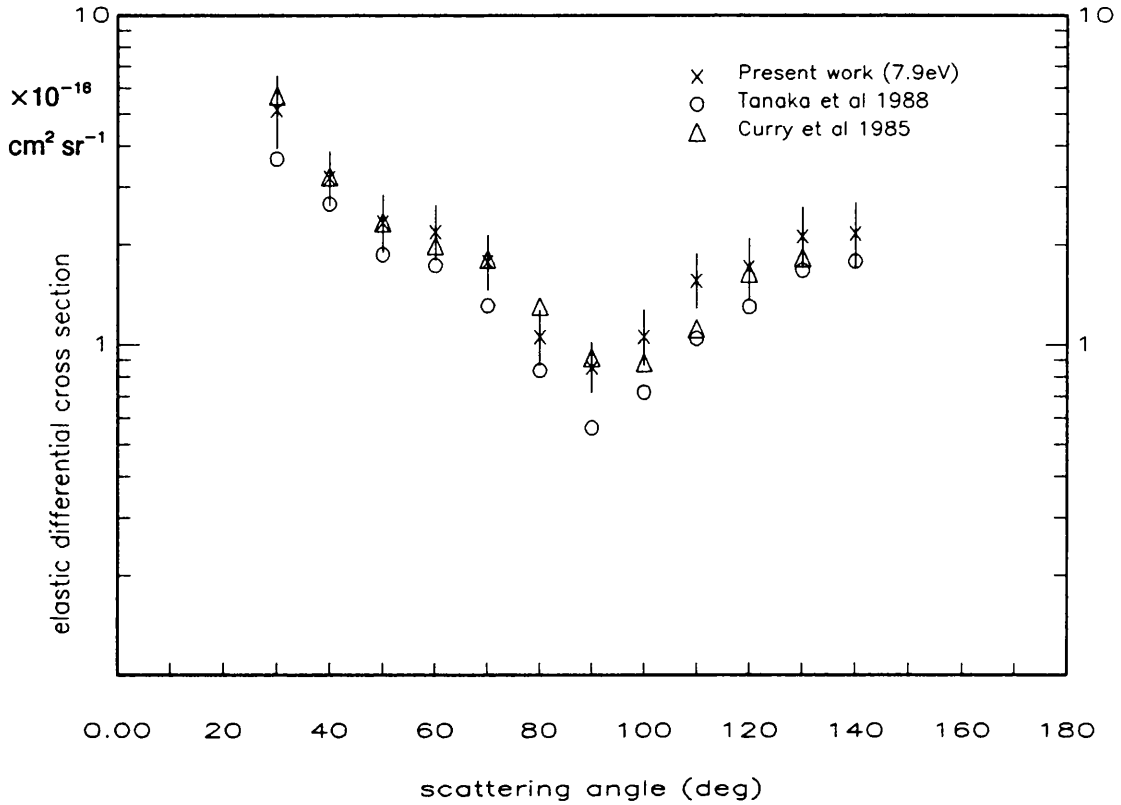

Figure 6.15 Ethane 6eV

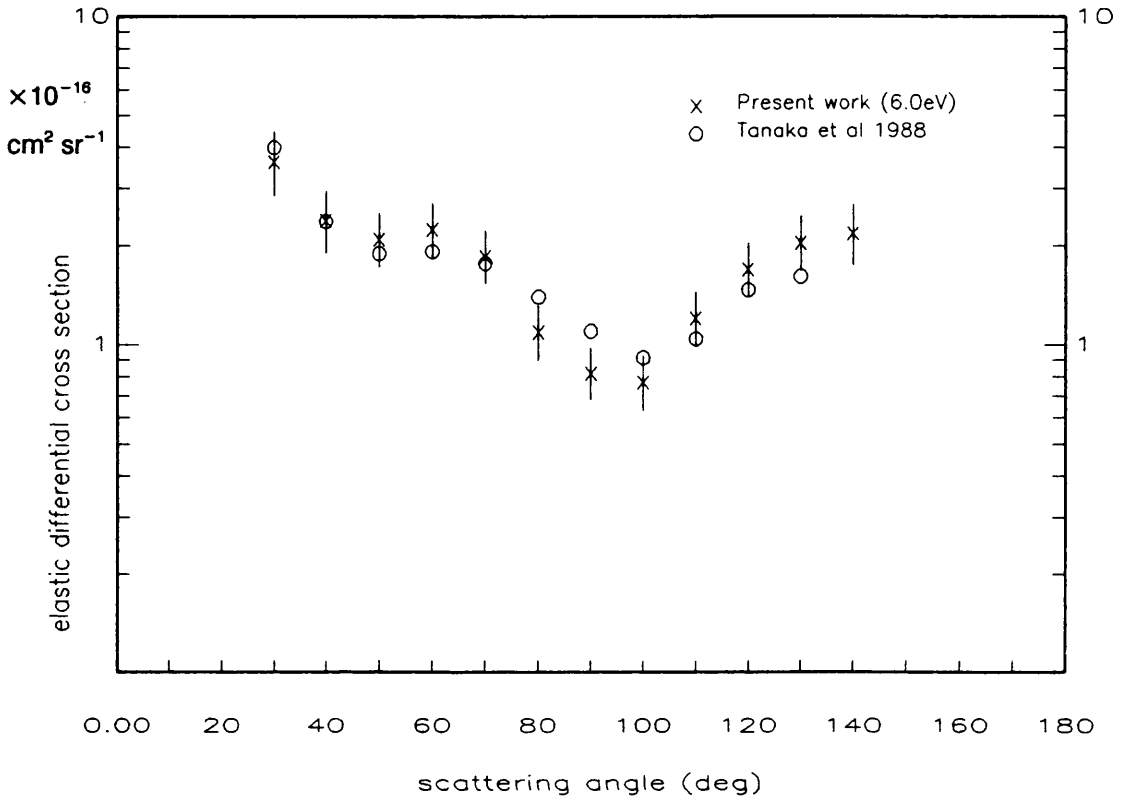

Figure 6.16 Ethane 5eV

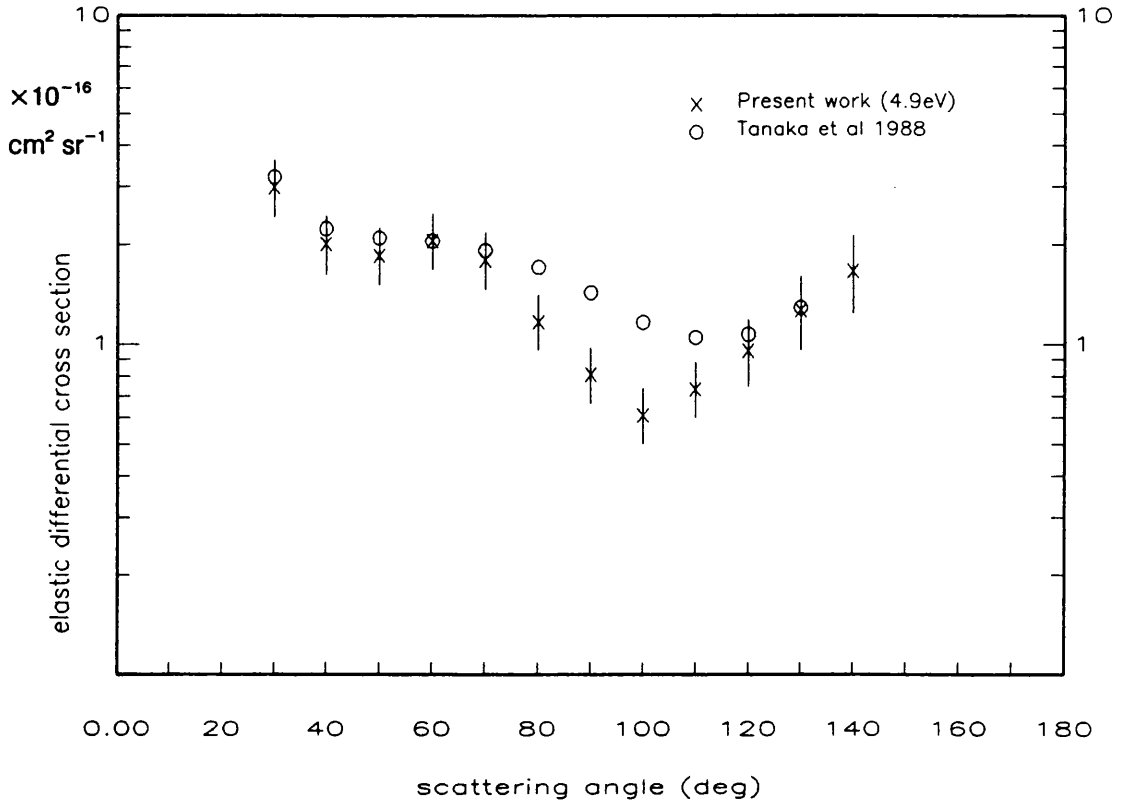

Figure 6.17 Ethane 4eV

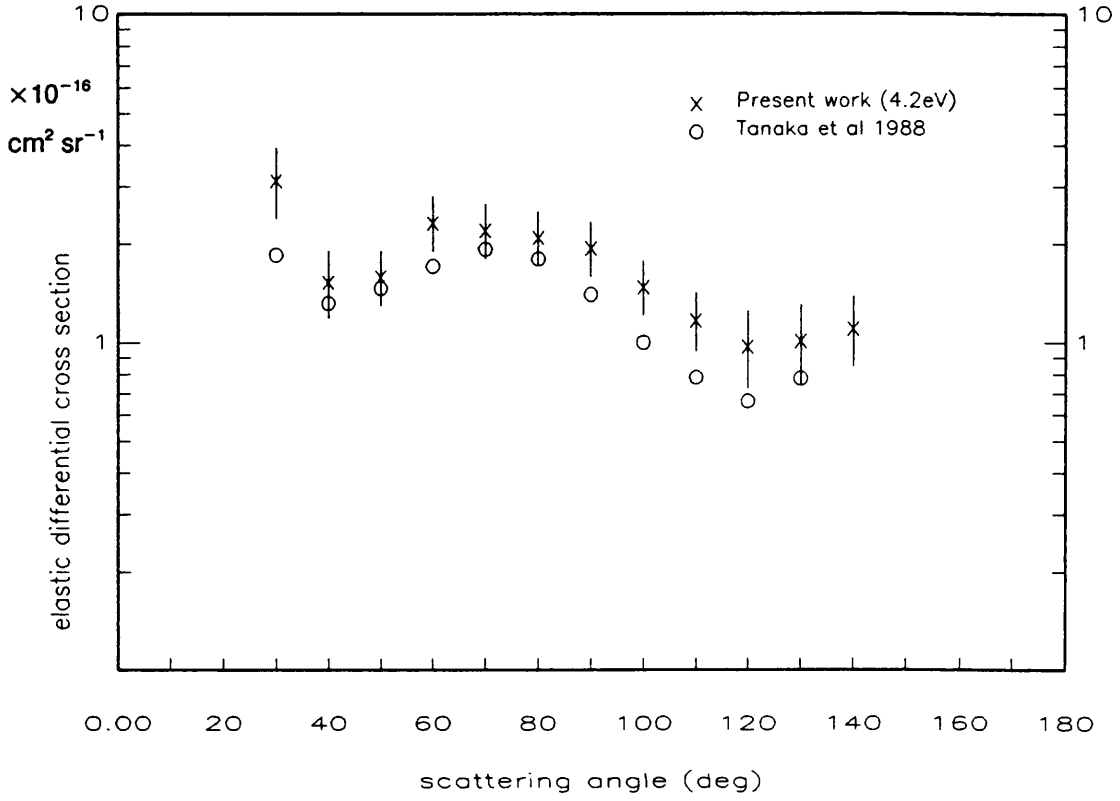

Figure 6.18 Ethane 3eV

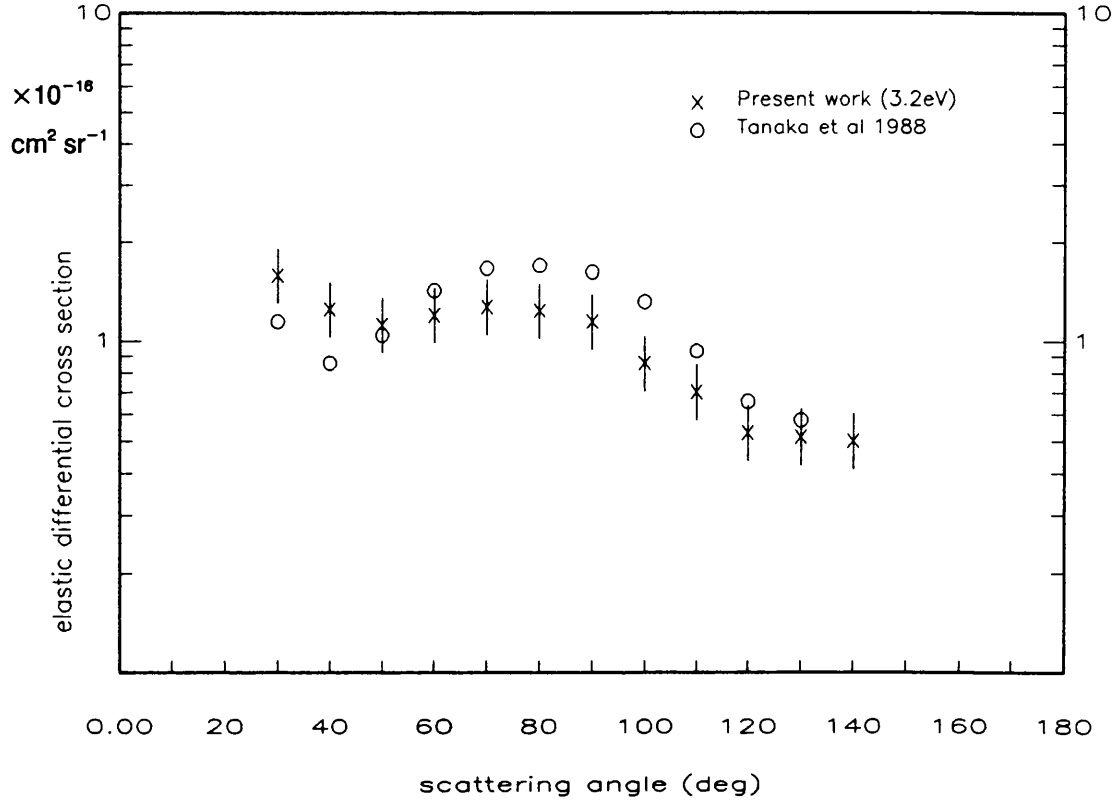

At 15eV, the curves agree well between 30 and 140°, all displaying a shallow minimum at 100°. At 7.5eV, good agreement is again achieved in the shape of the cross sections of the present work, Curry et al and Tanaka et al, all showing a minimum now at 90°, and a small plateau between 50 and 60°. The data of Curry et al is consistently lower in magnitude to both the present work and that of Tanaka et al, this is particularly noticeable at 90°.

In Figures 6.15 to 6.18 the present results are compared to those of Tanaka et al. At 6eV both cross sections show a shallow minimum at 50° with a deeper minimum at 100°. At 5eV the results of Tanaka et al display a plateau between 40 and 80°, falling to a shallow minimum between 110 and 120°. The present data has a shallow minimum at 50° and starts falling at 80° to a deeper minimum at 100°. Better agreement is found at 4eV, both cross sections displaying minima at 40 and 120°. At 3eV the data of Tanaka et al shows a maximum at 80°, rather than the plateau observed in the present data over the same angular range. The low angle minimum of Tanaka et al occurs at 40° whereas in the present data this minimum has shifted slightly to 50°. Both sets of data fall off at 100° with a low plateau starting at 130°.

Generally the ethane differential cross section exhibits the angular distribution characteristic of an f-wave resonance for energies greater than 4eV (5eV in the case of Tanaka et al), ie a minimum at about 45° followed by a local maximum around 65° and a deeper minimum at 90°. Ethane belongs to the D_{3d} point group. Its ground state electron configuration is $(C_{core})^4 - 2a_{1g}^2 2a_{2u}^2 1e_u^4 3a_{1g}^2 1e_g^4$ yielding the $\tilde{X}^1A_{1g}$ ground state symmetry. The two lowest allowed states are 1^1A_{2u} and 1^1E_u whose excitation energies correspond to the experimentally observed transition of 9.4eV (Johnson et al 1979). The two optically forbidden levels 1^3E_g and 1^3A_{1g} have small cross sections and so far have not been clearly observed. According to angular correlation theory (Read 1968, Andrick and Read 1971) the symmetry of these levels allows only the angular moments $L=0$, $L=2$ for A_{1g} and $L=2$, $L=4$ for E_g while the next two states A_{2u} and E_u both have quantum numbers $L=1$ and $L=3$. Therefore if the broad peak seen in the total cross section is a short lived shape resonance, and given the observed f-wave behaviour, it may be assumed that the dominant shape resonance is most probably a $^2A_{2u}$ /^2E_u state. The dominant partial waves of this resonance are then f and p waves with the former characterising the observed angular distribution.

Below 5eV the cross sections starts to exhibit d-wave characteristics, ie two minima near 60 and 120° with a maximum at 90°. The total cross section, however, shows no structure until the onset of the Ramsauer minimum. This suggests that non-resonant direct scattering arising from the $^1A_{1g}$ state, containing mainly $L=0$ and $L=2$ wave functions, determines the differential cross section.

6.5 Summary

The present measurements provide quantitative data for the elastic scattering of electrons by methane and ethane over the angular range from 30 to 140° and an energy range 3 to 15eV. Quantitative measurements are given for ethene over the same angular range at 7.5 and 15eV, while for energy range 3 to 6eV qualitative data are presented.

It was experimentally confirmed that the angular distribution for methane, in the energy range of 3 to 7.5eV, is dominated by a d wave scattering, as has been theoretically predicted, this being due to the excitation of the T_2 resonance state. The agreement between the present measurements and theoretical calculations indicate that polarisation effects are important over the energy range 3 to 7.5eV.

From the shape of the cross section no evidence was found for a resonance at 7.5eV in ethene, however at lower energies the scattering did display features characteristic of a f-wave. Ethane was found to display both f and d-wave features depending on the collision energy, the f wave characteristics, probably due to the $^2A_{2u}/^2E_u$ resonance state, being apparent for the energies between 4 and 15eV, with the d-wave becoming dominant at 3eV.

Tanaka et al (1982) used a modified partial wave fitting procedure, including polarisation corrections and the Born approximation for higher partial waves ($L > 3$) to smooth their differential cross sections over the range 30 to 140° and also to extrapolate the measurements between 0 to 30° and 140 to 180°. The total cross section was determined from the fits using

$$\sigma_T = 2\pi \int \frac{d\sigma}{d\Omega} \sin\theta \, d\theta. \tag{6.12}$$

Their results are plotted in Figure 1.1 where it can be seen that their calculated total cross section under estimates the most recently measured values by up to 25%. Caution must be exercised in the application of phase shift fitting techniques to experimental data as the requirements for this procedure to be valid are:-

a) Experimental precision in both calibration and resolution of both energy and angular scales.

b) As large an angular range as possible.

c) Knowledge of the roles played by open inelastic channels and exchange in the scattering process.

The problems indicated by the above would suggest that the application of this procedure to complex collision processes such as electrons scattering by methane, ethene and ethane is premature. Tanaka (1988), however, achieved rather better agreement with the measurements of Floeder et al(1985) and Brüche et al(1930) of the total cross section of ethane. Four phases plus a size factor were sufficient in the lower energy range, but beyond 20eV six phases were required. The fit misses some of the finer detail but represents the general shape well.

In order to achieve an accurate phase shift fit for molecules, a program needs to be developed which exceeds the simple physics embraced by the phase shift fitting of rare gases (Newell et al 1981). This would require more knowledge of the symmetry of the molecular wave functions and their cross section extrapolation to the small and large angles, and is work for future development.

Chapter 7 - Inelastic Scattering of Electrons From Methane, Ethene and Ethane

7.1 Introduction

The normalised absolute differential cross sections for the vibrational excitation of methane, ethene and ethane are presented in this chapter. These cross sections have been measured over the incident electron energy range of 3 to 15eV and angular range 30° to 140°. The method used to fit the energy loss spectrum and calculate these inelastic cross sections is described in Section 7.2. The shape of the spectra for each target gas is discussed in Section 7.3, this varying with the number of vibrational modes contributing to a particular peak in the energy loss spectrum. In Sections 7.4 and 7.5 of this chapter, the cross sections obtained in the present experiment are discussed and compared with other measurements. Finally in Section 7.6 the results of the present inelastic measurements are summarised.

7.2 Analysis of Results

The inelastic cross section is given by Equation 5.18. To calculate this for the vibrational peaks in the energy loss spectra of methane, ethene and ethane, it was therefore necessary to obtain the areas under the elastic and inelastic peaks displayed in each energy loss spectrum, after making the corrections described below.

Two interactive graphics programs were written to process the energy loss spectra. These programs yielded the areas under the elastic and inelastic peaks and estimates of their standard errors. Both programs were written in BBC BASIC to run on a BBC microcomputer.

The first of these programs (FIT-1) provided facilities to "tidy up" the energy loss spectra. This involved the removal of erroneous points caused by noise in the equipment, correction for the dc background noise and removal of any sloping continuum if present. The second program (FIT-2) was used to fit a set of Gaussian curves to the spectra, using a non-linear least squares technique.

Both programs had facilities for loading and saving data at any stage during the processing, changing graph scales, printing the data and producing graphical output on dot matrix printers. The first section below describes the typical features of the energy loss spectra to be processed. The method used to process the spectra and calculate the areas of the elastic and inelastic peaks is then described. The following two sections describe each of the data processing programs. Appendix E contains a detailed

description of the method used to fit the spectra and the program listings are contained in Appendix F.

7.2.1 Data Processing Technique

The typical features of an energy loss spectrum before processing are shown in Figure 7.1a. In all cases there is a dominant central elastic peak (PEAK 1) and two secondary inelastic peaks (PEAK 2 and PEAK 3). The spectra often had a flat continuum due to the dc background electrical noise (Z_d), this was always less than 1% of the height of the elastic peak. Occasionally there were obvious erroneous data points (N) which were caused by the detecting equipment. Some of the spectra (collected at 30° and 40°) also displayed a low intensity 'tail' on the energy loss side ($\frac{I_0}{e}W$) and this is illustrated in Figure 7.1b.

The procedure followed to process each energy loss spectrum is outlined below. The programs FIT-1 and FIT-2 are used to achieve these steps and these programs are described in more detail in sections 7.2.2 and 7.2.3.

1) Remove all erroneous data points from the spectrum. This is done by setting the number of counts at the particular step to zero. Any step with zero counts is then ignored in the following stages.

2) Remove the dc continuum signal. This is achieved by taking the average number of counts over a range of steps to the left of the elastic peak, then subtracting this average from each step. Any steps with zero counts are ignored when taking this average, and any steps which end up with a negative number of counts have their counts set to zero.

3) Apply the transmission correction to the 3.75 and 2.81eV spectra (see Section 3.10). The transmission data generated by the program described in Section 3.10 is loaded. Each point in the spectrum is then multiplied by the value of the transmission data ($T_d(E)/T_d(E-\Delta E)$)for the corresponding voltage step.

4) Remove the 'tail' if present. To do this, a line is drawn which runs through the rising continuum, then the area under the line is subtracted from the energy loss side of the spectrum.

The result of the above steps is a spectrum consisting of a central peak with two secondary peaks on a background continuum of zero (see Figure 7.1c). The next three processing steps are carried out by second program, FIT-2.

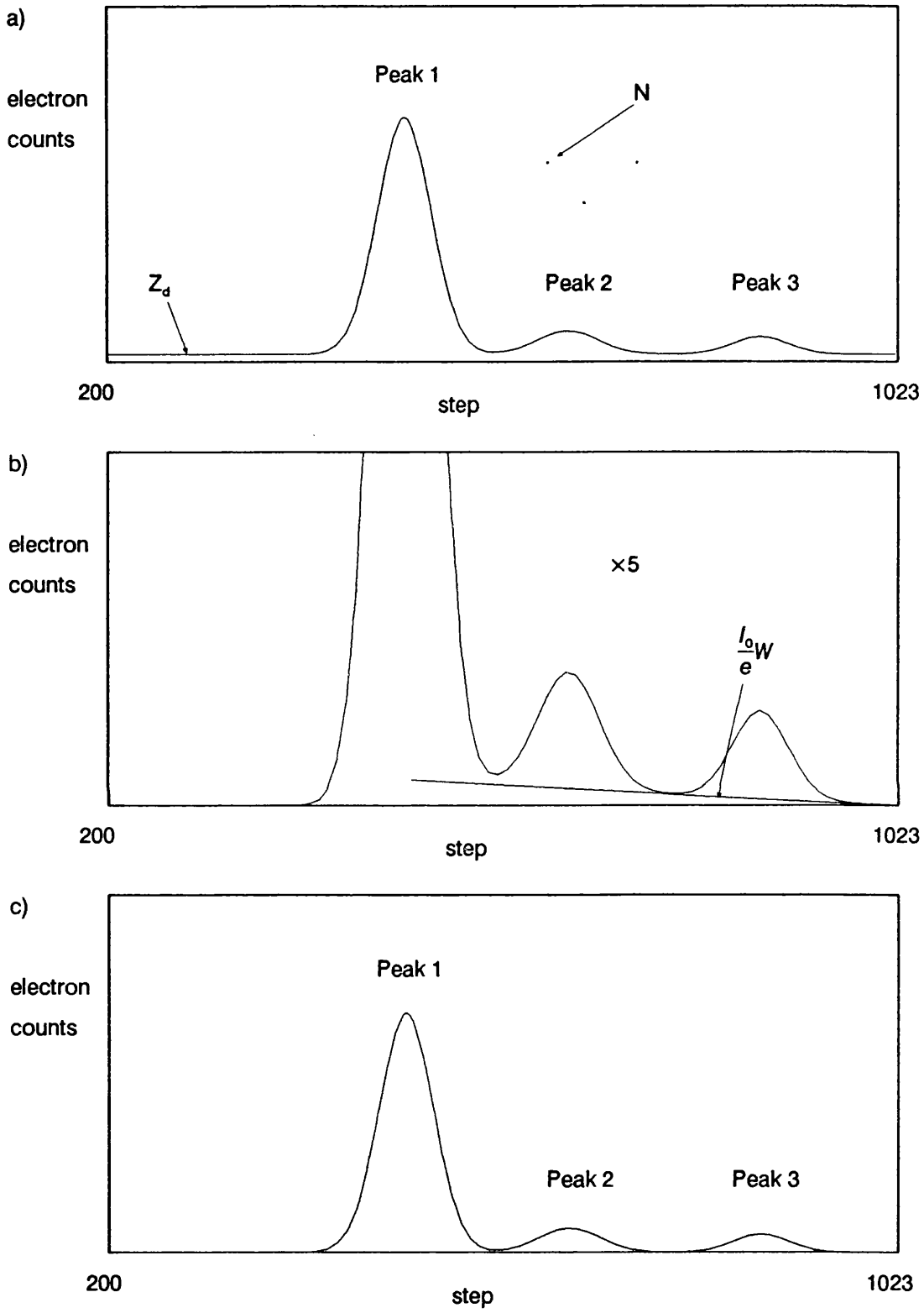

Figure 7.1 Illustration of the procedure used to 'clean up' the energy loss spectra.

a) Illustrates the noise features which may be visible on a spectrum.

b) Shows the spectrum after subtracting Z_d and N, the tail $(I_0/e)W$ is visible on expanding the y axis.

c) Shows a 'clean' spectrum, ready to be fitted.

5) Fit a Gaussian curve to PEAK 1 of the spectrum. The area under this curve is then subtracted from the spectrum.

6) In the same manner as step 5, fit Gaussian curves to the secondary peaks, subtracting each one from the spectrum in turn.

The areas under each of the three peaks is found from the fitted parameters, and the ratios PEAK 2/PEAK 1 and PEAK 3/PEAK 1 found. Estimates of the standard errors on these ratios are also calculated.

7.2.2 Program FIT-1

On running FIT-1, the user is presented with the following menu:-

```
1. LOAD DATA
2. LOAD TRANSMISSION DATA
3. CORRECT DATA
4. SAVE CORRECTED DATA
5. END PROGRAM
```

If an error occurs, or if the user presses the escape key, this menu is redisplayed. While at this menu, the user can submit operating system commands (such as looking at a disk) by pressing the '*' key.

Options 1 and 2 are used to load the counts stored for each step of the spectrum and the transmission correction data respectively. The user is asked to enter the names of the files containing the desired data. The filename for the energy loss spectra is usually of the form < letter > < date >, to signify the date on which data was collected and the set of data collected that day eg the file C10056 contains the third set of data collected on 10th May 1986. When the data is later saved, using option 4, it is saved into a file with the same name as the input file, but with a 'C' appended to it (eg C10056C).

Option 3 of the main menu leads to the interactive graphical data manipulation part of the program. The user must first of all select the range of steps to be displayed along the x-axis. This is usually 200 to 1023, as data was not normally collected over steps 0-199. Having entered the x-scale, the user is presented with a graph displaying the number of counts in each step. The y-axis of this graph is automatically scaled so that the elastic peak is as large as possible with scale gradations of 1,2 or 5 on the y-axis. On hitting the space bar, the scale of the y-axis is expanded by a factor of 5 and the graph redrawn. A pointer is also displayed, this can be moved around the screen using the cursor keys. The position of the pointer, in relation to the axes is displayed in a separate window on the screen. Various options can be selected by pressing keys, as follows.

<D> The present graph is saved to disk in a file name specified by the user, so that it can be printed out later.

<P> The graph displayed on the screen is copied to the printer.

<M> Control is returned to the main menu.

<F1> The data point at the graphics pointer is deleted from the screen and not used in any later analysis. This is used to remove obvious erroneous points (eg N in Figure 7.1a) generated by the detection circuits.

<F2> This is used to remove the electrical dc background signal from the spectrum (Z_d in Figure 7.1a). After pressing this key, the user selects two step positions along the x-axis (typically 200 to 350). The average count number between those two steps is then subtracted from the spectrum.

<F3> This is used to fit a line between two points selected using the pointer. The positive area under the line is then subtracted from the energy loss side of the spectrum. The option is used to remove any sloping continuum ($\frac{I_0}{e}W$ in Figure 7.1b).

<F4> This applies the transmission correction to the spectrum by multiplying the counts at each step of the spectrum by the corresponding value of $T_d(E)/T_d(E-\Delta E)$.

7.2.3 Program FIT-2

On running the second data processing program FIT-2, the user is presented with the following menu:-

```
1. LOAD CORRECTED DATA
2. LOAD FIT PARAMETERS
3. FIT DATA
4. CALCULATE AREAS
5. SAVE FIT PARAMETERS
6. END PROGRAM
```

As with the first program, if an error occurs this menu is redisplayed, and the operating system commands can be used by pressing the '*' key.

Option 1 loads in the corrected energy loss spectrum, output from FIT-1. Options 2 and 5 allow the user to load or save the Gaussian parameters for each peak in the spectrum. This can be done at any stage, so not all the peaks have to be fitted before saving. This also enables a complete fitted spectrum to be plotted (using option 3) at some later date, without having to re-fit the data. A similar file naming convention to that in FIT-1 is used. The file of fitted parameters has the letter 'P' appended to the original spectrum data file name. eg C10056P contains the fitted Gaussian parameters for the third set of data collected on 10th May 1986.

As with the first program, option 3 of the main menu leads to the interactive graphical data manipulation part of the program. This is virtually the same as for FIT-1, except the y-axis displays relative intensity with the height of the elastic peak set to 1 and the function keys F2, F3 and F4, now perform the following actions:-

<F2> This is used to activate the Gaussian fitting procedure. After pressing this key, the computer prompts for the lower and upper bounds of the steps to be included in the fit, the position of peak maximum and the lower and upper bounds of the peak at half height. These values are entered by moving the graphics pointer to the appropriate position, then pressing the return key. From the initial estimates of the peaks height, position and width, the computer iterates until the fit converges with an error less than 10^{-4}. If the process has not converged within 10 iterations, the program prompts the user as to whether it should continue. When the fit converges, the program prompts for the peak number, then stores the fitted parameters for future use.

<F3> This key allows the user to plot the fit for one peak, the user is then asked whether the area under the fitted peak is to be subtracted from the spectrum.

<F4> This option plots the complete fitted spectrum on the current axes.

Option 4 from the main menu calculates the ratio of areas, PEAK 2/PEAK 1 and PEAK3/PEAK 1, along with estimates of their standard errors. A further option is given to print these values.

7.2.4 Spectrum Fitting Method

Each energy loss spectrum is assumed to be composed of three superimposed Gaussian peaks, of the form

$$y = a \exp\left[-\frac{(x-c)^2}{b^2}\right]. \tag{7.1}$$

where a is the height of the peak

b is proportional to the width of the peak,

c is the position of the peak.

To calculate the inelastic cross sections of the two vibrational peaks it is necessary to calculate the ratios R_1 and R_2, where R_1 and R_2 are given by

$$R_1 = \frac{A_1}{A_e} \quad \text{and} \quad R_2 = \frac{A_2}{A_e} \ ,$$

where A_e is the area under the elastic peak,

A_1 is the area under the first inelastic peak,

A_2 is the area under the second inelastic peak.

These areas can be calculated by fitting Gaussian curves to each of the peaks in the spectrum. They are then given by

$$A_i = \sqrt{\pi}\, a_i b_i \tag{7.2}$$

where (a_i, b_i, c_i) are the Gaussian parameters for the peak.

R_2 and R_3 are therefore given by

$$R_1 = \frac{A_1}{A_e} = \frac{a_1 b_1}{a_e b_e}, \tag{7.3}$$

$$R_2 = \frac{A_2}{A_e} = \frac{a_2 b_2}{a_e b_e}, \tag{7.4}$$

where (a_e, b_e, c_e), (a_1, b_1, c_1) and (a_2, b_2, c_2) are the Gaussian parameters for the elastic peak and two inelastic peaks respectively.

The calculated areas A_i are approximately equal to the number of counts collected in each peak. Hence the standard errors on these values ΔA_i are approximately given by (Bevington 1969)

$$\Delta A_i = \sqrt{A_i}, \tag{7.5}$$

and the standard errors on R_1 and R_2 can be calculated from

$$\left(\frac{\Delta R_1}{R_1}\right)^2 = \left(\frac{\Delta A_1}{A_1}\right)^2 + \left(\frac{\Delta A_e}{A_e}\right)^2, \tag{7.6}$$

$$\left(\frac{\Delta R_2}{R_2}\right)^2 = \left(\frac{\Delta A_2}{A_2}\right)^2 + \left(\frac{\Delta A_e}{A_e}\right)^2. \tag{7.7}$$

The spectrum fitting method is to fit the elastic peak, then subtract it from the spectrum, fit the first inelastic peak and subtract it from the spectrum, and finally fit the second inelastic peak. Each peak is fitted using an iterative technique, from initial estimates of the Gaussian parameters a, b and c. Figure 7.2 shows a typical fit.

7.2.5 Calculation of Inelastic Cross sections

From Equation 5.18, it can be seen that the inelastic cross section at a given angle θ may be found from

$$\frac{d\sigma(E-\Delta E)}{d\Omega} = R_i \frac{d\sigma(E)}{d\Omega} \tag{7.8}$$

and the error on this cross section from

$$\left(\frac{\Delta\, d\sigma(E-\Delta E)/d\Omega}{d\sigma(E-\Delta E)/d\Omega}\right)^2 = \left(\frac{\Delta R_i}{R_i}\right)^2 + \left(\frac{\Delta\, d\sigma(E)/d\Omega}{d\sigma(E)/d\Omega}\right)^2 \tag{7.9}$$

$$= \left(\frac{\Delta A_i}{A_i}\right)^2 + \left(\frac{\Delta A_e}{A_e}\right)^2 + \left(\frac{\Delta\, d\sigma(E)/d\Omega}{d\sigma(E)/d\Omega}\right)^2. \tag{7.10}$$

Absolute inelastic cross sections may therefore be obtained by substituting absolute elastic cross sectional data into Equation 7.8

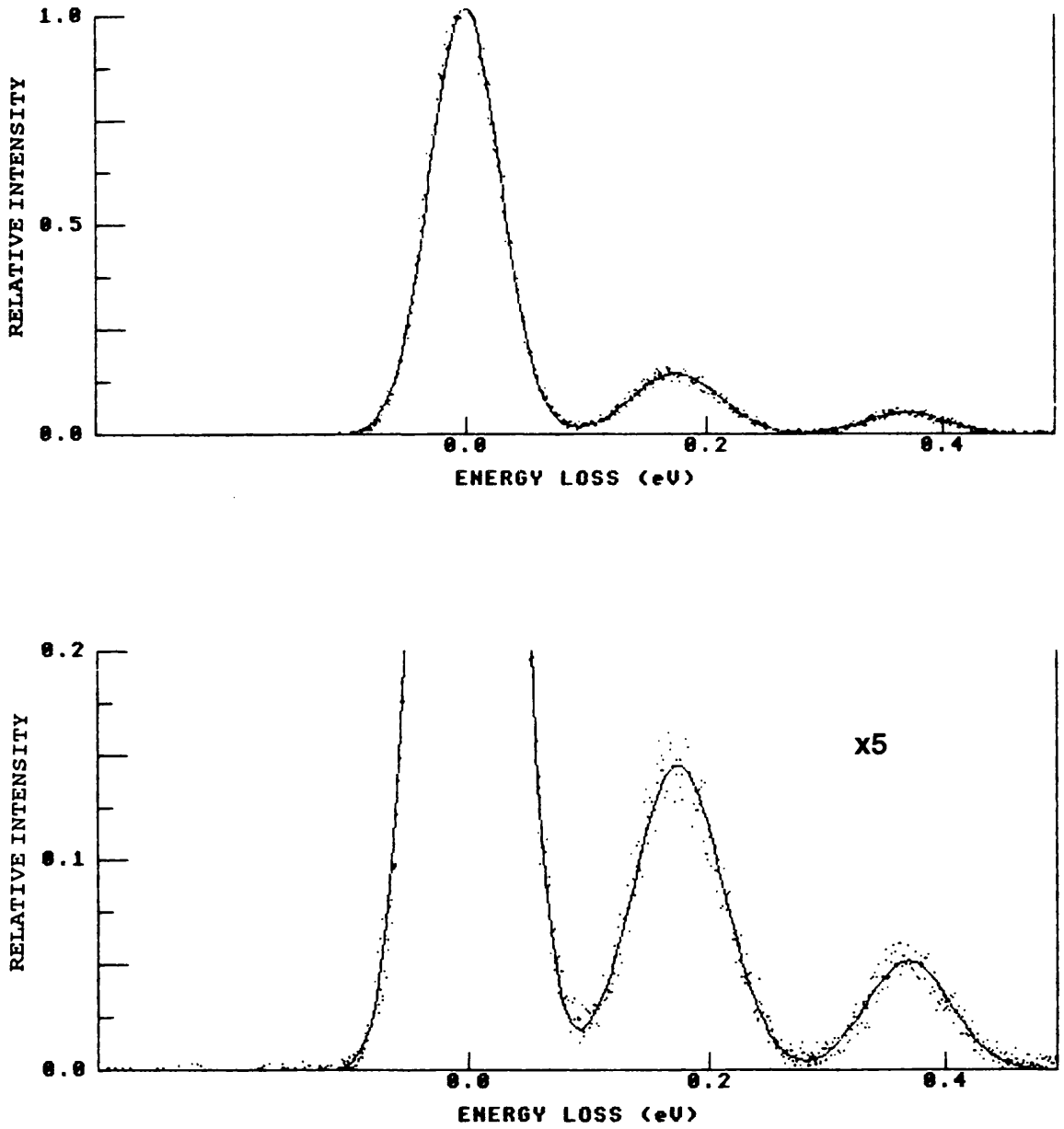

Figure 7.2 Fitted energy loss spectrum of methane at 3eV and 30°.

7.3 The Vibrational Structure of Methane, Ethene and Ethane

Typical energy loss spectra for the three target gases methane, ethene and ethane are given in Figures 7.3,7.4 and 7.5.

Methane has four vibrational modes donated by ν_1, ν_2, ν_3 and ν_4.The excitational energies associated with these modes, have been measured in infra-red and Raman spectroscopy experiments (Hertzberg 1945) and are 162, 190, 362, and 374meV. The overall resolution of the spectrometer during these measurements was between 50 and 60meV and was therefore insufficient to separate the peaks corresponding to the ν_2 and ν_4 modes and the ν_1 and ν_3 modes. These modes therefore appear as two composite peaks in the energy loss spectrum shown in Figure 7.3. As to be expected the FWHMs of the first and second vibrational peaks (76meV and 68meV respectively) are significantly larger than that of the elastic peak (59meV) due to the spread in energy of the composite modes.

Ethene has twelve vibrational normal modes (ν_1 to ν_{12}). These appear as the two composite peaks ν_i ($\nu_2, \nu_3, \nu_4, \nu_6, \nu_7, \nu_8, \nu_{10}, \nu_{12}$) and ν_j ($\nu_1, \nu_5, \nu_9, \nu_{11}$). The constituent modes of ν_i have an energy range of 0.102 to 0.210eV, resulting in the rather broad peak displayed in Figure 7.4. The constituents of the second composite peak have the smaller energy spread of 0.371 to 0.405eV.

Ethane also has twelve vibrational normal modes (ν_1 to ν_{12}). These appear as two composite peaks, the first ν_b ($\nu_2, \nu_3, \nu_6, \nu_8, \nu_{11}, \nu_{12}$) having excitational energies over the range 0.123 to 0.183eV, and the second ν_a ($\nu_1, \nu_5, \nu_7, \nu_{10}$) with an excitational energy range of 0.361 to 0.368eV. The modes ν_4 and ν_9 are situated at 0.036eV and 0.102eV respectively. The mode ν_4 is buried in the elastic peak and can not be observed, ν_9, however lies between the elastic and first inelastic peak and its presence can be deduced from the asymmetry of the first composite peak (see Figure 7.5). After subtracting the elastic and first composite peak ν_b, a small peak was observed due to this mode, however its magnitude was usually so small that it could not be fitted with any accuracy and so was ignored in the present analysis.

7.4 Inelastic Results for Methane and Comparison with Other Work

Trajmar et al (1983) have reviewed the cross section data for electron impact excitation of molecules and it is clear from this survey that only fragmentary information exists for vibrational (and electronic) excitations, even for the most common of molecular species. The only molecule for which a reasonably extensive set of differential and integral cross sections is available is nitrogen, although even in this case the data are far from complete and only accurate to ±30%.

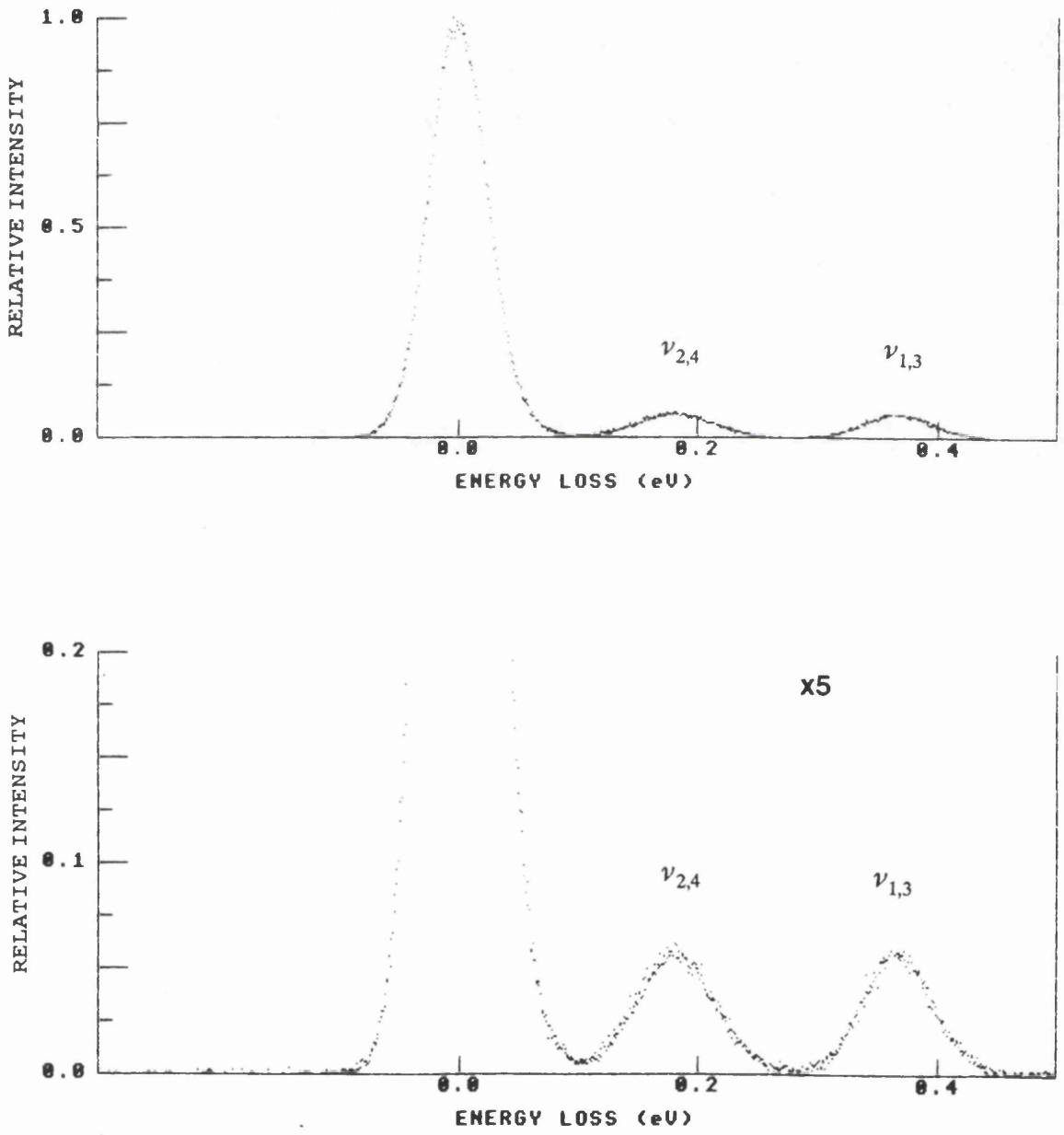

Figure 7.3 Energy loss spectrum of methane at 6eV and 100°.

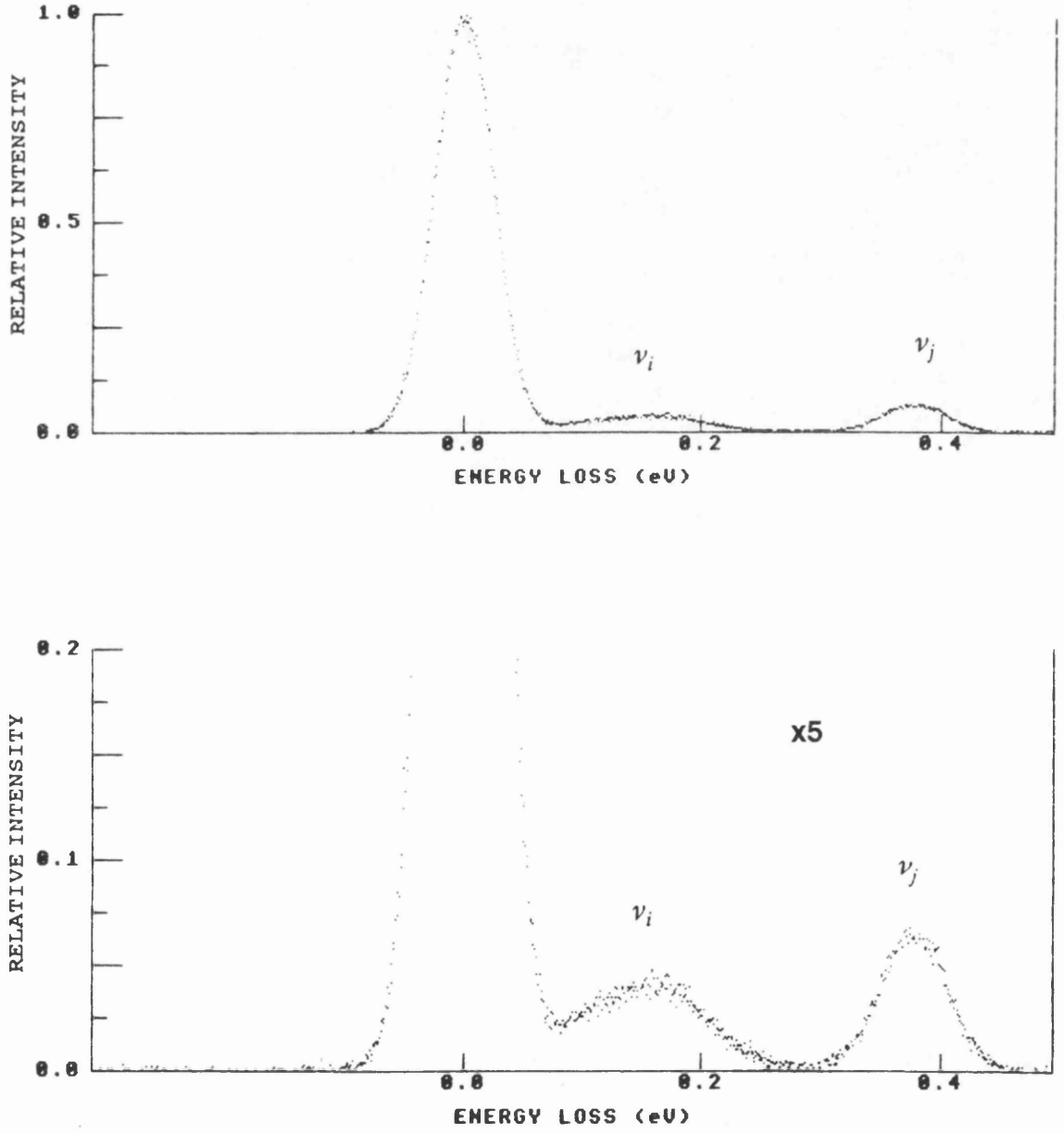

Figure 7.4 Energy loss spectrum of ethene at 6eV and 100°.

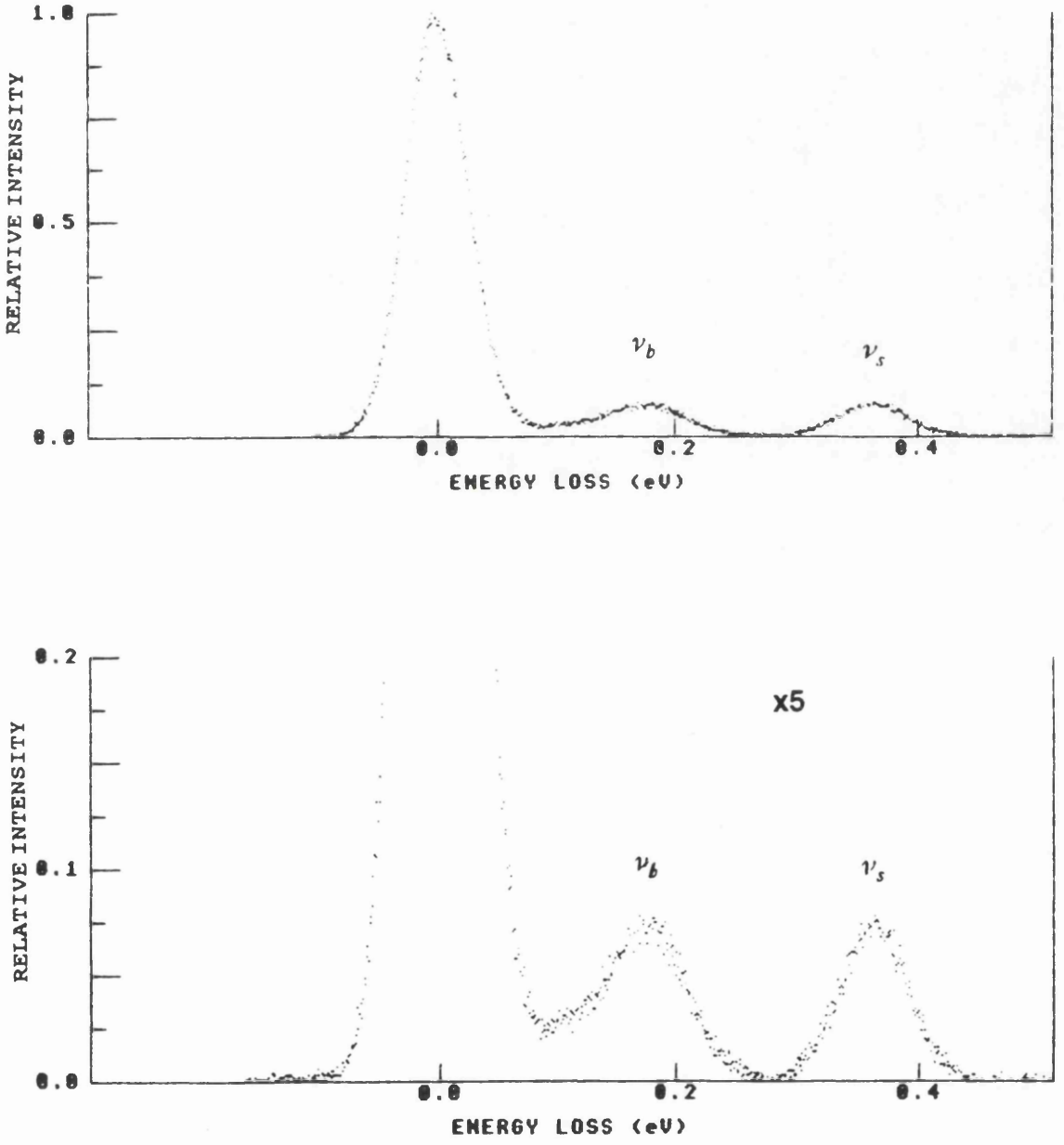

Figure 7.5 Energy loss spectrum of ethane at 6eV and 100°.

The renewed interest in the vibrational structure of methane stems from atmospheric physics, infra-red absorption bands have been identified in the spectra of the atmospheres of Jupiter and Saturn. Furthermore, in the field of laser research, methane has been the leading choice for use in backward Raman pulse compression of excimer lasers (eg the KrF laser which is used for laser fusion experiments) because the 361.5meV Q branch of the ν_1 symmetric stretch vibration of the molecule has a high Ramen cross section and dominates the spectrum (Murry et al 1979)). This feature of methane has prompted extensive study of the lineshape of the Q branch, but vibrational excitation by electron impact has not been investigated in sufficient detail.

The relationship between the Ramsauer minimum and vibrational excitation has been discussed by Barbarito et al (1979) as well as in papers on differential measurements by Rohr (1980) and Sohn et al (1983).

Swarm experiments (Pollack 1968, Duncan and Walker 1972) have shown that the low energy electrons can excite the vibrational levels of the methane molecule very efficiently, leading to their large vibrational cross sections (of the order of $10^{-16} cm^2$). Low energy electrons are very light compared to the molecular nuclei and it might be expected that the electron impact excitation of molecules is relatively unimportant, however electrons are in fact very effective in producing vibrational excitations, particularly at low impact energies, by interacting with the molecular electron distribution which is coupled with the nuclear vibrational motion. This is a resonance mechanism for vibrational excitation which involves a temporary electron capture. Resonances occurring in electron impact often enhance inelastic cross section by orders of magnitudes and occur in well defined energy ranges, at these energies electrons spend much more time in the neighbourhood of the molecule than is characteristic of the normal transit time. The electrons that are trapped in the neighbourhood of the molecule have an increased interaction time and cause a more efficient distortion of the molecule. This distortion leads to an enhancement in the vibrational excitation.

The nature of the vibrational excitation via resonant processes is strongly influenced by the lifetime of the resonance, in the case of a shape resonance the lifetime of the resonance is much smaller than a typical vibrational period ($\tau < 10^{-14} s$), so the nuclei cannot vibrate during the lifetime of the resonance. The incident electron under these circumstances attaches itself to the molecule (forming a resonance state) and the system decays by the emission of the extra electron, leaving the molecules in a vibrationally excited state. Because of the uncertainty principle this intermediate state has a large width in energy (few eV) and this leads to a broad peak in the energy dependence of the vibrational cross section.

Nonresonant cross sections generally show a smooth, slowly varying energy dependence and contribute a typical cross section of $10^{-18} cm^2$ for small non polar molecules, whereas resonant dependent cross sections are typically of the order of $10^{-16} cm^2$.

The absolute differential cross sections for the excitation of the $\nu_{1,3}$ and $\nu_{2,4}$ peaks are given in Tables 7.1 and 7.2 respectively and are plotted in Figures 7.6 to 7.17. The only reported data that overlap the energy range covered in the present experiment are the absolute differential cross sections of Tanaka et al (1983) and Curry et al (1985) and these measurements are shown with the present results at the appropriate energies; there is no theoretical data available for comparison.

All the measurements are in good agreement at 15eV. At this energy the differential cross sections of both composite peaks display a shallow minimum at 80° rising to a maximum at 130°, the maximum is more pronounced for the $\nu_{2,4}$ than the $\nu_{1,3}$ composite. At 7.5eV the present data and that of Tanaka et al exhibit shallow minima at 60 and 110° with a maximum at 90° for both composite peaks, whereas the data of Curry et al displays a maximum in the region of 100 to 130°. Tanaka et al have interpreted the angular distribution of their results as a consequence of resonant enhancement of the vibrational excitation channels induced by a d-wave dominated shape resonance in the elastic scattering cross section at approximately 7eV, the present results appear to support this.

Below 7.5eV. the present data for the $\nu_{2,4}$ composite and that of Tanaka et al display a shallow minimum again at 80° with a maximum at 130° down to 3eV where the curves are virtually isotropic. The angular distribution of the $\nu_{1,3}$ composite is also nearly isotropic at all the lower energies, the cross sections falling off slightly with increasing angle. The isotropic shape of the differential cross section indicates s-wave scattering.

As in the case of their elastic data, Tanaka et al used their differential measurements to extract the total cross sections for the excitation of the $\nu_{2,4}$ and $\nu_{1,3}$ vibrational modes of methane. The total cross sections for both composite peaks exhibit approximately the same variation with incident energy, rising rapidly from 1.5 $10^{-17} cm^2$ to a peak value of 7.5 $10^{-17} cm^2$ in the energy region 3 to 7.5eV, and decreasing to the same value at 20eV. This broad peak in the total cross section may be explained by the presence of the shape resonance.

7.5 Inelastic Results for Ethene and Ethane and Comparison with Other Work

There are no experiments or theoretical calculations to compare with the present measurements for ethene. The cross sections for the ν_i and ν_j composite peaks are given in Tables 7.3 and 7.4. and the data are presented in Figures 7.18 to 7.29. The cross sections at 15 and 7.5eV were found using the

	Incident energy (eV)					
Angle (deg)	15.4eV	7.9eV	6.0eV	4.9eV	4.2eV	3.2eV
30	4.01 ± 0.56	8.19 ± 1.25	5.52 ± 1.26	5.22 ± 1.04	4.52 ± 0.34	3.99 ± 0.62
40	3.06 ± 0.57	8.19 ± 1.32	5.01 ± 1.15	4.77 ± 0.64	3.84 ± 0.31	2.77 ± 0.54
50	2.91 ± 0.45	4.90 ± 0.73	5.42 ± 1.15	4.43 ± 0.62	3.23 ± 0.70	1.81 ± 0.30
60	2.72 ± 0.30	4.76 ± 0.68	4.99 ± 0.92	3.64 ± 0.47	3.29 ± 0.76	2.18 ± 0.37
70	2.01 ± 0.28	6.22 ± 0.84	4.68 ± 0.86	3.95 ± 0.56	3.39 ± 0.46	2.33 ± 0.53
80	1.98 ± 0.24	6.43 ± 0.96	5.10 ± 0.93	3.64 ± 0.51	3.18 ± 0.45	2.21 ± 0.52
90	2.25 ± 0.34	7.19 ± 0.96	5.26 ± 0.89	4.14 ± 0.62	3.17 ± 0.47	2.14 ± 0.36
100	2.76 ± 0.38	5.67 ± 0.78	6.31 ± 0.94	3.97 ± 0.47	3.31 ± 0.50	2.26 ± 0.37
110	3.20 ± 0.47	5.15 ± 1.43	5.82 ± 1.42	4.11 ± 0.51	3.52 ± 0.53	2.03 ± 0.33
120	3.14 ± 0.39	6.35 ± 2.10	7.78 ± 2.12	6.03 ± 1.41	5.74 ± 1.23	2.22 ± 0.60
130	3.23 ± 0.45	7.08 ± 2.21	8.32 ± 1.51	7.69 ± 1.76	5.51 ± 1.32	3.58 ± 1.43
140	2.85 ± 0.50	6.62 ± 1.32	5.52 ± 1.04	4.48 ± 0.69	3.65 ± 1.03	3.69 ± 1.23

Table 7.1 Differential inelastic cross sections for CH_4, $\nu_{2,4}$ ($\times 10^{-18}$cm^2 sr^{-1}).

	Incident energy (eV)					
Angle (deg)	15.4eV	7.9eV	6.0eV	4.9eV	4.2eV	3.2eV
30	1.82 ± 0.35	8.16 ± 1.54	5.43 ± 1.43	5.03 ± 0.66	4.23 ± 0.41	2.23 ± 0.20
40	1.83 ± 0.34	6.61 ± 1.30	5.38 ± 1.24	3.39 ± 0.26	3.98 ± 0.29	1.70 ± 0.33
50	1.98 ± 0.32	5.24 ± 1.03	5.10 ± 1.08	3.16 ± 0.38	3.34 ± 0.67	1.23 ± 0.23
60	1.90 ± 0.21	4.98 ± 0.81	5.06 ± 0.94	3.11 ± 0.40	3.19 ± 0.46	1.22 ± 0.21
70	1.36 ± 0.19	4.88 ± 0.72	4.63 ± 0.85	2.93 ± 0.41	2.59 ± 0.35	1.60 ± 0.33
80	1.11 ± 0.13	4.67 ± 0.74	5.35 ± 0.97	3.27 ± 0.45	2.49 ± 0.35	1.59 ± 0.30
90	1.15 ± 0.17	5.58 ± 0.80	5.04 ± 0.86	3.55 ± 0.66	2.83 ± 0.42	1.29 ± 0.22
100	1.47 ± 0.20	5.18 ± 0.75	5.67 ± 0.84	3.64 ± 0.42	2.82 ± 0.43	1.26 ± 0.20
110	1.59 ± 0.24	4.37 ± 0.93	4.87 ± 1.01	2.90 ± 0.43	2.79 ± 0.24	0.67 ± 0.16
120	1.81 ± 0.23	4.12 ± 1.20	5.01 ± 1.37	3.31 ± 1.37	3.06 ± 0.66	0.91 ± 0.25
130	1.89 ± 0.26	4.23 ± 1.76	4.10 ± 0.73	3.45 ± 0.56	1.96 ± 0.47	1.23 ± 0.49
140	2.02 ± 0.36	4.54 ± 0.81	3.77 ± 0.71	2.92 ± 0.22	1.87 ± 0.26	0.66 ± 0.22

Table 7.2 Differential inelastic cross sections for CH_4, $\nu_{1,3}$ ($\times 10^{-18}$cm^2 sr^{-1}).

Figure 7.6 Methane $\nu_{2,4}$ 15eV

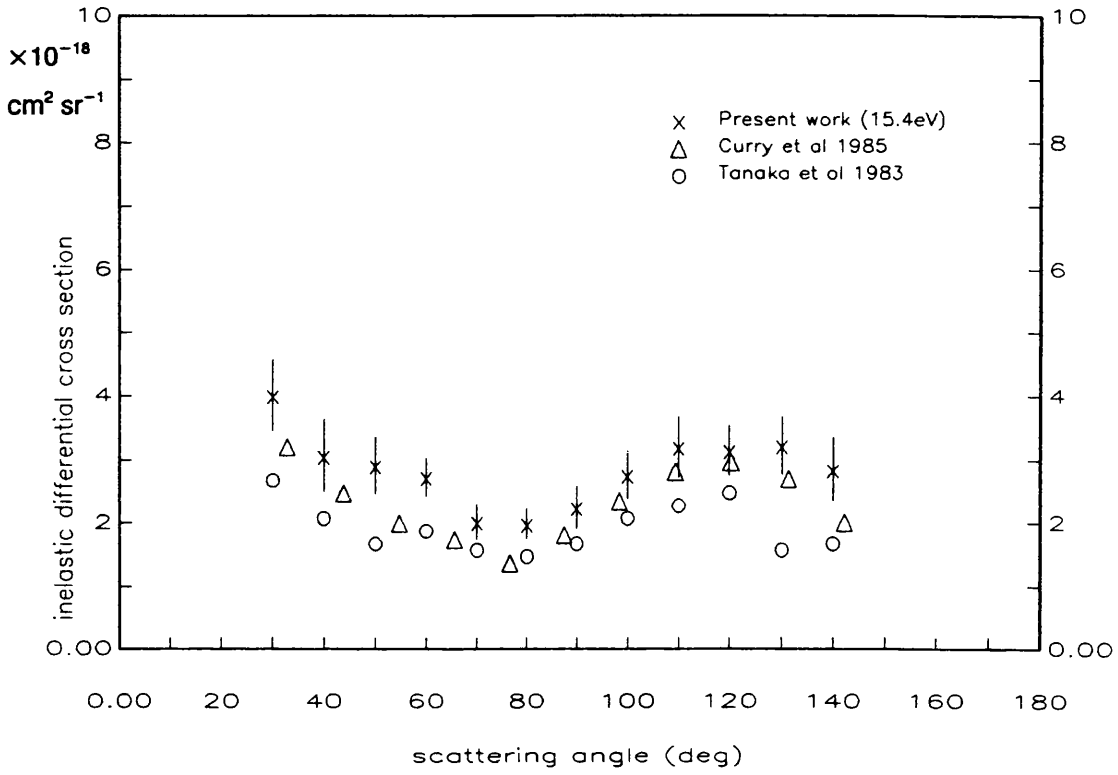

Figure 7.7 Methane $\nu_{2,4}$ 7.5eV

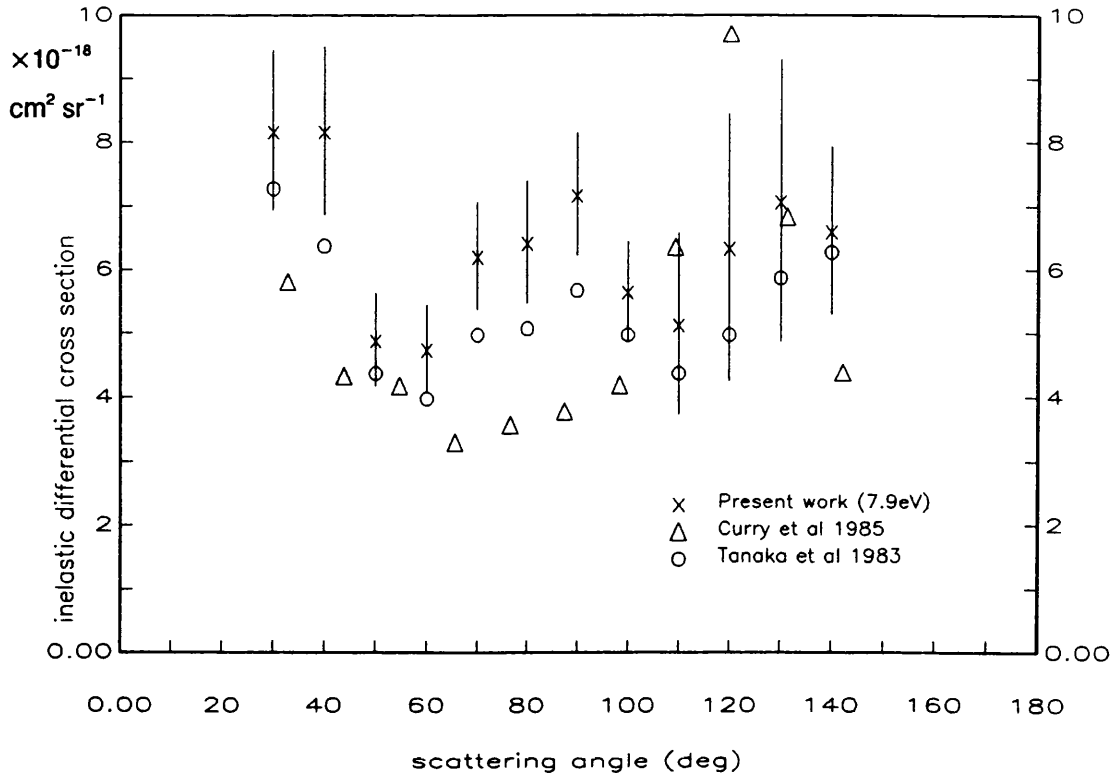

Figure 7.8 Methane $\nu_{2,4}$ 6eV

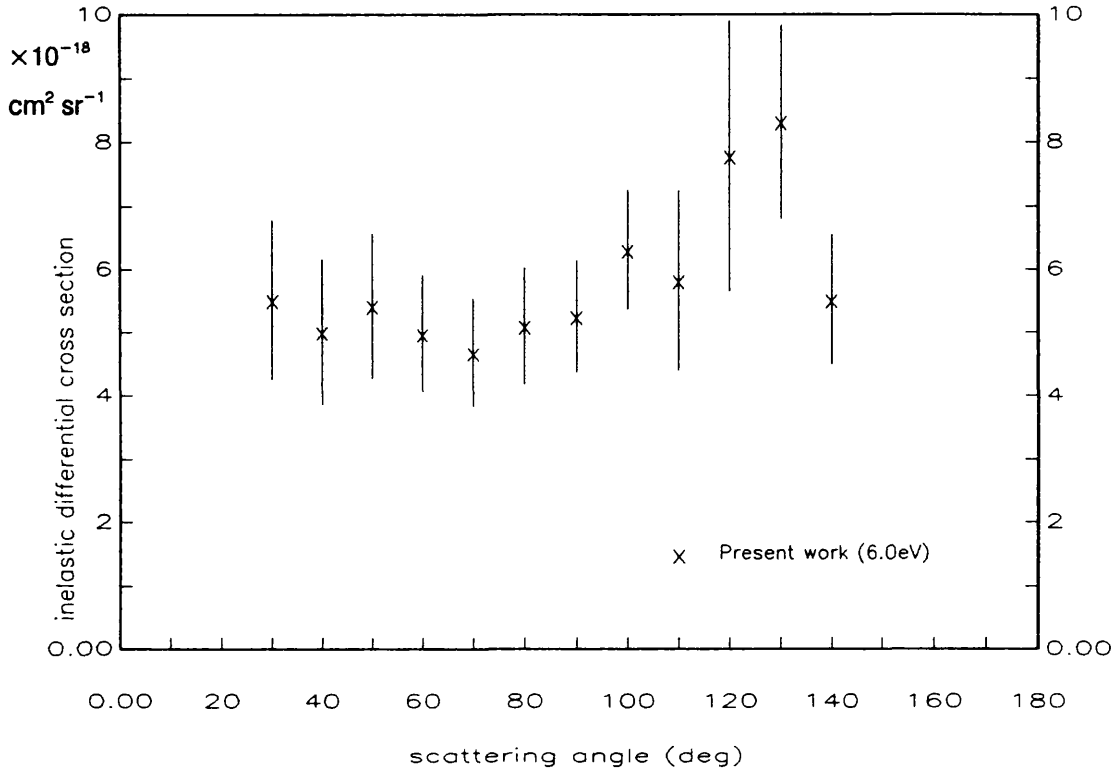

Figure 7.9 Methane $\nu_{2,4}$ 5eV

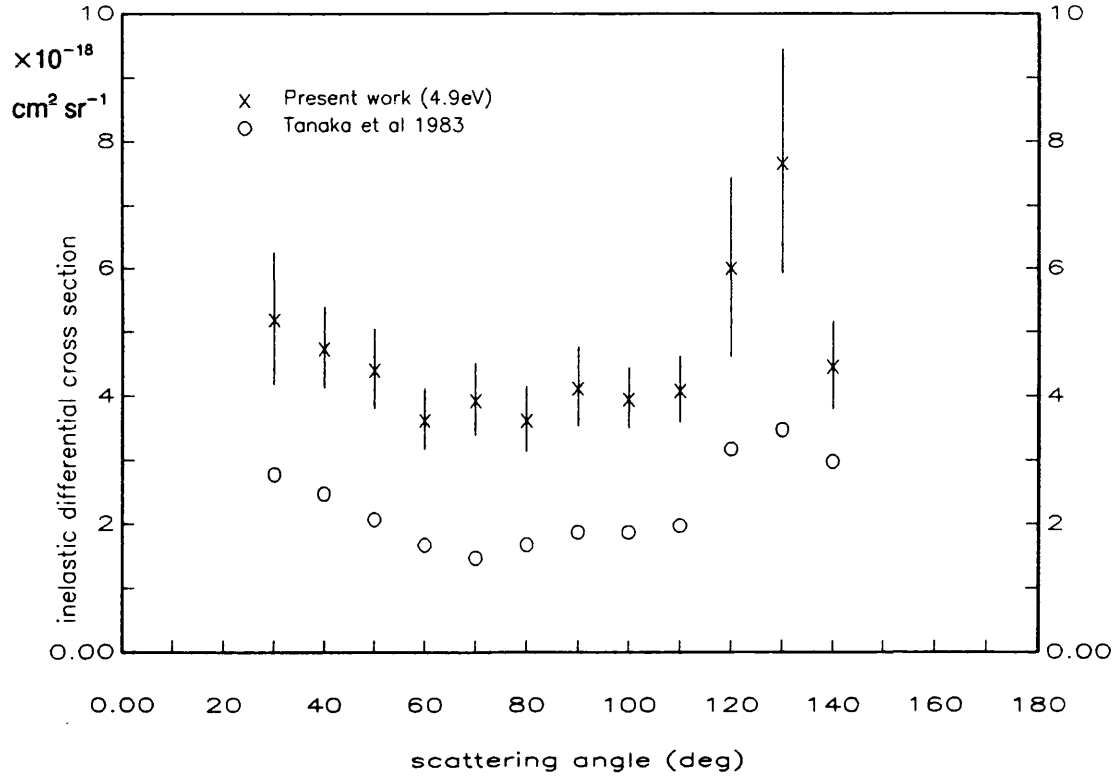

Figure 7.10 Methane $\nu_{2,4}$ 4eV

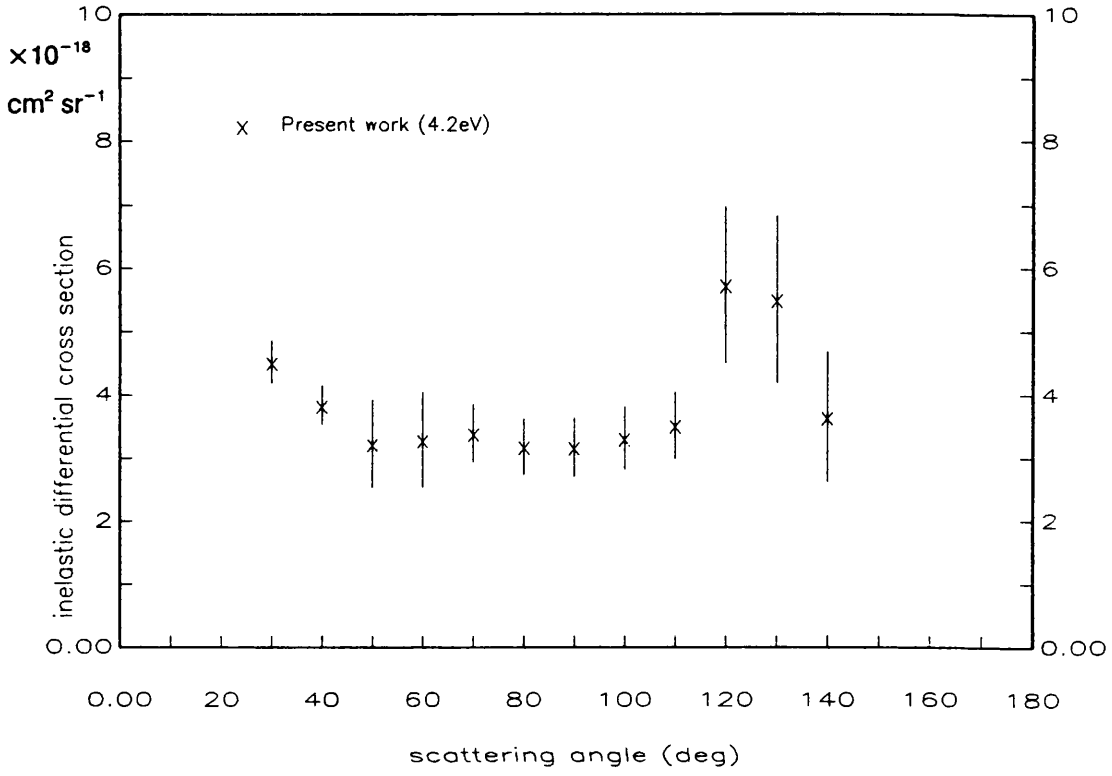

Figure 7.11 Methane $\nu_{2,4}$ 3eV

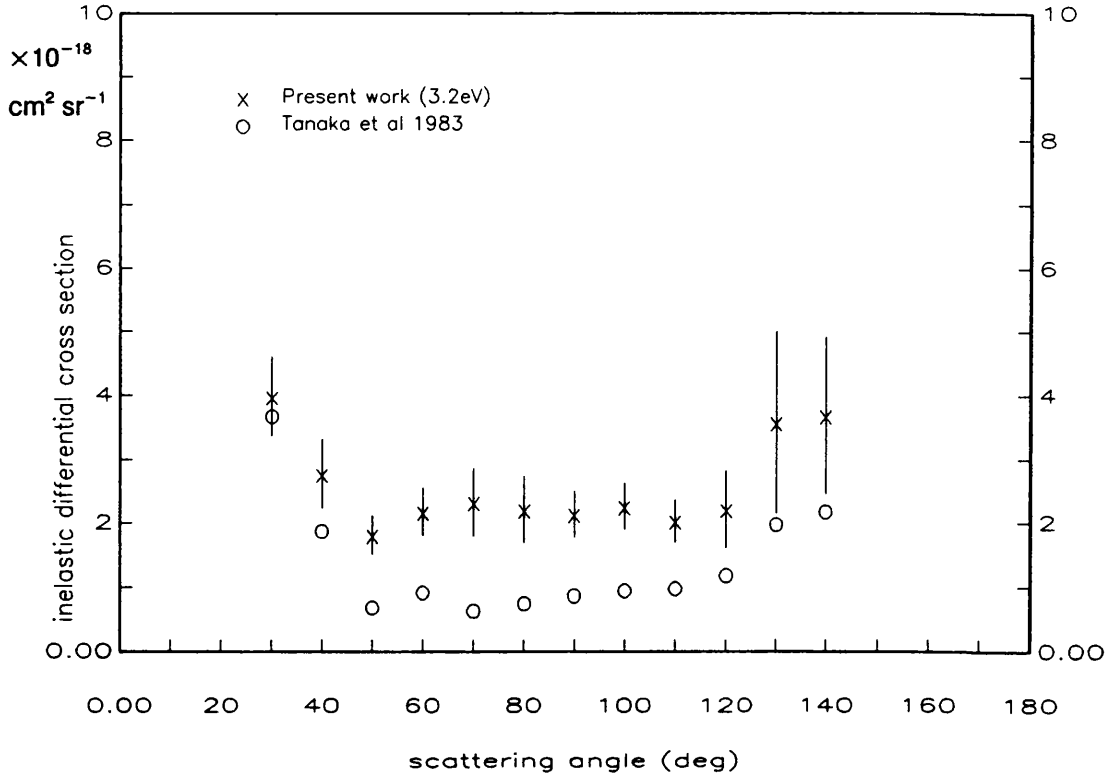

Figure 7.12 Methane $\nu_{1,3}$ 15eV

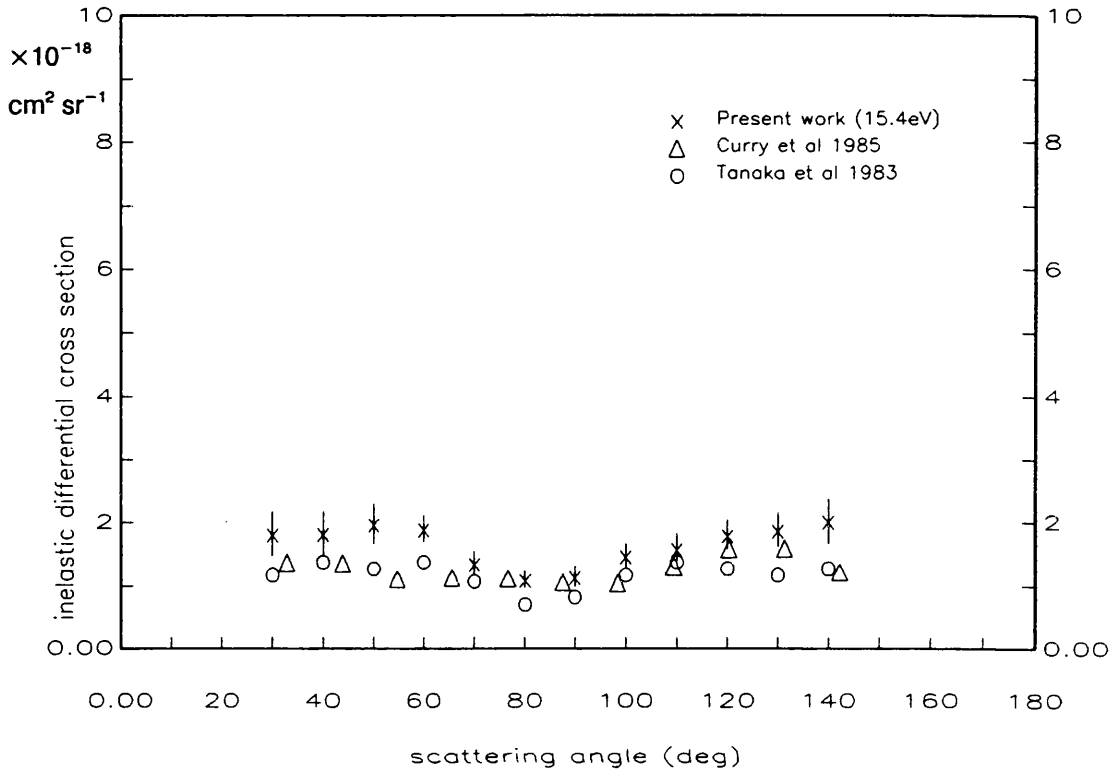

Figure 7.13 Methane $\nu_{1,3}$ 7.5eV

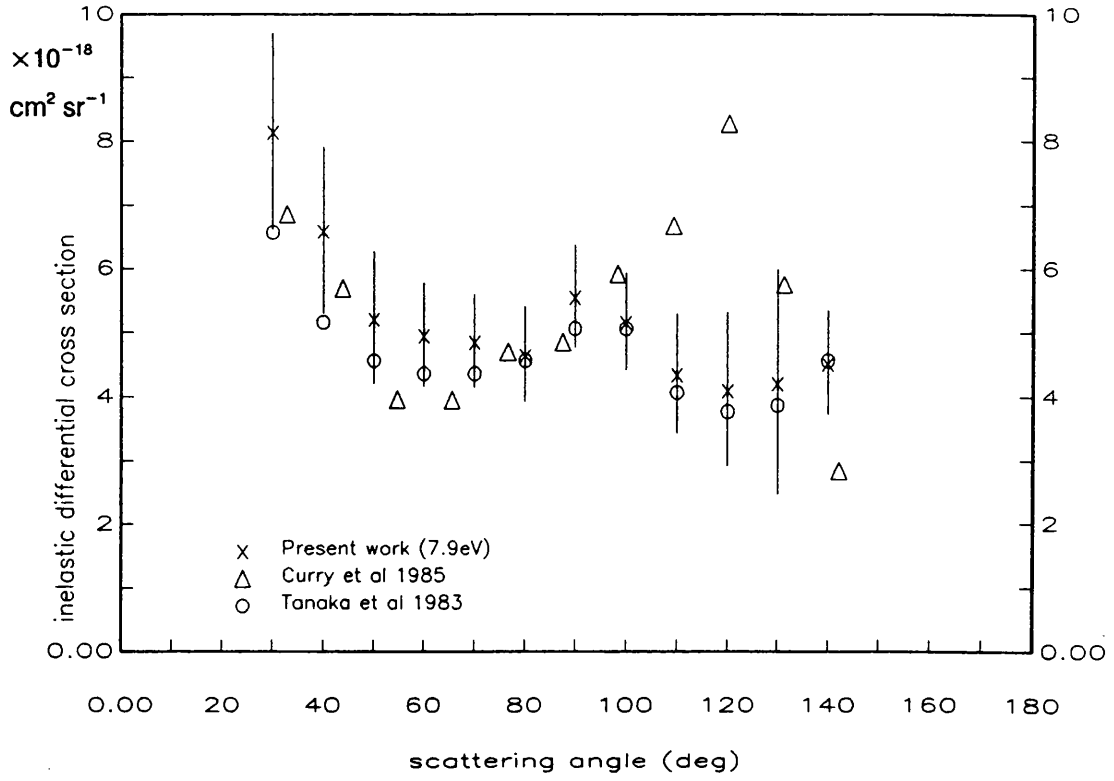

Figure 7.14 Methane $\nu_{1,3}$ 6eV

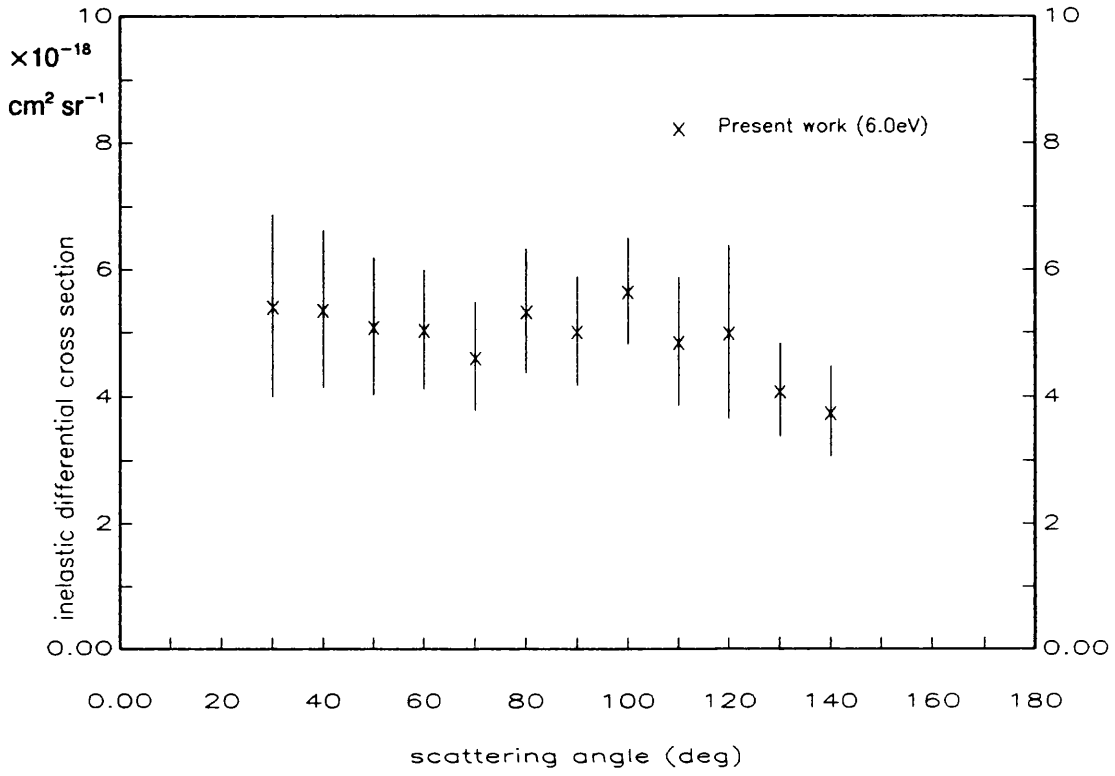

Figure 7.15 Methane $\nu_{1,3}$ 5eV

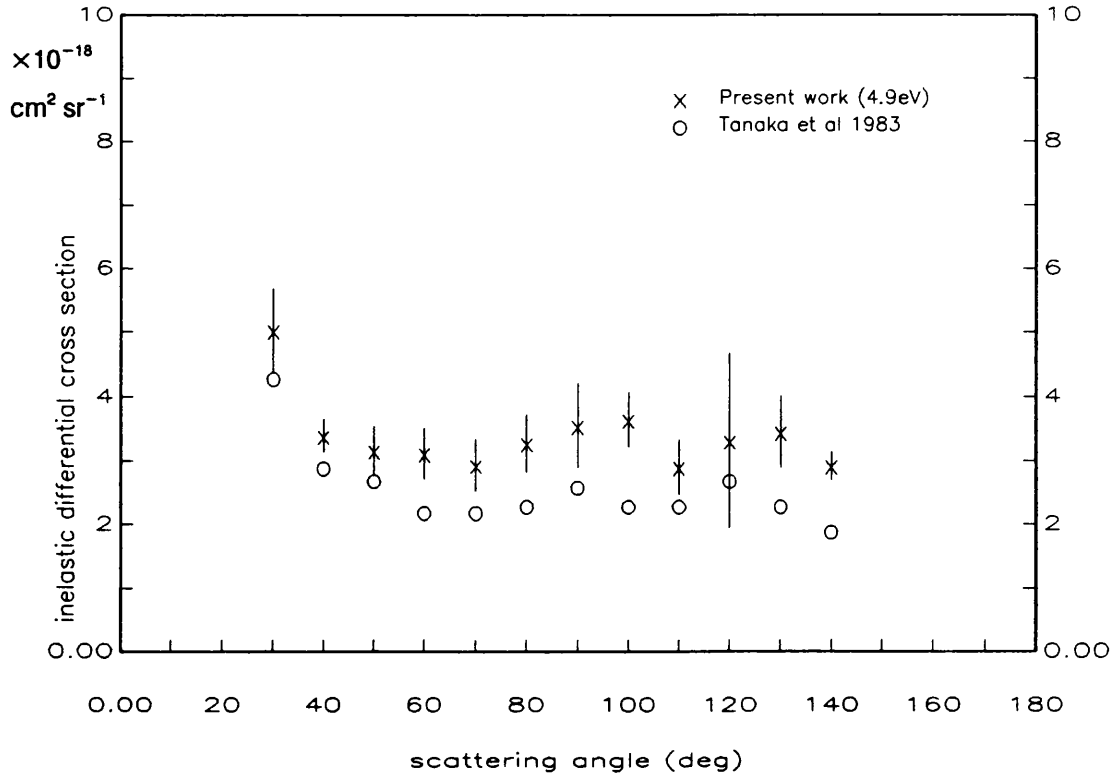

Figure 7.16 Methane $\nu_{1,3}$ 4eV

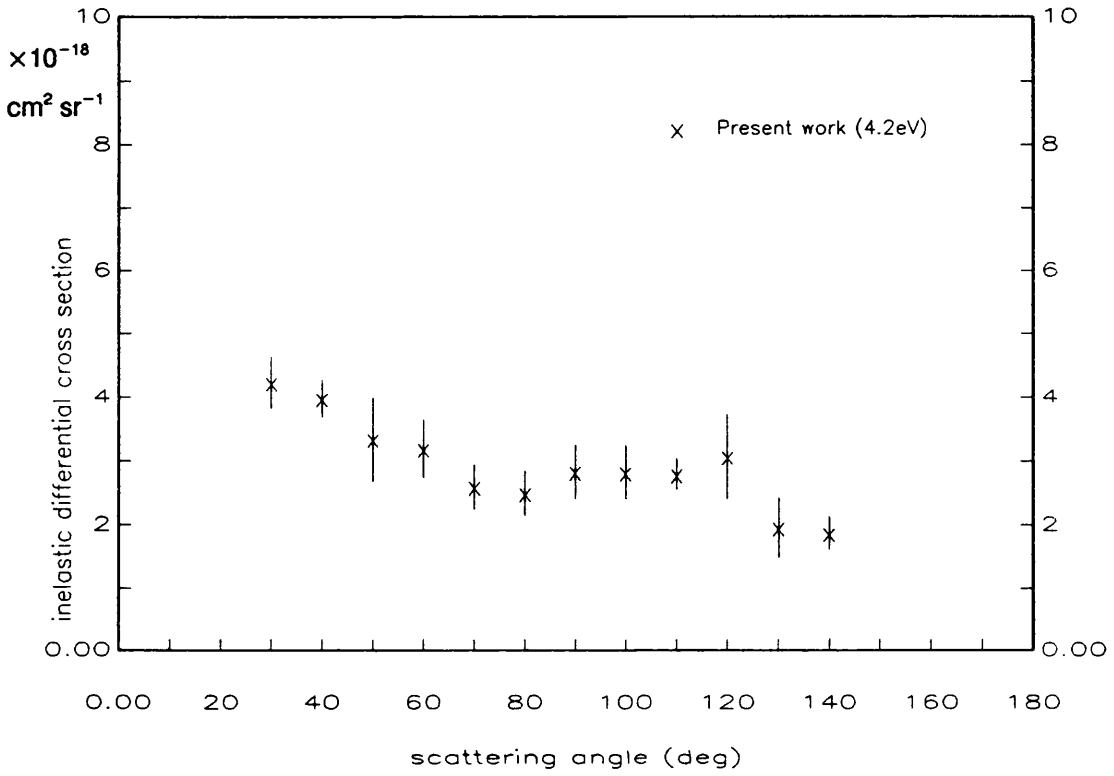

Figure 7.17 Methane $\nu_{1,3}$ 3eV

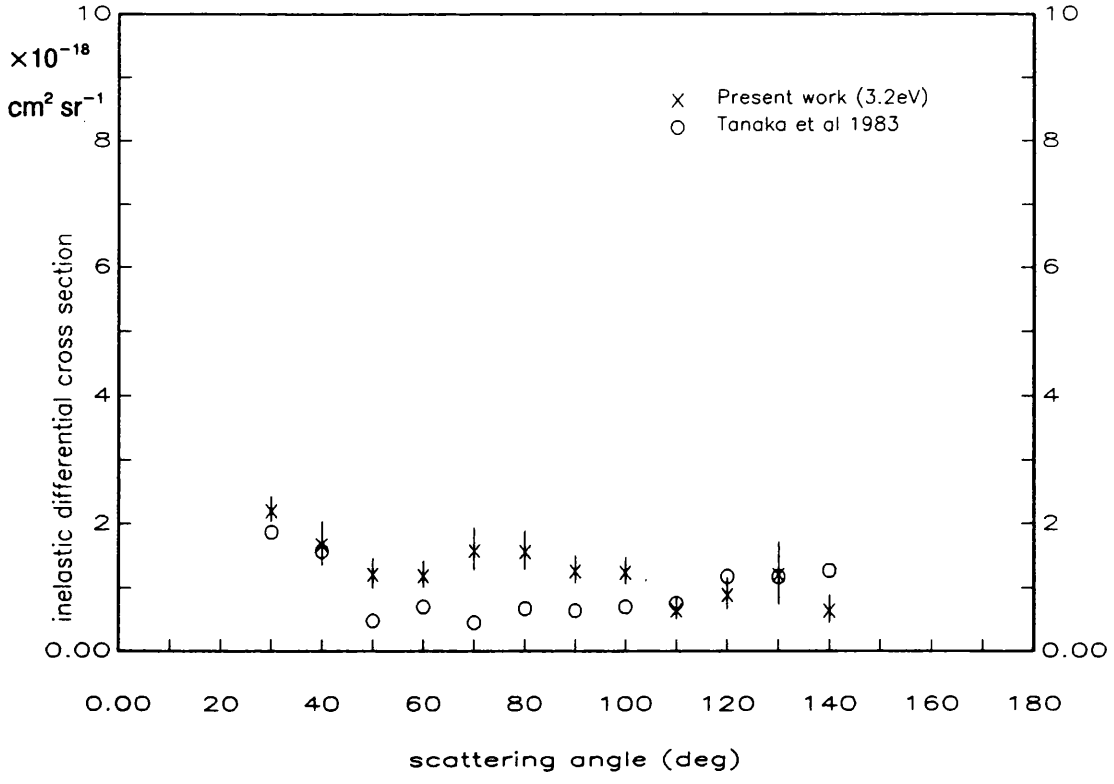

	Incident energy (eV)					
Angle (deg)	15.5eV	8.0eV	6.1eV	5.0eV	4.3eV	3.3eV
30	8.09 ± 1.03	12.99 ± 1.78	10.74 ± 1.14	10.23 ± 0.73	8.91 ± 0.84	9.23 ± 0.99
40	-	12.57 ± 1.21	10.50 ± 1.49	-	-	-
50	6.80 ± 0.64	11.51 ± 1.20	9.45 ± 1.48	8.97 ± 1.10	7.60 ± 0.74	8.43 ± 0.72
60	-	10.23 ± 1.25	8.99 ± 0.91	-	-	-
70	5.98 ± 0.48	10.42 ± 1.59	8.60 ± 0.77	8.95 ± 1.11	7.62 ± 0.76	8.98 ± 0.87
80	-	11.52 ± 0.87	9.02 ± 0.69	-	-	-
90	6.64 ± 0.55	11.53 ± 1.22	9.54 ± 0.62	9.48 ± 0.58	7.99 ± 0.82	8.54 ± 0.83
100	-	12.45 ± 1.19	10.23 ± 0.89	-	-	-
110	7.86 ± 0.92	12.57 ± 1.13	10.43 ± 0.88	10.23 ± 1.15	7.84 ± 0.61	7.75 ± 0.68
120	-	12.65 ± 0.84	10.67 ± 0.86	-	-	-
130	7.99 ± 1.22	12.60 ± 0.85	10.92 ± 1.18	10.45 ± 1.32	7.90 ± 0.78	7.89 ± 0.74
140	-	12.80 ± 1.49	11.02 ± 1.48	-	-	-

Table 7.3 Differential inelastic cross sections for C_2H_4, ν_i ($\times 10^{-18}$cm^2 sr^{-1} at 15 & 7.5eV).

	Incident energy (eV)					
Angle (deg)	15.5eV	8.0eV	6.1eV	5.0eV	4.3eV	3.3eV
30	2.88 ± 0.30	6.14 ± 0.63	9.12 ± 0.99	6.12 ± 0.61	5.73 ± 0.66	4.56 ± 0.45
40	-	6.12 ± 0.63	8.92 ± 0.86	-	-	-
50	1.78 ± 0.17	5.87 ± 0.57	8.53 ± 0.87	5.63 ± 0.54	5.25 ± 0.61	4.46 ± 0.43
60	-	5.64 ± 0.56	7.99 ± 0.79	-	-	-
70	1.51 ± 0.12	5.57 ± 0.56	8.32 ± 0.78	5.21 ± 0.54	4.95 ± 0.53	4.12 ± 0.42
80	-	5.33 ± 0.54	8.61 ± 0.86	-	-	-
90	1.85 ± 0.15	5.24 ± 0.53	8.59 ± 0.84	5.25 ± 0.52	4.85 ± 0.52	4.02 ± 0.42
100	-	5.33 ± 0.53	8.80 ± 0.89	-	-	-
110	2.24 ± 0.26	5.25 ± 0.52	8.60 ± 0.89	5.31 ± 0.59	4.63 ± 0.47	4.21 ± 0.39
120	-	5.23 ± 0.57	8.61 ± 0.92	-	-	-
130	2.45 ± 0.34	5.36 ± 0.54	8.72 ± 0.90	4.89 ± 0.46	4.21 ± 0.41	4.35 ± 0.49
140	-	5.41 ± 0.52	8.62 ± 0.93	-	-	-

Table 7.4 Differential inelastic cross sections for C_2H_4, ν_j ($\times 10^{-18}$cm^2 sr^{-1} at 15 & 7.5eV).

Figure 7.18 Ethene ν_i 15eV

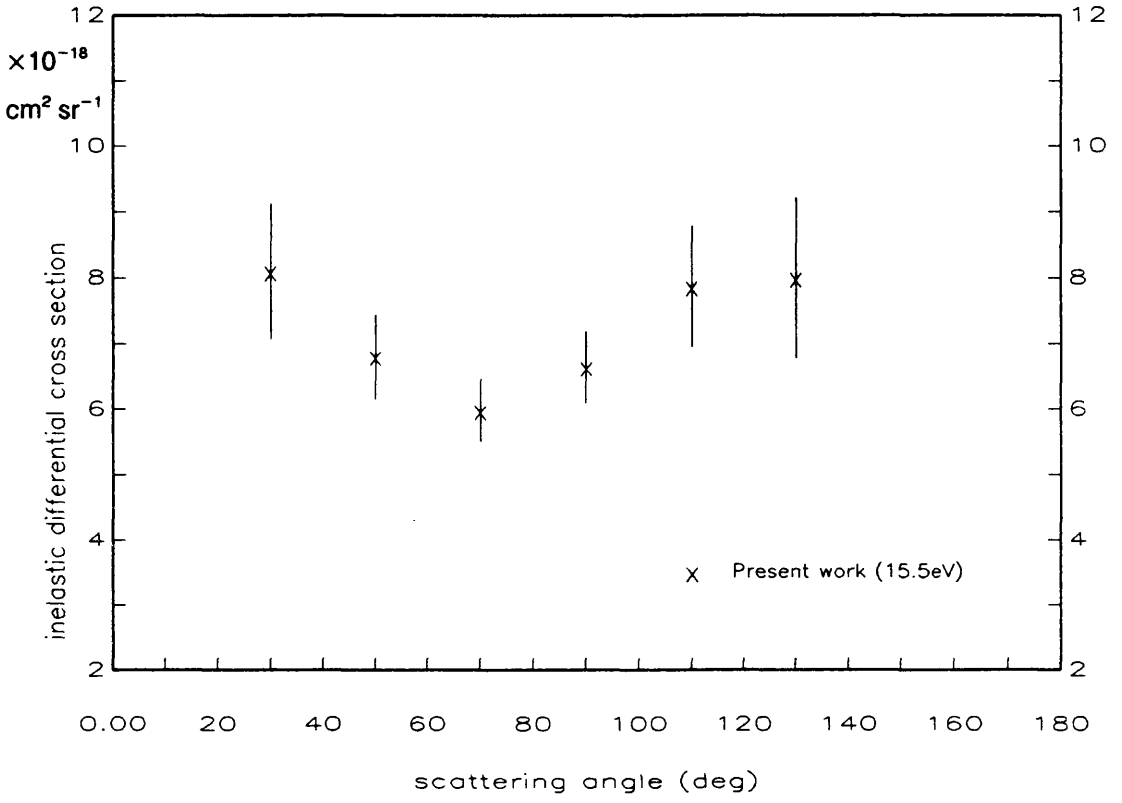

Figure 7.19 Ethene ν_i 7.5eV

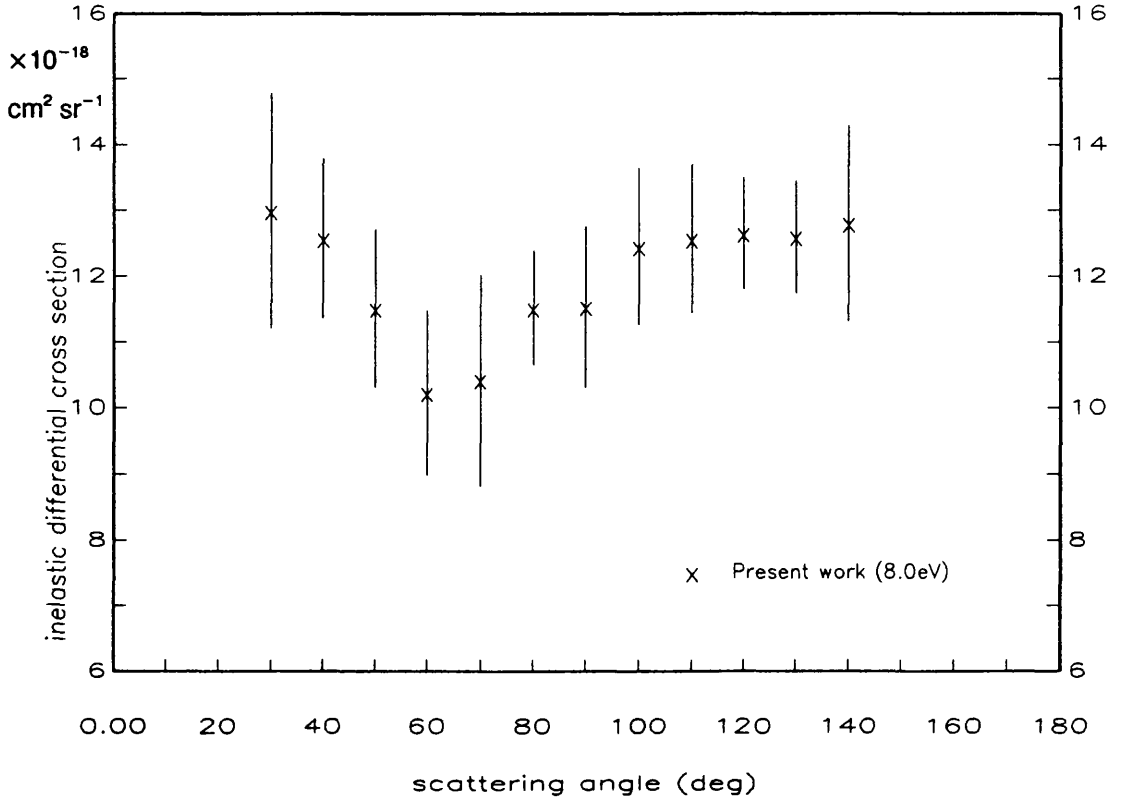

Figure 7.20 Ethene ν_i 4eV

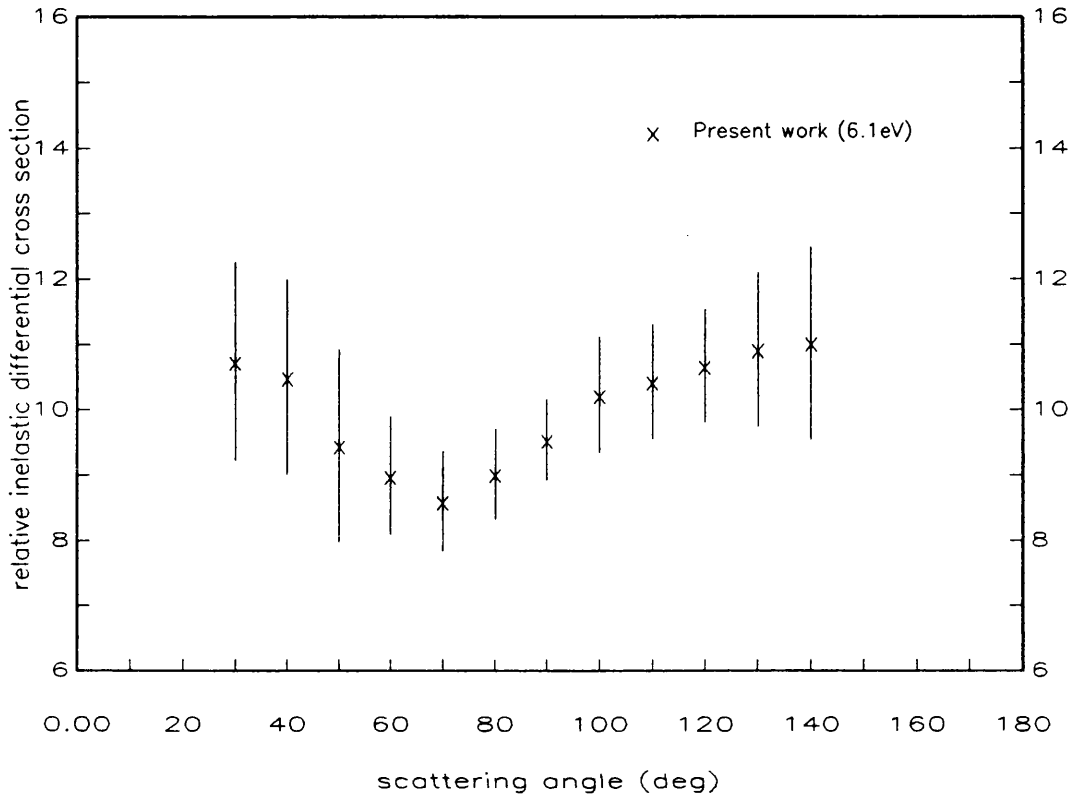

Figure 7.21 Ethene ν_i 5eV

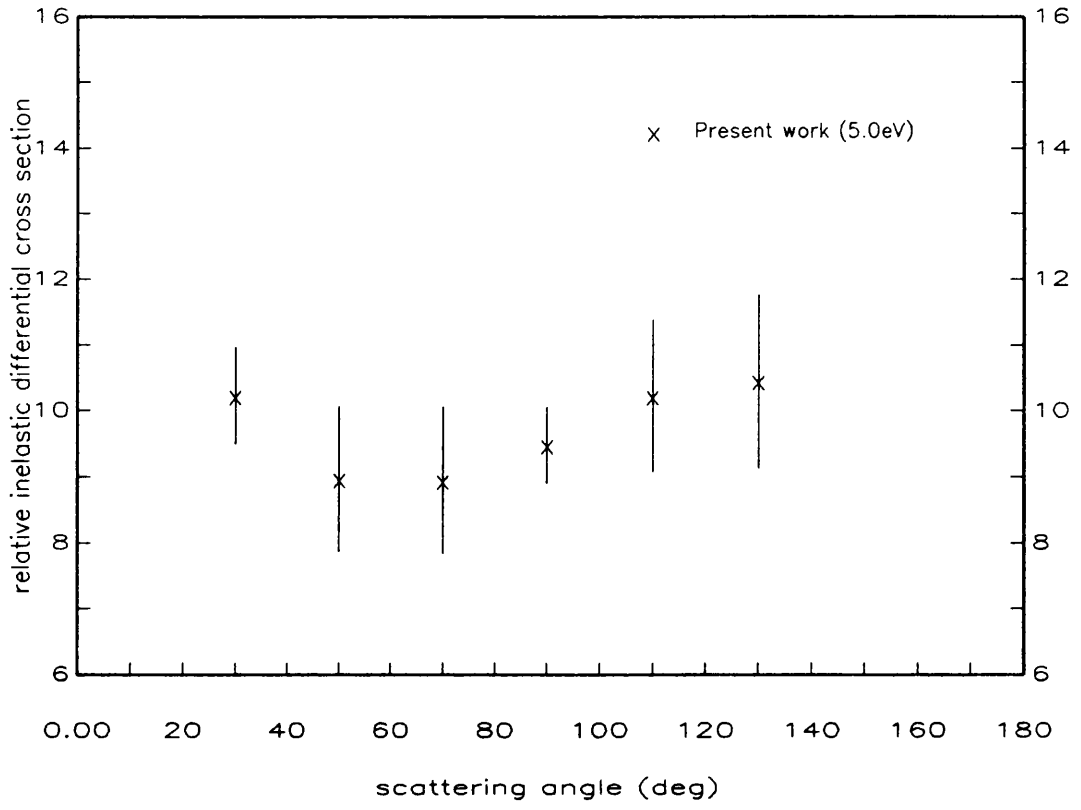

Figure 7.22 Ethene ν_i 6eV

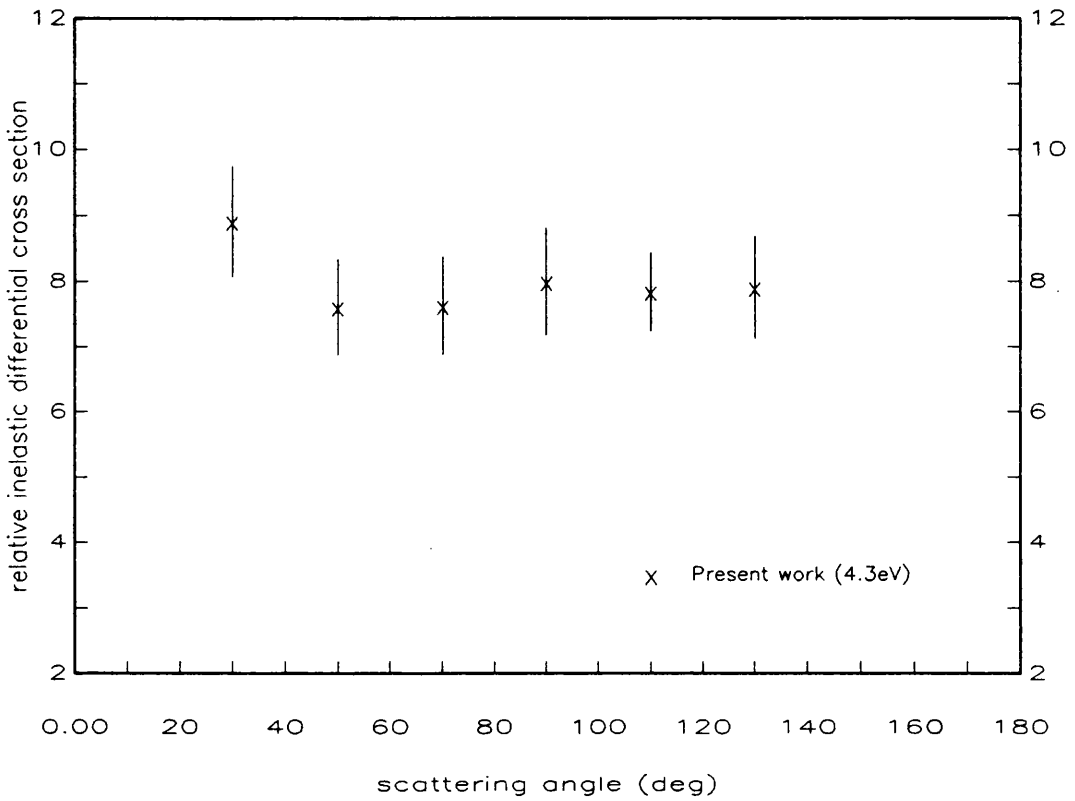

Figure 7.23 Ethene ν_i 3eV

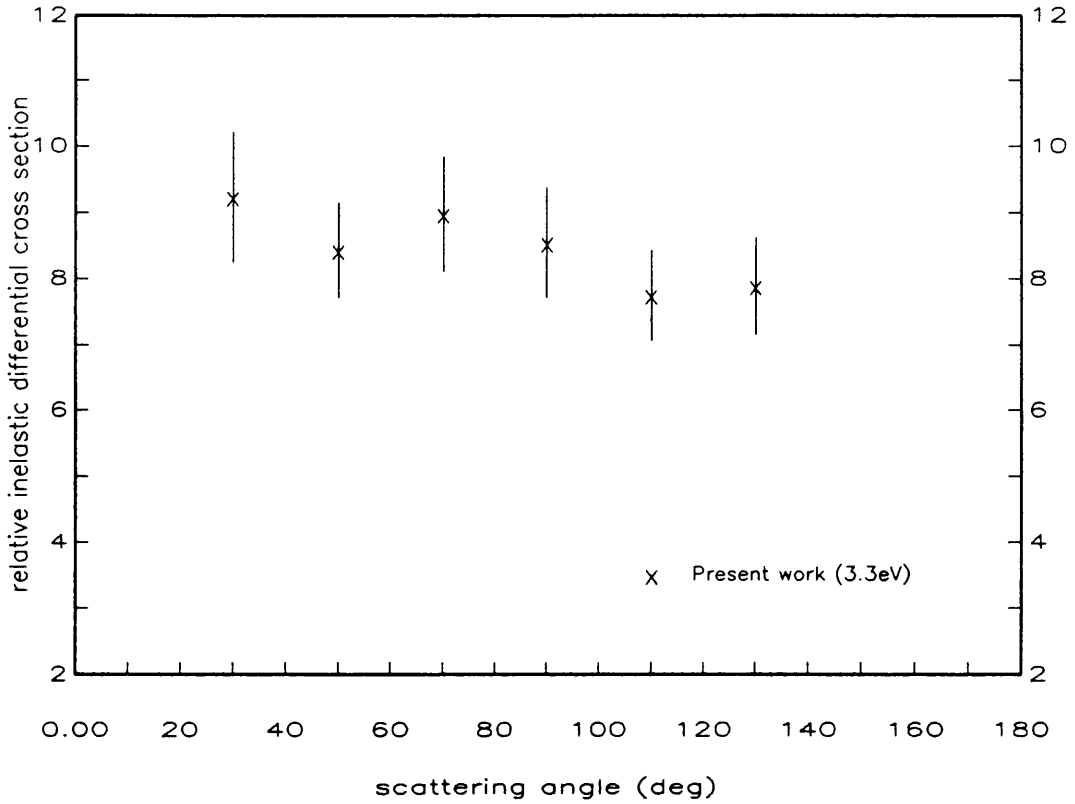

Figure 7.24 Ethene ν_j 15eV

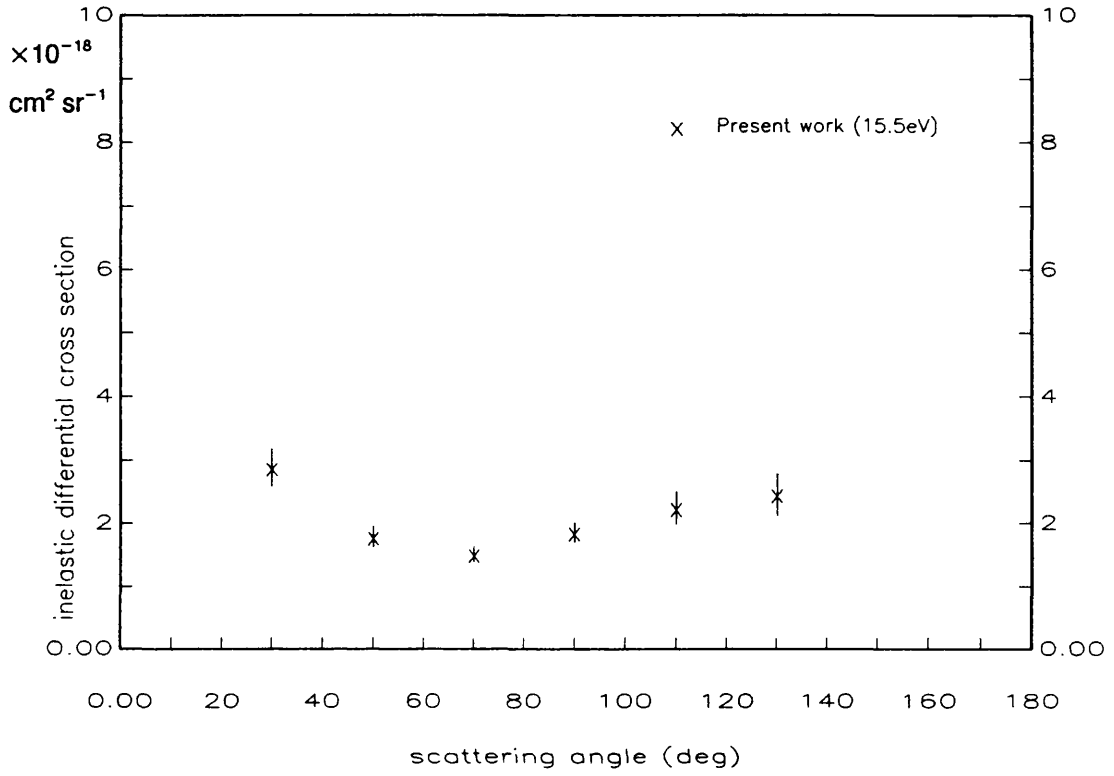

Figure 7.25 Ethene ν_j 7.5eV

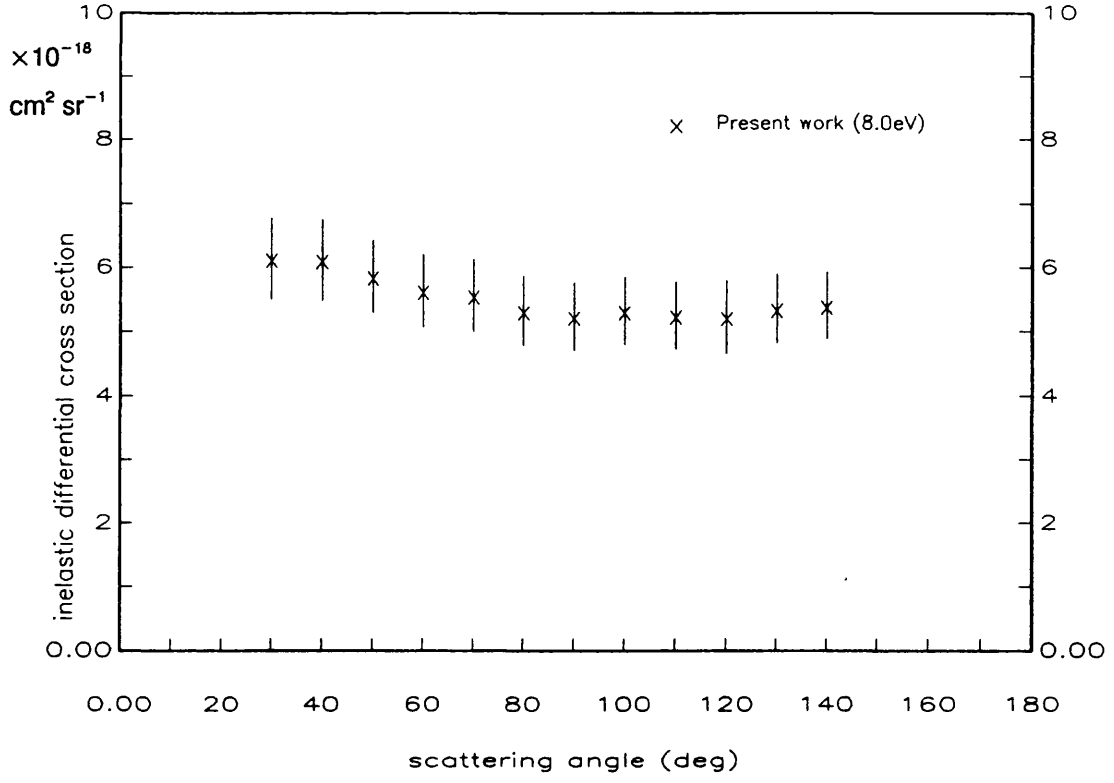

Figure 7.26 Ethene ν_j 6eV

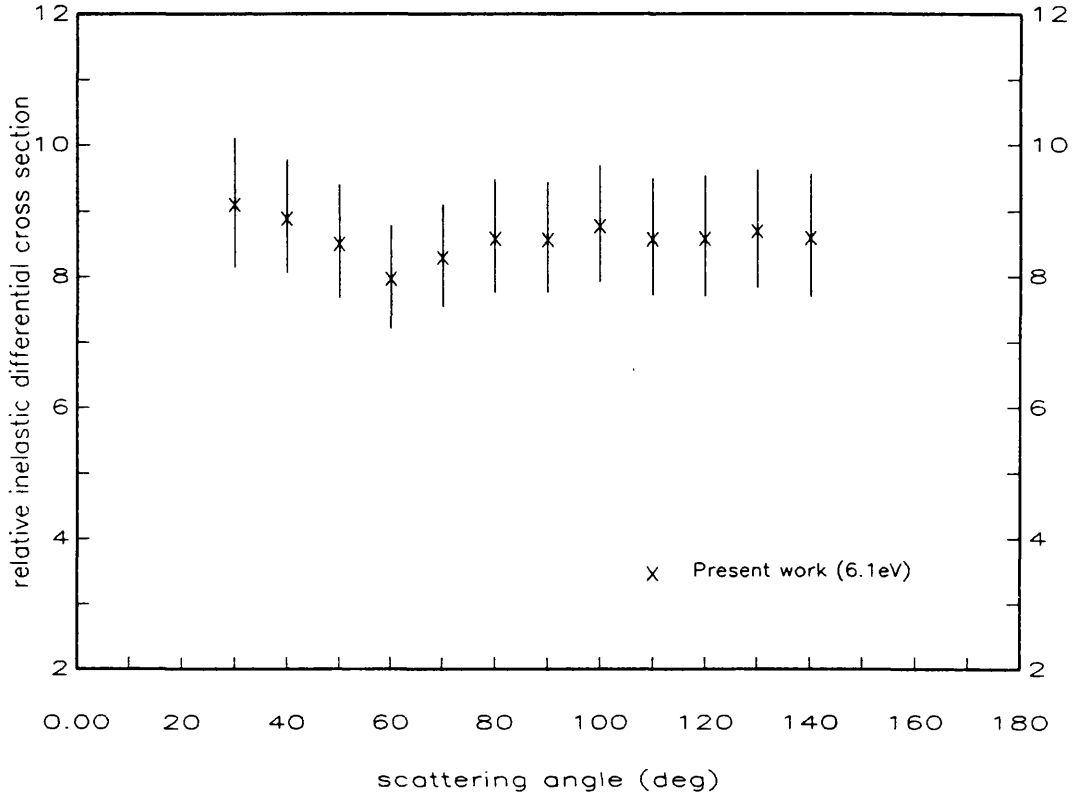

Figure 7.27 Ethene ν_j 5eV

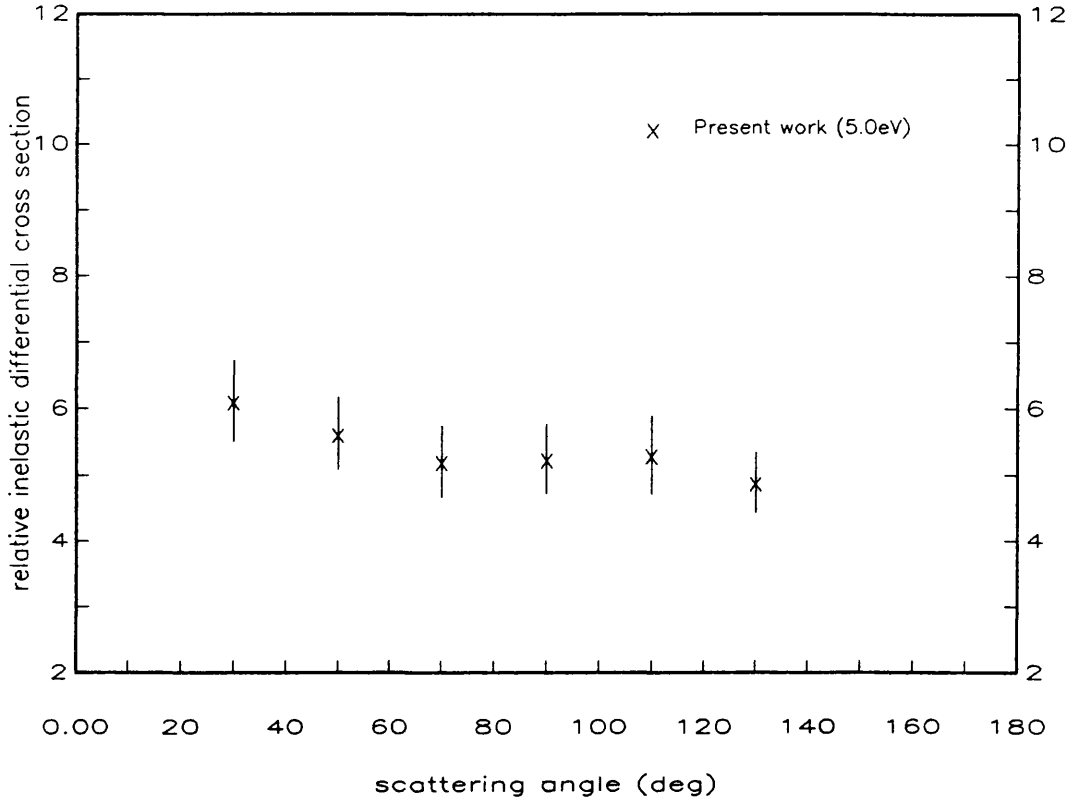

Figure 7.28 Ethene ν_j 4eV

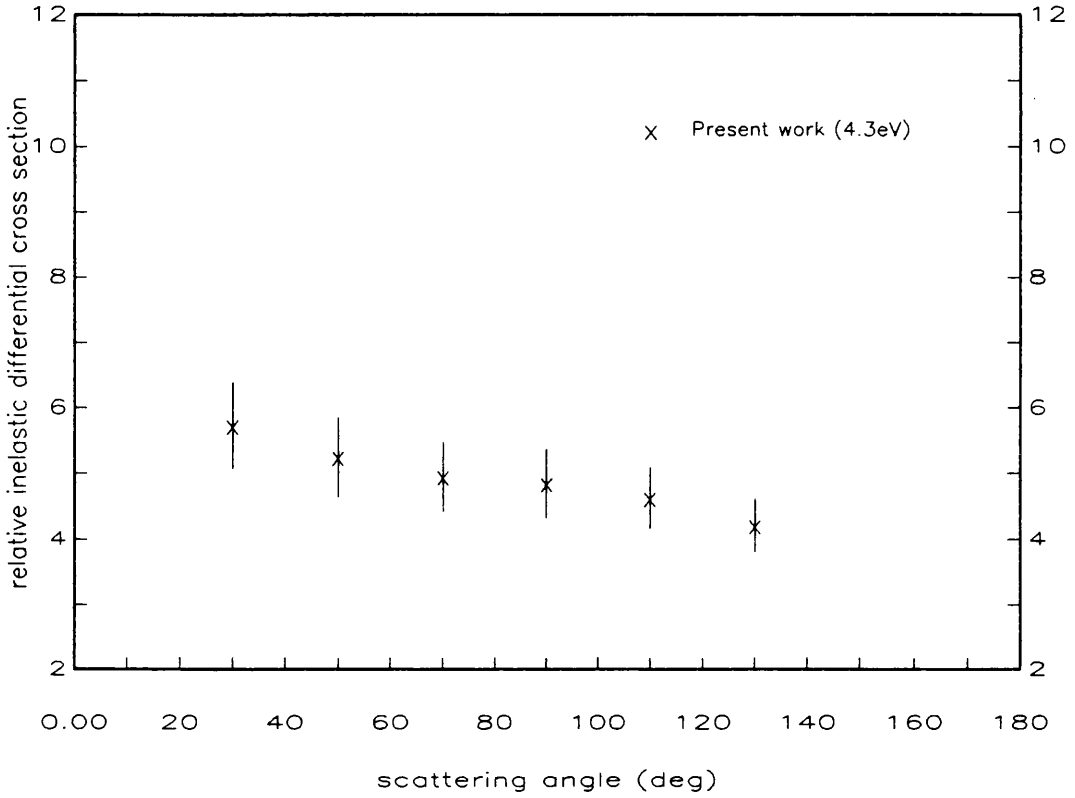

Figure 7.29 Ethene ν_j 3eV

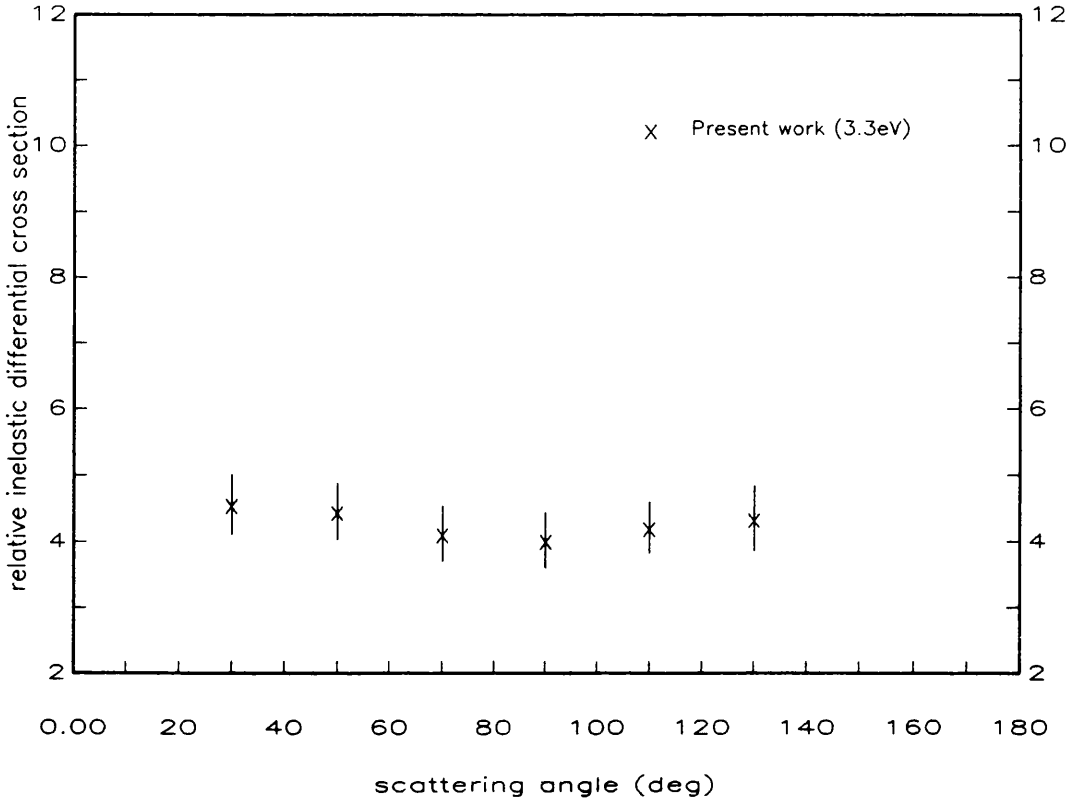

corresponding normalised absolute elastic cross sections, as no elastic data has been reported below 7.5eV, the elastic and therefore inelastic cross sections are relative over the energy range 3 to 6eV.

The ν_i excitation displays a minimum between 60 and 70° between 15 and 3eV, at the lower energies the angular distribution is virtually isotropic. The composite ν_j displays a shallow minimum at 70°, 15eV and becomes isotropic at the lower energies.

The data for the ethane excitations ν_b and ν_s are given in Tables 7.5 and 7.6 and are plotted in Figures 7.30 to 7.41. Swarm experiments (Duncan and Walker 1972) have indicated that the vibrational levels of ethane are excited with high efficiency by slow electrons as in the case of methane. However, the inability to include rotational and de-excitation processes in the analysis of these results, and the fact that the trial inelastic cross sections used considered single excitation of one vibrational mode only, usually the lowest infrared-active mode, limits the detailed information that can be obtained from this type of experiment.

The results for ethane are compared to the measured differential cross sections of Curry et al (1985) at 15 and 7.5eV, no other experimental or theoretical data is available for comparison. The present data is noticeably greater in magnitude than that of Curry et al, by up to a factor of 2. This is most likely a result of the different methods used to calculate the cross sections. In the present experiment the ratio of the areas of the inelastic peak to the elastic peak was taken to calculate the angular distribution, whereas Curry et al took the ratio of the peak heights. From Figure 7.5 it can be seen that due to the spread of excitation energies in the composite peaks ν_b and ν_s the FWHM of the elastic and inelastic peaks differ, being larger for the inelastic peaks. By taking the ratio of the areas, the full contributions of all the composite excitations is included, whereas the peak height ratios will under estimate the contributions of the excitations furthest from the peak centre. Tanaka et al (1983) also took the ratio of the peak heights when calculating the angular distributions of the composite peaks $\nu_{2,4}$ and $\nu_{1,3}$ for methane, however, as the inelastic peaks in the ethane energy loss spectra are broader than those in the methane spectra, the discrepancies in the magnitudes of the differential cross sections is greater for ethane.

At 15eV the shape of the present differential cross sections agrees well with that of Curry et al, in both sets of data the composite peaks ν_s and to a lessor extent ν_b display a shallow minimum at around 70°. The present results at 7.5eV for both composite peaks display a shallow minimum at 40° and a second broader minimum between 80 and 90° which is consistent with the presence of a weak f-wave dominated shape resonance in this energy region. This is also demonstrated by the elastic scattering results given in Section 6.4, at the same energy. As with methane the agreement with the results of Curry et al is less satisfactory at this energy, the earlier results for the ν_b composite being isotropic up to 90° then increasing in magnitude with scattering angle. The ν_s composite in the data of Curry et al,

	Incident energy (eV)					
Angle (deg)	15.4eV	7.9eV	6.0eV	4.9eV	4.2eV	3.2eV
30	6.46 ± 1.62	11.94 ± 2.98	9.67 ± 0.90	7.66 ± 1.50	5.99 ± 1.20	3.19 ± 0.56
40	5.34 ± 1.10	10.34 ± 1.97	8.24 ± 1.42	4.61 ± 0.93	5.30 ± 1.23	3.20 ± 0.56
50	4.99 ± 0.99	11.43 ± 2.27	8.41 ± 1.60	6.16 ± 1.21	4.34 ± 0.98	2.99 ± 0.54
60	4.55 ± 0.87	12.75 ± 2.43	8.51 ± 1.62	7.55 ± 1.44	6.47 ± 1.23	2.79 ± 0.53
70	4.64 ± 0.88	12.38 ± 2.35	8.38 ± 1.56	7.21 ± 1.43	5.95 ± 1.13	3.31 ± 0.55
80	4.58 ± 0.83	9.02 ± 1.72	7.16 ± 1.36	5.74 ± 1.09	6.81 ± 1.25	3.41 ± 0.65
90	5.56 ± 1.06	9.92 ± 1.72	6.94 ± 1.26	4.10 ± 0.78	6.14 ± 1.17	3.14 ± 0.60
100	5.70 ± 1.08	11.89 ± 2.26	7.82 ± 1.49	4.37 ± 0.83	6.58 ± 1.25	2.55 ± 0.49
110	5.51 ± 0.96	12.54 ± 1.66	8.89 ± 1.76	5.12 ± 0.97	6.71 ± 1.37	2.61 ± 0.50
120	5.31 ± 1.01	13.43 ± 1.67	9.66 ± 1.76	6.26 ± 1.42	5.46 ± 1.45	3.30 ± 0.63
130	5.65 ± 1.11	13.35 ± 1.79	10.98 ± 2.09	6.89 ± 1.72	5.15 ± 1.41	3.43 ± 0.65
140	6.03 ± 1.56	13.89 ± 2.50	11.25 ± 2.40	8.23 ± 2.19	5.28 ± 1.28	3.15 ± 0.60

Table 7.5 Differential inelastic cross sections for C_2H_6, ν_b ($\times 10^{-18}$cm^2 sr^{-1}).

	Incident energy (eV)					
Angle (deg)	15.4eV	7.9eV	6.0eV	4.9eV	4.2eV	3.2eV
30	5.70 ± 1.43	10.07 ± 2.51	8.97 ± 1.90	4.57 ± 0.90	4.23 ± 0.61	2.22 ± 0.42
40	5.72 ± 1.18	7.74 ± 1.47	8.38 ± 1.80	3.18 ± 0.64	4.03 ± 0.94	2.13 ± 0.40
50	5.55 ± 1.07	9.68 ± 1.92	7.47 ± 1.42	4.61 ± 0.91	3.98 ± 0.77	2.04 ± 0.39
60	4.76 ± 0.91	9.95 ± 1.89	8.05 ± 1.53	6.53 ± 1.24	4.94 ± 0.94	2.03 ± 0.39
70	4.08 ± 0.78	10.03 ± 1.91	9.51 ± 1.77	7.64 ± 1.51	4.93 ± 0.94	2.21 ± 0.42
80	3.98 ± 0.72	6.98 ± 1.33	7.23 ± 1.37	6.40 ± 1.22	4.95 ± 0.91	2.53 ± 0.48
90	4.86 ± 0.98	7.15 ± 1.24	6.41 ± 1.16	4.09 ± 0.78	4.13 ± 0.79	1.82 ± 0.35
100	5.19 ± 0.99	8.37 ± 1.59	6.90 ± 1.31	3.44 ± 0.65	4.16 ± 0.79	1.67 ± 0.32
110	5.27 ± 0.92	10.11 ± 2.12	7.61 ± 1.45	4.28 ± 0.82	4.53 ± 0.92	2.43 ± 0.46
120	5.39 ± 1.03	10.24 ± 2.13	8.94 ± 1.67	4.49 ± 1.02	4.04 ± 1.07	2.30 ± 0.44
130	6.64 ± 1.71	10.11 ± 2.12	10.49 ± 2.00	4.57 ± 1.14	2.77 ± 0.76	2.40 ± 0.46
140	6.63 ± 1.72	11.67 ± 2.61	11.53 ± 2.12	5.39 ± 1.44	2.94 ± 0.71	2.40 ± 0.46

Table 7.6 Differential inelastic cross sections for C_2H_6, ν_s ($\times 10^{-18}$cm^2 sr^{-1}).

Figure 7.30 Ethane ν_b 15eV

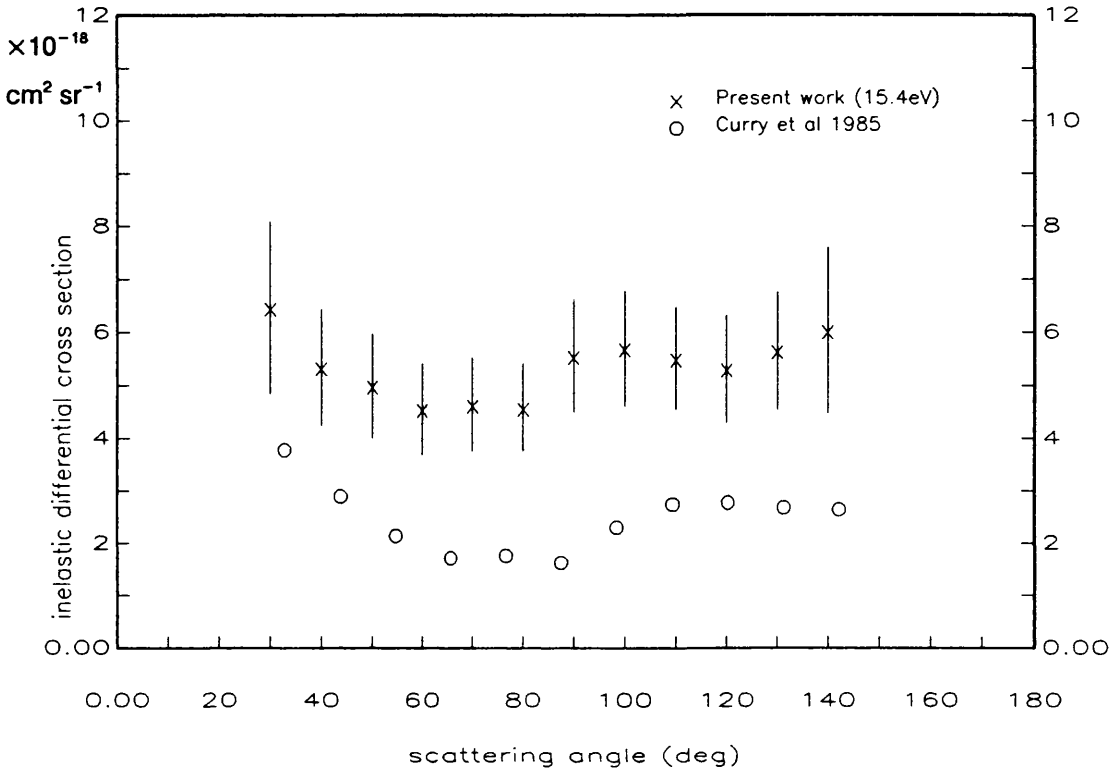

Figure 7.31 Ethane ν_b 7.5eV

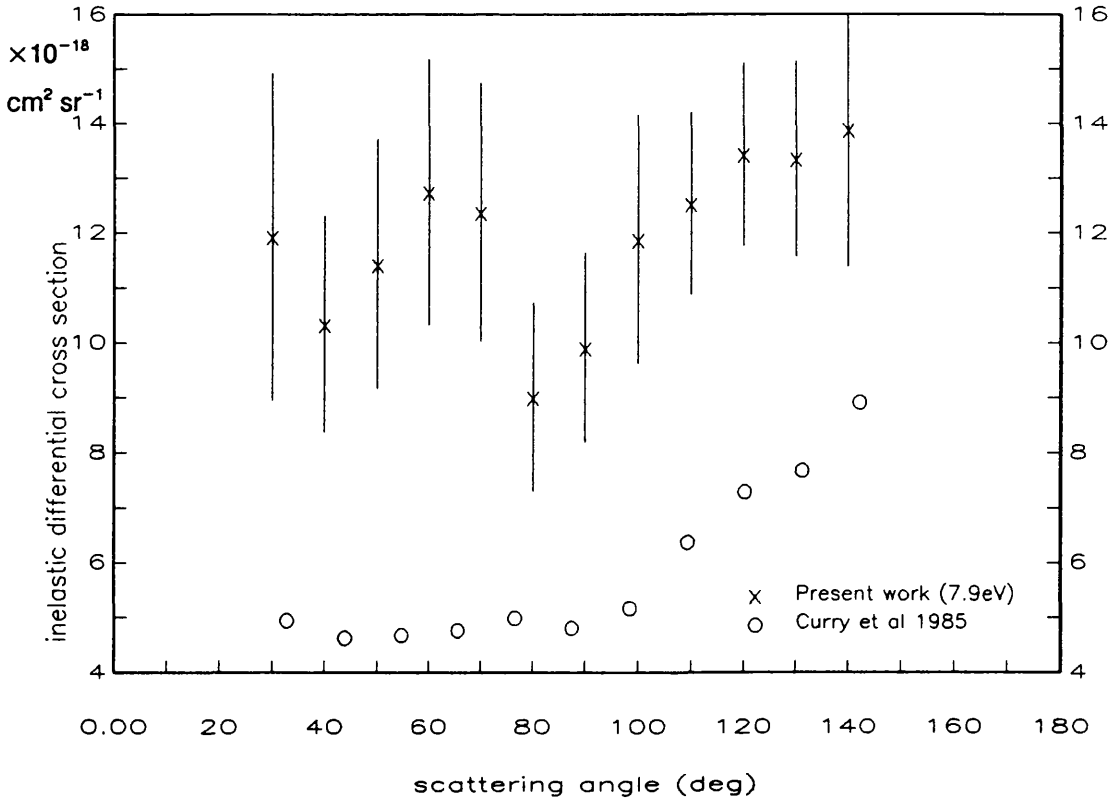

Figure 7.32 Ethane ν_b 6eV

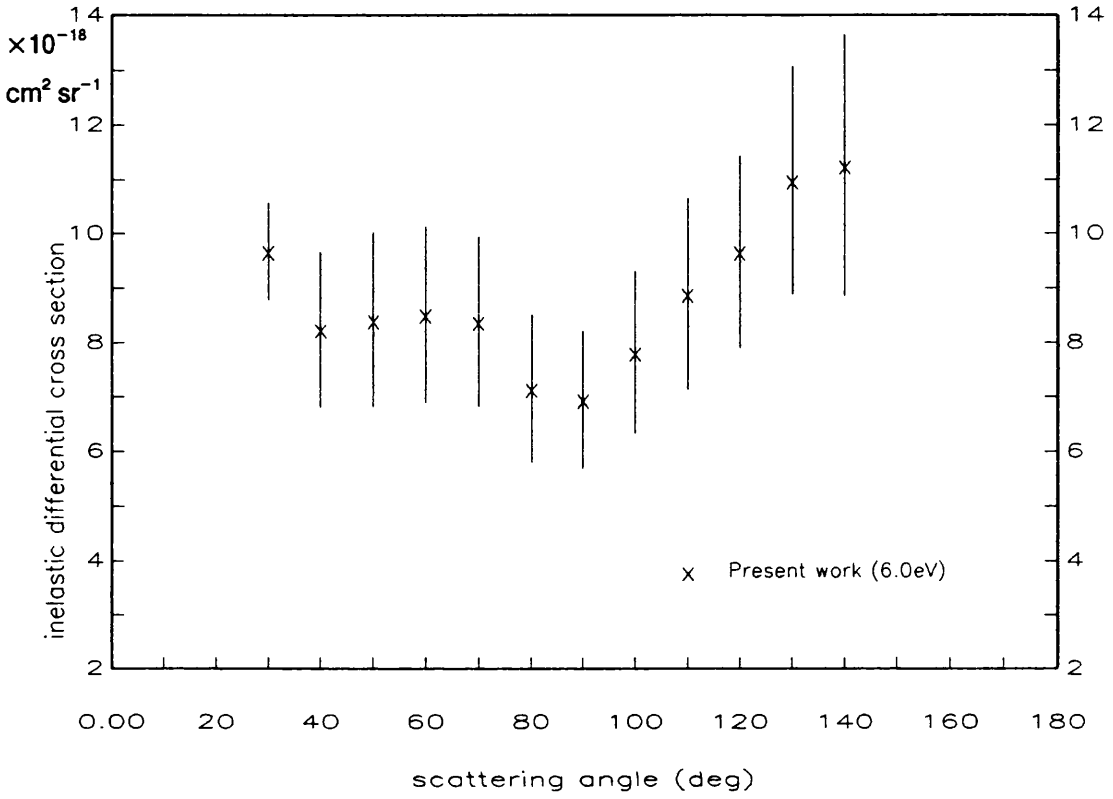

Figure 7.33 Ethane ν_b 5eV

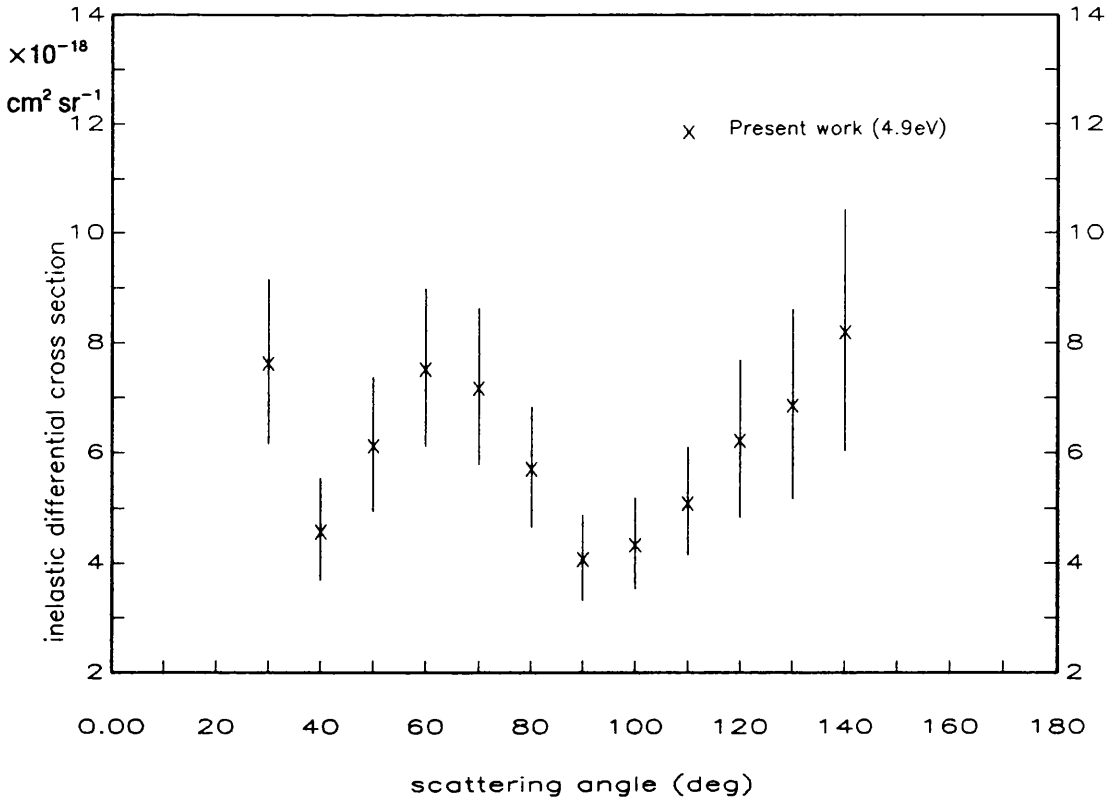

Figure 7.34 Ethane ν_b 4eV

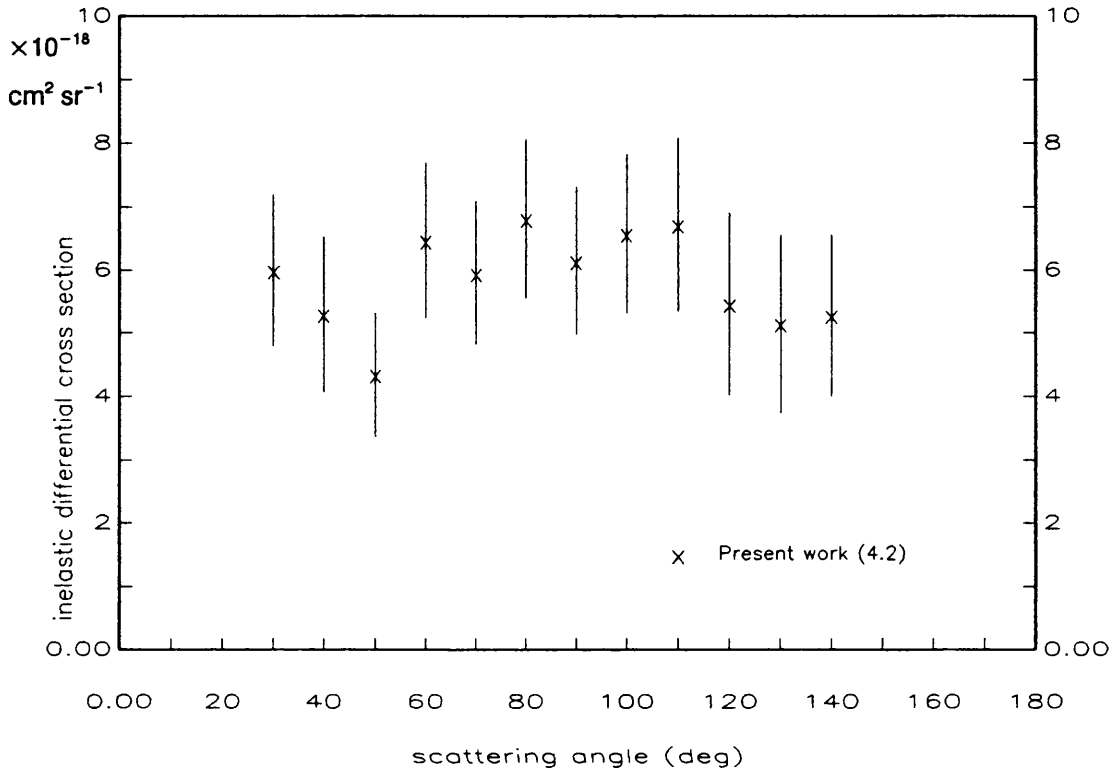

Figure 7.35 Ethane ν_b 3eV

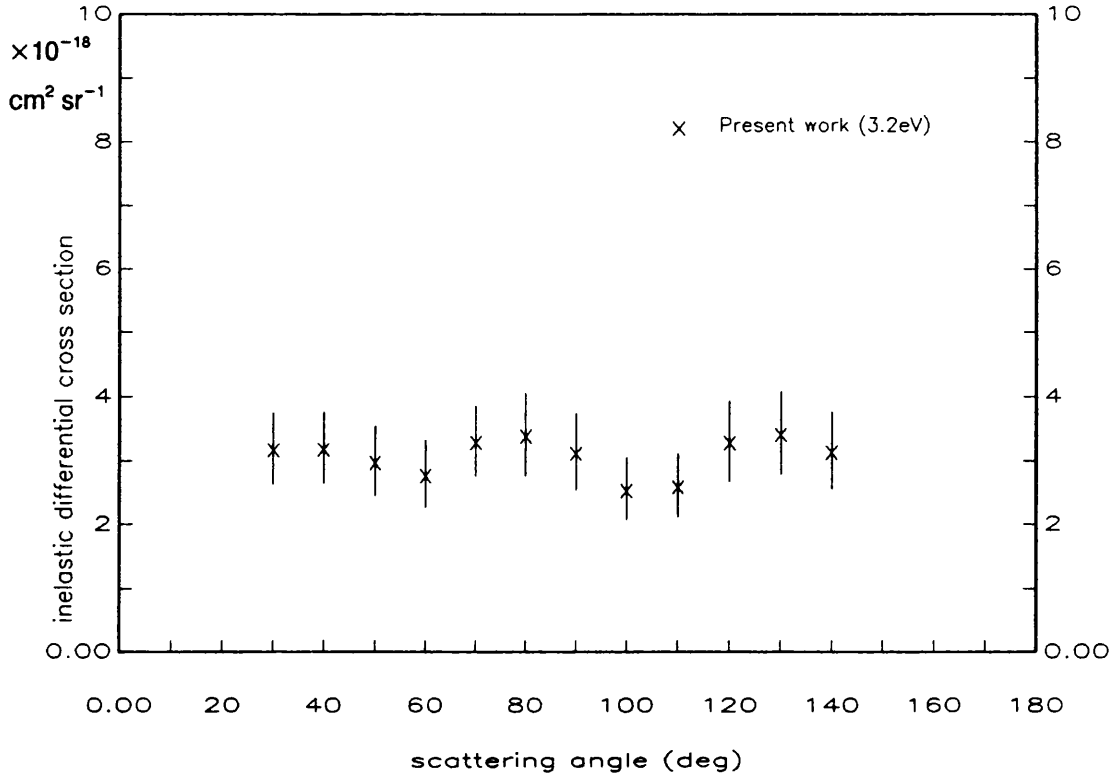

Figure 7.36 Ethane ν_s 15eV

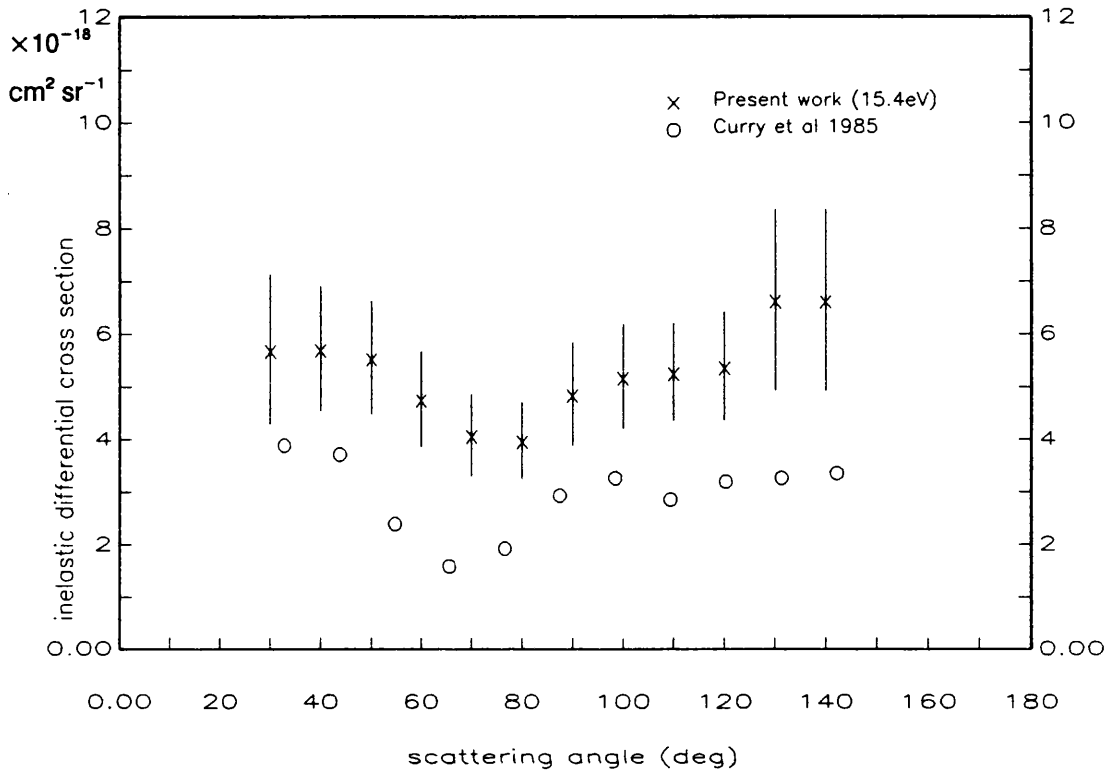

Figure 7.37 Ethane ν_s 7.5eV

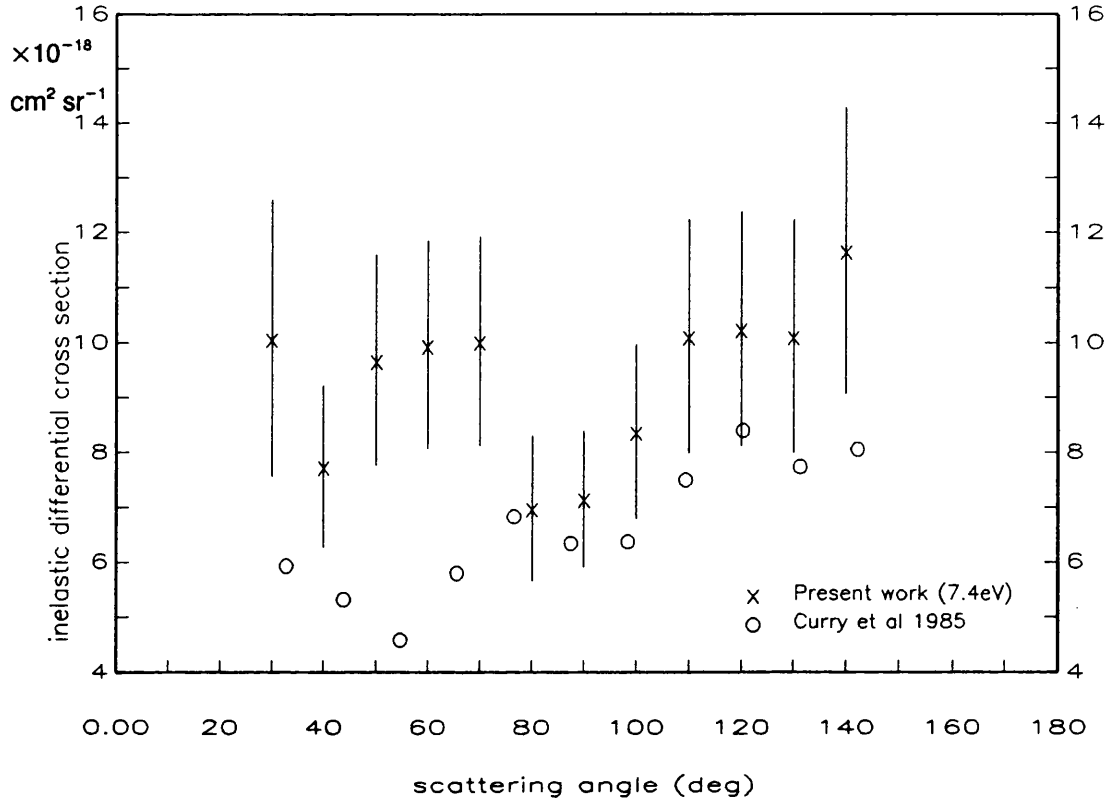

Figure 7.38 Ethane ν_s 6eV

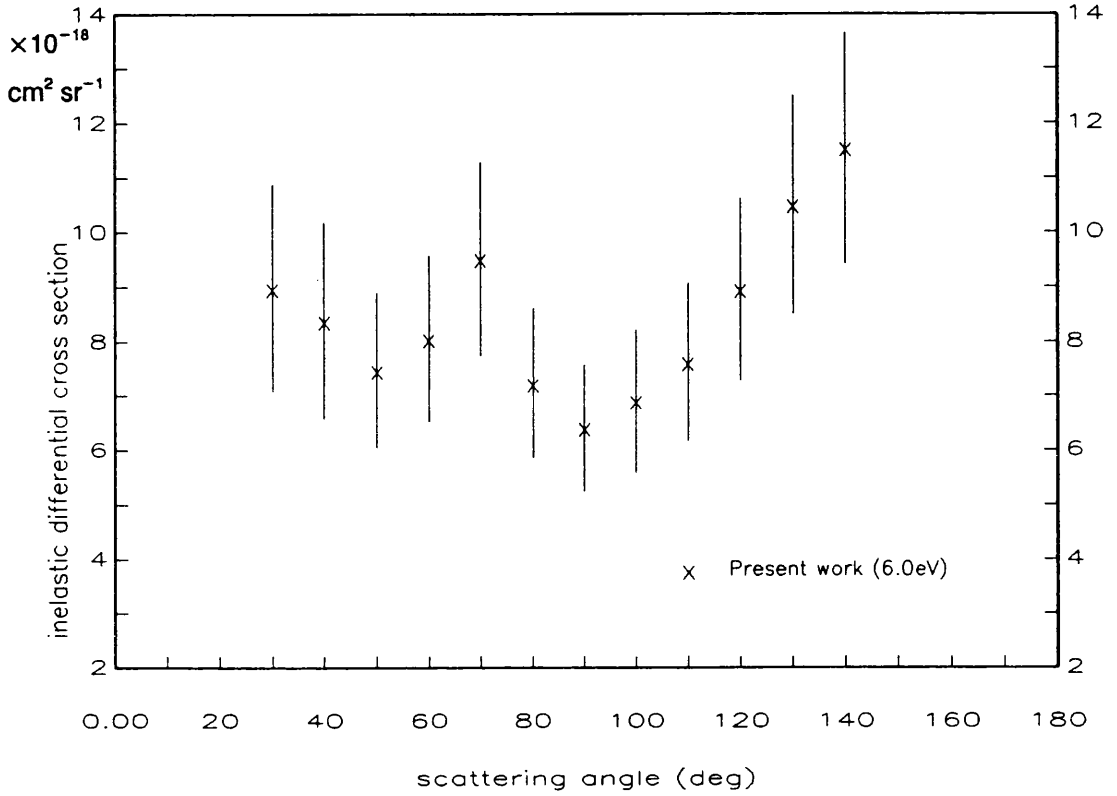

Figure 7.39 Ethane ν_s 5eV

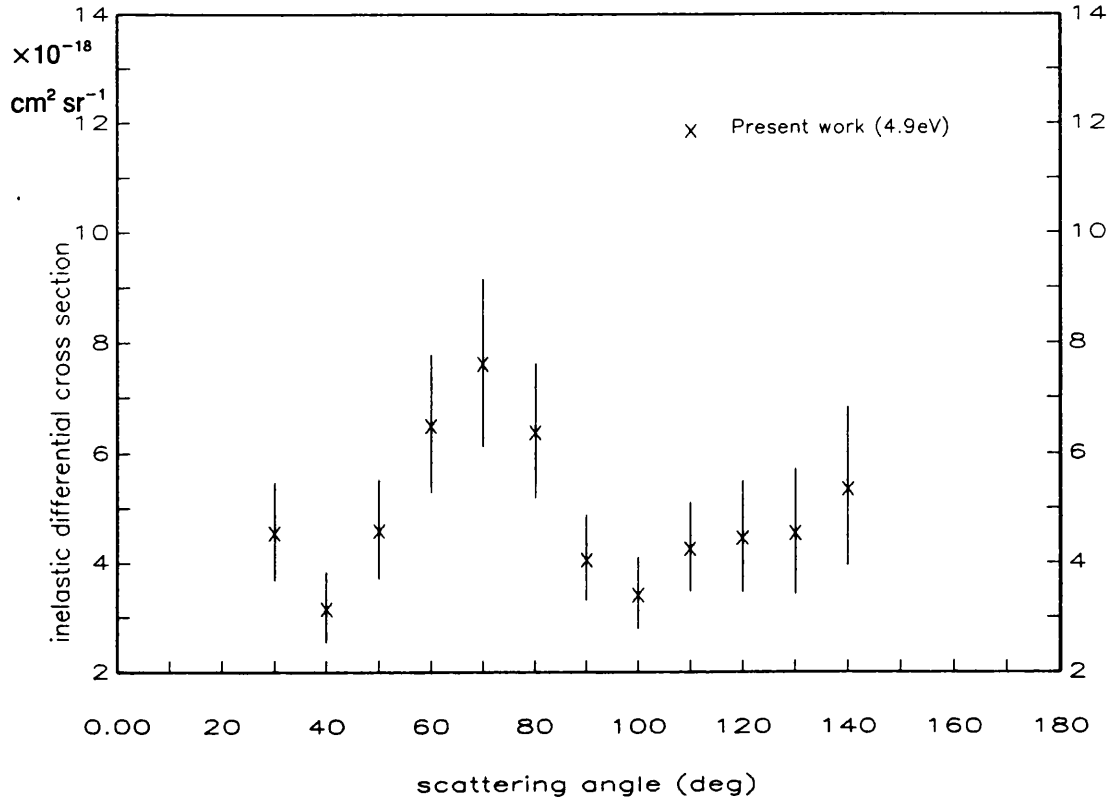

Figure 7.40 Ethane ν_s 4eV

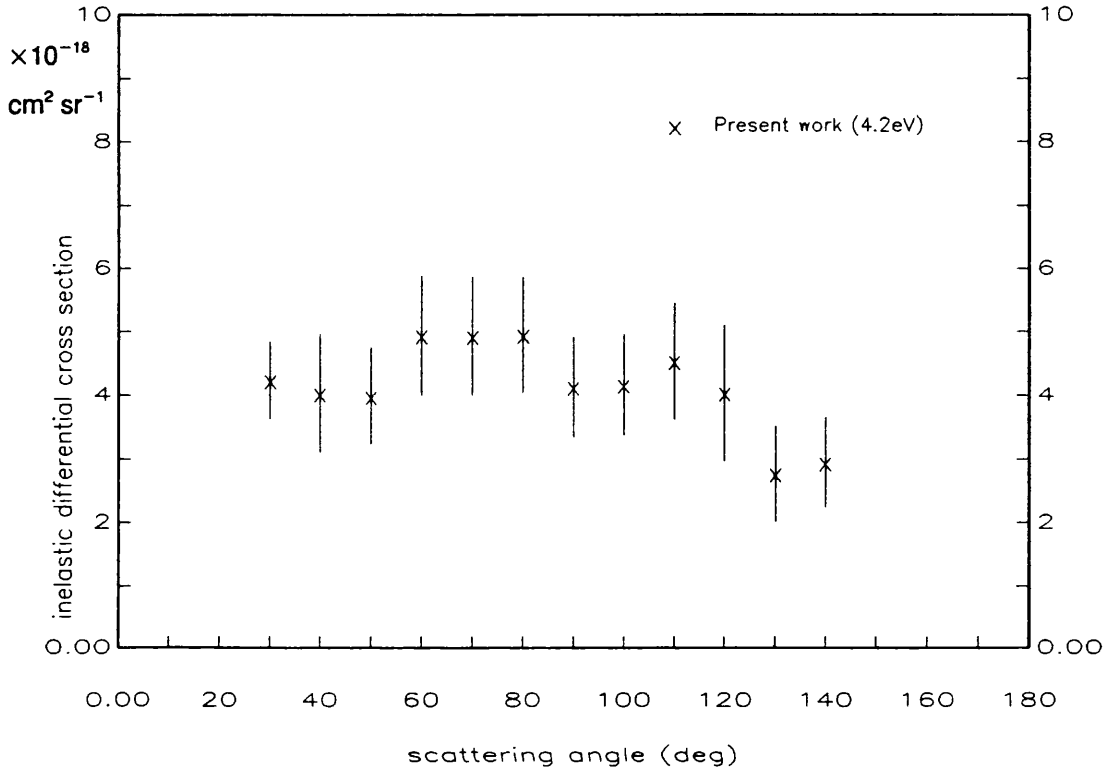

Figure 7.41 Ethane ν_s 3eV

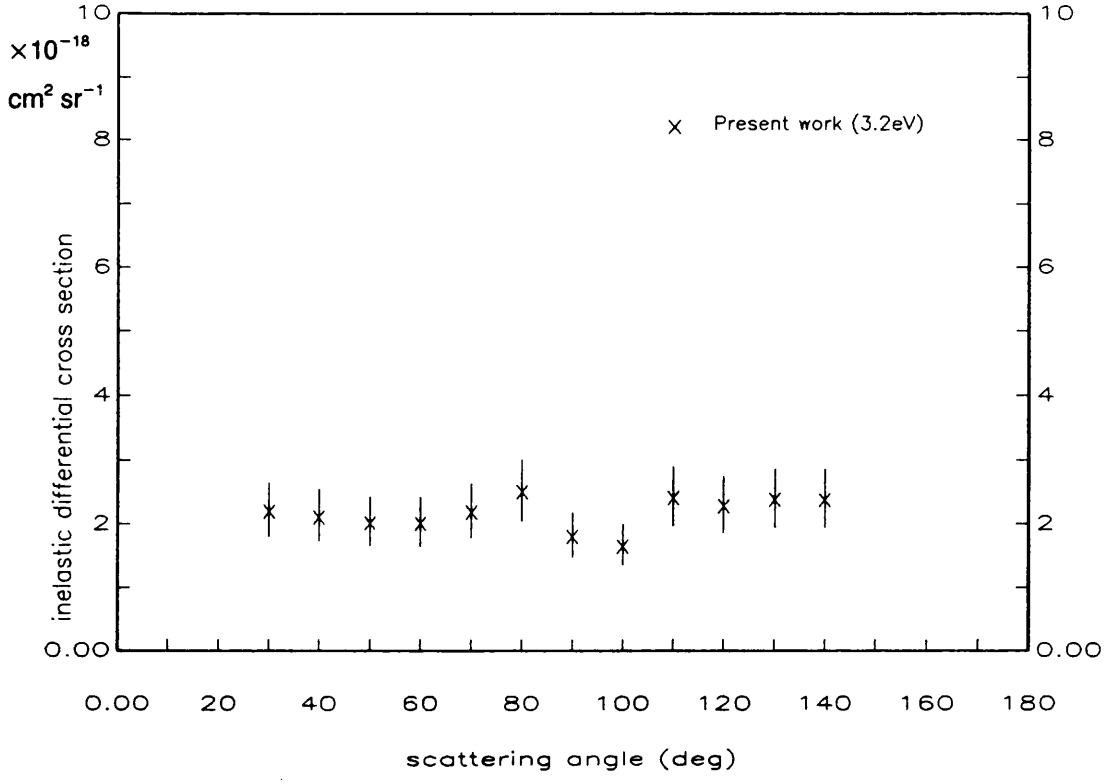

however, does displays a slight f-wave influence with very shallow minima at 50° and 100°. In the present measurements the ν_s and ν_b excitation continue to exhibit weak f-wave features down to 4eV. At 3eV both the ν_b and ν_s excitations have fairly isotropic angular distributions.

7.6 Summary

The present measurements provide a range of quantitative data for the $\nu_{1,3}$ and $\nu_{2,4}$ vibrational excitations of methane, over the incident energy range 3 to 15eV and angular range 30 to 140°. Measurements are also presented over the same energy and angular range for the excitations of the composite modes ν_b and ν_s of ethane and ν_i and ν_j of ethene.

The differential cross sections of both excitational peaks of methane show d-wave characteristics at 7.5eV, which indicate resonant enhancement of the vibrational excitation channels. Ethane displays f-wave characteristics at this energy, also for both excitational peaks, again this may be due to resonant enhancement of the vibrational excitation.

Further investigations are necessary to assess the contribution of resonance enhancement to the vibrational excitation cross section in this energy region. Such experiments would also stimulate developments in the theoretical treatment of vibrational excitation which to date has only been applied to a few simple molecules eg hydrogen, nitrogen and carbon dioxide.

Chapter 8 - Future Developments

The electron spectrometer worked well over the required energy range 3 to 15eV and no further modifications would appear to be necessary. The same is true of the interface which worked reliably during the course of the experiment. The interface, however, could be further developed as at the moment only one of the possible eight output voltages is being utilised. A second voltage ramp could be output and applied to the outer plate of the reference detector, allowing the voltage on this plate to be varied automatically to bring the data and reference elastic peaks into line when collecting elastic differential cross section data (see Section 4.4.2). As a further extension, variable voltages could be applied to the central elements of lenses G, H, I and the inner and outer hemispheres, the voltages on these elements could then be adjusted automatically to maximise the count rate at the data detector using a suitable algorithm.

The major outstanding improvement to the experimental apparatus is to allow for absolute elastic measurements to be made using the 'relative flow' technique. This technique has been described in detail by Srivastava et al (1981) and Nickel et al (1989) and was used by Tanaka et al (1982,1988) whose methane and ethane data were used to normalise the present results.

In this method the elastically scattered electrons from helium and the gas under study are measured at a given E and θ, under experimental conditions where the effective scattering volumes or their ratios can be easily measured and accurately established. Once this is achieved, the elastic differential cross section for the gas under study is found by substituting into

$$\frac{d\sigma(\theta)^{mol}/d\Omega}{d\sigma(\theta)^{He}/d\Omega} = \frac{D_{bc}^{mol}}{D_{bc}^{He}} \left(\frac{m_{He}}{m_{mol}}\right)^{\frac{1}{2}} \frac{N^{He}}{N^{mol}}, \tag{8.1}$$

where $d\sigma(\theta)/d\Omega$ = differential cross section,

D_{bc} = scattered electron count rate,

m = atomic/molecular mass,

N = flow rate of gas through needle.

This equation is valid provided that the angular distributions of the two gases are the same; this is the case provided

$$\lambda_{mol} = \lambda_{He}, \tag{8.2}$$

where λ is the mean free path of the target gas in the source region. To achieve this it is necessary to set (Orlander and Kruger 1970)

$$\frac{N_{mol}}{N_{He}} = \frac{\delta_{He}}{\delta_{mol}} \left(\frac{m_{He}}{m_{mol}} \right)^{\frac{1}{2}}, \tag{8.3}$$

where δ is the gas kinetic molecular diameter.

If the molecular beam volume defined by the electron and molecular beam intersection is well within the view cone of the detector and the electron beam flux is uniform, the relative flow method yields Equation 8.1 without the need for any flow rate condition. In this case although the shape of the molecular beam may vary with the flow rate, the total number of target particles in the scattering volume remains the same. To achieve this in the present experiment it would be necessary to move the hypodermic needle from its present position of -120° in the scattering plane and suspend it either above or below the scattering plane ensuring that the divergence of the gas beam at the scattering plane was always less than the size of the acceptance cone of the detector over the full operational energy range of the electron spectrometer.

The future experimental work using the present apparatus (incorporating the relative flow method described above) could develop in two main directions. Firstly a continuing program of research into electron - molecule scattering, aimed at providing accurate absolute elastic and inelastic cross section data of the molecules associated with the greenhouse effect eg CH_4, CO_2, H_2O. As there is little or no theoretical results for these molecules absolute cross sections are of particular interest.

The second direction of development is to extend the experiment to incorporate a laser beam. A continuous wave laser has already been used with the experimental tank (Curry et al 1984) so little structural work would be required for this. Such a laser may be used to populate higher lying vibrational levels, superelastic processes may then be studied using the present electron spectrometer. In addition off resonant 'excitations' combined with electron impact will lead to a study of simultaneous electron photon excitation processes in molecules. No work has yet been done on these systems, this process has just been confirmed as an excitation mechanism in atoms (Mason and Newell 1989).

Appendices

Appendix A - Electron Optics Summary

1) The voltages applied to the elements of a three element cylindrical lens determine the action of the lens, these voltages are usually numbered in the direction of travel of the electron beam. The other parameters which influence the action of the lens (D, A and G) are illustrated below.

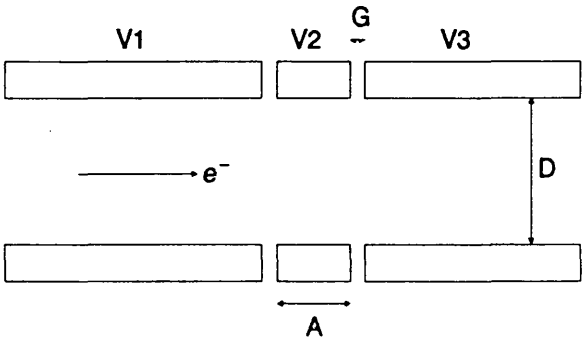

D = internal diameter of lens
A = length of middle element
G = gap between elements

Figure A.1 A three element cylinder lens.

2) The focal and mid-focal lengths $f1$, $f2$, $F1$ and $F2$, of an electron lens are dependent on the voltage ratios $V2/V1$ and $V3/V1$, these parameters are illustrated in Figure A.2 and are tabulated by Harting and Read (1976) for a given $V3/V2$ as a function of $V2/V1$ for a variety of lenses.

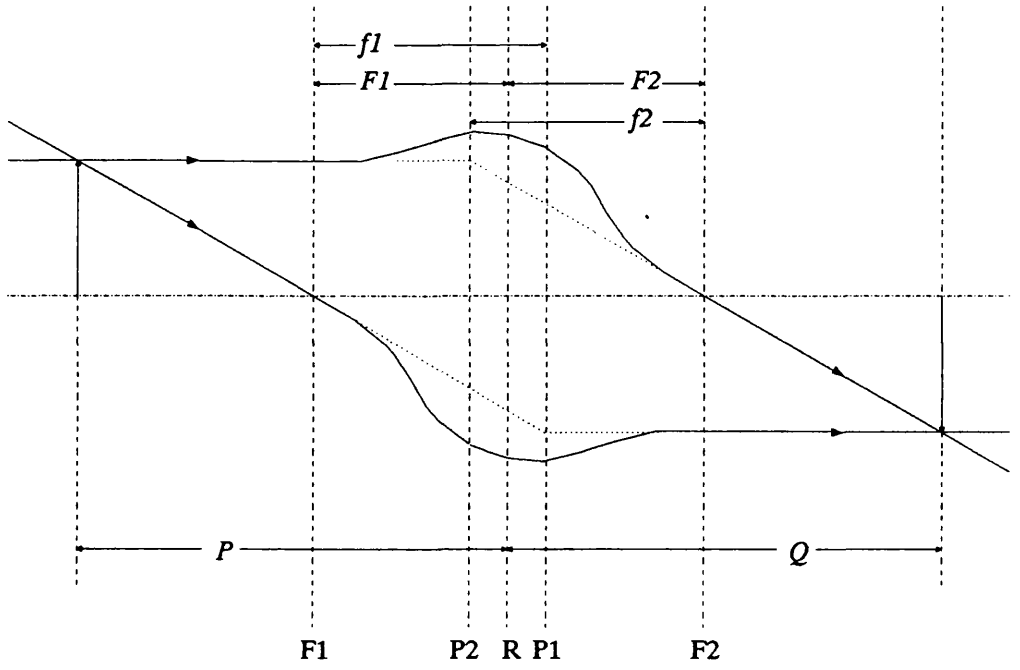

Figure A.2 Schematic representation of the four cardinal points, and the focal and mid-focal lengths. R is the reference plane of the lens, P1 and P2 are the first and second principal planes, F1 and F2 are the first and second principal foci and P and Q are the conjugate object and image distances.

3) The object and image distances (P, Q) may be found from

$$(P - F1)(Q - F2) = f1f2\,. \tag{A.1}$$

An object at infinity is imaged on to the second focal plane F2 and an object at the first focal plane F1, is imaged to infinity.

4) The object magnification is given by

$$M_L = \frac{\text{image size}}{\text{object size}} = \frac{-f1}{P - F1} = \frac{Q - F2}{f2} \tag{A.2}$$

and the spherical aberration, Δr is given by

$$\Delta r = M_L\, C_s\, \alpha_p^3\,, \tag{A.3}$$

where C_s is the third order spherical aberration coefficient and α_p is the pencil angle (see Figure A.3).

The full image size is therefore given by

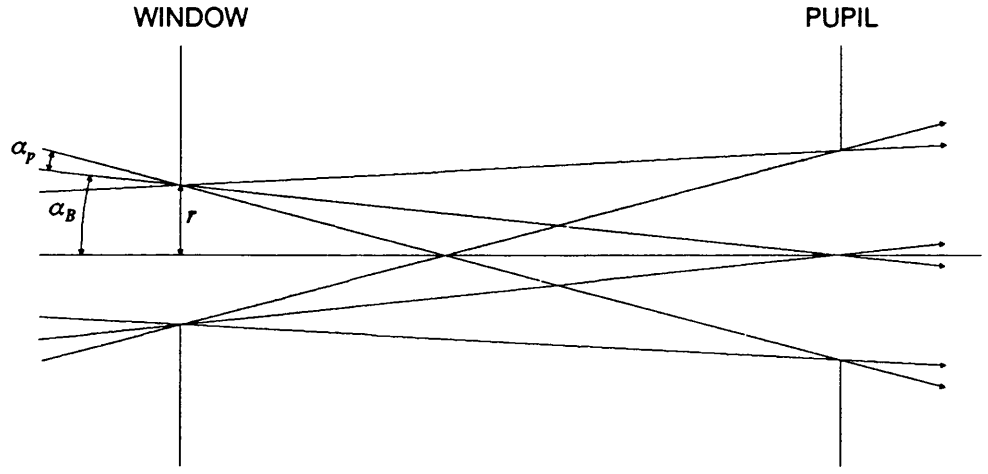

Figure A.3 An object is defined by two collimators, namely (i) a window to define the radius r and (ii) a pupil to define the pencil angle α_p. The beam angle α_B is also defined by these two collimators.

$$\text{image size} = \text{object size} \times M_L + 2\,\Delta r \tag{A.4}$$

5) The magnification of the pencil angle (see Figure A.3) is given by

$$M_\alpha = \frac{\alpha_{p\,\text{out}}}{\alpha_{p\,\text{in}}} \tag{A.5}$$

and may be found from the Helmholtz Lagrange law

$$M_\alpha M_L \left(\frac{V_3}{V_1}\right)^{1/2} = 1\,. \tag{A.6}$$

6) The lens filling factor *ff*, is given by

$$ff = \frac{y}{D} \times 100$$

$$= \frac{2P(\tan\alpha) + \text{object size}}{D}\,, \tag{A.7}$$

where $\alpha = \alpha_p + \alpha_b$ (see Figure A.3).

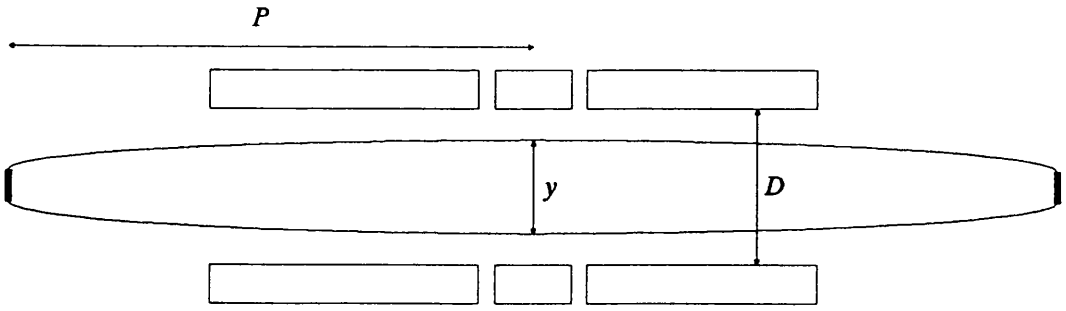

Figure A.4 Illustration of lens filling factor.

7) The formulae listed above are for accelerating lenses only, ie) $V3 > V1$. In the case of a decelerating lens, where $V3' < V1'$ the formulae may still be used provided the following substitutions are made:

$$P' = Q, Q' = P, F1' = F2, M_L' = \frac{1}{M_L} \text{ etc.}$$

8) Einzel lenses have $V1 = V3$. The principal planes of an Einzel lens lie very close together about the reference plane for all values of $V2/V1$. An object situated on the first principal plane of an einzel lens is imaged on to its second principal plane.

Appendix B - Electron Spectrometer Lens Data

Tables B.1 and B.2 contain the voltages, voltage ratios and lens data for the electron spectrometer lenses A to J for the six operational modes of the spectrometer ie 2.81,3.75,4.5,5.63,7.5 and 15eV.

For all lenses G/D = 0.1

For lens B, D = 7mm; for all other lenses, D = 10mm

For lenses F and G, A/D = 1.0; for all other lenses, A/D = 0.5

Lens	V3/V1	V2/V1	V1	V2	V3	f1	f2	F1	F2
A'	5.0	10.00	75.00	150.00	15.00	1.05	2.35	2.01	1.07
B	1.0	12.20	15.00	183.00	15.00	1.19	1.19	0.84	0.84
C'	2.0	7.65	15.00	57.40	7.50	1.50	2.11	1.96	1.45
D	3.0	5.35	7.50	40.10	22.50	2.11	3.65	3.17	2.35
E1	1.0	6.91	22.50	155.50	22.50	1.54	1.54	1.41	1.41
F1'	8.0	4.19	22.50	11.80	2.81	1.60	4.51	3.09	2.19
G1	8.0	4.19	2.81	11.80	22.50	1.60	4.51	3.09	2.19
H1	1.0	6.91	22.50	155.50	22.50	1.54	1.54	1.41	1.41
E2	1.0	6.61	22.50	148.70	22.50	1.60	1.60	1.47	1.47
F2'	6.0	4.81	22.50	18.00	3.75	1.71	4.18	3.28	2.04
G2	6.0	4.81	3.75	18.00	22.50	1.71	4.18	3.28	2.04
H2	1.0	6.61	22.50	148.70	22.50	1.60	1.60	1.47	1.47
E3	1.0	6.53	22.50	146.90	22.50	1.61	1.61	1.48	1.48
F3'	5.0	4.94	22.50	22.20	4.50	1.78	3.99	3.31	2.01
G3	5.0	4.94	4.50	22.20	22.50	1.78	3.99	3.31	2.01
H3	1.0	6.53	22.50	146.90	22.50	1.61	1.61	1.48	1.48
E4	1.0	6.53	22.50	146.90	22.50	1.61	1.61	1.48	1.48
F4'	4.0	4.95	22.50	27.90	5.63	1.89	3.78	3.30	2.01
G4	4.0	4.95	5.63	27.90	22.50	1.89	3.78	3.30	2.01
H4	1.0	6.53	22.50	146.90	22.50	1.61	1.61	1.48	1.48
E5	1.0	6.68	22.50	150.30	22.50	1.59	1.59	1.46	1.46
F5'	3.0	4.83	22.50	36.20	7.50	2.04	3.53	3.23	2.07
G5	3.0	4.83	7.50	36.20	22.50	2.04	3.53	3.23	2.07
H5	1.0	6.68	22.50	150.30	22.50	1.59	1.59	1.46	1.46
E6	1.0	7.36	22.50	165.60	22.50	1.48	1.48	1.32	1.32
F6'	1.5	4.08	22.50	61.20	15.00	2.39	2.92	2.79	2.29
G6	1.5	4.08	15.00	61.20	22.50	2.39	2.92	2.79	2.29
H6	1.0	7.36	22.50	165.60	22.50	1.48	1.48	1.32	1.32
I'	3.0	5.35	22.50	40.10	7.50	2.11	3.65	3.17	2.35
J	-	7.99	7.50	59.90	-	1.00	2.85	1.87	1.47

Table B.1 Voltage ratios, voltages and lens parameters for the six operational modes of the electron spectrometer corresponding to the interaction region energies of 2.81 to 15eV (labelled 1 to 6).

Lens	Ow	Op	α_b^{in}	α_p^{in}	Pw/D	Pp/D	Qw/D	Qp/D	M_L^w	M_L^p	M_α	Iw	Ip	α_b^{out}	α_p^{out}	ff
A'	0.30	0.10	1.73	3.13	1.75	2.41	5.64	3.85	3.50	1.75	0.65	1.05	0.18	1.97	2.03	33.00
B	1.05	0.18	1.97	2.03	0.35	2.21	0.35	1.86	1.00	0.87	1.00	1.05	0.16	2.23	2.03	20.00
C'	1.05	0.16	2.34	2.03	3.00	F1'	4.00	inf	1.36	1.00	1.04	1.43	0.16	0.00	2.11	55.00
D	0.50	0.16	0.00	2.11	5.00	inf	6.56	F2	1.15	1.00	0.50	0.58	0.16	0.50	1.06	42.00
E1	0.58	0.16	0.50	1.06	0.13	4.05	0.13	2.31	1.00	0.58	1.00	0.58	0.09	0.79	1.06	7.00
F1'	0.58	0.09	0.79	1.06	4.66	F1'	6.00	inf	1.82	1.00	1.55	1.06	0.09	0.00	1.65	36.00
G1	1.06	0.41	0.00	1.65	6.00	inf	4.66	F2	0.55	1.00	0.64	0.58	0.41	1.15	1.06	45.00
H1	0.58	0.41	1.15	1.06	0.13	2.31	0.13	4.05	1.00	1.71	1.00	0.58	0.70	0.88	1.06	7.00
E2	0.58	0.16	0.50	1.06	0.13	4.05	0.13	2.46	1.00	0.62	1.00	0.58	0.10	0.75	1.06	7.00
F2'	0.58	0.10	0.75	1.06	4.66	F1'	6.00	inf	1.59	1.00	1.54	0.92	0.10	0.00	1.63	35.00
G2	0.92	0.43	0.00	1.63	6.00	inf	4.66	F2	0.63	1.00	0.65	0.58	0.43	1.10	1.06	43.00
H2	0.58	0.43	1.10	1.06	0.13	2.46	0.13	4.05	1.00	1.62	1.00	0.58	0.70	0.88	1.06	7.00
E3	0.58	0.16	0.50	1.06	0.13	4.05	0.13	2.49	1.00	0.63	1.00	0.58	0.10	0.74	1.06	7.00
F3'	0.58	0.10	0.74	1.06	4.66	F1'	6.00	inf	1.50	1.00	1.49	0.87	0.10	0.00	1.58	35.00
G3	0.87	0.44	0.00	1.58	6.00	inf	4.66	F2	0.66	1.00	0.68	0.58	0.44	1.10	1.06	42.00
H3	0.58	0.44	1.10	1.06	0.13	2.49	0.11	4.05	1.00	1.59	1.00	0.58	0.70	0.88	1.06	7.00
E4	0.58	0.16	0.50	1.06	0.13	4.05	0.13	2.49	1.00	0.63	1.00	0.58	0.10	0.74	1.06	7.00
F4'	0.58	0.10	0.74	1.06	4.66	F1'	6.00	inf	1.42	1.00	1.40	0.83	0.10	0.00	1.49	35.00
G4	0.83	0.44	0.00	1.49	6.00	inf	4.66	F2	0.70	1.00	0.71	0.58	0.44	1.11	1.06	40.00
H4	0.58	0.44	1.11	1.06	0.13	2.49	0.13	4.05	1.00	1.59	1.00	0.58	0.70	0.88	1.06	7.00
E5	0.58	0.16	0.50	1.06	0.13	4.05	0.13	2.43	1.00	0.61	1.00	0.58	0.10	0.76	1.06	7.00
F5'	0.58	0.10	0.76	1.06	4.66	F1'	6.00	inf	1.36	1.00	1.27	0.79	0.10	0.00	1.35	35.00
G5	0.79	0.43	0.00	1.35	6.00	inf	4.66	F2	0.74	1.00	0.78	0.58	0.43	1.11	1.06	36.00
H5	0.58	0.43	1.11	1.06	0.13	2.43	0.13	4.05	1.00	1.64	1.00	0.58	0.70	0.88	1.06	7.00
E6	0.58	0.16	0.50	1.06	0.16	4.05	0.16	2.12	1.00	0.54	1.00	0.58	0.09	0.84	1.06	7.00
F6'	0.58	0.09	0.84	1.06	4.66	F1'	6.00	inf	1.27	1.00	0.96	0.74	0.09	0.00	1.02	37.00
G6	0.74	0.38	0.00	1.02	6.00	inf	4.66	F2	0.79	1.00	1.04	0.58	0.38	1.47	1.06	29.00
H6	0.58	0.38	1.47	1.06	0.16	2.12	0.16	4.05	1.00	1.85	1.00	0.58	0.70	0.88	1.06	7.00
I'	0.58	0.70	0.88	1.06	6.56	F1'	5.00	inf	0.87	1.00	2.00	0.50	0.70	0.00	2.13	50.00
J	0.50	0.70	0.00	2.11	2.50	inf	6.00	F2	1.59	1.00	0.22	0.80	0.70	0.82	0.47	23.40

Table B.2 Lens data for the electron spectrometer lenses A to J and the six interaction region energies 2.81 to 15eV (labelled 1 to 6).

O_w/I_w = window object and image sizes

O_p/I_p = pupil object and image sizes

α_b^{in} = entrance beam angle

α_p^{in} = entrance pencil angle

P_w/D, Q_w/D = object and image distances of window

P_p/D, Q_p/D = object and image distances of pupil

M_L^w = magnification of window

M_L^p = magnification of pupil

M_α = magnification of pencil angle

α_b^{out} = exit beam angle

α_p^{out} = exit pencil angle

Appendix C - E-LOSS Program Listing

```
 10 REM***********************************************
 20 REM* E-LOSS - INELASTIC DATA COLLECTION PROGRAM *
 30 REM* ISABELLA MAPSTONE                           *
 40 REM***********************************************
 50 REM main program
 60 ON ERROR GOTO100
 70 DIM C1%(1023),L(4)
 80 PROCinit
 90 PROCassembly
100 MODE7
110 PRINTTAB(5,5)"********** MENU *************"
120 PRINTTAB(5,7)"1","COLLECT DATA"
130 PRINTTAB(5,8)"2","DISPLAY DATA"
140 PRINTTAB(5,9)"3","PLOT DATA"
150 PRINTTAB(5,10)"4","SAVE DATA ON DISC"
160 PRINTTAB(5,11)"5","LOAD DATA FROM DISC"
170 PRINTTAB(5,12)"6","END PROGRAM"
180 PRINTTAB(5,14)"*******************************"
190 PRINTTAB(5,19)"PRESS KEY FOR REQUIRED OPTION";
200 G$=GET$
210 IF G$="1" THEN PROCcollect
220 IF G$="2" THEN PROCdisplay
230 IF G$="3" THEN MODE0:PROCplot:MODE7
240 IF G$="4" THEN PROCsave
250 IF G$="5" THEN PROCload
260 IF G$="6" THEN PROCend
270 IF G$="*" THEN PROCstar
280 GOTO100
290 REM*******************************
300 DEF PROCscreensave
310 REM saves a 20k screen to disc
320 PRINTTAB(1,30)"ENTER FILE NAME FOR SAVED SCREEN ";
330 INPUT $&100
340 PRINTTAB(1,30)SPC(78);
350 $&100="SAVE "+$&100+" 3000+5000"
360 ON ERROR GOTO 420
370 *FX 111,0
380 OSCLI($&100)
390 *FX 111,1
400 ON ERROR GOTO 4150
410 ENDPROC
420 *FX 111,1
430 GOTO 4150
440 REM*******************************
450 DEF PROCinit
460 REM set up first 6522 registers
470 ?&FDF2=&83
480 ?&FDF3=&FF
490 ?&FDFB=&A0
500 ?&FDFC=&0A
510 ?&FDFD=&FF
520 ?&FDFE=&3F
530 ?&FDFE=&C0
540 ENDPROC
```

```
550 REM*******************************
560 DEF PROCassembly
570 LOCAL M%,pass%
580 DIM M%150
590 FOR pass%=1 TO 2
600   P%=M%
610   [OPT 0
620   .init%  LDA &206           \save old vector
630           STA oldv%
640           LDA &207
650           STA oldv%+1
660           RTS
670   .enint% SEI                \enable interface interrupts
680           LDA #int% MOD 256  \low byte of address
690           STA &206
700           LDA #int% DIV 256  \high byte of address
710           STA &207
720           CLI
730           RTS
740   .disint% SEI               \disable interface interrupts
750           LDA oldv%          \restore vector
760           STA &206
770           LDA oldv%+1
780           STA &207
790           CLI
800           RTS
810   .int%   LDA &FDFD          \interface interrupt routine
820           AND #&40           \test bit 6 of IFR
830           BEQ exit%          \exit if bit 6 not set
840           LDA #&40           \clear flag
850           STA &FDFD
860           LDA #1             \set memory location &70 to 1
870           STA &70
880   .exit%  JMP (oldv%)        \continue interrupt chain
890   .oldv%  EQUW0              \reserve two bytes
900   .read%  LDA #0             \zero memory locations used in r1%
910           STA &78
920           STA &79
930           RTS
940   .c%     LDA &72            \send out ramp voltage
950           STA &FDF0
960           LDA &71
970           STA &FDF1
980           LDA #&FF           \set up counters
990           STA &FDF8
1000          STA &FDF9
1010          LDA #0             \zero &70
1020          STA &70
1030          LDA &75            \start decrementing T1
1040          STA &FDF5
1050  .z%     LDA &70            \wait for interrupt
1060          BEQ z%
1070  .r1%    LDA #&FF           \calculate COUNTS 1
1080          SEC
1090          SBC &FDF8
1100          STA &76
1110          LDA #&FF
1120          SBC &FDF9
```

```
1130           STA &77
1140           RTS
1150   ]
1160   NEXT pass%
1170 REM execute init%
1180 CALL init%
1190 ENDPROC
1200 REM*******************************
1210 DEF PROCcollect
1220 ON ERROR GOTO 4110
1230 LOCAL NSCANS%,STIME%,A$,B$,J%,S$,FS%,IS%
1240 CALL enint%
1250 CALLread%
1260 CLS
1270 INPUTTAB(0,4)"NUMBER OF SCANS? "NSCANS%
1280 INPUTTAB(0,6)"INITIAL STEP NUMBER (0-1023)? "IS%
1290 IF IS%>1023 GOTO 1260
1300 INPUT"FINAL STEP NUMBER (0-1023)? "FS%
1310 IF FS%>1023 GOTO 1260
1320 INPUTTAB(0,9)"STEP TIME (1-65535)us? "STIME%
1330 PRINTTAB(0,11)"DELETE CURRENT DATA (Y/N)? ";
1340 A$=GET$
1350 PRINTA$
1360 PRINTTAB(0,13)"DO YOU WANT TO EDIT THE ABOVE (Y/N)? ";
1370 B$=GET$
1380 PRINTB$;
1390 IF B$<>"N" THEN GOTO 1260
1400 PROCwork
1410 IF A$="Y"THEN FOR I%=0 TO 1023:C1%(I%)=0:NEXT
1420 ?&75=STIME% DIV 256
1430 ?&FDF4=STIME% MOD 256
1440 @%=3:PRINTTAB(13,18)"SCAN";:*FX15,1
1450 FOR J%=1 TO NSCANS%:S$=INKEY$(1):IF S$<>"" GOTO1480 ELSE
PRINTTAB(17,18)J%;
1460   FOR !&71=IS% TO FS%:CALLc%:C1%(!&71)=C1%(!&71)+!&76:NEXT
1470   NEXT
1480 CALL disint%
1490 PRINTTAB(13,20)"       "
1500 PRINTTAB(13,21)"       "
1510 *FX15,1
1520 PRINTTAB(0,25)"PRESS ANY KEY FOR MENU";
1530 VDU7:A$=INKEY$(100):IF A$="" GOTO1530
1540 ENDPROC
1550 @%=10
1560 REM*******************************
1570 DEF PROCdisplay
1580 CLS
1590 @%=&0000B
1600 REM set paged mode
1610 PRINTCHR$(14)
1620 PRINT"TO CONTINUE SCROLLING PRESS <SHIFT>"
1630 PRINTTAB(8,5)"STEP      DATA"
1640 FOR I%=0 TO 1023
1650   PRINTI%,C1%(I%):NEXT
1660 @%=10
1670 PRINT
1680 PRINTTAB(7,24)"PRESS <M> FOR MENU";
1690 REPEAT UNTIL GET$="M"
```

```
1700 ENDPROC
1710 REM*****************************
1720 DEF PROCplot
1730 ON ERROR GOTO 4150
1740 LOCALG%,MV%,EPT%,SF%,S,XMIN%,XMAX%,SX,SCALE,SF,T$,LEPT%,J%,
K%,M%,P%
1750 REM switch off cursor
1760 VDU23;8202;0 ;0;0;
1770 CLS
1780 PRINTTAB(25,10)"1   COMPLETE PLOT"
1790 PRINTTAB(25)"2   PARTIAL PLOT"
1800 PRINTTAB(25,16)"PRESS <M> FOR MENU"
1810 G%=GET
1820 IF G%=49 THEN PROCcompl
1830 IF G%=50 THEN PROCpartl
1840 IF G%=77 THEN ENDPROC
1850 GOTO 1770
1860 REM*********************************
1870 DEF PROCcompl
1880 CLS
1890 REM calculate Y scale
1900 MV%=C1%(0)
1910 FOR I%=1 TO 1023
1920   IF C1%(I%)>MV% THEN MV%=C1%(I%)
1930   NEXT
1940 PROCscale(MV%)
1950 REM plot points
1960 M%=1
1970 S=SF%/M%*10^EPT%
1980 FOR I%=0 TO 1023
1990   PLOT 69,I%+256,C1%(I%)/S+160
2000   NEXT
2010 REM draw and label axes
2020 PROCaxes("ENERGY LOSS SPECTRUM",0,1023)
2030 PROCnumberY
2040 REM test for <M>, space bar, <D> or <P>
2050 PRINTTAB(1,31)" <M> FOR MENU, SPACE BAR TO EXTEND Y AXIS, <D>
FOR DISC OR <P> FOR PRINTER DUMP";
2060 P%=GET
2070 IF P%=77 ENDPROC
2080 IF P%=32 CLS:M%=M%*5:GOTO 1970
2090 IF P%=68 PRINTTAB(1,31)SPC(78);:PROCscreensave
:PRINTTAB(1,31)"<M> FOR MENU, SPACE BAR TO EXTEND Y AXIS, <D> FOR
DISC OR <P> FOR PRINTER DUMP";
2100 IF P%=80 PRINTTAB(1,31)SPC(78);:PROCcopy
2110 GOTO 2060
2120 REM*********************************
2130 DEF PROCpartl
2140 PRINTTAB(25,20)"ENTER STEP RANGE TO BE PLOTTED"
2150 INPUTTAB(25,22)"LOWEST STEP "IS%
2160 INPUTTAB(25)"HIGHEST STEP "FS%
2170 CLS
2180 REM calculate Y scale for X range
2190 MV%=C1%(IS%)
2200 FOR J%=IS% TO FS%
2210   IF C1%(J%)>MV% THEN MV%=C1%(J%)
2220   NEXT
2230 PROCscale(MV%)
```

```
2240 REM plot points
2250 M%=1
2260 SX=1024/(FS%-IS%)
2270 S=SF%/M%*10^EPT%
2280 FOR J%=IS% TO FS%
2290   PLOT69,(J%-IS%)*SX+256,C1%(J%)/S+160
2300   NEXT
2310 REM draw and label axes
2320 PROCaxes("ENERGY LOSS SPECTRUM",IS%,FS%)
2330 PROCnumberY
2340 REM test for <M>, space bar, <D> or <P>
2350 PRINTTAB(1,31)" <M> FOR MENU, SPACE BAR TO EXTEND Y AXIS, <D>
FOR DISC OR <P> FOR PRINTER DUMP";
2360 P%=GET
2370 IF P%=77 ENDPROC
2380 IF P%=32 CLS:M%=M%*5:GOTO 2270
2390 IF P%=68 PROCscreensave
2400 IF P%=80 PROCcopy
2410 GOTO 2360
2420 REM*********************************
2430 DEF PROCscale(MV%)
2440 SCALE=MV%/800
2450 EPT%=INT(LOG(SCALE))
2460 SF=SCALE/10^EPT%
2470 IF SF=1 THEN SF%=1
2480 IF SF>1 AND SF<=2 THEN SF%=2
2490 IF SF>2 AND SF<=5 THEN SF%=5
2500 IF SF>5 AND SF<=10 THEN SF%=10
2510 ENDPROC
2520 REM*********************************
2530 DEF PROCaxes(T$,IS%,FS%)
2540 REM draw axes
2550 MOVE 256,959
2560 DRAW 256,160
2570 DRAW 1279,160
2580 REM label axes
2590 PRINTTAB(0,0)SPC(38);T$;SPC(22)
2600 PRINTTAB(0,1)SPC(79)
2610 @%=&00004
2620 PRINTTAB(39,28)IS%;" TO ";FS%;" STEPS"
2630 PRINTTAB(0,10)"COUNTS"
2640 ENDPROC
2650 REM*********************************
2660 DEF PROCnumberY
2670 IF SF%=1 THEN L(4)=8.0/M%:LEPT%=2+EPT%
2680 IF SF%=2 THEN L(4)=1.6/M%:LEPT%=3+EPT%
2690 IF SF%=5 THEN L(4)=4.0/M%:LEPT%=3+EPT%
2700 IF SF%=10 THEN L(4)=8.0/M%:LEPT%=3+EPT%
2710 L(3)=3*L(4)/4
2720 L(2)=L(4)/2
2730 L(1)=L(4)/4
2740 IF L(4)<1:FOR K%=1 TO 4:L(K%)=L(K%)*10:NEXT:LEPT%=LEPT%-
1:GOTO2740
2750 REM print at graphics cursor
2760 VDU5
2770 REM print numeric labels
2780 MOVE176,176
2790 PRINT"0.00"
```

```
2800 FOR K%=1 TO 4
2810   @%=&20203
2820   MOVE176,176+K%*200
2830   PRINTL(K%)
2840   MOVE256,160+K%*200
2850   DRAW288,160+K%*200
2860   MOVE256,60+K%*200
2870   DRAW272,60+K%*200
2880   NEXT
2890 IF LEPT%=0 GOTO 2940
2900 @%=&00001
2910 MOVE48,656
2920 PRINTLEPT%
2930 REM PRINT AT TEXT CURSOR
2940 VDU4
2950 PRINTTAB(0,12)"/10"
2960 @%=10
2970 ENDPROC
2980 REM*************************
2990 DEF PROCcopy
3000 REM for use with a NEC printer
3010 LOCAL XMAX%,XMIN%,XSTEP%,YMAX%,YMIN%,YSTEP%,DYMAX%,
DYSTEP%,BACK%,BPL%
3020 PRINTTAB(1,30)SPC(78)
3030 LOCAL BPL1%,BPL2%,BPL3%,Y%,B%,X%,D%
3040 YMAX%=992:YMIN%=0:YSTEP%=-32
3050 XMAX%=1276:XMIN%=0:XSTEP%=2
3060 DYMAX%=28:DYSTEP%=DYMAX% DIV 8+1
3070 BACK%=0
3080 BPL%=(XMAX%-XMIN%) DIV XSTEP%+1
3090 BPL1%=BPL% DIV 100+&30
3100 BPL%=BPL%-100*(BPL% DIV 100)
3110 BPL2%=BPL% DIV 10+&30
3120 BPL%=BPL%-10*(BPL% DIV 10)
3130 BPL3%=BPL%+&30
3140 VDU 26,2,1,13,1,27,1,84,1,&31,1,&36
3150 FORY%=992TO0STEP-32:B%=0:VDU 1,27,1,83,1,&30,1,BPL1%,1,
BPL2%,1,BPL3%:FORX%=0TO1276STEP2:FORD%=0TO28STEP4
:B%=B%+B%-(POINT(X%,Y%+D%)0):NEXT:VDU 1,B%:NEXT
:VDU1,13,1,27,1,&72,1,13,1,27,1,&66,1,13:NEXT
3160 VDU 1,27,1,&41,3
3170 ENDPROC
3180 REM*****************************
3190 DEF PROCsave
3200 LOCAL O$,fil$,out%,heading$,L%,A$
3210 ON ERROR GOTO 4330
3220 CLS
3230 PRINTTAB(9,6)"1   SAVE SPECTRUM"
3240 PRINTTAB(9,8)"PRESS <M> FOR MENU";
3250 O$=GET$
3260 IF O$="1" PROCsave1
3270 IF O$="M" ENDPROC
3280 IF O$="*" PROCstar
3290 GOTO 3220
3300 REM*******************************
3310 DEF PROCsave1
3320 INPUTTAB(0,12)"FILENAME FOR SPECTRUM? "fil$
3330 REM save data file and heading on disc
```

```
3340 out%=OPENOUT(fil$)
3350 INPUTLINE"FILE HEADING FOR SPECTRUM? "heading$
3360 PROCwork
3370 PROCwriteline(out%,heading$)
3380 FOR I%=0TO 1023
3390   PROCwriteline(out%,STR$(C1%(I%)))
3400   NEXT
3410 CLOSE#out%
3420 OSCLI("ACCESS "+fil$+" L")
3430 ENDPROC
3440 REM*****************************
3450 DEF PROCwriteline(out%,A$)
3460 REM write the string a$ to the file on channel out%
3470 REM so that file can be viewed by wordwise
3480 L%=LENA$
3490 IF L%=0 GOTO 2290
3500 REPEAT
3510   L%=L%-1
3520   BPUT#out%,ASCA$
3530   A$=RIGHT$(A$,L%)
3540   UNTIL L%=0
3550 BPUT#out%,13
3560 ENDPROC
3570 REM*************************
3580 DEF PROCload
3590 ON ERROR GOTO 4470
3600 LOCAL fil$,in%,heading$,A%,A$,K$
3610 CLS
3620 PRINTTAB(0,4)"IS THE DATA ON DISC TO BE ADDED TO THE"
3630 PRINTTAB(0,5)"PRESENT DATA (Y/N)? ";
3640 K$=GET$
3650 PRINTK$
3660 INPUTTAB(0,7)"FILENAME? "fil$
3670 REM READ IN FILE HEADING AND DATA
3680 in%=OPENIN(fil$)
3690 heading$=FNreadline(in%)
3700 PRINTTAB(0,9)"FILE HEADING: ";heading$
3710 PROCwork
3720 IF K$="Y" FOR I%=0TO 1023:C1%(I%)=EVAL(FNreadline(in%))
+C1%(I%):NEXT
3730 IF K$<>"Y" FOR I%=0TO 1023:C1%(I%)=EVAL(FNreadline(in%)):NEXT
3740 CLOSE#in%
3750 ENDPROC
3760 REM*****************************
3770 DEF FNreadline(in%)
3780 REM return a record from the file on channel in%.
3790 REM the record ends with a carriage return character
3800 REM reserve string space
3810 A$=STRING$(255,"*")
3820 A$=""
3830 REPEAT
3840   A%=BGET#in%
3850   A$=A$+CHR$A%
3860   UNTIL A%=13 OR EOF#in%
3870 =LEFT$(A$,LENA$-1)
3880 REM*****************************
3890 DEF PROCwork
3900 PRINTTAB(11,20)CHR$(136);CHR$(141)"WORKING";
```

```
3910 PRINTTAB(11,21)CHR$(136);CHR$(141)"WORKING";
3920 ENDPROC
3930 REM*******************************
3940 DEF PROCend
3950 PRINT
3960 END
3970 REM*******************************
3980 DEF PROCstar
3990 LOCAL L$,Z$
4000 ON ERROR GOTO 4560
4010 CLS
4020 PRINTTAB(0,6)"*";
4030 INPUT LINE""L$
4040 OSCLI(L$)
4050 PRINTTAB(7,24)"PRESS <M> FOR MENU";
4060 Z$=GET$
4070 IF Z$="M" ENDPROC
4080 IF Z$="*" GOTO 4010
4090 GOTO 4060
4100 REM******* COLLECT ERRORS *******
4110 CALLdisint%
4120 @%=10
4130 GOTO 100
4140 REM******* PLOT ERRORS **********
4150 MODE7:@%=10
4160 IF ERR=17 GOTO 100
4170 IF ERR=15 PRINTTAB(11,12)"STEP OUT OF RANGE"
4180 IF ERR=18 PRINTTAB(9,12)"STEP RANGE INCORRECT"
4190 IF ERR=22 AND XMIN%>XMAX% PRINTTAB(9,12)"STEP RANGE INCORRECT"
4200 IF ERR=22 AND XMIN%<=XMAX% PRINTTAB(16,12)"NO DATA"
4210 IF ERR=204 PRINTTAB(13,12)"BAD FILENAME!"
4220 IF ERR=195 PRINTTAB(14,12)"FILE LOCKED"
4230 IF ERR=197 PRINTTAB(8,12)"DRIVES ARE SWITCHED OFF!"
4240 IF ERR=190 PRINTTAB(12,12)"CATALOGUE FULL!"
4250 IF ERR=198 PRINTTAB(15,12)"DISC FULL!"
4260 PRINTTAB(9,14)"PRESS <C> TO CONTINUE";
4270 REPEAT UNTIL GET$="C"
4280 MODE0
4290 PROCplot
4300 MODE7
4310 GOTO100
4320 REM******* SAVE ERRORS **********
4330 CLOSE#out%
4340 IF ERR=17 GOTO100
4350 CLS
4360 IF ERR=204 PRINTTAB(13,12)"BAD FILENAME!"
4370 IF ERR=195 PRINTTAB(14,12)"FILE LOCKED"
4380 IF ERR=197 PRINTTAB(8,12)"DRIVES ARE SWITCHED OFF!"
4390 IF ERR=198 PRINTTAB(15,12)"DISC FULL!"
4400 IF ERR=190 PRINTTAB(12,12)"CATALOGUE FULL!"
4410 IF ERR=26 PRINTTAB(9,12)"MISSING FILE HEADING"
4420 PRINTTAB(9,14)"PRESS <C> TO CONTINUE";
4430 REPEAT UNTIL GET$="C"
4440 PROCsave
4450 GOTO 100
4460 REM******* LOAD ERRORS ********
4470 IF ERR=17 GOTO100
4480 CLS
```

```
4490 IF ERR=222 PRINTTAB(11,12)"FILE NOT FOUND"
4500 IF ERR=26 PRINTTAB(10,12)"INCOMPLETE FILE"
4510 IF ERR=204 PRINTTAB(10,12)"INVALID FILENAME"
4520 PRINTTAB(9,14)"PRESS <M> FOR MENU";
4530 REPEAT UNTIL GET$="M"
4540 GOTO 100
4550 REM******* STAR ERRORS ***********
4560 IF ERR=17 GOTO 100
4570 PRINTTAB(10,12)"STATEMENT INCORRECT"
4580 PRINTTAB(9,14)"PRESS <C> TO CONTINUE";
4590 REPEAT UNTIL GET$="C"
4600 GOTO100
```

Appendix D - DIFF Program Listing

```
  10 REM*****************************************
  20 REM* DIFF - ELASTIC DATA COLLECTION PROGRAM *
  30 REM* ISABELLA MAPSTONE                      *
  40 REM*****************************************
  50 REM main program
  60 ON ERROR GOTO100
  70 DIM C1%(1023),C2%(1023),L(4)
  80 PROCinit
  90 PROCassembly
 100 MODE7
 110 PRINTTAB(5,5)"********** MENU *************"
 120 PRINTTAB(5,7)"1","SET STEP RANGES"
 130 PRINTTAB(5,8)"2","PLOT DATA"
 140 PRINTTAB(5,9)"3","COLLECT DATA"
 150 PRINTTAB(5,10)"4","COLLECT NOISE"
 160 PRINTTAB(5,11)"5","DISPLAY DATA"
 170 PRINTTAB(5,12)"6","CALCULATE COUNTRATES"
 180 PRINTTAB(5,13)"7","END PROGRAM"
 190 PRINTTAB(5,15)"*******************************"
 200 PRINTTAB(5,20)"PRESS KEY FOR REQUIRED OPTION";
 210  G$=GET$
 220 IF G$="1" PROCsetup
 230 IF G$="2" MODE0:PROCplot:MODE7
 240 IF G$="3" PROCcollect
 250 IF G$="4" PROCnoise
 260 IF G$="5" PROCdisplay
 270 IF G$="6" PROCcount
 280 IF G$="7" PROCend
 290 GOTO100
 300 REM*******************************
 310 DEF PROCscreensave
 320 PRINTTAB(14,31)SPC(65);
 330 PRINTTAB(14,30)"ENTER FILE NAME FOR SAVED SCREEN ";
 340 INPUT $&100
 350 $&100="SAVE "+$&100+" 3000+5000"
 360 ON ERROR GOTO 440
 370 *FX 111,0
 380 OSCLI($&100)
 390 *FX 111,1
 400 PRINTTAB(14,30)SPC(65);
 410 PRINTTAB(14,31)"PRESS <M> FOR MENU, SPACE BAR TO EXTEND Y AXIS,
<D> FOR DISC DUMP";
 420 ON ERROR GOTO 4970
 430 ENDPROC
 440 *FX 111,1
 450 GOTO4970
 460 REM*******************************
 470 DEF PROCinit
 480 REM set up first 6522 registers
 490 ?&FDF2=&83
 500 ?&FDF3=&FF
 510 ?&FDF4=&FF
 520 ?&FDFB=&A0
 530 ?&FDFC=&0A
```

```
 540 ?&FDFD=&FF
 550 ?&FDFE=&3F
 560 ?&FDFE=&C0
 570 REM set up second 6522 registers
 580 ?&FDE2=0
 590 ?&FDEB=&20
 600 ?&FDEC=0
 610 ?&FDED=&FF
 620 ?&FDEE=&7F
 630 ENDPROC
 640 REM*******************************
 650 DEF PROCassembly
 660 LOCAL M%,pass%
 670 DIM M%150
 680 FOR pass%=1 TO 2
 690   P%=M%
 700   [OPT 0
 710   .init%  LDA &206           \save old vector
 720           STA oldv%
 730           LDA &207
 740           STA oldv%+1
 750           RTS
 760   .enint% SEI                \enable interface interrupts
 770           LDA #int% MOD 256  \low byte of address
 780           STA &206
 790           LDA #int% DIV 256  \high byte of address
 800           STA &207
 810           CLI
 820           RTS
 830   .disint% SEI               \disable interface interrupts
 840           LDA oldv%          \restore vector
 850           STA &206
 860           LDA oldv%+1
 870           STA &207
 880           CLI
 890           RTS
 900   .int%   LDA &FDFD          \interface interrupt routine
 910           AND #&40           \test bit 6 of IFR
 920           BEQ exit%          \exit if bit 6 not set
 930           LDA #&40           \clear flag
 940           STA &FDFD
 950           LDA #1             \set memory location &70 to 1
 960           STA &70
 970   .exit%  JMP (oldv%)        \continue interrupt chain
 980   .oldv%  EQUW0              \reserve two bytes
 990   .read%  LDA #0             \zero memory locations used in r%
1000           STA &78
1010           STA &79
1020           STA &82
1030           STA &83
1040           RTS
1050   .c%     LDA &72            \send out ramp voltage
1060           STA &FDF0
1070           LDA &71
1080           STA &FDF1
1090           LDA #&FF           \set up counters
1100           STA &FDF8
1110           STA &FDF9
```

```
1120            STA &FDE8
1130            STA &FDE9
1140            LDA #0              \zero &70
1150            STA &70
1160            LDA #&FF            \start decrementing T1
1170            STA &FDF5
1180    .z%     LDA &70             \wait for interrupt
1190            BEQ z%
1200    .r%     LDA #&FF            \calculate COUNTS 1
1210            SEC
1220            SBC &FDF8
1230            STA &76
1240            LDA #&FF
1250            SBC &FDF9
1260            STA &77
1270            LDA #&FF            \calculate COUNTS  2
1280            SEC
1290            SBC &FDE8
1300            STA &80
1310            LDA #&FF
1320            SBC &FDE9
1330            STA &81
1340            RTS
1350    ]
1360    NEXT pass%
1370 REM execute init%
1380 CALL init%
1390 ENDPROC
1400 REM*******************************
1410 DEF PROCsetup
1420 ON ERROR GOTO 4890
1430 LOCAL A$,B$,I%,NSCANS%,J%,cs%,sr%
1440 CALL enint%
1450 CALLread%
1460 CLS
1470 INPUTTAB(0,4)"NUMBER OF SCANS? "NSCANS%
1480 INPUTTAB(0,7)"ESTIMATED CENTRE STEP (0-1023)? "cs%
1490 IF cs%>1023 GOTO 1460
1500 INPUT"SCAN RANGE (+/-)? "sr%
1510 IS%=cs%-sr%:FS%=cs%+sr%
1520 PRINTTAB(0,11)"DELETE CURRENT DATA (Y/N)? ";
1530 A$=GET$
1540 PRINTA$
1550 PRINTTAB(0,13)"DO YOU WANT TO EDIT THE ABOVE (Y/N)? ";
1560 B$=GET$
1570 IF B$<>"N" THEN GOTO 1460
1580 PROCwork
1590 IF A$="Y"THEN FOR I%=0 TO
1023:C1%(I%)=0:C2%(I%)=0:TSCANS%=0:NEXT
1600 @%=3:PRINTTAB(13,18)"SCAN ";
1610 FOR J%=1 TO NSCANS%:PRINTTAB(18,18)J%;
1620   FOR !&71=IS% TO FS%:CALLc%
:C1%(!&71)=C1%(!&71)+!&76:C2%(!&71)=C2%(!&71)+!&80:NEXT:NEXT
1630 TSCANS%=NSCANS%+TSCANS%
1640 @%=10
1650 CALL disint%
1660 PRINTTAB(13,20)"       "
1670 PRINTTAB(13,21)"       "
```

```
1680 PRINTTAB(0,25)"PRESS ANY KEY FOR MENU";
1690 *FX15,1
1700 VDU7:A$=INKEY$(100):IF A$=""GOTO1700
1710 PROCmaxmin
1720 ENDPROC
1730 REM*****************************
1740 DEF PROCcollect
1750 ON ERROR GOTO 4890
1760 LOCAL A$,B$,J%,I%,NSCANS%,is%,fs%,cs%,sr%
1770 CALL enint%
1780 CALLread%
1790 CLS
1800 @%=1
1810 MINC%=10000
1820 PRINTTAB(0,2)"MINIMUM COUNTS IN EITHER PEAK= "MINC%
1830 NSCANS%=INT((MINC%-MINV%)*TSCANS%/MINV%)+1
1840 PRINTTAB(0,4)"NUMBER OF REQUIRED SCANS= "NSCANS%:@%=10
1850 INPUTTAB(0,7)"CENTRE STEP (0-1023)? "cs%
1860 INPUT"SCAN RANGE (+/-)? "sr%
1870 is%=cs%-sr%:fs%=cs%+sr%
1880 IF is%<IS% OR is%>FS% PRINTTAB(0,10)"INITIAL STEP IS OUT OF PRE-
VIOUS RANGE"
1890 IF fs%>FS% OR fs%<IS% PRINTTAB(0,11)"FINAL STEP IS OUT OF PRE-
VIOUS RANGE"
1900 IF is%<IS% OR is%>FS% PRINTTAB(0,13)"CURRENT DATA WILL BE
DELETED":A$="Y"
1910 IF fs%>FS% OR fs%<IS% PRINTTAB(0,13)"CURRENT DATA WILL BE
DELETED":A$="Y"
1920 PRINTTAB(0,14)"DO YOU WANT TO EDIT THE ABOVE (Y/N)? ";
1930 B$=GET$
1940 PRINTB$;
1950 IF B$<>"N":A$="":GOTO 1790
1960 IS%=is%:FS%=fs%
1970 PROCwork
1980 IF A$="Y"THEN FOR I%=0 TO
1023:C1%(I%)=0:C2%(I%)=0:TSCANS%=0:NEXT
1990 @%=3:PRINTTAB(12,18)"SCAN ";
2000 FOR J%=1 TO NSCANS%:PRINTTAB(17,18)J%;
2010   FOR !&71=IS% TO FS%:CALLc%
:C1%(!&71)=C1%(!&71)+!&76:C2%(!&71)=C2%(!&71)+!&80:NEXT:NEXT
2020 TSCANS%=NSCANS%+TSCANS%
2030 @%=10
2040 CALL disint%
2050 PRINTTAB(13,20)"       "
2060 PRINTTAB(13,21)"       "
2070 PRINTTAB(0,25)"PRESS ANY KEY FOR MENU";
2080 *FX15,1
2090 VDU7:A$=INKEY$(100):IF A$=""GOTO2090
2100 PROCmaxmin
2110 ENDPROC
2120 REM*****************************
2130 DEF PROCnoise
2140 ON ERROR GOTO 4890
2150 LOCAL B$,NSCANS%,J%,cs%,sr%
2160 CALL enint%
2170 CALLread%
2180 CLS
2190 INPUTTAB(0,4)"NUMBER OF SCANS? "NSCANS%
```

```
2200 @%=0
2210 cs%=0:PRINTTAB(0,7)"CENTRE STEP= "cs%
2220 sr%=0:PRINT"SCAN RANGE (+/-)= "sr%
2230 PRINTTAB(0,13)"DO YOU WANT TO EDIT THE ABOVE (Y/N)? ";
2240 B$=GET$
2250 IF B$<>"N" THEN GOTO 1460
2260 PROCwork
2270 TSCANS%=0:C1%(0)=0:C2%(0)=0:IS%=0:FS%=0
2280 @%=3:PRINTTAB(13,18)"SCAN ";
2290 FOR J%=1 TO NSCANS%:PRINTTAB(18,18)J%;
2300   !&71=0:CALLc%:C1%(0)=C1%(0)+!&76:C2%(0)=C2%(0)+!&80:NEXT
2310 TSCANS%=NSCANS%
2320 @%=10
2330 CALL disint%
2340 PRINTTAB(13,20)"        "
2350 PRINTTAB(13,21)"        "
2360 PRINTTAB(0,25)"PRESS ANY KEY FOR MENU";
2370 *FX15,1
2380 VDU7:A$=INKEY$(100):IF A$=""GOTO1700
2390 PROCmaxmin
2400 ENDPROC
2410 REM*********************************
2420 DEF PROCmaxmin
2430 MV1%=0:MV2%=0:MAXV%=0:MINV%=0:CS1%=0:CS2%=0
2440 FOR I%=IS% TO FS%
2450   IF C1%(I%)>MV1% THEN MV1%=C1%(I%):CS1%=I%
2460   IF C2%(I%)>MV2% THEN MV2%=C2%(I%):CS2%=I%
2470   NEXT
2480 IF MV1%>=MV2% THEN MAXV%=MV1% ELSE MAXV%=MV2%
2490 IF MAXV%=MV1% THEN MINV%=MV2% ELSE MINV%=MV1%
2500 ENDPROC
2510 REM*******************************
2520 DEF PROCdisplay
2530 ON ERROR GOTO 5140
2540 CLS
2550 @%=&0000B
2560 REM set paged mode
2570 PRINTCHR$(14)
2580 PRINT"TO CONTINUE SCROLLING PRESS <SHIFT>"
2590 PRINTTAB(8,5)"STEP      DATA    REFERENCE"
2600 FOR I%=IS% TO FS%
2610   PRINTI%,C1%(I%),C2%(I%):NEXT
2620 @%=10
2630 PRINT
2640 PRINTTAB(7,24)"PRESS <M> FOR MENU";
2650 REPEAT UNTIL GET$="M"
2660 ENDPROC
2670 REM*****************************
2680 DEF PROCplot
2690 ON ERROR GOTO 4970
2700 LOCALG%,EPT%,SF%,S,SX,SCALE,SF,T$,LEPT%,I%,K%,M%,P%,Y$,OW%,OP%
2710 REM switch off cursor
2720 VDU23;8202;0 ;0;0;
2730 CLS
2740 PRINTTAB(25,10)"1   DATA COUNTS"
2750 PRINTTAB(25)"2   REFERENCE COUNTS"
2760 PRINTTAB(25)"3   DATA AND REFERENCE COUNTS"
2770 PRINTTAB(25,16)"PRESS <M> FOR MENU"
```

```
2780 G%=GET
2790 IF G%=49 THEN PROCpart1
2800 IF G%=50 THEN PROCpart2
2810 IF G%=51 THEN PROCpart12
2820 IF G%=77 THEN ENDPROC
2830 GOTO 2730
2840 REM*********************************
2850 DEF PROCpart1
2860 CLS
2870 PROCscale(MV1%)
2880 REM plot points
2890 M%=1
2900 SX=1024/(FS%-IS%)
2910 S=SF%/M%*10^EPT%
2920 FOR I%=IS% TO FS%
2930   PLOT69,(I%-IS%)*SX+256,C1%(I%)/S+160
2940   NEXT
2950 REM draw and label axes
2960 PROCaxes("DATA COUNTS     ")
2970 PROCnumberY
2980 REM draw centre line
2990 MOVE(CS1%-IS%)*SX+256,160
3000 DRAW(CS1%-IS%)*SX+256,MV1%/S+160
3010 PRINTTAB(16,28)SPC(55)
3020 PRINTTAB(16,28)"IS LINE POSITION OK (Y/N)?";:Y$=GET$
3030 IF Y$="N" PROCadjust1:GOTO2990
3040 IF Y$<>"N" @%=1:PRINTTAB(16,28)"CENTRE STEP="CS1%,"
MAX.COUNTS="MV1%:@%=10
3050 REM test for <M>, space bar and <D>
3060 PRINTTAB(14,31)"PRESS <M> FOR MENU, SPACE BAR TO EXTEND Y AXIS,
<D> FOR DISC DUMP";
3070 P%=GET
3080 IF P%=77 ENDPROC
3090 IF P%=32 CLS:M%=M%*5:GOTO 2910
3100 IF P%=68 PROCscreensave
3110 GOTO 3070
3120 REM*********************************
3130 DEF PROCpart2
3140 CLS
3150 PROCscale(MV2%)
3160 M%=1
3170 SX=1024/(FS%-IS%)
3180 S=SF%/M%*10^EPT%
3190 FOR I%=IS% TO FS%
3200   PLOT69,(I%-IS%)*SX+256,C2%(I%)/S+160
3210   NEXT
3220 REM draw and label axes
3230 PROCaxes("REFERENCE COUNTS")
3240 PROCnumberY
3250 REM draw centre line
3260 MOVE(CS2%-IS%)*SX+256,160
3270 DRAW(CS2%-IS%)*SX+256,MV2%/S+160
3280 PRINTTAB(16,29)SPC(55)
3290 PRINTTAB(16,29)"IS LINE POSITION OK (Y/N)?";:Y$=GET$
3300 IF Y$="N" PROCadjust2:GOTO 3260
3310 IF Y$<>"N" @%=1:PRINTTAB(16,29)"CENTRE STEP="CS2%,"
MAX.COUNTS="MV2%:@%=10
3320 REM test for <M>, space bar and <D>
```

```
3330 PRINTTAB(14,31)"PRESS <M> FOR MENU, SPACE BAR TO EXTEND Y AXIS,
<D> FOR DISC DUMP";
3340 P%=GET
3350 IF P%=77 ENDPROC
3360 IF P%=32 CLS:M%=M%*5:GOTO 3180
3370 IF P%=68 PROCscreensave
3380 GOTO 3340
3390 REM*********************************
3400 DEF PROCpart12
3410 CLS
3420 OP%=1
3430 PROCscale(MAXV%)
3440 REM plot points
3450 M%=1
3460 SX=1024/(FS%-IS%)
3470 S=SF%/M%*10^EPT%
3480 MOVE 256,160
3490 FOR I%=IS% TO FS%:PLOT5,(I%-IS%)*SX+256,C1%(I%)/S+160:NEXT
3500 MOVE 256,160
3510 FOR I%=IS% TO FS%:PLOT29,(I%-IS%)*SX+256,C2%(I%)/S+160:NEXT
3520 REM draw and label axes
3530 PROCaxes("DATA & REFERENCE(DOTTED) COUNTS")
3540 PROCnumberY
3550 REM draw centre line
3560 MOVE(CS1%-IS%)*SX+256,160
3570 DRAW(CS1%-IS%)*SX+256,MV1%/S+160
3580 PRINTTAB(16,28)SPC(55)
3590 PRINTTAB(16,28)"IS DATA LINE POSITION OK (Y/N)?";:Y$=GET$
3600 IF Y$="N" PROCadjust1:GOTO 3560
3610 IF Y$<>"N" @%=1:PRINTTAB(16,28)"DATA: CENTRE STEP
COUNTS1="CS1%,"     MAX. COUNTS="MV1%:@%=10
3620 MOVE(CS2%-IS%)*SX+256,160
3630 DRAW(CS2%-IS%)*SX+256,MV2%/S+160
3640 PRINTTAB(16,29)SPC(55)
3650 PRINTTAB(16,29)"IS REFERENCE LINE POSITION OK (Y/N)?";:Y$=GET$
3660 IF Y$="N" OW%=CS1%:PROCadjust2:GOTO 3620
3670 IF Y$<>"N" @%=1:PRINTTAB(16,29)"REF.: CENTRE STEP
COUNTS2="CS2%,"     MAX.COUNTS="MV2%:@%=10
3680 REM test for <M>, space bar and <D>
3690 PRINTTAB(14,31)"PRESS <M> FOR MENU, SPACE BAR TO EXTEND Y AXIS,
<D> FOR DISC DUMP";
3700 P%=GET
3710 IF P%=77 OP%=0:ENDPROC
3720 IF P%=32 CLS:M%=M%*5:GOTO 3470
3730 IF P%=68 PROCscreensave
3740 GOTO 3700
3750 REM*********************************
3760 DEF PROCscale(MV%)
3770 SCALE=MV%/800
3780 EPT%=INT(LOG(SCALE))
3790 SF=SCALE/10^EPT%
3800 IF SF=1 THEN SF%=1
3810 IF SF>1 AND SF<=2 THEN SF%=2
3820 IF SF>2 AND SF<=5 THEN SF%=5
3830 IF SF>5 AND SF<=10 THEN SF%=10
3840 ENDPROC
3850 REM*********************************
3860 DEF PROCaxes(T$)
```

```
3870 REM draw axes
3880 MOVE 256,959
3890 DRAW 256,160
3900 DRAW 1279,160
3910 REM label axes
3920 PRINTTAB(0,0)SPC(30);T$;SPC(20)
3930 PRINTTAB(0,1)SPC(79)
3940 @%=&00004
3950 PRINTTAB(63,27)IS%;" TO ";FS%;" STEPS"
3960 PRINTTAB(0,10)"COUNTS"
3970 ENDPROC
3980 REM*********************************
3990 DEF PROCnumberY
4000 IF SF%=1 THEN L(4)=8.0/M%:LEPT%=2+EPT%
4010 IF SF%=2 THEN L(4)=1.6/M%:LEPT%=3+EPT%
4020 IF SF%=5 THEN L(4)=4.0/M%:LEPT%=3+EPT%
4030 IF SF%=10 THEN L(4)=8.0/M%:LEPT%=3+EPT%
4040 L(3)=3*L(4)/4
4050 L(2)=L(4)/2
4060 L(1)=L(4)/4
4070 IF L(4)<1:FOR K%=1 TO 4:L(K%)=L(K%)*10:NEXT:LEPT%=LEPT%-
1:GOTO4070
4080 REM print numeric labels
4090 REM print at graphics cursor
4100 VDU5
4110 MOVE176,176
4120 PRINT"0.00"
4130 FOR K%=1 TO 4
4140   @%=&20203
4150   MOVE176,176+K%*200
4160   PRINTL(K%)
4170   MOVE256,160+K%*200
4180   DRAW288,160+K%*200
4190   MOVE256,60+K%*200
4200   DRAW272,60+K%*200
4210   NEXT
4220 IF LEPT%=0 GOTO 4270
4230 @%=&00001
4240 MOVE48,656
4250 PRINTLEPT%
4260 REM PRINT AT TEXT CURSOR
4270 VDU4
4280 PRINTTAB(0,12)"/10"
4290 @%=10
4300 ENDPROC
4310 REM*************************
4320 DEF PROCadjust1
4330 LOCAL R%
4340 INPUTTAB(16,28)"ENTER RELATIVE POSITION OF PEAK CENTRE FROM
LINE "R%
4350 IF CS1%+R%>FS% OR CS1%+R%<IS% PRINTTAB(16,28)"OUT OF RANGE!
PRESS ANY KEY TO CONTINUE";SPC(15):K$=GET$:GOTO4340
4360 REM overwrite old line
4370 MOVE(CS1%-IS%)*SX+256,160
4380 IF CS1%<>IS% PLOT6,(CS1%-IS%)*SX+256,MV1%/S+160
4390 PLOT69,(CS1%-IS%)*SX+256,MV1%/S+160
4400 PLOT69,(CS1%-IS%)*SX+256,160
4410 IF OP%=1:PLOT69,(CS1%-IS%)*SX+256,C2%(CS1%)/S+160
```

```
4420 REM adjust centre
4430 CS1%=CS1%+R%
4440 MV1%=C1%(CS1%)
4450 ENDPROC
4460 REM*********************************
4470 DEF PROCadjust2
4480 LOCAL R%
4490 INPUTTAB(16,29)"ENTER RELATIVE POSITION OF PEAK CENTRE FROM
LINE "R%
4500 IF CS2%+R%>FS% OR CS2%+R%<IS% PRINTTAB(16,29)"OUT OF RANGE!
PRESS ANY KEY TO CONTINUE";SPC(15):K$=GET$:GOTO4490
4510 REM overwrite old line
4520 IF CS2%=OW% MOVE(CS1%-IS%)*SX+256,160:PLOT6,(CS1%-
IS%)*SX+256,MV1%/S+160
4530 MOVE(CS2%-IS%)*SX+256,160
4540 IF CS2%<>IS% PLOT6,(CS2%-IS%)*SX+256,MV2%/S+160
4550 PLOT69,(CS2%-IS%)*SX+256,MV2%/S+160
4560 PLOT69,(CS2%-IS%)*SX+256,160
4570 IF OP%=1:PLOT69,(CS2%-IS%)*SX+256,C1%(CS2%)/S+160
4580 REM adjust centre
4590 CS2%=CS2%+R%
4600 MV2%=C2%(CS2%)
4610 ENDPROC
4620 REM*********************************
4630 DEF PROCcount
4640 LOCAL CR1,CR2,DCR1,DCR2,M$
4650 CR1=MV1%/(.0655365*TSCANS%)
4660 CR2=MV2%/(.0655365*TSCANS%)
4670 DCR1=SQR(MV1%)/(.0655365*TSCANS%)
4680 DCR2=SQR(MV2%)/(.0655365*TSCANS%)
4690 CLS
4700 @%=&10509
4710 PRINTTAB(11,6)"COUNTRATES (Hz)"
4720 PRINT STRING$(35,"_")
4730 PRINTTAB(0,9)"DATA      : "CR1;" +/-"DCR1
4740 PRINTTAB(0,11)"REFERENCE : "CR2;" +/-"DCR2
4750 @%=10
4760 PRINTTAB(11,20)"PRESS <M> FOR MENU";
4770 REPEAT UNTIL GET$="M"
4780 ENDPROC
4790 REM*********************************
4800 DEF PROCwork
4810 PRINTTAB(11,20)CHR$(136);CHR$(141)"WORKING";
4820 PRINTTAB(11,21)CHR$(136);CHR$(141)"WORKING";
4830 ENDPROC
4840 REM*********************************
4850 DEF PROCend
4860 PRINT
4870 END
4880 REM******* COLLECT ERRORS *******
4890 CALLdisint%
4900 @%=10
4910 IF ERR=26 CLS:PRINTTAB(9,12)"SET STEP RANGE FIRST"
:PRINTTAB(9,14)"PRESS <C> TO CONTINUE";:REPEAT UNTIL GET$="C"
4920 IF ERR=15 CLS:PRINTTAB(9,12)"SCAN RANGE TOO LARGE!"
:PRINTTAB(9,14)"PRESS <C> TO CONTINUE";:REPEAT UNTIL GET$="C"
```

```
4930 IF ERR=18 CLS:IF MV2%=MINV% PRINTTAB(4,12)"REFERENCE DETECTOR
COUNTRATE=0":PRINTTAB(9,14)"PRESS <C> TO CONTINUE";:REPEAT UNTIL
GET$="C"
4940 IF ERR=18 CLS:IF MV1%=MINV% PRINTTAB(7,12)"DATA DETECTOR
COUNTRATE=0":PRINTTAB(9,14)"PRESS <C> TO CONTINUE";:REPEAT UNTIL
GET$="C"
4950 GOTO 100
4960 REM******* PLOT ERRORS **********
4970 MODE7:@%=10
4980 IF ERR=17 OP%=0:GOTO 100
4990 IF ERR=18 PRINTTAB(12,12)"ONLY ONE POINT!";
5000 IF ERR=22 PRINTTAB(16,12)"NO DATA!";
5010 IF ERR=26 PRINTTAB(9,12)"SET STEP RANGE FIRST"
5020 IF ERR=204 PRINTTAB(13,12)"BAD FILENAME!"
5030 IF ERR=195 PRINTTAB(14,12)"FILE LOCKED"
5040 IF ERR=197 PRINTTAB(8,12)"DRIVES ARE SWITCHED OFF!"
5050 IF ERR=190 PRINTTAB(12,12)"CATALOGUE FULL!"
5060 IF ERR=198 PRINTTAB(15,12)"DISC FULL!"
5070 PRINTTAB(9,14)"PRESS <C> TO CONTINUE";
5080 REPEAT UNTIL GET$="C"
5090 MODE0
5100 PROCplot
5110 MODE7
5120 GOTO100
5130 REM********* DISPLAY ERRORS *******
5140 IF ERR=17 GOTO100
5150 CLS
5160 IF ERR=26 PRINTTAB(16,12)"NO DATA"
5170 PRINTTAB(9,14)"PRESS <C> TO CONTINUE";
5180 REPEAT UNTIL GET$="C"
5190 GOTO100
```

Appendix E - Details of the Guassian Fit

A Gaussian curve takes the form

$$y = a \exp\left[-\frac{(x-c)^2}{b^2}\right], \tag{E.1}$$

where a is the height of the peak,

b is proportional to the width of the peak,

c is the position of the peak.

The best fit to a Gaussian occurs where χ^2 is a minimum, where χ^2 is given by

$$\chi^2 = \sum_i \left[y_i - e_i(a, b, c)\right]^2, \tag{E.2}$$

where

$$e_i = a \exp\left[-\frac{(x_i - c)^2}{b^2}\right]$$

and (x_i, y_i) are the points to be fitted.

The minimum of χ^2 occurs where

$$\frac{\partial}{\partial a}\chi^2 = 0, \tag{E.3}$$

$$\frac{\partial}{\partial b}\chi^2 = 0, \tag{E.4}$$

$$\frac{\partial}{\partial c}\chi^2 = 0. \tag{E.5}$$

Let

$$F_0(a,b,c) = \frac{\partial}{\partial a}\chi^2 , \tag{E.6}$$

$$F_1(a,b,c) = \frac{\partial}{\partial b}\chi^2 , \tag{E.7}$$

$$F_2(a,b,c) = \frac{\partial}{\partial c}\chi^2 . \tag{E.8}$$

Then, by differentiating the above expressions,

$$F_0(a,b,c) = \frac{\partial}{\partial a}\chi^2 = \frac{1}{a}\sum_i e_i d_i , \tag{E.9}$$

$$F_1(a,b,c) = \frac{\partial}{\partial b}\chi^2 = -\frac{2}{b^3}\sum_i u_i^4 e_i d_i , \tag{E.10}$$

$$F_2(a,b,c) = \frac{\partial}{\partial c}\chi^2 = -\frac{2}{b^4}\sum_i u_i^3 e_i d_i , \tag{E.11}$$

where

$$u_i = x_i - c ,$$

$$e_i = a \exp\left[-\frac{u_i^2}{b^2}\right] ,$$

$$d_i = y_i - e_i .$$

the problem is then to find a, b and c for $F_0 = F_1 = F_2 = 0$. This can be done by using Newton's method for simultaneous non-linear equations (Burden and Faires 1985):

The general form of a system of nonlinear equations is:

$$
\begin{aligned}
f_1(x_1, x_2, \ldots, x_n) &= 0, \\
f_2(x_1, x_2, \ldots, x_n) &= 0, \\
&\vdots \\
f_n(x_1, x_2, \ldots, x_n) &= 0,
\end{aligned}
\tag{E.12}
$$

or in matrix notation

$$
\mathbf{F}(\mathbf{x}) = \mathbf{0}\,. \tag{E.13}
$$

Newton's method for nonlinear systems is to generate successively more accurate solutions $\mathbf{x}^{(k)}$ to $\mathbf{F}(\mathbf{x}) = \mathbf{0}$ from $\mathbf{x}^{(k-1)}$ using the iteration procedure

$$
\mathbf{x}^{(k)} = \mathbf{x}^{(k-1)} - \mathbf{J}(\mathbf{x}^{(k-1)})^{-1}\,\mathbf{F}(\mathbf{x}^{(k-1)})\,, \tag{E.14}
$$

where $\mathbf{J}(\mathbf{x})$ is the Jacobian matrix

$$
\mathbf{J}(\mathbf{x}) = \begin{bmatrix}
\dfrac{\partial f_1(\mathbf{x})}{\partial x_1} & \dfrac{\partial f_1(\mathbf{x})}{\partial x_2} & \cdots & \dfrac{\partial f_1(\mathbf{x})}{\partial x_n} \\
\dfrac{\partial f_2(\mathbf{x})}{\partial x_1} & \dfrac{\partial f_2(\mathbf{x})}{\partial x_2} & \cdots & \dfrac{\partial f_2(\mathbf{x})}{\partial x_n} \\
\vdots & \vdots & & \vdots \\
\dfrac{\partial f_n(\mathbf{x})}{\partial x_1} & \dfrac{\partial f_n(\mathbf{x})}{\partial x_2} & \cdots & \dfrac{\partial f_n(\mathbf{x})}{\partial x_n}
\end{bmatrix} \tag{E.15}
$$

This method is expected to give quadratic convergence to a solution, provided a sufficiently accurate starting value is known.

In this case

$$
\mathbf{x} = \begin{bmatrix} a \\ b \\ c \end{bmatrix}, \tag{E.16}
$$

$$
\mathbf{F} = \begin{bmatrix} F_0 \\ F_1 \\ F_2 \end{bmatrix} \tag{E.17}
$$

and the terms of the Jacobian $\mathbf{J}$ are

$$J_{11} = -\frac{1}{a^2}\sum_i e_i^2 ,$$

$$J_{12} = \frac{F_1}{a} + \frac{2}{a\,b^5}\sum_i u_i^4\, e_i^2 ,$$

$$J_{13} = \frac{F_2}{a} + \frac{2}{a\,b^4}\sum_i u_i^3\, e_i^2 ,$$

$$J_{21} = J_{12} ,$$

$$J_{22} = -\frac{5\,F_1}{b} + \frac{4}{b^{10}}\sum_i u_i^8\, e_i\, d_i - \frac{4}{b^{10}}\sum_i u_i^8\, e_i^2 ,$$

$$J_{23} = -\frac{4F_2}{b} + \frac{4}{b^9}\sum_i u_i^7\, e_i\, d_i - \frac{4}{b^9}\sum_i u_i^7\, e_i^2 ,$$

$$J_{31} = J_{13} ,$$

$$J_{32} = J_{23} ,$$

$$J_{33} = \frac{6}{b^4}\sum_i u_i^2\, e_i\, d_i + \frac{4}{b^8}\sum_i u_i^6\, e_i\, d_1 - \frac{4}{b^8}\sum_i u_i^6\, e_i^2 ,$$

where

$$F_0 = \frac{1}{a}\sum_i e_i\, d_i ,$$

$$F_1 = \frac{-2}{b^5}\sum_i u_i^4\, e_i\, d_i ,$$

$$F_2 = -\frac{2}{b^4}\sum_i u_i^3\, e_i\, d_i .$$

Appendix F - Program Listings for FIT-1 and FIT-2

```
  10 REM*************************************
  20 REM* FIT-1 - SPECTRUM PROCESSING PROGRAM *
  30 REM* ISABELLA MAPSTONE                   *
  40 REM*************************************
  50 REM main program
  60 ON ERROR GOTO80
  70 DIM A(1,1023),L(4)
  80 MODE7
  90 PRINTTAB(3,5)"************* MENU **************"
 100 PRINTTAB(3,7)"1","LOAD DATA"
 110 PRINTTAB(3,8)"2","LOAD TRANSMISSION DATA"
 120 PRINTTAB(3,9)"3","CORRECT DATA"
 130 PRINTTAB(3,10)"4","SAVE CORRECTED DATA"
 140 PRINTTAB(3,11)"5","END PROGRAM"
 150 PRINTTAB(3,13)"*********************************"
 160 PRINTTAB(5,18)"PRESS KEY FOR REQUIRED OPTION";
 170 G$=GET$
 180 IF G$="1" THEN PROCload
 190 IF G$="2" THEN PROCloadtrcure
 200 IF G$="3" THEN MODE0:PROCplot:MODE7
 210 IF G$="4" THEN PROCsave
 220 IF G$="5" THEN PROCend
 230 IF G$="*" THEN PROCstar
 240 GOTO80
 250 REM*******************************
 260 DEF PROCscreensave
 270 REM saves a 20k screen to disc
 280 PRINTTAB(1,30)"ENTER FILE NAME FOR SAVED SCREEN ";
 290 INPUT $&100
 300 PRINTTAB(1,30)SPC(78);
 310 $&100="SAVE "+$&100+" 3000+5000"
 320 ON ERROR GOTO 380
 330 ?&FE34=0
 340 OSCLI($&100)
 350 ?&FE34=255
 360 ON ERROR GOTO 5170
 370 ENDPROC
 380 ?&FE34=255
 390 GOTO5170
 400 REM*****************************
 410 DEF PROCplot
 420 ON ERROR GOTO 5170
 430 LOCALG%,MV,EPT%,SF%,S,XMIN%,XMAX%,SX,SCALE,SF,T$,LEPT%,J%,
K%,M%,P%
 440 REM switch off cursor
 450 VDU23;8202;0 ;0;0;
 460 CLS
 470 PRINTTAB(25,10)"1   COMPLETE PLOT"
 480 PRINTTAB(25)"2   PARTIAL PLOT"
 490 PRINTTAB(25,16)"PRESS <M> FOR MENU"
 500 G%=GET
 510 IF G%=49 THEN IS%=200:FS%=1023:CLS:PROCpart1
 520 IF G%=50 THEN PROCxrange:PROCpart1
 530 IF G%=77 THEN ENDPROC
```

```
 540 GOTO 460
 550 REM*********************************
 560 DEF PROCxrange
 570 PRINTTAB(25,20)"ENTER STEP RANGE TO BE PLOTTED"
 580 INPUTTAB(25,22)"LOWEST STEP "IS%
 590 INPUTTAB(25)"HIGHEST STEP "FS%
 600 CLS
 610 ENDPROC
 620 REM*********************************
 630 DEF PROCpart1
 640 REM calculate Y scale for X range
 650 MV=A(1,IS%)
 660 FOR J%=IS% TO FS%
 670   IF A(1,J%)>MV THEN MV=A(1,J%)
 680   NEXT
 690 PROCscale(MV)
 700 REM plot points within graphics window
 710 M%=1
 720 SX=1024/(FS%-IS%+1)
 730 S=SF%/M%*10^EPT%
 740 VDU 24,258;164;1278;960;
 750 FOR J%=IS% TO FS%
 760   PLOT69,(J%-IS%)*SX+256,A(1,J%)/S+160
 770   NEXT
 780 REM default windows
 790 VDU 26
 800 REM draw and label axes
 810 PROCaxes("",IS%,FS%)
 820 PROCnumberY
 830 REM test for <M>, space bar, <D> or <P>
 840 PRINTTAB(1,31)" <M> FOR MENU, SPACE BAR TO EXTEND Y AXIS, <D>
FOR DISC OR <P> FOR PRINTER DUMP";
 850 REM define graphics window
 860 VDU 24,258;164;1278;960;
 870 REM initialise and turn on graphics cursor, disable text cursor
editing
 880 PROCpointerinit
 890 PROCpointeron
 900 *FX 4,1
 910 REM read keyboard
 920 IF INKEY-122 PROCrightpointer
 930 IF INKEY-26 PROCleftpointer
 940 IF INKEY-58 PROCuppointer
 950 IF INKEY-42 PROCdownpointer
 960 IF INKEY-102 PROCpointeroff
:OSCLI("FX 4,0"):OSCLI("FX 15,1"):VDU 26:ENDPROC
 970 IF INKEY-99 PROCpointeroff:CLS:M%=M%*5:GOTO 730
 980 IF INKEY-51 PROCpointeroff:PRINTTAB(1,31)SPC(78);
:OSCLI("FX 15,1"):PROCscreensave:PRINTTAB(1,31)" <M> FOR MENU, SPACE
BAR TO EXTEND Y AXIS, <D> FOR DISC OR <P> FOR PRINTER DUMP";
:PROCpointeron
 990 IF INKEY-56 PROCpointeroff:PRINTTAB(1,31)SPC(78);
:PROCcopy:PRINTTAB(1,31)" <M> FOR MENU, SPACE BAR TO EXTEND Y AXIS,
<D> FOR DISC OR <P> FOR PRINTER DUMP";:PROCpointeron
1000 IF INKEY-114 PROCzappoint
1010 IF INKEY-115 PROCsubtracteb:PROCpointeroff:PRINTTAB(1,31)" <M>
FOR MENU, SPACE BAR TO EXTEND Y AXIS, <D> FOR DISC OR <P> FOR
PRINTER DUMP";:PROCpointeron
```

```
1020 IF INKEY-116 PROCtranscorrection:PROCpointeroff:PRINTTAB(1,31)"
 FOR MENU, SPACE BAR TO EXTEND Y AXIS, <D> FOR DISC OR <P> FOR
PRINTER DUMP";:PROCpointeron
1030 IF INKEY-21  PROCsubtractslope:PROCpointeroff
:PRINTTAB(1,31)"<M> FOR MENU, SPACE BAR TO EXTEND Y AXIS,
<D> FOR DISC OR <P> FOR PRINTER DUMP";:PROCpointeron
1040 IF INKEY-117 PROCevlabel
1050 REM flush buffers
1060 *FX 15,1
1070 GOTO 920
1080 REM*********************************
1090 DEF PROCscale(MV)
1100 SCALE=MV/800
1110 EPT%=INT(LOG(SCALE))
1120 SF=SCALE/10^EPT%
1130 IF SF=1 THEN SF%=1
1140 IF SF>1 AND SF<=2 THEN SF%=2
1150 IF SF>2 AND SF<=5 THEN SF%=5
1160 IF SF>5 AND SF<=10 THEN SF%=10
1170 ENDPROC
1180 REM*********************************
1190 DEF PROCaxes(T$,IS%,FS%)
1200 REM draw axes
1210 MOVE 256,960
1220 DRAW 256,160
1230 DRAW 1279,160
1240 DRAW 1279,960
1250 DRAW 256,960
1260 REM label axes
1270 PRINTTAB(0,0)SPC(38);T$;SPC(22)
1280 @%=&00004
1290 PRINTTAB(39,28)IS%;" TO ";FS%;" STEPS"
1300 PRINTTAB(0,10)"COUNTS"
1310 ENDPROC
1320 REM*********************************
1330 DEF PROCnumberY
1340 IF SF%=1 THEN L(4)=8.0/M%:LEPT%=2+EPT%
1350 IF SF%=2 THEN L(4)=1.6/M%:LEPT%=3+EPT%
1360 IF SF%=5 THEN L(4)=4.0/M%:LEPT%=3+EPT%
1370 IF SF%=10 THEN L(4)=8.0/M%:LEPT%=3+EPT%
1380 L(3)=3*L(4)/4
1390 L(2)=L(4)/2
1400 L(1)=L(4)/4
1410 IF L(4)<1:FOR K%=1 TO 4:L(K%)=L(K%)*10:NEXT:LEPT%=LEPT%-
1:GOTO1410
1420 REM print at graphics cursor
1430 VDU5
1440 REM print numeric labels
1450 MOVE176,176
1460 PRINT"0.00"
1470 FOR K%=1 TO 4
1480   @%=&20203
1490   MOVE176,176+K%*200
1500   PRINTL(K%)
1510   MOVE256,160+K%*200
1520   DRAW288,160+K%*200
1530   MOVE256,60+K%*200
1540   DRAW272,60+K%*200
```

```
1550   NEXT
1560 IF LEPT%=0 GOTO 1610
1570 @%=&00001
1580 MOVE48,656
1590 PRINTLEPT%
1600 REM PRINT AT TEXT CURSOR
1610 VDU4
1620 PRINTTAB(0,12)"/10"
1630 @%=10
1640 ENDPROC
1650 REM************************
1660 DEF PROCcopy
1670 REM for use with a KAGA printer
1680 LOCAL XMAX%,XMIN%,XSTEP%,YMAX%,YMIN%,YSTEP%,DYMAX%,
DYSTEP%,BACK%,BPL%
1690 LOCAL Y%,B%,X%,D%
1700 VDU 26,2,1,13,1,27,1,65,1,8
1710 FORY%=992TO0STEP-32:B%=0:VDU 1,27,1,42,1,1,1,&80,1,2
:FORX%=0TO1278STEP2:FORD%=28TO0STEP-4
:B%=B%+B%-(POINT(X%,Y%+D%)0):NEXT:VDU 1,B%:NEXT:VDU1,13:NEXT
1720 VDU 1,27,1,80,3
1730 ENDPROC
1740 REM*******************************
1750 DEF PROCsave
1760 LOCAL A$,fil$,out%,heading$,L%
1770 ON ERROR GOTO 5370
1780 CLS
1790 PRINTTAB(0,3)"CORRECTED DATA SET ";datafile$
1800 PRINTTAB(0,7)"FILENAME ";datafile$;"C"
1810 PRINTTAB(0,10)"INSERT DISK AND PRESS <S> TO SAVE DATA";
1820 PRINTTAB(5,19)"PRESS <M> FOR MENU";
1830 A$=GET$
1840 IF A$="*" PROCstar:GOTO1830
1850 IF A$="S" PROCsave1
1860 IF A$="M" ENDPROC
1870 GOTO 1830
1880 REM********************************
1890 DEF PROCsave1
1900 REM save corrected data file and heading on disc
1910 out%=OPENOUT(datafile$+"C")
1920 heading$="CORRECTED DATA SET "+datafile$
1930 PROCwork
1940 PROCwriteline(out%,heading$)
1950 FOR I%=0TO 1023
1960   PROCwriteline(out%,STR$(A(1,I%)))
1970   NEXT
1980 CLOSE#out%
1990 OSCLI("ACCESS "+ datafile$ + "C L")
2000 ENDPROC
2010 REM*******************************
2020 DEF PROCwriteline(out%,A$)
2030 REM write the string a$ to the file on channel out%
2040 REM so that file can be viewed by wordwise
2050 L%=LENA$
2060 IF L%=0 GOTO 760
2070 REPEAT
2080   L%=L%-1
2090   BPUT#out%,ASCA$
```

```
2100   A$=RIGHT$(A$,L%)
2110   UNTIL L%=0
2120 BPUT#out%,13
2130 ENDPROC
2140 REM*************************
2150 DEF PROCload
2160 ON ERROR GOTO 5510
2170 LOCAL fil$,in%,heading$,A%,A$,K$
2180 CLS
2190 PRINTTAB(0,4)"LOAD DATA FROM DISC"
2200 INPUTTAB(0,7)"FILENAME? "fil$
2210 REM read in file heading and data
2220 in%=OPENIN(fil$)
2230 heading$=FNreadline(in%)
2240 PRINTTAB(0,9)"FILE HEADING: ";heading$
2250 PROCwork
2260 FOR I%=0TO 1023:A(1,I%)=VAL(FNreadline(in%)):NEXT
2270 CLOSE#in%
2280 datafile$=fil$
2290 IF RIGHT$(datafile$,1)="C" OR RIGHT$(datafile$,1)="c"
datafile$=LEFT$(fil$,LEN(fil$)-1)
2300 ENDPROC
2310 REM*************************
2320 DEF PROCloadtrcurve
2330 ON ERROR GOTO 5510
2340 LOCAL fil$,in%,heading$,A%,A$,K$
2350 CLS
2360 INPUTTAB(0,7)"FILENAME? "fil$
2370 REM READ IN FILE HEADING AND DATA
2380 in%=OPENIN(fil$)
2390 heading$=FNreadline(in%)
2400 PRINTTAB(0,9)"FILE HEADING: ";heading$
2410 PROCwork
2420 FOR I%=0TO 1023:A(0,I%)=EVAL(FNreadline(in%)):NEXT
2430 CLOSE#in%
2440 ENDPROC
2450 REM ******************************
2460 DEF FNreadline(in%)
2470 REM return a record from the file on channel in%.
2480 REM the record ends with a carriage return character
2490 REM reserve string space
2500 A$=STRING$(255,"*")
2510 A$=""
2520 REPEAT
2530   A%=BGET#in%
2540   A$=A$+CHR$A%
2550   UNTIL A%=13 OR EOF#in%
2560 =LEFT$(A$,LENA$-1)
2570 REM******************************
2580 DEF PROCwork
2590 PRINTTAB(11,20)CHR$(136);CHR$(141)"WORKING";
2600 PRINTTAB(11,21)CHR$(136);CHR$(141)"WORKING";
2610 ENDPROC
2620 REM******************************
2630 DEF PROCend
2640 PRINT
2650 END
2660 REM******************************
```

```
2670 DEF PROCstar
2680 LOCAL L$,Z$
2690 ON ERROR GOTO 5610
2700 CLS
2710 PRINTTAB(0,6)"*";
2720 INPUT LINE""L$
2730 OSCLI(L$)
2740 PRINTTAB(7,24)"PRESS <M> FOR MENU";
2750 Z$=GET$
2760 IF Z$="M" ENDPROC
2770 IF Z$="*" GOTO 2700
2780 GOTO 2750
2790 REM*********************************
2800 DEF PROCpointerinit
2810 REM initialise graphics cursor
2820 px=0:py=0
2830 ENDPROC
2840 REM*********************************
2850 DEF PROCpointeron
2860 REM defines & clears text window for cursor coordinates
2870 VDU28,0,3,8,1,12
2880 PROCdrawpointer(px,py)
2890 ENDPROC
2900 REM*********************************
2910 DEF PROCpointeroff
2920 PROCdrawpointer(px,py)
2930 REM clears and cancels curso text window
2940 VDU12,26
2950 ENDPROC
2960 REM*********************************
2970 DEF PROCdrawpointer(px,py)
2980  REM draw (or undraw) pointer at (px,py) relative to the origin
2990 LOCAL @%,X%,Y%,N%,M%
3000 N%=12:M%=8
3010 X%=px*2+256
3020 Y%=py*2+160
3030 GCOL4,1
3040 MOVE X%-N%,Y%:PLOT 6,X%-M%,Y%:MOVE X%+N%,Y%:PLOT 6,X%+M%,Y%
3050 MOVE X%,Y%-N%:PLOT 6,X%,Y%-M%:MOVE X%,Y%+N%:PLOT 6,X%,Y%+M%
3060 GCOL0,1
3070 @%=&408
3080 PRINT2*px/SX+IS%'2*py*S
3090 ENDPROC
3100 REM*********************************
3110 DEF PROCrightpointer
3120 REM move pointer right while the right cursor key is being
pressed
3130 LOCAL I%,N%,T%
3140 N%=20:I%=1
3150 PROCdrawpointer(px,py)
3160 T%=FALSE
3170 REPEAT
3180   IF T% PROCdrawpointer(px,py):T%=FALSE
3190   IF px<512 px=px+1:I%=I%+1
3200   IF I% MOD N%=0 PROCdrawpointer(px,py):T%=TRUE
3210   UNTIL NOTINKEY-122
3220 IF NOT T% PROCdrawpointer(px,py)
3230 ENDPROC
```

```
3240 REM*******************************
3250 DEF PROCleftpointer
3260 REM move pointer left while the left cursor key is being pressed
3270 LOCAL I%,N%,T%
3280 N%=20:I%=1
3290 PROCdrawpointer(px,py)
3300 T%=FALSE
3310 REPEAT
3320   IF T% PROCdrawpointer(px,py):T%=FALSE
3330   IF px>0 px=px-1:I%=I%+1
3340   IF I% MOD N%=0 PROCdrawpointer(px,py):T%=TRUE
3350   UNTIL NOTINKEY-26
3360 IF NOT T% PROCdrawpointer(px,py)
3370 ENDPROC
3380 REM*******************************
3390 DEF PROCuppointer
3400 REM move pointer up while the up cursor key is being pressed
3410 LOCAL I%,N%,T%
3420 N%=20:I%=1
3430 PROCdrawpointer(px,py)
3440 T%=FALSE
3450 REPEAT
3460   IF T% PROCdrawpointer(px,py):T%=FALSE
3470   IF py<462 py=py+1:I%=I%+1
3480   IF I% MOD N%=0 PROCdrawpointer(px,py):T%=TRUE
3490   UNTIL NOTINKEY-58
3500 IF NOT T% PROCdrawpointer(px,py)
3510 ENDPROC
3520 REM*******************************
3530 DEF PROCdownpointer
3540 REM move pointer down while the down cursor key is being pressed
3550 LOCAL I%,N%,T%
3560 N%=20:I%=1
3570 PROCdrawpointer(px,py)
3580 T%=FALSE
3590 REPEAT
3600   IF T% PROCdrawpointer(px,py):T%=FALSE
3610   IF py>0 py=py-1:I%=I%+1
3620   IF I% MOD N%=0 PROCdrawpointer(px,py):T%=TRUE
3630   UNTIL NOTINKEY-42
3640 IF NOT T% PROCdrawpointer(px,py)
3650 ENDPROC
3660 REM *******************************
3670 DEF PROCzappoint
3680 REM set ordinate of point(s) under graphics cursor to zero
3690 PROCcalcposition
3700 A%=FNlimit(xpos-xpres,0,1023):B%=FNlimit(xpos+xpres,0,1023)
3710 FOR T%=A% TO B%
3720   IF A(1,T%)<ypos+ypres AND A(1,T%)>ypos-ypres THEN
GCOL0,0:PLOT69,(T%-IS%)*SX+256,A(1,T%)/S+160:GCOL1,0:A(1,T%)=0
3730   NEXT
3740 ENDPROC
3750 REM *******************************
3760 DEF PROCcalcposition
3770 REM calculate position of graphics cursor and positional
resolution
3780 LOCAL A%,B%,T%
3790 xpos=2*px/SX+IS%
```

```
3800 xpres=3/SX
3810 ypos=2*py*S
3820 ypres=6*S
3830 ENDPROC
3840 REM*******************************
3850 DEF FNlimit(X,XL,XH)
3860 REM return value in range [XL,XH]
3870 IF X<XL THEN =XL
3880 IF X>XH THEN =XH
3890 =X
3900 REM*******************************
3910 DEF PROCsubtracteb
3920 REM calculate the average ordinate between two points and
subtract from the whole spectrum
3930 LOCAL T%,N%,T,M,X1%,X2%
3940 REM set initial channel to 200
3950  X1%=200
3960 PROCpointeroff
3970 PRINT TAB(1,31)SPC(78);:PRINT TAB(1,31)"DC BACKGROUND
CORRECTION - SELECT END CHANNEL WITH POINTER, PRESS <RETURN>
3980 PROCpointeron
3990 *FX 15,1
4000 IF INKEY-122 PROCrightpointer
4010 IF INKEY-26 PROCleftpointer
4020 IF INKEY-58 PROCuppointer
4030 IF INKEY-42 PROCdownpointer
4040 IF INKEY-74 X2%=FNlimit(2*px/SX+IS%,0,1023):GOTO4060
4050 GOTO3990
4060 *FX 15,1
4070 PROCpointeroff
4080 PRINT TAB(1,31)SPC(78);
4090 PROCpointeron
4100 REM calculate average a between X1% and X2%
4110 N%=0:T=0
4120 FOR T%=X1% TO X2%
4130   IF A(1,T%)>0 N%=N%+1:T=T+A(1,T%)
4140   NEXT
4150 IF N%>0 M=T/N% ELSE M=0
4160 IF M=0 ENDPROC
4170 REM delete current data
4180 GCOL0,0
4190 FOR T%=IS% TO FS%
4200   PLOT69,(T%-IS%)*SX+256,A(1,T%)/S+160
4210   NEXT
4220 GCOL0,1
4230 REM subtract M from data
4240 FORT%=0TO1023
4250   A(1,T%)=A(1,T%)-M
4260   IF A(1,T%)<0 A(1,T%)=0
4270   NEXT
4280 REM plot resultant data
4290 FOR T%=IS% TO FS%
4300   PLOT69,(T%-IS%)*SX+256,A(1,T%)/S+160
4310   NEXT
4320 MOVE 256,160:DRAW 1279,160
4330 ENDPROC
4340 REM*******************************
4350 DEF PROCsubtractslope
```

```
4360 REM calculate the equation of a line between two points and
subtract from the the spectrum to the right of the central peak
4370 LOCAL T%,N%,T,M,C,X1%,X2%,X3%,Y1%,Y2%
4380 PROCpointeroff
4390 PRINT TAB(1,31)SPC(78);:PRINT TAB(1,31)"SLOPE CORRECTION -
SELECT INITIAL CHANNEL WITH POINTER, PRESS <RETURN>
4400 PROCpointeron
4410 *FX 15,1
4420 IF INKEY-122 PROCrightpointer
4430 IF INKEY-26 PROCleftpointer
4440 IF INKEY-58 PROCuppointer
4450 IF INKEY-42 PROCdownpointer
4460 IF INKEY-74 X1%=2*px/SX+IS%:Y1%=2*py*S:GOTO4480
4470 GOTO4410
4480 *FX 15,1
4490 PROCpointeroff
4500 PRINT TAB(1,31)SPC(78);:PRINT TAB(1,31)"SLOPE CORRECTION -
SELECT END CHANNEL WITH POINTER, PRESS <RETURN>
4510 PROCpointeron
4520 REPEAT UNTIL NOT INKEY-74
4530 *FX 15,1
4540 IF INKEY-122 PROCrightpointer
4550 IF INKEY-26 PROCleftpointer
4560 IF INKEY-58 PROCuppointer
4570 IF INKEY-42 PROCdownpointer
4580 IF INKEY-74 X2%=2*px/SX+IS%:Y2%=2*py*S:GOTO4600
4590 GOTO4530
4600 *FX 15,1
4610 REPEAT UNTIL NOT INKEY-74
4620 PROCpointeroff
4630 PRINT TAB(1,31)SPC(78);:PRINT TAB(1,31)"SLOPE CORRECTION -
SELECT CENTRE OF MAIN PEAK WITH POINTER, PRESS <RETURN>
4640 PROCpointeron
4650 *FX 15,1
4660 IF INKEY-122 PROCrightpointer
4670 IF INKEY-26 PROCleftpointer
4680 IF INKEY-58 PROCuppointer
4690 IF INKEY-42 PROCdownpointer
4700 IF INKEY-74 X3%=FNlimit(2*px/SX+IS%,0,1023):GOTO4720
4710 GOTO4650
4720 *FX 15,1
4730 REM calculate equation of line
4740 IF X2%=X1% ENDPROC
4750 M=(Y2%-Y1%)/(X2%-X1%)
4760 C=Y1%-M*X1%
4770 REM ensure the line correction only corrects the data to the
right of the X intercept
4780 IF M<>0 THEN IF -C/M>X3% X3%=FNlimit(-C/M,0,1023)
4790 REM delete displayed data
4800 GCOL 0,0
4810 FOR T%=X3% TO FS%
4820   PLOT69,(T%-IS%)*SX+256,A(1,T%)/S+160
4830   NEXT
4840 GCOL 0,1
4850 REM correct data
4860 FOR T%=X3% TO 1023
4870   A(1,T%)=A(1,T%)-M*T%-C
4880   IF A(1,T%)<0 A(1,T%)=0
```

```
4890   NEXT
4900 REM plot resultant data
4910 FOR T%=X3% TO FS%
4920   PLOT69,(T%-IS%)*SX+256,A(1,T%)/S+160
4930   NEXT
4940 MOVE 256,160:DRAW 1279,160
4950 ENDPROC
4960 REM*******************************
4970 DEF PROCtranscorrection
4980 REM multiply data array by transmission array
4990 LOCAL T%
5000 PROCpointeroff
5010 PRINT TAB(1,31)SPC(78);:PRINT TAB(1,31)"TRANSMISSION
CORRECTION";
5020 PROCpointeron
5030 GCOL0,0
5040 FOR T%=IS% TO FS%
5050   PLOT69,(T%-IS%)*SX+256,A(1,T%)/S+160
5060   NEXT
5070 GCOL0,1
5080 FORT%=0TO1023
5090   A(1,T%)=A(1,T%)*A(0,T%)
5100   NEXT
5110 FOR T%=IS% TO FS%
5120   PLOT69,(T%-IS%)*SX+256,A(1,T%)/S+160
5130   NEXT
5140 MOVE 256,160:DRAW 1279,160
5150 ENDPROC
5160 REM******* PLOT ERRORS **********
5170 MODE7:@%=10
5180 VDU23,48,&3C,&66,&6E,&7E,&76,&66,&3C,0
5190 *FX 4,0
5200 IF ERR=17 GOTO 80
5210 IF ERR=15 PRINTTAB(11,12)"STEP OUT OF RANGE"
5220 IF ERR=18 PRINTTAB(9,12)"STEP RANGE INCORRECT"
5230 IF ERR=22 AND XMIN%>XMAX% PRINTTAB(9,12)"STEP RANGE INCORRECT"
5240 IF ERR=22 AND XMIN%<=XMAX% PRINTTAB(16,12)"NO DATA"
5250 IF ERR=204 PRINTTAB(13,12)"BAD FILENAME!"
5260 IF ERR=195 PRINTTAB(14,12)"FILE LOCKED"
5270 IF ERR=197 PRINTTAB(8,12)"DRIVES ARE SWITCHED OFF!"
5280 IF ERR=190 PRINTTAB(12,12)"CATALOGUE FULL!"
5290 IF ERR=198 PRINTTAB(15,12)"DISC FULL!"
5300 PRINTTAB(9,14)"PRESS <C> TO CONTINUE";
5310 REPEAT UNTIL GET$="C"
5320 MODE0
5330 PROCplot
5340 MODE7
5350 GOTO80
5360 REM******* SAVE ERRORS **********
5370 CLOSE#out%
5380 IF ERR=17 GOTO80
5390 CLS
5400 IF ERR=204 PRINTTAB(13,12)"BAD FILENAME!"
5410 IF ERR=195 PRINTTAB(14,12)"FILE LOCKED"
5420 IF ERR=197 PRINTTAB(8,12)"DRIVES ARE SWITCHED OFF!"
5430 IF ERR=198 PRINTTAB(15,12)"DISC FULL!"
5440 IF ERR=190 PRINTTAB(12,12)"CATALOGUE FULL!"
5450 IF ERR=26 PRINTTAB(6,12)"DATA MUST BE LOADED FIRST!";
```

```
5460 PRINTTAB(9,14)"PRESS <C> TO CONTINUE";
5470 REPEAT UNTIL GET$="C"
5480 PROCsave
5490 GOTO 80
5500 REM******* LOAD ERRORS ********
5510 IF ERR=17 GOTO80
5520 CLS
5530 IF ERR=222 PRINTTAB(11,12)"FILE NOT FOUND"
5540 IF ERR=26 PRINTTAB(10,12)"INCOMPLETE FILE"
5550 IF ERR=204 PRINTTAB(10,12)"INVALID FILENAME"
5560 PRINTTAB(9,14)"PRESS <M> FOR MENU";
5570 REPEAT UNTIL GET$="M"
5580 PROCload
5590 GOTO 80
5600 REM******* STAR ERRORS ***********
5610 IF ERR=17 GOTO 80
5620 PRINTTAB(10,12)"STATEMENT INCORRECT"
5630 PRINTTAB(9,14)"PRESS <C> TO CONTINUE";
5640 REPEAT UNTIL GET$="C"
5650 GOTO80
5660 REM********************************
5670 DEF PROCevlabel
5680 X1=(511-IS%)*SX+256
5690 X2=(716-IS%)*SX+256
5700 X3=(921-IS%)*SX+256
5710 MOVE X1,160
5720 DRAW X1,192
5730 MOVE X2,160
5740 DRAW X2,192
5750 MOVE X3,160
5760 DRAW X3,192
5770 PROCpointeroff
5780 PRINTTAB(0,28)SPC(78);
5790 PROCpointeron
5800 VDU 5
5810 VDU 24,256;0;1279;1023;
5820 MOVE X1-24,152:PRINT"0.0";
5830 MOVE X2-24,152:PRINT"0.2";
5840 MOVE X3-24,152:PRINT"0.4";
5850 MOVE 640,88:PRINT"ENERGY LOSS (eV)";
5860 VDU 4
5870 VDU 24,258;164;1278;960;
5880 ENDPROC
```

```
  10 REM************************************
  20 REM* FIT-2 - SPECTRUM FITTING PROGRAM *
  30 REM* ISABELLA MAPSTONE                *
  40 REM************************************
  50 ON ERROR GOTO100
  60 DIM A(1023),PEAK(3,2),defined%(3),L(4),C(2),y(2),f(2),j(2,2),
k(2,2),temp(2,2)
  70 datafile$=" "
  80 defined%(1)=FALSE:defined%(2)=FALSE:defined%(3)=FALSE
  90 tol=1E-4
 100 MODE7
 120 VDU3
 130 *FX 4,0
 140 PRINTTAB(5,5)"********** MENU *************"
 150 PRINTTAB(5,7)"1","LOAD CORRECTED DATA"
 160 PRINTTAB(5,8)"2","LOAD FIT PARAMETERS"
 170 PRINTTAB(5,9)"3","FIT DATA"
 180 PRINTTAB(5,10)"4","CALCULATE AREAS"
 190 PRINTTAB(5,11)"5","SAVE FIT PARAMETERS"
 200 PRINTTAB(5,12)"6","END PROGRAM"
 210 PRINTTAB(5,14)"*******************************"
 220 PRINTTAB(5,19)"PRESS KEY FOR REQUIRED OPTION";
 230 G$=GET$
 240 IF G$="1" THEN PROCload
 250 IF G$="2" THEN PROCloadfitpars
 260 IF G$="3" THEN MODE0:PROCplot:MODE7
 270 IF G$="4" THEN PROCareas
 280 IF G$="5" THEN PROCsavefit
 290 IF G$="6" THEN PROCend
 300 IF G$="*" THEN PROCstar
 310 GOTO100
 320 REM*********************************
 330 DEF PROCscreensave
 340 PRINTTAB(1,30)"ENTER FILE NAME FOR SAVED SCREEN ";
 350 INPUT $&100
 360 PRINTTAB(1,30)SPC(78);
 361 OSCLI("SSAVE "+$&100)
 370 REM$&100="SAVE "+$&100+" 3000+5000"
 380 REMON ERROR GOTO 440
 390 REM?&FE34=0
 400 REMOSCLI($&100)
 410 REM?&FE34=255
 420 ON ERROR GOTO 4270
 430 ENDPROC
 440 REM?&FE34=255
 450 REMGOTO4270
 460 REM*********************************
 470 DEF PROCplot
 480 ON ERROR GOTO 4270
 490 LOCALG%,MV,EPT%,SF%,S,XMIN%,XMAX%,SX,SCALE,SF,T$,LEPT%,J%,
K%,M%,P%
 500 VDU23;8202;0 ;0;0;
 510 CLS
 520 PRINTTAB(25,10)"1   COMPLETE PLOT"
 530 PRINTTAB(25)"2   PARTIAL PLOT"
 540 PRINTTAB(25,16)"PRESS <M> FOR MENU"
 550 G%=GET
 560 IF G%=49 THEN IS%=200:FS%=1023:CLS:PROCpart1
```

```
 570 IF G%=50 THEN PROCxrange:PROCpart1
 580 IF G%=77 THEN ENDPROC
 590 GOTO 510
 600 REM*********************************
 610 DEF PROCxrange
 620 PRINTTAB(25,20)"ENTER STEP RANGE TO BE PLOTTED"
 630 INPUTTAB(25,22)"LOWEST STEP "IS%
 640 INPUTTAB(25)"HIGHEST STEP "FS%
 650 CLS
 660 ENDPROC
 670 REM*********************************
 680 DEF PROCpart1
 690 MV=A(IS%)
 700 FOR J%=IS% TO FS%
 710   IF A(J%)>MV THEN MV=A(J%)
 720   NEXT
 730 M%=1
 740 SX=1024/(FS%-IS%+1)
 750 S=MV/(800*M%)
 760 VDU 24,258;164;1278;960;
 770 FOR J%=IS% TO FS%
 780   PLOT69,(J%-IS%)*SX+256,A(J%)/S+160
 790   NEXT
 800 VDU 26
 810 PROCaxes("",IS%,FS%)
 820 PROCnumberY
 830 PRINTTAB(1,31)" <M> FOR MENU, SPACE BAR TO EXTEND Y AXIS, <D>
FOR DISC OR <P> FOR PRINTER DUMP";
 840 VDU 24,258;164;1278;960;
 850 PROCpointerinit
 860 PROCpointeron
 870 *FX 4,1
 880 PROCmovepointer
 890 IF INKEY-102 PROCpointeroff
:OSCLI("FX 4,0"):OSCLI("FX 15,1"):VDU26:ENDPROC
 900 IF INKEY-99 PROCpointeroff:VDU26:CLS:M%=M%*5:GOTO 750
 910 IF INKEY-51 PROCpointeroff:PRINTTAB(1,31)SPC(78);
:OSCLI("FX 15,1"):PROCscreensave:PRINTTAB(1,31)" <M> FOR MENU, SPACE
BAR TO EXTEND Y AXIS, <D> FOR DISC OR <P> FOR PRINTER DUMP";
:PROCpointeron
 920 IF INKEY-56 PROCpointeroff:PRINTTAB(1,31)SPC(78);
:PROCcopy:PRINTTAB(1,31)" <M> FOR MENU, SPACE BAR TO EXTEND Y AXIS,
<D> FOR DISC OR <P> FOR PRINTER DUMP";:PROCpointeron
 930 REM function keys
 950 IF INKEY-115 PROCfitpeak:PROCpointeroff:PRINTTAB(1,31)" <M> FOR
MENU, SPACE BAR TO EXTEND Y AXIS, <D> FOR DISC OR <P> FOR PRINTER
DUMP";:PROCpointeron
 960 IF INKEY-116 PROCpeakplot:PROCpointeroff:PRINTTAB(1,31)" <M>
FOR MENU, SPACE BAR TO EXTEND Y AXIS, <D> FOR DISC OR <P> FOR
PRINTER DUMP";:PROCpointeron
 980 IF INKEY-21 PROCspectrumplot:PROCpointeroff:PRINTTAB(1,31)" <M>
FOR MENU, SPACE BAR TO EXTEND Y AXIS, <D> FOR DISC OR <P> FOR
PRINTER DUMP";:PROCpointeron
 990 IF INKEY-118 PROCevlabel
1000 *FX 15,1
1010 GOTO 880
1020 REM*********************************
1030 DEF PROCaxes(T$,IS%,FS%)
```

```
1040 MOVE 256,959
1050 DRAW 256,160
1060 DRAW 1279,160
1070 DRAW 1279,960
1080 PRINTTAB(0,0)SPC(38);T$;SPC(22)
1090 @%=&00004
1100 PRINTTAB(39,28)IS%;" TO ";FS%;" STEPS"
1110 ENDPROC
1120 REM*********************************
1130 DEF PROCnumberY
1140 FOR K%=1 TO 4
1150   MOVE176,176+K%*200
1160   MOVE256,160+K%*200
1170   DRAW288,160+K%*200
1180   MOVE256,60+K%*200
1190   DRAW272,60+K%*200
1200   NEXT
1210 ENDPROC
1220 REM*********************************
1230 DEF PROCcopy
1240 LOCAL XMAX%,XMIN%,XSTEP%,YMAX%,YMIN%,YSTEP%,DYMAX%,
DYSTEP%,BACK%,BPL%
1250 LOCAL Y%,B%,X%,D%
1260 VDU 26,2,1,13,1,27,1,65,1,8
1270 FORY%=992TO0STEP-32:B%=0:VDU 1,27,1,42,1,1,1,&80,1,2
:FORX%=0TO1278STEP2:FORD%=28TO0STEP-4
:B%=B%+B%-(POINT(X%,Y%+D%)0):NEXT:VDU 1,B%:NEXT:VDU1,13:NEXT
1280 VDU 1,27,1,80,3
1290 ENDPROC
1300 REM*********************************
1310 DEF PROCsavefit
1320 ON ERROR GOTO 4450
1330 LOCAL A$,in%,T%,heading$
1340 CLS
1350 PRINTTAB(0,3)"FITTED PARAMETERS FOR DATA SET "+datafile$
1360 PRINTTAB(0,7)"FILENAME ";datafile$;"P"
1370 PRINTTAB(0,11)"(DATA SENT TO DRIVE 2)";
1380 A$=GET$
1390 out%=OPENOUT(":2."+datafile$+"P")
1400 heading$="FITTED PARAMETERS FOR DATA SET "+datafile$
1410 PROCwork
1420 PROCwriteline(out%,heading$)
1430 FOR T%=1 TO 3
1440   PROCwriteline(out%,STR$(defined%(T%)))
1450   PROCwriteline(out%,STR$(PEAK(T%,0)))
1460   PROCwriteline(out%,STR$(PEAK(T%,1)))
1470   PROCwriteline(out%,STR$(PEAK(T%,2)))
1480   NEXT
1490 CLOSE #out%
1500 ENDPROC
1510 REM*********************************
1520 DEF PROCwriteline(out%,A$)
1530 L%=LENA$
1540 IF L%=0 GOTO 780
1550 REPEAT
1560   L%=L%-1
1570   BPUT#out%,ASCA$
1580   A$=RIGHT$(A$,L%)
```

```
1590   UNTIL L%=0
1600 LOCAL X1,X2,X3
1610 BPUT#out%,13
1620 ENDPROC
1630 REM*********************************
1640 DEF PROCload
1650 ON ERROR GOTO 4580
1660 LOCAL fil$,in%,heading$,A%,A$,K$
1670 CLS
1680 PRINTTAB(0,4)"LOAD DATA FROM DISC"
1690 INPUTTAB(0,7)"FILENAME? "fil$
1700 datafile$=fil$
1710 IF RIGHT$(datafile$,1)="C" OR RIGHT$(datafile$,1)="c"
datafile$=LEFT$(fil$,LEN(fil$)-1)
1720 in%=OPENIN(fil$)
1730 heading$=FNreadline(in%)
1740 PRINTTAB(0,9)"FILE HEADING: ";heading$
1750 PROCwork
1760 IF K$="Y" FOR I%=0TO 1023:A(I%)=EVAL(FNreadline(in%))+A(I%):NEXT
1770 IF K$ <> "Y" FOR I%=0TO 1023:A(I%)=EVAL(FNreadline(in%)):NEXT
1780 CLOSE#in%
1790 ENDPROC
1800 REM*********************************
1810 DEF PROCloadfitpars
1820 ON ERROR GOTO 4580
1830 LOCAL A$,in%,heading$
1840 CLS
1850 PRINTTAB(0,4)"LOAD FITTED PARAMETERS FROM DISC"
1860 PRINTTAB(0,7)"FILENAME : :2.";datafile$;"P"
1870 PRINTTAB(0,10)"INSERT DISK AND PRESS RETURN"
1880 A$=GET$
1890 in%=OPENIN(":2."+datafile$+"P")
1900 heading$=FNreadline(in%)
1910 PROCwork
1920 FOR T%=1 TO 3
1930   defined%(T%)=VAL(FNreadline(in%))
1940   PEAK(T%,0)=VAL(FNreadline(in%))
1950   PEAK(T%,1)=VAL(FNreadline(in%))
1960   PEAK(T%,2)=VAL(FNreadline(in%))
1970   NEXT
1980 CLOSE#in%
1990 ENDPROC
2000 REM*********************************
2010 DEF FNreadline(in%)
2020 A$=STRING$(255,"*")
2030 A$=""
2040 REPEAT
2050   A%=BGET#in%
2060   A$=A$+CHR$A%
2070   UNTIL A%=13 OR EOF#in%
2080 =LEFT$(A$,LENA$-1)
2090 REM*********************************
2100 DEF PROCwork
2110 PRINTTAB(11,20)CHR$(136);CHR$(141)"WORKING";
2120 PRINTTAB(11,21)CHR$(136);CHR$(141)"WORKING";
2130 ENDPROC
2140 REM*********************************
2150 DEF PROCend
```

```
2160 PRINT
2170 END
2180 REM*********************************
2190 DEF PROCstar
2200 LOCAL L$,Z$
2210 ON ERROR GOTO 4670
2220 CLS
2230 PRINTTAB(0,6)"*";
2240 INPUT LINE""L$
2250 OSCLI(L$)
2260 PRINTTAB(7,24)"PRESS <M> FOR MENU";
2270 Z$=GET$
2280 IF Z$="M" ENDPROC
2290 IF Z$="*" GOTO 2220
2300 GOTO 2270
2310 REM*********************************
2320 DEF PROCpointerinit
2330 px=0:py=0
2340 ENDPROC
2350 REM*********************************
2360 DEF PROCpointeron
2370 VDU28,0,3,8,1,12
2380 PROCdrawpointer(px,py)
2390 ENDPROC
2400 REM*********************************
2410 DEF PROCpointeroff
2420 PROCdrawpointer(px,py)
2430 VDU12,28,0,31,79,0
2440 ENDPROC
2450 REM*********************************
2460 DEF PROCdrawpointer(px,py)
2470 LOCAL @%,X%,Y%,N%,M%
2480 N%=12:M%=8
2490 X%=px*2+256
2500 Y%=py*2+160
2510 GCOL4,1
2520 MOVE X%-N%,Y%:PLOT 6,X%-M%,Y%:MOVE X%+N%,Y%:PLOT 6,X%+M%,Y%
2530 MOVE X%,Y%-N%:PLOT 6,X%,Y%-M%:MOVE X%,Y%+N%:PLOT 6,X%,Y%+M%
2540 GCOL0,1
2550 @%=&408
2560 PRINT2*px/SX+IS%'2*py*S
2570 ENDPROC
2580 REM*********************************
2590 DEF PROCrightpointer
2600 LOCAL I%,N%,T%
2610 N%=20:I%=1
2620 PROCdrawpointer(px,py)
2630 T%=FALSE
2640 REPEAT
2650   IF T% PROCdrawpointer(px,py):T%=FALSE
2660   IF px<512 px=px+1:I%=I%+1
2670   IF I% MOD N%=0 PROCdrawpointer(px,py):T%=TRUE
2680   UNTIL NOTINKEY-122
2690 IF NOT T% PROCdrawpointer(px,py)
2700 ENDPROC
2710 REM*********************************
2720 DEF PROCleftpointer
2730 LOCAL I%,N%,T%
```

```
2740 N%=20:I%=1
2750 PROCdrawpointer(px,py)
2760 T%=FALSE
2770 REPEAT
2780   IF T% PROCdrawpointer(px,py):T%=FALSE
2790   IF px>0 px=px-1:I%=I%+1
2800   IF I% MOD N%=0 PROCdrawpointer(px,py):T%=TRUE
2810   UNTIL NOTINKEY-26
2820 IF NOT T% PROCdrawpointer(px,py)
2830 ENDPROC
2840 REM*********************************
2850 DEF PROCuppointer
2860 LOCAL I%,N%,T%
2870 N%=20:I%=1
2880 PROCdrawpointer(px,py)
2890 T%=FALSE
2900 REPEAT
2910   IF T% PROCdrawpointer(px,py):T%=FALSE
2920   IF py<462 py=py+1:I%=I%+1
2930   IF I% MOD N%=0 PROCdrawpointer(px,py):T%=TRUE
2940   UNTIL NOTINKEY-58
2950 IF NOT T% PROCdrawpointer(px,py)
2960 ENDPROC
2970 REM*********************************
2980 DEF PROCdownpointer
2990 LOCAL I%,N%,T%
3000 N%=20:I%=1
3010 PROCdrawpointer(px,py)
3020 T%=FALSE
3030 REPEAT
3040   IF T% PROCdrawpointer(px,py):T%=FALSE
3050   IF py>0 py=py-1:I%=I%+1
3060   IF I% MOD N%=0 PROCdrawpointer(px,py):T%=TRUE
3070   UNTIL NOTINKEY-42
3080 IF NOT T% PROCdrawpointer(px,py)
3090 ENDPROC
3100 REM*********************************
3110 DEF PROCcalcposition
3120 LOCAL A%,B%,T%
3130 xpos=2*px/SX+IS%
3140 xpres=3/SX
3150 ypos=2*py*S
3160 ypres=6*S
3170 ENDPROC
3180 REM*********************************
3190 DEF FNlimit(X,XL,XH)
3200 IF X<XL THEN =XL
3210 IF X<XH THEN =XH
3220 =X
3230 REM*********************************
3240 DEF PROCmovepointer
3250 IF INKEY-122 PROCrightpointer
3260 IF INKEY-26 PROCleftpointer
3270 IF INKEY-58 PROCuppointer
3280 IF INKEY-42 PROCdownpointer
3290 ENDPROC
3300 REM*********************************
3310 DEF PROCfjcalc(X1%,X2%)
```

```
3320 REM procedure to calculate components of the vector f and
matrix j
3330 LOCAL i%,temp, u, e, d, u2, u3, u4, u6, u7, u8, e2i, edi, e2,
ed, u2ed, u3ed, u4ed, u6ed, u7ed, u8ed, u3e2, u4e2, u6e2, u7e2,
u8e2, a14, a15, a18, a19, a110
3340 REM set all sum totals to zero
3350
e2=0:ed=0:u2ed=0:u3ed=0:u4ed=0:u6ed=0:u7ed=0:u8ed=0:u3e2=0:u4e2=0
:u6e2=0:u7e2=0:u8e2=0
3360 REM Calculate sums
3370 FOR i%=X1% TO X2%
3380   IF A(i%)=0 GOTO 3630
3390   u=i%-C(2)
3400   e=C(0)*EXP(-((u/C(1))^2))
3410   d=A(i%)-e
3420   u2=u^2
3430   u3=u2*u
3440   u4=u3*u
3450   u6=u4*u2
3460   u7=u6*u
3470   u8=u7*u
3480   e2i=e^2
3490   edi=e*d
3500   e2=e2+e2i
3510   ed=ed+edi
3520   u2ed=u2ed+u2*edi
3530   u3ed=u3ed+u3*edi
3540   u4ed=u4ed+u4*edi
3550   u6ed=u6ed+u6*edi
3560   u7ed=u7ed+u7*edi
3570   u8ed=u8ed+u8*edi
3580   u3e2=u3e2+u3*e2i
3590   u4e2=u4e2+u4*e2i
3600   u6e2=u6e2+u6*e2i
3610   u7e2=u7e2+u7*e2i
3620   u8e2=u8e2+u8*e2i
3630   NEXT
3640 REM Calculate powers of C(1)
3650 a14=C(1)^4
3660 a15=a14*C(1)
3670 a18=a14^2
3680 a19=a14*a15
3690 a110=a15^2
3700 REM Calculate f
3710 f(0)=ed/C(0)
3720 f(1)=-2*u4ed/a15
3730 f(2)=-2*u3ed/a14
3740 REM Calculate Jacobian j
3750 j(0,0)=-e2/C(0)^2
3760 j(0,1)=f(1)/C(0)+2*u4e2/C(0)/a15
3770 j(0,2)=f(2)/C(0)+2*u3e2/C(0)/a14
3780 j(1,0)=j(0,1)
3790 j(1,1)=-5*f(1)/C(1)+4*u8ed/a110-4*u8e2/a110
3800 j(1,2)=-4*f(2)/C(1)+4*u7ed/a19-4*u7e2/a19
3810 j(2,0)=j(0,2)
3820 j(2,1)=j(1,2)
3830 j(2,2)=6*u2ed/a14+4*u6ed/a18-4*u6e2/a18
3840 ENDPROC
```

```
3850 REM*********************************
3860 DEF PROCnewton(tol,maxit%,X1%,X2%)
3870 REM calculate the best fit to a Gaussian using Newton's
technique for solving nonlinear simultaneous equations
3880 LOCAL i%,n%
3890 i%=1
3900 REPEAT
3910   REM calculate the Jacobian J and function f
3920   PROCfjcalc(X1%,X2%)
3930   REM calculate the inverse k of the Jacobian j
3940   PROCinvert
3950   y(0)=k(0,0)*f(0)+k(0,1)*f(1)+k(0,2)*f(2)
3960   y(1)=k(1,0)*f(0)+k(1,1)*f(1)+k(1,2)*f(2)
3970   y(2)=k(2,0)*f(0)+k(2,1)*f(1)+k(2,2)*f(2)
3980   REM calculate a better estimate to the fit parameters and the
error delta
3990   C(0)=C(0)-y(0)
4000   C(1)=C(1)+y(1)
4010   C(2)=C(2)+y(2)
4020   delta=SQR((y(0)/C(0))^2+(y(1)/C(1))^2+(y(2)/C(2))^2)
4030   PROCprompt("GAUSSIAN FIT - ITERATION "+STR$(i%)+", ERROR
"+STR$(delta))
4040   i%=i%+1
4050   UNTIL i%>maxit% OR delta<tol
4060 *FX 15,1
4070 i%=i%-1
4080 IF delta>tol PROCprompt("GAUSSIAN FIT - ITERATION "+STR$(i%)+",
ERROR "+STR$(delta)+"  CONTINUE (Y/N)?"):A$=GET$:IF A$="Y" OR A$="y"
maxit%=maxit%+10:PROCprompt("GAUSSIAN FIT - ITERATION "+STR$(i%)+",
ERROR "+STR$(delta)):GOTO 3900
4090 ENDPROC
4100 REM*********************************
4110 DEF PROCinvert
4120 REM invert the matrix j, storing the result in matrix k
4130 LOCAL I%,J%,detm
4140 detm=j(0,0)*(j(1,1)*j(2,2)-j(1,2)*j(2,1))-j(0,1)*(j(1,0)*j(2,2)-
j(1,2)*j(2,0))+j(0,2)*(j(1,0)*j(2,1)-j(1,1)*j(2,0))
4150 FORI%=0TO2:FORJ%=0TO2:k(I%,J%)=j(J%,I%):NEXT:NEXT
4160 k(0,0)=( j(1,1)*j(2,2)-j(1,2)*j(2,1))/detm
4170 k(0,1)=(-j(1,0)*j(2,2)+j(1,2)*j(2,0))/detm
4180 k(0,2)=( j(1,0)*j(2,1)-j(1,1)*j(2,0))/detm
4190 k(1,0)=(-j(0,1)*j(2,2)+j(0,2)*j(2,1))/detm
4200 k(1,1)=( j(0,0)*j(2,2)-j(0,2)*j(2,0))/detm
4210 k(1,2)=(-j(0,0)*j(2,1)+j(0,1)*j(2,0))/detm
4220 k(2,0)=( j(0,1)*j(1,2)-j(0,2)*j(1,1))/detm
4230 k(2,1)=(-j(0,0)*j(1,2)+j(0,2)*j(1,0))/detm
4240 k(2,2)=( j(0,0)*j(1,1)-j(0,1)*j(1,0))/detm
4250 ENDPROC
4260 REM******* PLOT ERRORS **********
4270 MODE7:@%=10
4280 IF ERR=17 GOTO 100
4290 IF ERR=15 PRINTTAB(11,12)"STEP OUT OF RANGE"
4300 IF ERR=18 PRINTTAB(9,12)"STEP RANGE INCORRECT"
4310 IF ERR=22 AND XMIN% > XMAX% PRINTTAB(9,12)"STEP RANGE INCORRECT"
4320 IF ERR=22 AND XMIN% <= XMAX% PRINTTAB(16,12)"NO DATA"
4330 IF ERR=204 PRINTTAB(13,12)"BAD FILENAME!"
4340 IF ERR=195 PRINTTAB(14,12)"FILE LOCKED"
4350 IF ERR=197 PRINTTAB(8,12)"DRIVES ARE SWITCHED OFF!"
```

```
4360 IF ERR=190 PRINTTAB(12,12)"CATALOGUE FULL!"
4370 IF ERR=198 PRINTTAB(15,12)"DISC FULL!"
4380 PRINTTAB(9,14)"PRESS <C> TO CONTINUE";
4390 REPEAT UNTIL GET$="C"
4400 MODE0
4410 PROCplot
4420 MODE7
4430 GOTO100
4440 REM******* SAVE ERRORS **********
4450 CLOSE#out%
4460 IF ERR=17 GOTO100
4470 CLS
4480 IF ERR=195 PRINTTAB(14,12)"FILE LOCKED"
4490 IF ERR=197 PRINTTAB(8,12)"DRIVES ARE SWITCHED OFF!"
4500 IF ERR=198 PRINTTAB(15,12)"DISC FULL!
4510 IF ERR=190 PRINTTAB(12,12)"CATALOGUE FULL!"
4520 IF ERR=26 PRINTTAB(9,12)"LOAD DATA FIRST!"
4530 PRINTTAB(9,14)"PRESS <C> TO CONTINUE";
4540 REPEAT UNTIL GET$="C"
4550 PROCsavefit
4560 GOTO 100
4570 REM******* LOAD ERRORS ********
4580 IF ERR=17 GOTO100
4590 CLS
4600 IF ERR=222 PRINTTAB(11,12)"FILE NOT FOUND"
4610 IF ERR=26 PRINTTAB(10,12)"LOAD DATA FIRST!"
4620 IF ERR=204 PRINTTAB(10,12)"INVALID FILENAME"
4630 PRINTTAB(9,14)"PRESS <M> FOR MENU";
4640 REPEAT UNTIL GET$="M"
4650 GOTO 100
4660 REM******* STAR ERRORS ***********
4670 IF ERR=17 GOTO 100
4680 PRINTTAB(10,12)"STATEMENT INCORRECT"
4690 PRINTTAB(9,14)"PRESS <C> TO CONTINUE";
4700 REPEAT UNTIL GET$="C"
4710 GOTO100
4720 REM******* AREA  ERRORS **********
4730 IF ERR=17 GOTO 100
4740 IF ERR =18 PRINTTAB(10,12)"FIT PEAKS FIRST!"
4750 PRINTTAB(9,14)"PRESS <C> TO CONTINUE";
4760 REPEAT UNTIL GET$="C"
4770 GOTO100
4780 REM*********************************
4790 DEF PROCpeakplot
4800 REM plot the gaussian curve fitted to a selected part of the
spectrum,
4810 REM and give the option to subtract the peak from the spectrum
4820 LOCAL A$,L%
4830 PROCpointeroff
4840 PRINT TAB(1,31)SPC(78);:PRINT TAB(1,31)"PLOT PEAK FIT - PEAK
NUMBER (1,2, OR 3)? ";
4850 A$=GET$
4860 IF A$<>"1" AND A$<>"2" AND A$<>"3" GOTO 4850
4870 PRINT A$;
4880 L%=VAL(A$)
4890 IF NOT defined%(L%) GOTO 4840
4900 PROCpointeron
4910 PROCpeakplot1(L%)
```

```
4920 ENDPROC
4930 REM*********************************
4940 DEF PROCpeakplot1(L%)
4950 REM plot the gaussian curve with parameters PEAK(L%) and give
the option
4960 REM to subtract the peak from the spectrum
4970 LOCAL T%,S%,D%,E%,F%,a,b,c
4980 a=PEAK(L%,0):b=PEAK(L%,1):c=PEAK(L%,2)
4990 Y=a*EXP(-(((IS%-c)/b)^2))
5000 S%=(FS%-IS%) DIV 127
5010 IF S%<1 S%=1
5020 MOVE 256,Y/S+160
5030 FOR T%=IS% TO FS% STEP S%
5040   Y=a*EXP(-(((T%-c)/b)^2))
5050   DRAW (T%-IS%)*SX+256,Y/S+160
5060   NEXT
5070 PROCpointeroff
5080 PRINT TAB(1,31)SPC(78);:PRINT TAB(1,31)"PLOT OF PEAK FIT -
SUBTRACT FROM SPECTRUM (Y/N)? ";c;
5090 A$=GET$
5100 PROCclg
5110 IF A$<>"Y" AND A$<>"y" PRINT"N";:GOTO 5200
5120 PRINT"Y";
5130 D%=b*SQR(LN(a)+LN(2))+0.5
5140 E%=FNlimit(c-D%,0,1023)
5150 F%=FNlimit(c+D%,0,1023)
5160 FOR T%=E% TO F%
5170   A(T%)=A(T%)-a*EXP(-(((T%-c)/b)^2))
5180   IF A(T%)<0 A(T%)=0
5190   NEXT
5200 FOR T%=IS% TO FS%
5210   PLOT 69,(T%-IS%)*SX+256,A(T%)/S+160
5220   NEXT
5230 PROCpointeron
5240 ENDPROC
5250 REM*********************************
5260 DEF PROCclg
5270 CLG
5280 FOR T%=1 TO 4
5290   MOVE256,160+T%*200
5300   DRAW288,160+T%*200
5310   MOVE256,60+T%*200
5320   DRAW272,60+T%*200
5330   NEXT
5340 ENDPROC
5350 REM*********************************
5360 DEF PROCprompt(A$)
5370 REM display the message A$ at the bottom of the screen
5380 PROCpointeroff
5390 PRINT TAB(1,31)SPC(78);:PRINT TAB(1,31)A$;
5400 PROCpointeron
5410 ENDPROC
5420 REM*********************************
5430 DEF PROCfitpeak
5440 REM select the range of points to be included in the fit,
select initial
5450 REM estimates for the fit parameters, then fit and plot a
gaussian
```

```
5460 LOCAL T%,L%,A1,A2,X1%,X2%,h
5470 PROCprompt("GAUSSIAN FIT - SELECT LOWER BOUND OF RANGE")
5480 *FX 15,1
5490 PROCmovepointer
5500 IF INKEY-74 X1%=FNlimit(2*px/SX+IS%,0,1023):GOTO5520
5510 GOTO 5480
5520 *FX 15,1
5530 PROCprompt("GAUSSIAN FIT - SELECT UPPER BOUND OF RANGE")
5540 *FX 15,1
5550 PROCmovepointer
5560 IF INKEY-74 X2%=FNlimit(2*px/SX+IS%,0,1023):GOTO5580
5570 GOTO 5540
5580 *FX 15,1
5590 PROCprompt("GAUSSIAN FIT - SELECT PEAK MAXIMUM POSITION")
5600 *FX 15,1
5610 PROCmovepointer
5620 IF INKEY-74 C(2)=2*px/SX+IS%:C(0)=2*py*S:GOTO5640
5630 GOTO5600
5640 GCOL 4,1
5650 h=py
5660 MOVE 258,160+h:PLOT 29,1278,160+h
5670 PROCprompt("GAUSSIAN FIT - SELECT LOWER BOUND AT HALF HEIGHT")
5680 *FX 15,1
5690 PROCmovepointer
5700 IF INKEY-74 A1=2*px/SX+IS%:GOTO5720
5710 GOTO 5680
5720 PROCprompt("GAUSSIAN FIT - SELECT UPPER BOUND AT HALF HEIGHT")
5730 *FX 15,1
5740 PROCmovepointer
5750 IF INKEY-74 A2=2*px/SX+IS%:GOTO5770
5760 GOTO5730
5770 C(1)=(A2-A1)/1.665
5780 GCOL 4,1
5790 MOVE 258,160+h:PLOT 29,1278,160+h
5800 PROCprompt("GAUSSIAN FIT - ITERATE? (Y/N) ")
5810 *FX 15,1
5820 A$=GET$
5830 IF A$="N" GOTO 5880
5840 REM fit gaussian curve to selected peak
5850 PROCnewton(tol,10,X1%,X2%)
5860 IF delta>tol ENDPROC
5870 REM if the fit has converged store the fit parameters
5880 PROCpointeroff
5890 *FX 15,1
5900 PRINT TAB(1,31)SPC(78);:PRINT TAB(1,31)"GAUSSIAN FIT - PEAK
NUMBER (1,2, OR 3)? ";
5910 A$=GET$
5920 IF A$<>"1" AND A$<>"2" AND A$<>"3" GOTO 5910
5930 PRINT A$;
5940 L%=VAL(A$)
5950 defined%(L%)=TRUE
5960 PEAK(L%,0)=C(0):PEAK(L%,1)=C(1):PEAK(L%,2)=C(2)
5970 PROCpointeron
5980 PROCpeakplot1(L%)
5990 ENDPROC
6000 REM*********************************
6010 DEF PROCspectrumplot
6020 REM plot the complete spectrum fit
```

```
6030 LOCAL T%,S%
6040 PROCprompt("FITTED SPECTRUM PLOT")
6050 S%=(FS%-IS%) DIV 255
6060 IF S%<1 S%=1
6070 MOVE256,160
6080 FOR T%=IS% TO FS% STEP S%
6090   Y=0
6100   IF defined%(1) Y=Y+PEAK(1,0)*EXP(-(((T%-
PEAK(1,2))/PEAK(1,1))^2))
6110   IF defined%(2) Y=Y+PEAK(2,0)*EXP(-(((T%-
PEAK(2,2))/PEAK(2,1))^2))
6120   IF defined%(3) Y=Y+PEAK(3,0)*EXP(-(((T%-
PEAK(3,2))/PEAK(3,1))^2))
6130   DRAW (T%-IS%)*SX+256,Y/S+160
6140   NEXT
6150 ENDPROC
6160 REM*********************************
6170 DEF PROCareas
6180 REM calculate the areas under each peak of the spectrum, and
their errors
6190 LOCAL A,B,C,A$,@%
6200 @%=&10409
6210 CLS
6220 PRINT"AREAS UNDER PEAKS FOR DATA SET ";datafile$
6230 PRINT"-------------------------------------"
6240 A=SQR(PI)*PEAK(1,0)*PEAK(1,1)
6250 PRINT'"AREA UNDER PEAK 1 = ";A;" +/- ";SQR(A);"POS.=";PEAK(1,2)
6260 B=SQR(PI)*PEAK(2,0)*PEAK(2,1)
6270 PRINT'"AREA UNDER PEAK 2 = ";B;" +/- ";SQR(B);"POS.=";PEAK(2,2)
6280 C=SQR(PI)*PEAK(3,0)*PEAK(3,1)
6290 PRINT'"AREA UNDER PEAK 3 = ";C;" +/- ";SQR(C);"POS.=";PEAK(3,2)
6300 IF B<>0 PRINT''"AREA PEAK 2/PEAK 1= ";B/A;" +/-
";B/A*(1/SQR(A)+1/SQR(B))
6310 IF C<>0 PRINT'"AREA PEAK 3/PEAK 1= ";C/A;" +/-
";C/A*(1/SQR(A)+1/SQR(C))
6320 PRINT'''"DO YOU WISH TO PRINT THE ABOVE?";
6330 A$=GET$
6340 IF A$<>"Y" AND A$<>"y" ENDPROC
6350 CLS
6360 VDU 2
6370 PRINT"AREAS UNDER PEAKS FOR DATA SET ";datafile$
6380 PRINT"-------------------------------------"
6390 PRINT'"AREA UNDER PEAK 1 = ";A;" +/- ";SQR(A);"POS.=";PEAK(1,2)
6400 PRINT'"AREA UNDER PEAK 2 = ";B;" +/- ";SQR(B);"POS.=";PEAK(2,2)
6410 PRINT'"AREA UNDER PEAK 3 = ";C;" +/- ";SQR(C);"POS.=";PEAK(3,2)
6420 IF B<>0 PRINT''"AREA PEAK 2/PEAK 1= ";B/A;" +/-
";B/A*(1/SQR(A)+1/SQR(B))
6430 IF C<>0 PRINT'"AREA PEAK 3/PEAK 1= ";C/A;" +/-
";C/A*(1/SQR(A)+1/SQR(C))
6440 PRINT'''
6450 VDU 3
6460 ENDPROC
6470 REM*********************************
6940 DEF PROCevlabel
6950 X1=(PEAK(1,2)-IS%)*SX+256
6960 X2=(PEAK(1,2)+205-IS%)*SX+256
6970 X3=(PEAK(1,2)+410-IS%)*SX+256
6980 MOVE X1,160
```

```
6990 DRAW X1,192
7000 MOVE X2,160
7010 DRAW X2,192
7020 MOVE X3,160
7030 DRAW X3,192
7040 PROCpointeroff
7050 PRINTTAB(0,28)SPC(78);
7060 PROCpointeron
7070 VDU 5
7080 VDU 24,256;0;1279;1023;
7090 MOVE X1-24,152:PRINT"0.0";
7100 MOVE X2-24,152:PRINT"0.2";
7110 MOVE X3-24,152:PRINT"0.4";
7120 MOVE 640,88:PRINT"ENERGY LOSS (eV)";
7130 VDU 4
7140 VDU 24,258;164;1278;960;
7150 ENDPROC
```

References

Abusalbi N, Eades R A, Nam T, Thirumalai D, Dixon D A and Truhlar D G (1983) *J. Chem. Phys.* **78** 1213

Adams A and Read F H (1975a) *J. Phys. E: Sci. Instrum.* **5** 150

——— (1975b) *J. Phys. E: Sci. Instrum.* **5** 156

Arnot F L (1931) *Proc. Roy. Soc. London A* **133** 615

Altmann S L and Cracknell A P (1965) *Rev. Mod Phys.***37** 19

Altshuler S (1965) *Phys. Rev..***107** 114

Andrick D and Bitsch A (1975) *J. Phys B: At. Mol. Phys.* **8** 393

Andrick D and Read F H (1971) *J. Phys B: At. Mol. Phys.* **4** 389

Arthurs A M and Dalgarno A (1960) *Proc. Roy. Soc. London A* **256** 540

Barbarito E, Basta M and Caliechio M (1979) J. Chem Phys. **71** 54

Bederson B & Kieffer L S (1971) *Rev. Mod. Phys* **43** 601

Bevington P R (1969) 'Data Reduction and Error Analysis for the Physical Sciences' McGraw-Hill

Boness M J W, Larkin I W, Hasted J B and Moore L (1967) *Chem. Phys. Letters* **1** 292

Born M (1926) *Z. Phys.* **38** 803

Botz F K and Glick R E (1975) *Chem. Phys. Letters* **33** 279

Brewer D F C Newell W R and Smith A C H (1980) *J. Phys. E: Sci. Instrum.* **13** 123

Brinkmann R T and Trajmar S (1980) *J. Phys. E: Sci. Instrum.* **14** 255

Brode R B (1925) Phys. Rev. **25** 636

Brüch E (1927) *Ann. Phys. Lpz.* **83** 1065

——— (1929) *Ann. Phys. Lpz.* **2** 909

——— (1930) *Ann. Phys. Lpz.* **4** 387

Brunt J N H and Read F H (1975) *J. Phys. E: Sci. Instrum.* **8** 1015

Brunt J N H, Read F H and King G C (1977) *J. Phys. E: Sci. Instrum.* **10** 134

Bullard E C and Massey H S W (1931) *Proc. Roy. Soc. London A* **133** 637

Burden R L and Faires J D (1985) 'Numerical Analysis third edition' Prindle, Weber & Schmidt, Boston

Chang E S (1981) *J. Phys B: At. Mol. Phys.* **14** 893

Chantry P J *J. Chem. Phys.* **55** 2746

Choi B H and Poe R T (1977a) *Phys. Rev. A* **14** 1321

——— (1977b) *Phys. Rev. A* **16** 1831

Chutjian A (1974) *J. Chem. Phys.* **61** 4279

——— (1979) *Rev. Sci. Instrum.* **50** 347

Cotterill T L, and Walker I C (1965) *Trans. Faraday Soc.* **61** 1585

——— (1967) *Trans. Faraday Soc.* **63** 549

Cotton F A (1971) 'Chemical Applications of Group Theory' Wiley-Interscience

Curry P J (1984) Phd Thesis, London University

Curry P J, Newell W R and Smith A C H (1985) *J. Phys B: At. Mol. Phys.* **18** 2303

Deuring A, Floeder K, Fromme D, Raith W, Schwab A, Sinapius G, Zitzewitz P W and Krug J *J. Phys B: At. Mol. Phys.* **16** 1633

Duncan C W and Walker I C (1972) *J. Chem Soc* **68** 1514

Fano U (1970) *Comments on Atomic and Molecular Physics* **2** 47
Ferch J, Granitza B, Masche C and Raith W (1985a) *J. Phys B: At. Mol. Phys.* **18** 967
Ferch J, Granitza and Raith W (1985b) *J. Phys B: At. Mol. Phys.* **18** L445
Fink M, Jost K and Hermann D (1975) *J. Chem. Phys.* **63** 1985
Floeder K, Fromme D, Raith W, Schwab A and Sinapius G (1985) *J. Phys B: At. Mol. Phys.* **18** 3347
Gianturco F A and Thompson D G (1976) *J. Phys B: At. Mol. Phys.* **9** L383
——— (1980) *J. Phys B: At. Mol. Phys.* **13** 613
Gerjuoy E and Stein S (1955a) *Phys. Rev.* **97** 1671
——— (1955b) *Phys. Rev.* **98** 1848
Grivet P (1965) 'Electron Optics' Pergamon, Oxford
Harting E and Burrows (1970) *Rev. Sci. Instrum.* **41** 97
Harting E and Read F H (1976) 'Electron Optics' Elsevier, Amsterdam
Heddle D W O (1968) 'The measurement of the optical excitation Functions' in 'Methods of Experimental Physics' Vol 7 Part A (eds Bederson B and Fite W L) Academic Press
Herzberg G (1945) 'Molecular spectra and molecular structure' Vol 2 'Infrared and Raman spectra of polyatomic molecules' Princeton N. J
Hughs A C and McMillan J H (1933) *Phys. Rev.* **44** 876
Hunt G E (1980) 'Planetary Exploration' in 'The State of the Universe' Ed Bath G T Claredon Press Oxford
——— (1985) *J. British Interplanetary Soc.* **38** 217
Jain A and Thompson D G (1982) *J. Phys B: At. Mol. Phys.* **15** L631
——— (1989) Private communication
Johnson K E, Kim K, Johnston D B and Lipsky S (1979) *J. Chem. Phys.* **70** 2189
Jones R K (1985) *J. Chem. Phys.* **82** 5424
Jost K (1979) *J. Phys. E: Sci. Instrum.* **12** 1001
Kempler O and Barnett M E (1971) 'Electron Optics' Cambridge University Press
Kuyatt C E (1968) 'Measurement of Electron Scattering From a Static Gas Target' in 'Methods of Experimental Physics' Vol 7 Part A (eds Bederson B and Fite W L) Academic Press
Kuyatt C E and Simpson J A (1967) *Rev. Sci. Instrum.* **38** 103
Lima M A P, Gibson T L, Huo W M and McKoy V (1985) *Phys. Rev. A* **32** 2696
Lucas C B (1972) *Vacuum* **23** 295
Mason N J and Newell W R (1989) *J. Phys B: At. Mol. Phys.* **22** 777
Massey H S W (1930) *Proc. Roy. Soc. London A* **129** 616
——— (1932) *Proc. Cam. Phil. Soc.* **28** 99
Massey H S W and Burhop E H S (1969) 'Electronic and Ionic Impact Phenomena, Vol. 1 Collisions of Electrons with Atoms' Oxford: University Press
Massey H S W and Mohr C B O (1931) *Proc. Roy. Soc. London A* **132** 605
——— (1932a) *Proc. Roy. Soc London. A* **135** 258
——— (1932b) *Proc. Roy. Soc London. A* **136** 259
——— (1934) *Proc. Roy. Soc. London A* **143** 880
Mathur D (1980) *J. Phys B: At. Mol. Phys.* **13** 4703

McCorkle D L, Christophorou L G, Maxey D V and Carter J G (1978) *J. Phys B: At. Mol. Phys.* **11** 3067

McKoy (1987) Private communication

McGowan J W (1967) *Rev. Sci. Instrum.* **38** 285

Mohr C B O and Nicholl F H (1932) *Proc. Roy. Soc. London A* **138** 469

Murry J R, Goldhar J, Eimerl D and Szoke A (1979) *I.E.E.E. J. Quant. Elec.* **15** 342

Nesbit R K (1979) *Phys. Rev. A* **20** 58

Newell W R, Brewer D F C and Smith A C H (1979) Proc. 11th Int. Conf. on Physics of Electronic and Atomic Collisions (Kyoto) Abstracts 308

——— (1981) *J. Phys B: At. Mol. Phys.* **14** 3209

Nickel J C, Zetner P W, Shen G and Trajmar S (1989) *J. Phys. E: Sci. Instrum.* **22** 730

O'Malley T F (1963) *Phys. Rev.* **130** 1020

Oppenheimer J R (1928) *Phys.Rev* **32** 361

Orlander DE R and Kruger (1970) *J. App. Phys.* **41** 2769

Parker J H and Warren R W (1962) *Rev. Sci. Instrum.* **33** 948

Petley C H (1971) *Mullard Tech. Rev* **24** 130

Pollock W J (1968) *Trans. Faraday Soc.* **64** 2919

Purcell E M (1938) *Phys. Rev.* **54** 818

Ramsauer C (1921) *Ann. Phy.* **64** 513

Ramsauer C and Kollath R (1930) *Ann. Phys. Lpz.* **4** 91

Read F H (1968) *J. Phys B:(Proc. Phys. Soc)* **1** 893

Read F H (1975) *J. Phys B: At. Mol. Phys.* **8** 1034

Read F H, Comer J, Imhof R E, Brunt J N H and Harting E (1974) J. *Elect. Spec. & Rel. Phenon.* **4** 293

Register D F, Trajmar S and Srivastava S K (1980) *Phys. Rev. A* **21** 1134

Riley M E and Truhlar D G (1975) *J. Chem. Phys.* **63** 2182

Rohr K (1980) *J. Phys B: At. Mol. Phys.* **13** 4897

Sanche L and Schulz G J (1973) *J. Chem. Phys.* **58** 479

Sevier K D (1972) 'Low Energy Electron Spectrometry' Wiley

Shyn T W, Stolarski R S and Carignan G R (1972) *Phys. Rev. A* **6** 1002

Simpson (1964) *Rev. Sci. Instrum.* **35** 1698

Sohn W, Jung K and Ehrhardt H (1983) *J. Phys B: At. Mol. Phys.* **16** 891

Sohn W, Kochem K H, Scheuerlein K M, Jung K and Ehrhardt (1986) *J. Phys B: At. Mol. Phys.* **19** 3625

Srivastava S K, Chutjian A and Trajmar S (1975) *J. Chem. Phys.* **63** 2659

——— (1981) *Phys. Rev. A* **23** 2156

Steph N C, McDonald L and Golden D E (1979) *J. Phys B: At. Mol. Phys.* **12** 1507

Sueoka O, and Mori S (1986) *J. Phys B: At. Mol. Phys.* **19** 4035

Takatsuka K, McKoy V (1981) *Phys. Rev. A* **24** 2473

——— (1984) *Phys. Rev. A* **30** 1734

Tanaka H, Okada T, Boesten L, Suzuki T, Yamamoto T and Kubo H (1982) *J. Phys B: At. Mol. Phys.* **15** 3305

Tanaka H, Kubo M, Onodera N and Suzuki A (1983) *J. Phys B: At. Mol. Phys.* **16** 2861

Tanaka H, Boesten L, Matsunaga D and Kubo T (1988) *J. Phys B: At. Mol. Phys.* **21** 1255

Temkin A (1957) *Phys. Rev.* **107** 1004

Trajmar S and Register D F (1984) ' Experimental Techniques for Cross Section Measurements' in Electron-Molecule Collisions' New York: Plenum Press

Trajmar S, Register D F and Chutjian A (1983) *Physics Reports* **97** 219

Valone S M, Truhlar D G and Thirumalai D (1982) *Phys. Rev. A* **25** 3003

Vuskovic L and Trajmar S (1983) *J. Chem. Phys.* **78** 4947

Wayne R P (1985) 'Chemistry of Atomospheres' Oxford Science Publications

Williams S F *J. Phys B: At. Mol. Phys.* **12** 265